FORMATION, DEPOSITIONAL HISTORY AND MAGNETIC PROPERTIES OF LOESSIC SILT FROM THE TIBETAN FRONT, CHINA.

Thesis submitted for the degree of
Doctor of Philosophy
at the University of Leicester

by

Michèle Louise Clarke BSc (Sussex) MSc (London) GRSC
Department of Geography
University of Leicester

September 1992

7501440835

CONTENTS

Acknowledgements

This work was funded by a NERC studentship (GT4/88/GS/61) and was supervised by Professor Edward Derbyshire of Leicester University and Dr John Shaw of Liverpool University. It is the result of a cooperative venture between several institutions in both the U.K. and China, and, as such, I have pleasure in acknowledging the help of a number of people who gave their time to contribute to the successful completion of this work.

Christine Scott spent 4 months in China acting as my field assistant, which involved non-stop sampling and sub-sampling under trying conditions. I am most grateful for her patience, enthusiasm and continued encouragment as well as her helpful comments on drafts of this manuscript.

Professor Wang Jingtai, of the Gansu Academy of Sciences, allowed me use his Institute as my home and laboratory, and offered his staff, Meng Xingming, Ma Jinhui and Xiao Wei, to help on fieldwork. He arranged for us to join the Sino-Soviet Tibetan Plateau Expedition after my numerous attempts at gaining permission to enter Tibet had failed. Thanks are also due to his wife for cooking such authentic food.

Dr. Jennifer King accompanied me on part of my first visit to China in 1989 and arranged for me to visit Xian. We shared some difficult times and I am particularly grateful for her organisation skills, especially during the aftermath of 'Tiananmen Square'. Professor An Zhisheng of the Xian Laboratory for Loess and Quaternary Geology arranged access to Weinan and Duanjiapo sections.

In researching this thesis, I have spent time at both the Geography Department, University of Leicester and the Geomagnetism Laboratory, University of Liverpool. At Leicester, I have benefitted from the help of Brian White who demonstrated how best to use the magnetic equipment; Rod Branson who taught me the ins and outs of the Hitachi Scanning Electron Microscope; and both Dr Andy Saunders and Brian Dickie of the Geology Department who helped me with the rare earth element analysis and commented on my draft manuscript. The chemical analysis was carried out in the ICPAES laboratory by Brian Dickie and Adelaide Holmes.

The nine months I spent in the Geomagnetism Laboratory at Liverpool were especially productive due to the research environment created by my fellow "spinners". Particular thanks are due to Del Atkinson, who showed me how to use most of the equipment and contributed endless suggestions on methods of improvement. Dr. Graham Sherwood and Dr. Tim Rolph helped me get to grips with the mainframe and associated programmes and both gave helpful comments on improving the written manuscript. Grateful thanks to Dr John Share for arranging the emergency flight from China after Tiananmen Square and organising my stay at Liverpool.

In addition to the above, I have benefitted from the advice and enouragement of Dr. Ann Wintle, Dr. Helen Rendell, Dr. Zhou Liping, Fang Xiaomin, Prof. Ian Smalley and Dr. Ernie Hailwood who ran the torsion fibre anisotropy. Kate Richardson, Fiona Musson, Geoff Duller and Li Shenghua supported my efforts on the final draft.

For my family, for all I have put them through.

The night is always blackest before the dawn - Chinese Proverb.

1. INTRODUCTION

Sedimentary sequences are widely used to obtain proxy records of climate change. Oxygen isotopic variations ($\delta^{18}O$) within planktonic and benthonic foraminifera obtained from deep sea sediments have allowed reconstruction of continental ice volume changes and have therefore been used to delineate glacial and interglacial periods (Shackleton and Opdyke, 1973). However, the accumulation rates of deep sea sediments are too low to permit recovery of an accurate Pleistocene climatic variability (Shackleton *et. al.*, 1990). Higher deposition rates exist on the continents, although undisturbed thick sedimentary sequences are rare. The study of deuterium, aerosol and greenhouse gas concentrations, taken from ice cores from Greenland, Antarctica and Tibet, have provided climatic information covering the Holocene and Late Pleistocene (Jouzel *et. al.*, 1990; Thompson *et. al.*, 1989). However the length of record is limited by ice flow and deformation which increases with depth. The thick Pleistocene loess sequences which exist in Europe, Pakistan, Kazakhstan, China, New Zealand and north America provide another possible proxy indicator. Loess, which is considered to be a cold climate deposit is often intercalated with soil horizons suggesting periods of climatic amelioration. The Loess Plateau of China contains the thickest of these sedimentary records and is thought to have 27 palaeosol horizons related to interglacial climates. Thus the Chinese loess-palaeosol sequences have excellent potential for use as a comprehensive palaeoclimatic indicator.

1.1 Scope and objectives of the thesis

The silt particles which form the Chinese Loess Plateau have long been thought to derive from the desert regions of northern China and Mongolia (Liu Tungsheng *et. al.*, 1985; Wu Zirong and Gao Fuqing, 1991). However, the mechanisms by which the constituent silt particles of loess are formed are a major source of contention, with both desert and mountain environments cited as the production area of these particles. Geochemical fingerprinting, using rare earth elements, has suggested that the loess deposits within the big bend of the Yellow River were formed within the Tengger desert (Wen Qizhong *et. al.*, 1983). The Loess Plateau of China lies in close proximity to the vast high level Tibetan Plateau and Kunlun, Qilian and A'nyêmaqen Mountains in addition to large areas of sand and gravel (gobi) desert. The tectonically active mountain areas of Tibet which lie to the immediate west of the Loess Plateau have been proposed as a source area for material in the western Loess Plateau around Lanzhou (Bowler *et.al.*, 1987; Zhang Linyuan *et.al.*, 1991). One of the objectives of this thesis is to use rare earth elements to compare silts sampled from the mountain environments with the loess of the western Loess Plateau.

The deposits of the western Loess Plateau represent the thickest accumulations of loess in the world (Derbyshire, 1983) with more than 300 metres exposed on the terrace gravels of the Yellow River near the city of Lanzhou. These thick continental loess-palaeosol sequences have been used as a proxy indicator of climatic change and, as such, have been correlated with climatic records obtained from deep sea cores (Kukla *et.al.*, 1987) and ice cores (Chen Fahu *et.al.*, 1991). Recently the variation in magnetic susceptibility with depth throughout loess profiles in China has been used as an indicator of climatic change due to the fact that palaeosols have a higher magnetic susceptibility than loess. The cause of this variation in loess and palaeosols is a contentious issue (Zhou Liping *et.al.*, 1990; Maher and Thompson, 1991). Magnetic susceptibility is dependent upon the concentration, size, shape and mineralogy of magnetic grains within the sediment and therefore to understand the variation in magnetic susceptibility within loess and palaeosols some understanding of the mineralogy and grain size of the magnetic particles within these sequences is needed. Studies of the variation in magnetic mineralogy of loess-palaeosol sequences have been carried out for sites within the central Loess Plateau, an area affected by the East Asian monsoon (Zhou Liping, 1991; Liu Xiuming *et.al.*, 1992). Part of this thesis study was undertaken to examine the variation in magnetic mineralogy throughout a series of loess-palaeosol transitions in the Lanzhou area where the climate is more arid (the monsoon winds are blocked by the mountains associated with the Tibetan Plateau) and the loess accumulation is greater in order to characterise the different magnetic assemblages in the soils and loess.

One of the problems concerning the study of loess is a lack in chronological control due to the limits of radiocarbon dating and the effects of underestimation of the thermoluminescence signal (Debenham, 1985; Wintle, 1990). Magnetostratigraphy may lend a relative chronology to a particular sediment section and has been extensively employed in China for this purpose (Heller and Liu Tungsheng, 1984; Rolph *et.al.*, 1989). Recognition of the magnetic excursion known as the Blake Event, which is thought to have occurred 115-120ka (Tric *et.al.*, 1991) during the last interglacial would form a useful stratigraphic marker horizon within these thick massive deposits. To date, convincing evidence for the Blake Event is absent from Chinese deposits.

The use of sedimentary sequences as palaeoclimatic indicators necessitates that the deposits are primary and undisturbed. Loess is thought to be an isotropic air fall deposit which may undergo reworking by slope processes or alluviation. Magnetic fabric techniques have been used within this thesis to assess the primary nature of the loess. Slopes of 35° are common on the western Loess Plateau, an area affected by neotectonic-related earthquakes (Derbyshire *et.al.*, 1991). Reworking of deposits may be prevalent in this type of environment.

1.2 Aims of the thesis:

1. To study the variation in magnetic mineralogy through loess-palaeosol transitions at sites within the western Loesss Plateau near Lanzhou and attempt to characterise the different magnetic assemblages within the loess and palaeosols.
2. To compile a magnetostratigraphy of these sections with the aim of observing the Blake Event.
3. To study the magnetic fabric of the loess deposits to assess the primary nature of the sediment fabric.
4. To compare the rare earth element geochemistry of Tibetan sediments obtained from the Qaidam Basin and Kunlun Mountains (which have been proposed as source areas for loess at Lanzhou (Bowler *et.al.*, 1987)) with those of the Lanzhou loess and compare it with existing data on Tengger desert sand and loess from the central Loess Plateau (Wen Qizhong *et.al.*, 1983).

1.3 Loess

Loess has been defined as a clastic deposit which consists primarily of quartz particles 20-50µm in diameter and which occurs as wind-lain sheets (Smalley and Vita-Finzi, 1968). The 20µm lower threshold was chosen to separate loess from the finer aerosolic dust <10µm (Smalley and Derbyshire, 1990). Along with quartz, loess may also contain feldpsars, micas, carbonates and clay minerals. It is characteristically a buff colour, although this can vary, and highly porous with no visible evidence of bedding structures. Unweathered loess is poorly sorted and usually exhibits positively skewed particle size values, indicating a tail of fines (Pye, 1987).

Smalley and Vita-Finzi (1968) have stressed that the aeolian origin of loess is an integral part of its definition, stating that once such material is redeposited by water, mass movement or any other agency, it forfeits the right to be called loess and should be termed 'redeposited loess material'. In this study the nomenclature: loessic alluvium and loessic colluvium, has been favoured for secondary redeposited loessic material.

The processes by which the constituent silt-sized quartz particles of loess are formed has been a source of contention for the last 25 years. Smalley (1966) described how the high energy grinding action of glaciers upon the underlying bedrock produces quartz 'flour' in the size range characteristic of loess. More recently, the action of frost within high periglacial mountain areas (Minervin, 1974; Konischev, 1987) has been suggested as a further 'cold environment' source of silt grains resulting in the distinction between 'ice sheet' and 'mountain' loess (Smalley and Smalley, 1983; Smalley and Derbyshire, 1990).

The production of silt-sized material from bedrock is aided by the presence of microcracks within quartz crystals (Reizebos and Van de Waals, 1974; Moss and Green, 1975) which can be exploited by salts and frost (Whalley *et. al.*, 1982b; Minervin 1974). In some environments weathering may occur by the combined action of frost and salt, with the presence of salts enhancing frost action (Goudie, 1974; Williams and Robinson, 1981), although this view is currently disputed (McGreevy, 1982).

Various mechanisms have been postulated for the hot climate formation of silt within deserts. Salt weathering has been suggested as an efficient producer of silt-sized particles (Goudie *et. al.*, 1979). *In situ* salt weathering may occur by several mechanisms, for example, the crystallisation of salt from supersaturated solutions in confined spaces; or the alternate hydration-dehydration of salts, which can occur diurnally *e.g.* thenardite (Na_2SO_4) to mirabilite ($Na_2SO_4.10H_2O$) (Pye and Sperling, 1983). The thenardite-mirabilite system is particularly effective in weathering due to its solubility characteristics and crystal shape: thenardite solubility decreases rapidly below 32.3°C and would therefore crystallise at night when the temperature falls producing prismatic or acicular crystals which concentrate crystal growth along one axis promoting disruption in confined spaces (Cooke, 1979). However, McGreevy and Smith (1982) emphasize that much work has been based on sodium sulphate, whereas calcium carbonate, calcium sulphate and sodium chloride are also prevalent in deserts and may play an important rôle.

Aeolian attrition during desert storms can produce quartz fragments by chipping off angular edges and causing rounding of sand grains (Whalley *et. al.*, 1982a; 1987). A substantial proportion of the quartz fragments produced in this way are within the size range of loess and the authors suggest that the Chinese loess could have been so produced within the Gobi desert. In humid tropical climates, where there has been no Quaternary glaciation, silt-sized quartz can be produced by chemical solution of regolith (Nahon and Trompette, 1982; Pye, 1983).

Once the silt constituent of loess has been formed, it undergoes a series of transportation and deposition stages. Smalley (1980) recognised a nine event sequence for the Tashkent loess (Kazakhstan) and Smalley and Smalley (1983) proposed a similar eleven event sequence for the Chinese loess. Both of these theories are based on the contention that the silt is formed only in cold mountain environments and is then transported by the action of both rivers and wind into the central Asian deserts, which act as a sediment trap. It is from these accumulations that silt is deflated to form loess.

1.4 Loess in China

1.4.1 Distribution

Loess is widely distibuted across China, with deposits ranging from the Liangdong Peninsula on the eastern Bohai Sea, to the far western piedmont of the Tien Shan in northern Xinjiang and as far south as Nanjing (figure

1.2). The thickest deposits occur on the Loess Plateau which covers an area of 273,000km^2 (Liu Tungsheng *et.al.*, 1985), encompassing the middle reaches of the Yellow River in the central Chinese provinces of Gansu, Shaanxi, Shanxi and Ningxia (figure 1.3).

The distribution of loess within the Loess Plateau is closely related to the desert and Gobi regions to the north and northwest (Wu Zirong and Gao Fuqing, 1991). Liu Tungsheng *et.al.* (1985) believe that the Cenozoic and Mesozoic detrital sediments which make up these deserts, constitutes the source material of the loess. Silt, resident within the deserts, is deflated and carried in the lower 1.5km of the atmosphere by cold, low-level northwesterly winds associated with the Mongolian anticyclone (Pye and Zhou Liping, 1989; figure 1.4). During atmospheric transport the heavier particles are "rained out" and particle size fractionation occurs (figure 1.4) with the finest particles being deposited furthest from the source area. The southeastward gradation from gravel desert (gobi) to sand desert to loess is a result of this type of sorting by deflation (Wang Yongyan, 1983).

1.4.2 Formation

The formation of silt within the Chinese deserts is also a source of contention (Smalley and Krinsley, 1978). Tsoar and Pye (1987) stress that the ultimate origin of silt within the Ordos Desert, thought to be the main source of silt for the central loess plateau, is uncertain. They argue that a proportion may have been derived from fluvioglacial outwash in the Yellow River (Huang He) floodplain. This suggests that the deserts act as both a source of silt and a storage area of secondary redeposited silt formed elsewhere, conforming to the transport and deposition stages of Smalley and Smalley (1983). Recently Bowler *et.al.* (1987) have described a depositional pathway for the westernmost Loess Plateau involving silt derived from the mountains fringing the Tibetan Plateau (see chapter 2). This silt is formed under glacial and periglacial conditions and transported to the Qaidam Basin from where it is deflated by northwesterly winds.

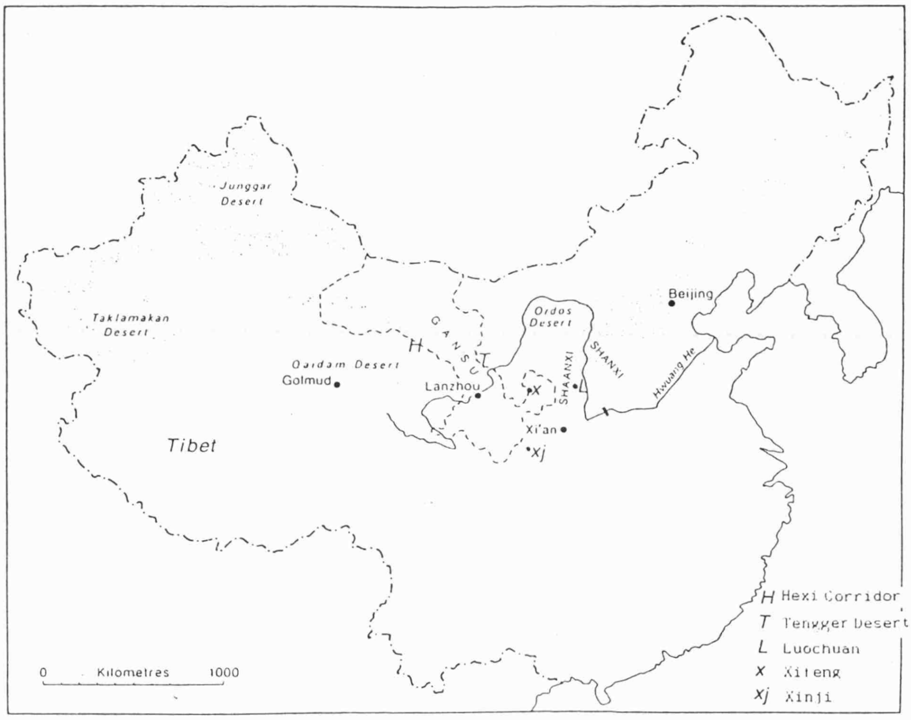

Figure 1.1 Map showing locations mentioned in the text

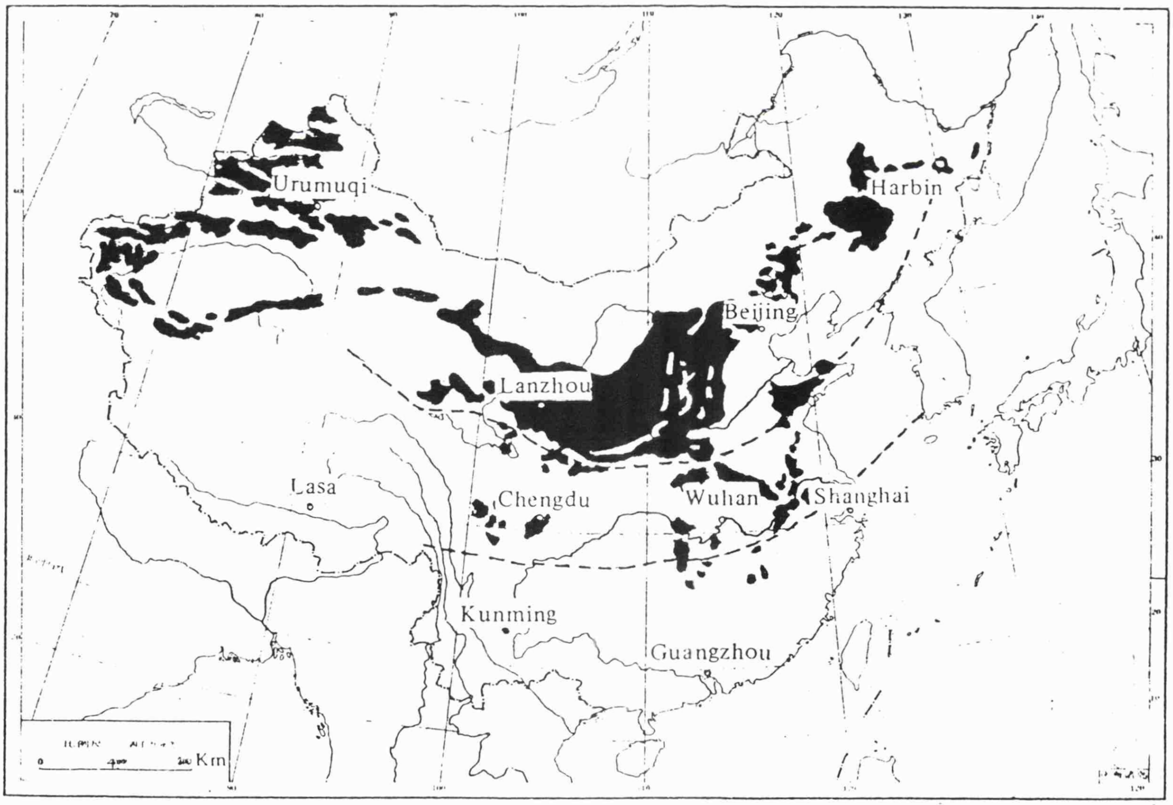

Figure 1.2 Map showing the distribution of loess in China

(Liu Tungsheng *et. al.*, 1985)

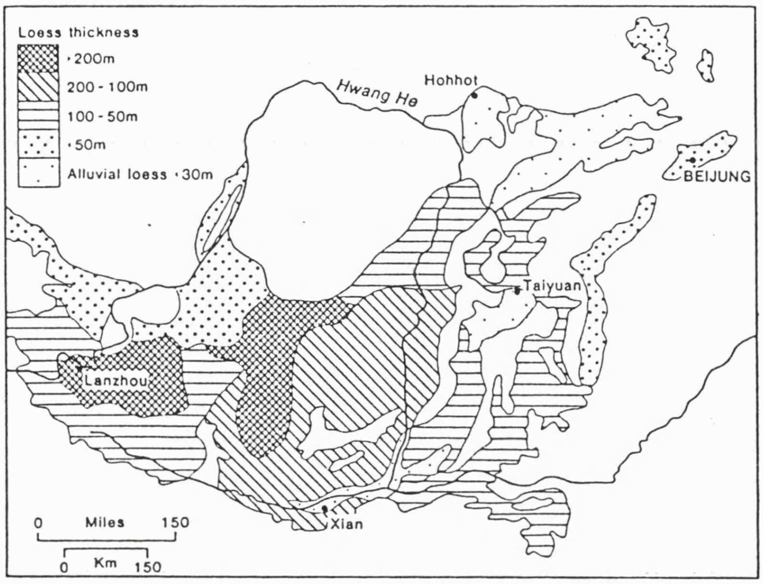

Figure 1.3 Distribution of loess thickness in the central Loess Plateau (Derbyshire, 1983)

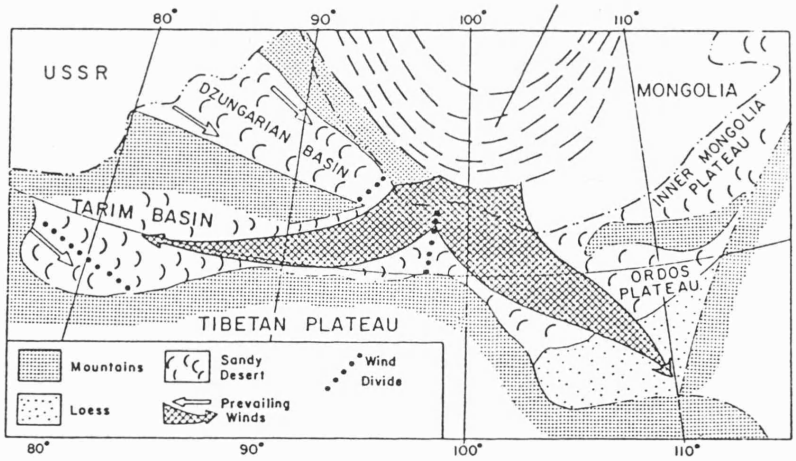

Figure 1.4 Direction of the prevailing winter winds in northwestern China (Chao Sungqiao, 1984)

This thesis is based on a study of the westernmost edge of the Loess Plateau and the deposits found in the mountain chains that make up the edge of the Tibetan Plateau. For this reason the area studied has been termed the 'Tibetan Front'.

1.4.3 Stratigraphy

The thick loess sequences that comprise the Loess Plateau are thought to represent a complete stratigraphic record covering the Quaternary period (Liu Tungsheng, *et.al.*, 1985). Cold, dry periods with strong northwesterly winds, associated with glacial climates, are thought to favour loess accumulation, with pedogenesis forming palaeosols within interglacial periods following the incursion of moister warmer air from the southerly monsoons (Liu Tungsheng and Ding Menglin, 1985). The loess in China is divided into four chronostratigraphical units: the Early Pleistocene Wucheng loess (Q_1); Middle Pleistocene Lishi Loess (Q_2) - which is often subdivided into Upper Lishi (Q_2^2) and Lower Lishi (Q_2^1); the Late Pleistocene Malan Loess (Q_3); and Holocene Potou Loess. The Wucheng loess commonly rests upon Neogene red clays, sands and gravels containing Pliocene faunas of the three-toed horse ***Hipparion*** and rhinocerus ***Chilotherium spp*** (Liu Tungsheng *et.al.*, 1987). The Wucheng loess in the Lanzhou area rests on terrace gravels of the Yellow River which planated the Pliocene red clays. The Wucheng loess contains Nihewan faunas, which have been correlated with the Villefranchian faunas of Europe. Vertebrate fossils from the Nihewan series are characteristic in that they contain both remnants of Pliocene species as well as forerunners of Pleistocene species, such as the early horse ***Proboschihipparion sinensis***. Nihewan Early Pleistocene faunas are found in lacustrine sediments at Yangyuan, Hebei Province and Yuanmou, Yunnan Province as well as within the Wucheng loess (Liu Tungsheng and Ding Menglin, 1985). Pollen of arboreal species (***Pinus***, ***Quercus***, ***Acer***) and grasses sugggest that the Wucheng loess sustained a forest-steppe environment (Derbyshire, 1983). The basal ten metres of the Wucheng loess in Gansu consists of fluvial or lacustrine reworked loessic silt, being visibly stratified and imbricated.

The Lishi loess contains mainly herb pollen with arboreal pollen rare, suggesting that it sustained a continental (steppe) environment, whereas the Malan loess sustained a bush and grass flora with the virtual disappearance of trees indicating a progressive dessication (Derbyshire, 1983). The presence of palaeosols within the loess sections has allowed stratigraphic correlation. Palaeosols are numbered S0, S1, S2 from the top of the section, with intervening loesses numbered L1, L2, L3 accordingly. S0 is a Holocene palaeosol (~10ka), with S1 representing the last interglacial (80-125ka) and the boundary between the Malan (L1) and Lishi loess (L2). The Upper Lishi is denoted as the loess existing between S1 and the well-developed triple palaeosol S5. The Lower Lishi ranges between S5 and S14 and is underlain by the Wucheng loess. This use of palaeosols to denote chronology is open to error if the section contains dicontinuities or erosional hiatuses.

The mean particle size of the loess units decreases with age, so that the Malan loess is generally coarser than the Lishi and the Wucheng (figure 1.5). Voids ratios decrease accordingly, due to the particle size and the effects of compaction.

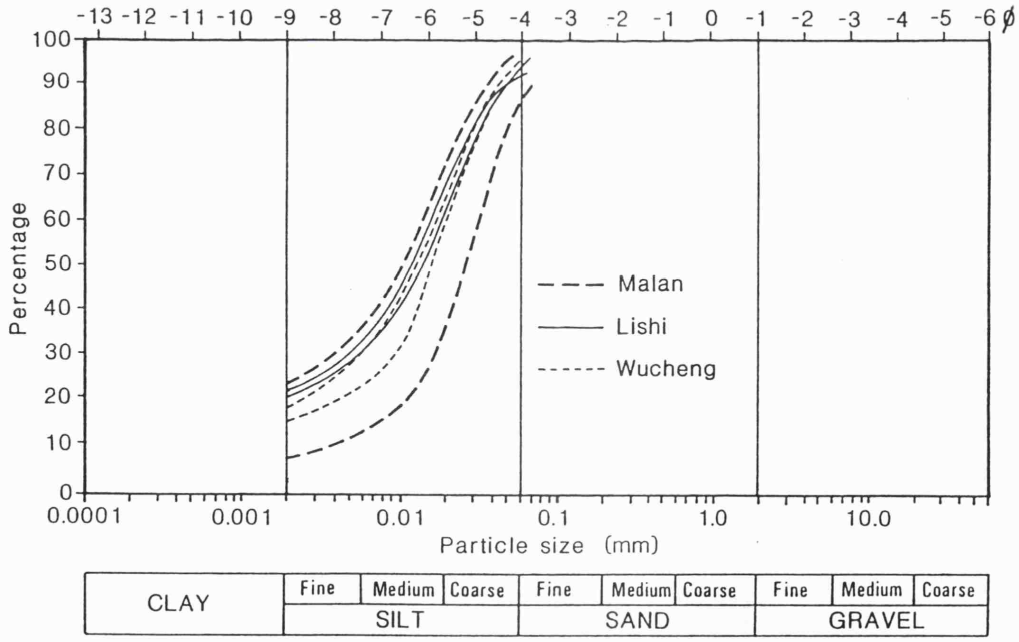

Figure 1.5 Particle size envelopes for Malan, Lishi and Wucheng loesses from Jiuzhoutai (Derbyshire, 1988)

The Luochuan and Xifeng loess sections, in central China (figure 1.6), have been extensively studied and are well documented (Liu Tungsheng *et. al.*, 1985; Liu Xiuming *et. al.* 1988a). These sections are thought to represent a stratigraphic sequence covering the Quaternary period, with a basal age indicating the onset of deposition at about 2.4Ma, based on magnetic reversal stratigraphy (figure 1.7). The Brunhes-Matuyama polarity boundary, dated at 730ka by fission track methods (Jacobs, 1984), occurs in L8 between palaeosols S7 and S8 (Liu Tungsheng *et. al.*, 1985). A recent study by Rolph *et. al.* (1989) suggests that the loess on the western edge of the Loess Plateau, at Lanzhou, also has a basal age of ~2.4Ma, contrary to the initial findings of Burbank and Li Jijun (1985) who believed that uplift of the mountains fringing the Tibetan Plateau inhibited deposition in the Lanzhou Basin until 1.3Ma.

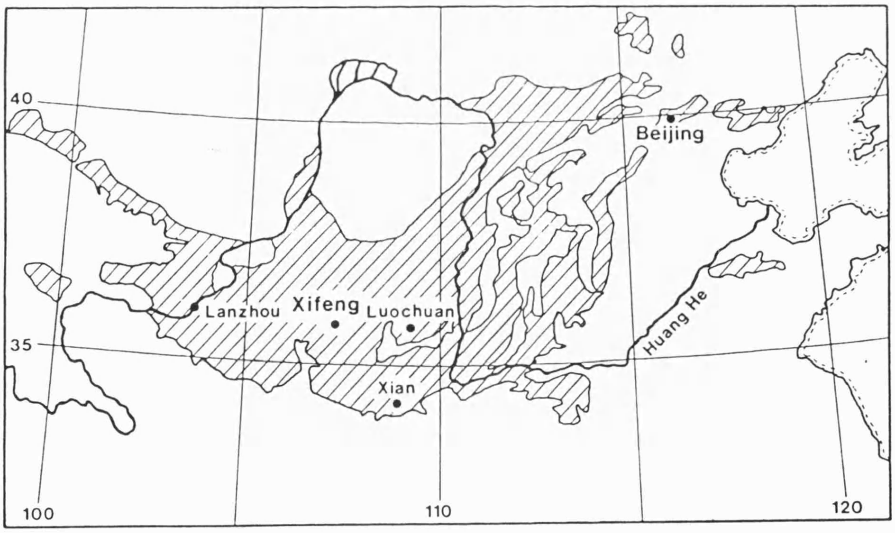

Figure 1.6 The position of the Luochuan, Xifeng and Lanzhou sections in relation to the central Loess Plateau (Kukla and An Zhisheng, 1989)

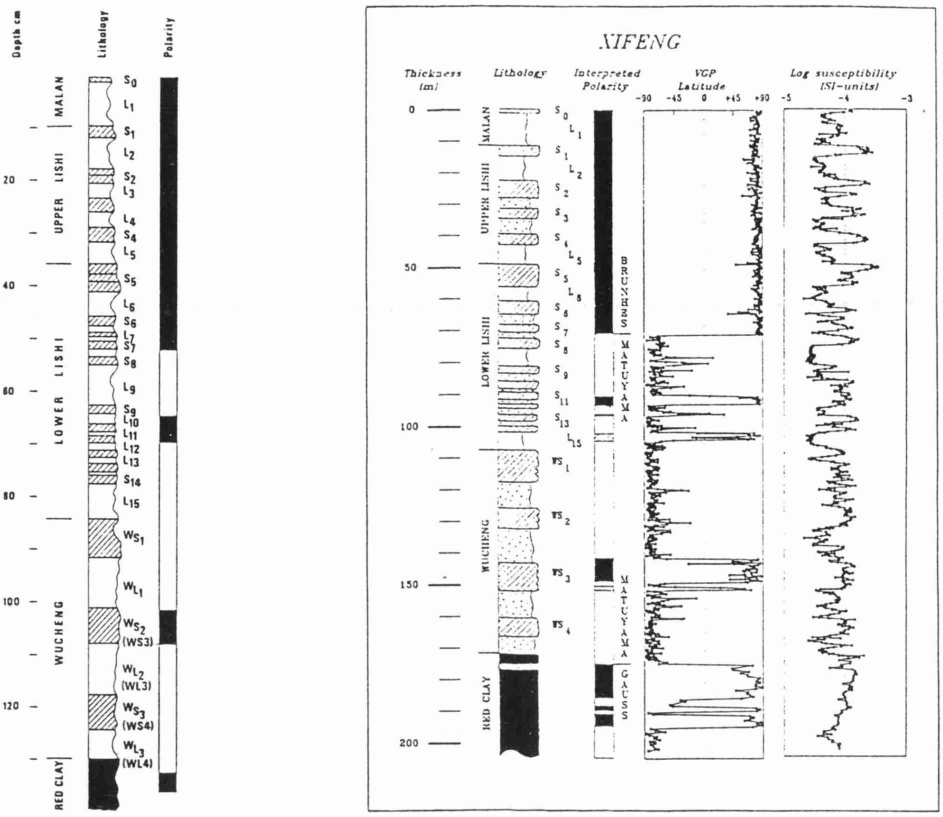

Figure 1.7 The sections at Luochuan and Xifeng (Kukla, 1987).

1.5 Quaternary glaciation and uplift of Tibet and the Himalayas

The rapid uplift of the Tibetan Plateau and the Himalayas as a result of the Tertiary tectonic collision between India and south Tibet has had a critical affect upon the climate of the surrounding regions. In northwest China this continued uplift has strengthened both the Siberian-Mongolian high pressure system and the Chinese monsoon system to cause a progressive increase in aridity (Chao Sungchiao, 1984). The rate and time of uplift is important as initial uplift of the Himalayas and Tibet above the firnline caused the onset of glacierisation; subsequent uplift had the opposite effect, cutting off moisture from the Indian monsoon and thus reducing glacierisation on the northern Himalayan slopes (Osmaston, 1989). The relationship between uplift and climate of Tibet is relevant to this study because of the proximity of the western Loess Plateau to Tibet, this being a possible source area for the constituent silt particles of loess. The relationship between high altitude silt production processes (cold weathering and glaciation) is linked to the present conflict of opinion on the degree of Quaternary glaciation of the Tibetan Plateau (Kuhle, 1987b; Zheng Benxing 1989b): Kuhle's ice sheet would produce vast amounts of glacially ground silt whereas Zheng Benxing's limited glaciation would lead to a progressive dominance of silt produced by cold weathering over the unglaciated plateau surface. Although there is a strong body of opinion that the grinding action at the bed of glaciers and ice sheets is the only mechanism capable of producing the large volumes of silt represented by the world's loess deposits (Smalley and Cabrera, 1970; Boulton, 1978) both field data and laboratory experimentation have clearly shown that the processes of hydration, salt weathering and frost weathering are capable of rapid and substantial production of silt from breakdown of quartz blocks (Prebble, 1967; Goudie, 1974; Goudie, 1983; Bradley, Hutton and Twidale, 1978; Sperling and Cooke, 1985). Discrimination of glacial from non-glacial silts, despite the well known work of Krinsley (Krinsley and Doornkamp, 1973; cf Bull *et. al.*, 1986), remains a doubtful practice. Scanning electron microscope examination of the fragments produced in the climatic-cabinet experiments of Sperling and Cooke (1985), for example, revealed conchoidal and stepped fracture surfaces which are indistinguishable from those attributed by some authors to glacial crushing alone.

1.5.1 Glaciation theories

Chinese workers have found evidence for four major Quaternary glaciations within Tibet, named the Xixabangma (Early Pleistocene); Nieniexongla (Nyanyaxongla; Middle Pleistocene); Late Pleistocene Qomolomgma I and Qomolongma II. The Middle Pleistocene Nieniexongla glaciation was thought to be the most extensive (Zheng Benxing, 1989a). A contrasting view of Tibetan glacial stratigraphy is provided by Matthias Kuhle on the basis of three expeditions to the area (Kuhle, 1986; 1987a; 1987b; 1988; 1989; 1990). He cites evidence for a large inland ice sheet 2.0 to 2.4 million km^2 covering Tibet, at the time of the last ice age (Late Pleistocene). These two opposing strategies have been recently criticised on the grounds that they attempt to make field evidence fit preconceived theories (Osmaston, 1989; Burbank and Cheng, 1991).

A major difficulty facing scientific reconstruction in Tibet is that as a politically sensitive area under military supervision by China, it is closed to foreign travel and study, with few exceptions. Thus the majority of work is unverifiable at present, fuelling the controvesy. The following section summarises present theories of Quaternary glaciation and outlines the stratigraphical evidence for them. The areas of Tibet studied in this thesis are presented in chapter 2.

1.5.2 Morphology, biostratigraphy and sedimentary evidence from Tibet

The Indian plate is presently converging on the Eurasian plate at between five to six centimetres a year (Howell, 1989). This rate of collision has remained fairly constant over the last 40Ma resulting in the present average elevation of 5000m for the Tibetan Plateau (Molnar, 1986). The rate of uplift of the plateau has been inferred from pollen and faunal fossils found in sedimentary sequences from both the Tibetan Plateau and Himalayan intermontane basins.

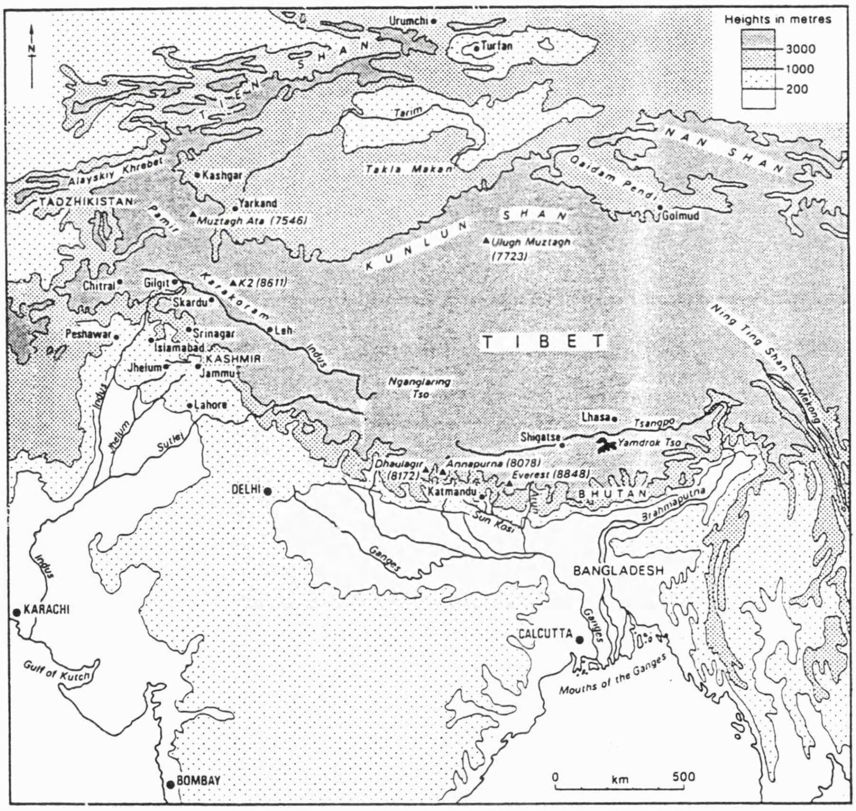

Figure 1.8 Map of Tibet and the Himalayas
Xixabangma is located just west of Everest (Qomolongma).

In the interior of the Tibetan Plateau, in the Bulong basin, south of the Tanggula Mountains, faunal remains of the Pliocene-age 3-toed horse ***Hipparion Xizangensis*** were found in the late 1970's. This species has the same characteristics as the European ***Hipparion Primigenius*** suggesting that during the Pliocene epoch the Tibetan Plateau sustained a forest and grassland ecology (Zheng Zuoxin *et.al.*, 1981). This is confirmed by Wang Fubao and Li Bingyuan (1985) who report that during this period, the plateau was also occupied by a number of large lakes whose sediments contained rich tropical and subtropical sporo-pollen. The ***Chilotherium*** (rhinocerus) species found in the Bulong basin are comparable to those found in the Siwalik Hills of south Asia suggesting that in the Early Pliocene the Himalayas were not a significant barrier to faunal migration and that the Tibetan Plateau was at an elevation of 500-1000m (Zheng Benxing, 1989a). At this time the Siberian-Mongolian high pressure system had not yet formed and there existed only a weak high pressure belt near Lhasa at a latitute of about 30°N (Chao Sungchiao, 1984).

During the Late Miocene and Pliocene the tectonic activity which caused the progressive rise of the Himalaya also produced parallel east-west trending basins. In these large lacustrine sedimentary sequences were deposited as a result of the northward drainage from the Himalayas. The initiation of extensional tectonics led to several grabens being formed across the lacustrine depressions, which were rapidly filled in with erosional debris from the upthrown blocks, forming (Gongba) conglomerate beds (Fort, 1989). Thick Plio-Pleistocene basin sedimentary sequences in the Xixabangma and Qomolongma (Everest) Himalaya have been used to reconstruct the uplift history and palaeoclimatic evolution of the Himalaya-Tibet region.

Unlike the Pliocene sediments, those of the Pleistocene in the Himalaya-Tibet region are open to varying interpretations as to their age and their genesis. Glacial features may be highly weathered and similar in nature to periglacial and fluvioglacial deposits (and *vice versa*), leading to problems of identification and interpretation. The stratigraphic evidence and differing interpretations are outlined here with particular reference to the Xixabangma and Qomolongma (Everest) regions.

In the Woma basin, south of Gyirong, between Mt. Xixabangma (8013m) and Mt. Ganesh (7429m), fossil faunas of ***Hipparion gyirongensis, Chilotherium xiganzensis*** (Asian rhinocerus), ***Metacervulus capreolinus*** (deer), ***Hyaena sp., Palaeotragus microdon, Gazella gaudryi*** and ***Ochotona gyirongensis*** (Gyirong pika) were found within a sedimentary series of sandstones, siltstones and mudstones known as the Jilong Group (Zheng Zouxing et.al., 1981). At Gyirong, the Jilong Group is overlain by the Gongba conglomerate which is indicative of the beginning of intense uplift of the plateau (Wang Fubao and Li Bingyuan, 1985). Further east at Nieniexongla, on the north slope of Xixabangma, just south of the Lalung La Pass there are Plio-Pleistocene deposits exposed next to the Sino-Nepal Highway at 5000m in which ***Hipparion*** remains are also found beneath the Gongba conglomerate (figure 1.9). In addition to the fauna fossils, pollen of ***Cedrus***, ***Quercus***, and ***Picea*** were found suggesting that uplift of the area had reached 2000-3000m during the Late Pliocene and early Pleistocene (Osmaston, 1989).

On the Lalung La, a 30km wide ridge just over 5000m on the edge of the Tibetan Plateau, Pleistocene gravels and cobbles lie uncomformably over Pliocene beds (Osmaston, 1989). The interpretation of these gravels varies. Zheng Benxing (1989a) has mapped them to be partly glacial (with 5 morainic surfaces demonstrating the retreat phases of a piedmont glacier) and part fluvioglacial outwash, which he assigns to the Middle Pleistocene extensive Nieniexongla glaciation (see figure 1.10). Osmaston (1989) on the other hand disputes that a glacier existed on the Lalung La and argues that they should not be used as a type site for the supposed Nieniexongla glaciation until the morainic nature of these deposits is unequivocally established. Derbyshire *et.al.* (1991b) recently argued for the glacial nature of the deposits correlating them with tills at the Yaruxongla site (called Nyanyanxongla in figure 1.9) next to the Sino-Nepal highway. They suggest that the Nieniexongla was a major piedmont glaciation covering about 1140km^2.

North of Xixabangma, there exists a wide apron of bouldery gravels sloping from 6200m to 5000m and incised by deep glacial valleys. Zheng Benxing (1989a) interprets this apron as a morainal plateau of the Early Pleistocene Xixabangma glaciation, with lower deposits interpreted as moraines from subsequently younger glaciations. However, Osmaston (1989) believes that it may be a reworked periglacial deposit, as the morainic nature of the deposit rests principally upon its topographical relationship with other moraines.

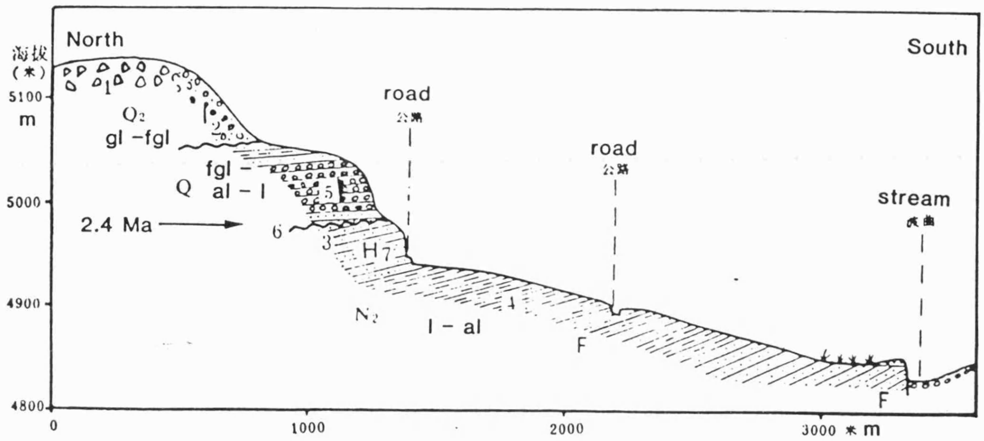

gl = glacial, fgl = fluvioglacial, l = lacustrine, al = alluvial, H = Hipparion fossils, F = Lamellibranch & Gasteropod fossils.
1. Moraine, 2. Fluvioglacial gravel, 3. Sandstone layers, 4. Mudstone layers, 5. Conglomerate, 6. Unconformity, 7. Hipparion fossils.

Figure 1.9 Road cut on the Sino-Nepal highway, just south of Nieniexongla and the Lalung, exposing Plio-Pleistocene deposits (Osmaston, 1989).

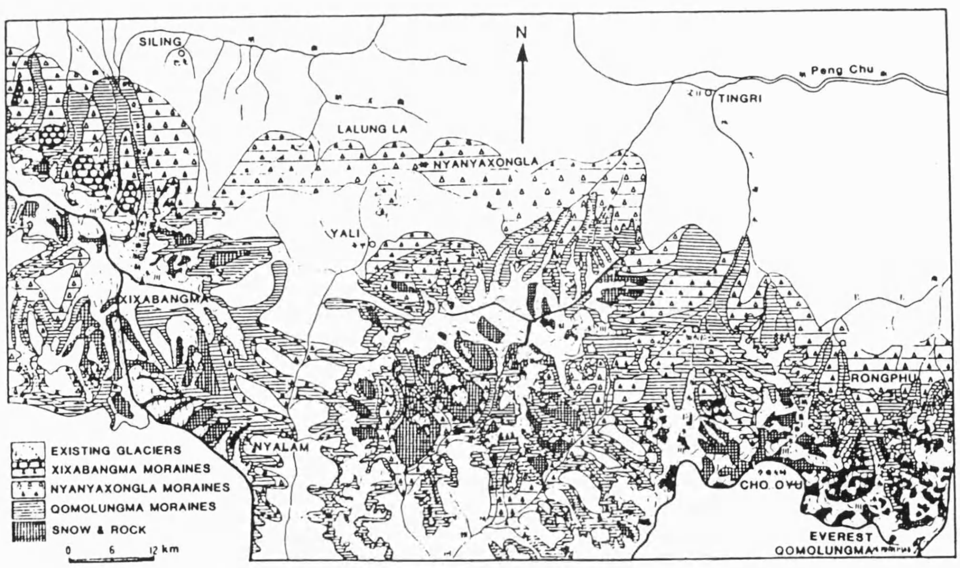

Figure 1.10 Qomolongma-Xixabagma region showing the moraines mapped by Zheng Benxing and Li Jijun (Osmaston, 1989).

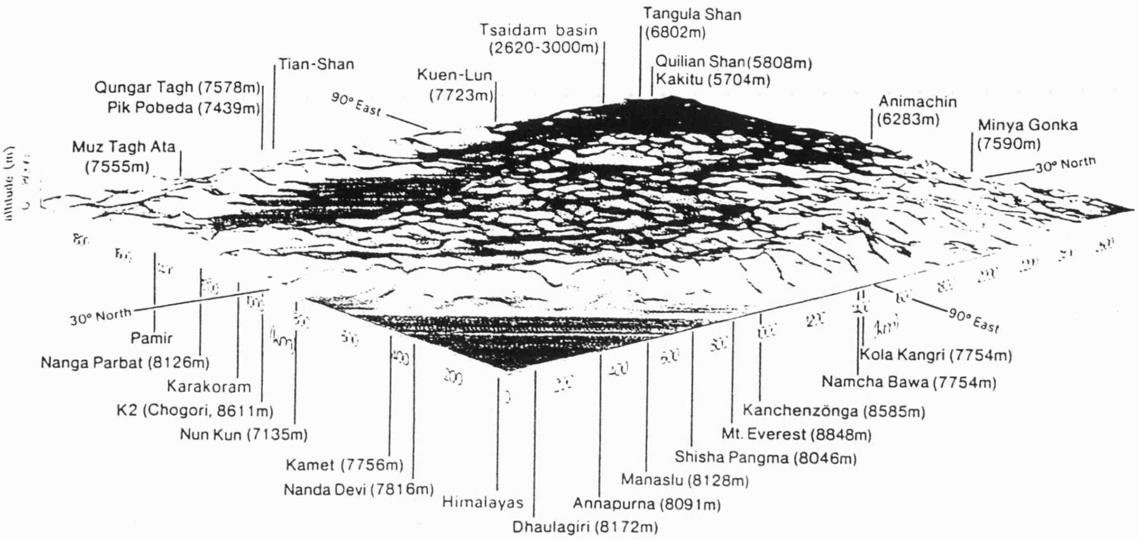

Figure 1.11a Tibetan highland and bordering mountain chains under present day conditions without glaciation (Kuhle, 1987b).

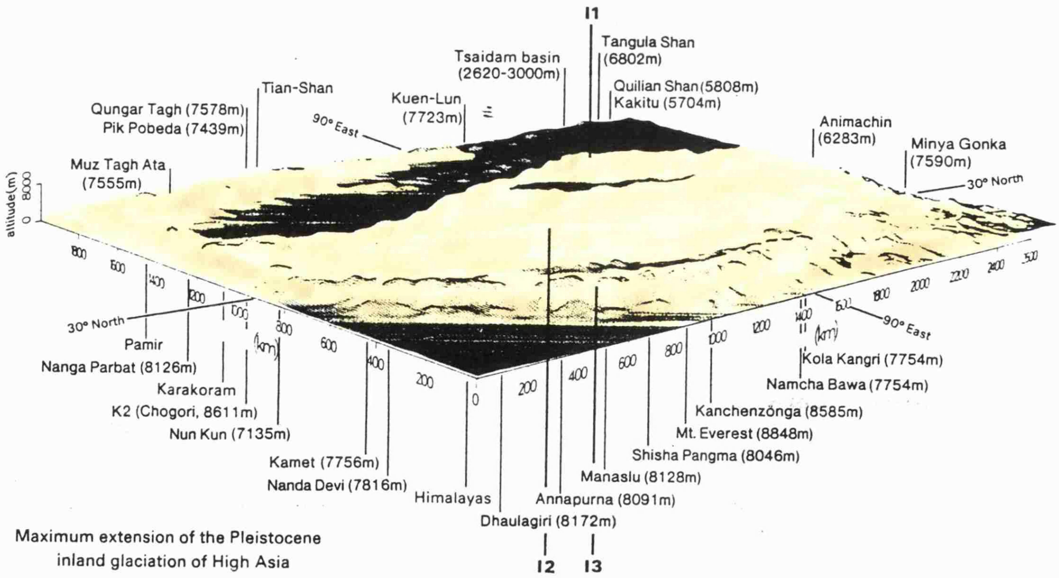

Figure 1.11b Model of the 2.4 million km² Late Pleistocene ice sheet over Tibet (coloured yellow). Only peaks exceeding 6000-6500m project above the glacier surface. I1, I2 and I3 represent the centres of glaciation (Kuhle, 1987b).

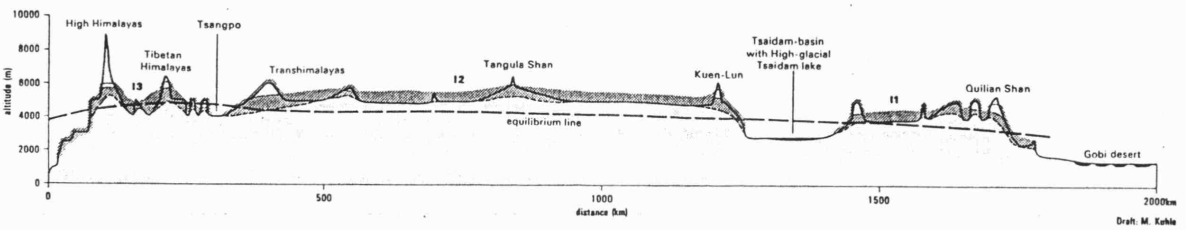

Figure 1.12a A cross section of Tibet showing the ice cover during the Late Pleistocene according to Kuhle (1987b).

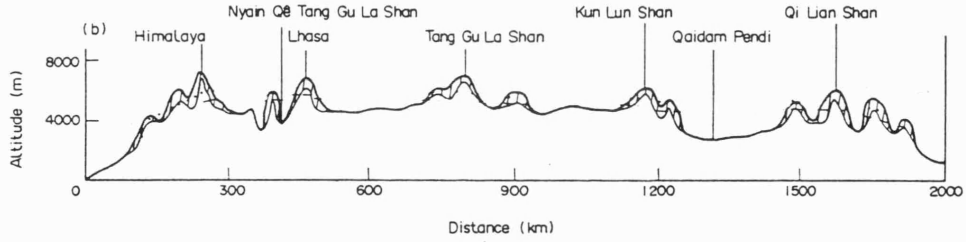

Figure 1.12b A cross section of Tibet showing the maximum extension of the Pleistocene glaciation according to the Chinese hypothesis (Derbyshire *et. al.*, 1991b)

Table 1.1 The different chronological interpretations of Zheng Benxing (1989a) and Kuhle (1988) of Tibetan moraines.

ZHENG 1989	age	KUHLE 1988	age
		Sub-Recent/Recent stadium	<30a
		Stadium X }	
		Stadium IX }	320-30a
Neoglaciation	<10ka	Stadium VIII	c.320a
		Stadium VII	c.440a
		Middle Dhualagiri Stadium VII	2ka
		Early Dhualagiri Stadium VI	2.4-2ka
Qomolongma II}		Nauri Stadium V	5-4ka
Qomolomgma I }	Late Pleistocene	Sirkung Stadium IV }	
Qomolongma I }		Dhampu Stadium III }	Late
Nieniexongla	Middle Pleistocene	Taglung Stadium II }	Glacial
Xixabangma	Early Pleistocene	Ghasa Stadium I }	

On the northern slopes of Qomolongma (8848m) in the Rongbu Valley, Zheng Benxing (1989a) has recognised Holocene and Late Pleistocene moraines associated with the Rongbu glacier, which he has assigned a type location for the Late Pleistocene. An end moraine near the Rongbu temple, 8km from the glacier snout (Qomolongma II) and a series of converging lateral moraines near the Jilong temple 5km from the snout (Qomolongma I) have been interpreted to represent sub-stages of the Late Pleistocene glaciation.

Recent re-evaluation of these moraines, on the basis of weathering characteristics of boulders found along moraine crests, suggests that they are, in fact, considerably older than the previously assigned ages and may include deposits from the Middle Pleistocene (Burbank and Cheng, 1991). This interpretation, and that of Zheng (1989), is in direct contrast with the ice sheet hypothesis of Kuhle.

Kuhle (1987b) argues that in the highly active mountain regions of Tibet it is extremely unlikely that easily eroded loose rock like moraines would remain *in situ* over a long time period *ie* since the penultimate ice age or earlier. Using evidence from the Tibetan margins he concluded that during the late glacial stage (LGS) a large inland ice sheet 2.0-2.4 million km^2 covered Tibet (figure 1.11) with separate outlet glaciers flowing down through the bordering mountain chains to altitudes of 2300 metres on the northern (Kunlun) scarp and 1100 metres on the southern Himalayan slopes (Kuhle, 1987). Terminal moraines, in the form of ice marginal ramps (bortensanders) are found in the Qaidam and Tarim Basins (Kuhle, 1990).

Kuhle (1989) summarises the evidence for large scale glaciation in south

Tibet on the basis of the morphogenetic characteristics of moraines and the existence of erratic blocks. From these features he concludes that: outlet glaciers from the 2.4 million km² ice sheet left moraines in the lower Mayangdi Khola and Thak Khola (Dhualgiri-Annapurna area) down to 1100m asl; while 300km to the east an outlet glacier flowed through the Bo Chu valley down to 1600m; and the Dudh Khosi glacier draining the Cho Oyu, Qomolongma and Lhotse area reached down to 1800m.

Cross sections of Tibet showing maximum glacial cover are shown in figure 1.12 indicating the disparity between the present theories.

1.6 Loess in Tibet

Redeposited and primary tan coloured loess has been reported from the Yarlung Zangpo valley and tributary valley systems of south Tibet (Péwé *et.al.*, 1987; in press; figure 1.13). The silt is thickest near the rivers, on pediments and blanketing alluvial fans where it also occurs within the matrix, occasionally interspersed with sand and gravel layers. It is prevalent within the matrix of fans or near the edges of flat, gently sloping valley floors where it is 1-2m thick (Péwé *et.al.*, in press). The thickest deposits are 10-20 metres of loess overlying till at Yangbajain on the southern foot of the Nyainqêntanglha Peak (7162m), northwest of Lhasa (Péwé et.al., in press), with a further free standing 15 metre vertical road-cut along the main highway south of Xigaze (Péwé et.al., 1987). Particle size analysis of some of the sites gave results varying from 8-55% sand; 26-75% silt and 2-67% clay. Unfortunately neither of these papers deal with the silt-producing mechanisms and thus the source of the loess, although Péwé et.al. (in press) disregard the possibility of *in situ* frost action on bedrock and stress the aeolian nature of the material.

Further north, thin loessic silt has been described blanketing the Tanggula Mountains (Xu Shuying, 1981) and the Qaidam Basin (Bowler *et.al.*, 1987; see chapter 2). Hövermann (1987) reports that loess cover in northeast Tibet is extensive with 0.33mm deposited *per annum*. He states that loess dominates east-facing slopes in the A'nyêmaqen Mountains (with west-facing slopes dominated by gelifluction), maximum cover occurring at altitudes of 3500-3900m where alpine meadow vegetation traps the loess. He also argues that in the past a thick cover of loess was formed on the north slopes of the Kunlun Mountains (between 3000-4100m) and the Qilian

Mountains (2000-3300) being formed "not from the sandfields in the deserts, but primarily from the piedmont regions. The periglacial region receives loess rather than supplying it (Hövermann, 1987, p.126)".

Intercalations of loess within aeolian sands have been documented within the Kulapundaiya Valley, near the village of Pulu (Li Baosheng *et.al.*, 1988). Pulu is located in the Kunlun Mountains 450km west of Ulugh Muztagh (figure 1.7). In addition to the buried layers, loess is also found blanketing the topography of this area up to an altitude of 4500m.

Kuhle (1987a) describes frost-induced polygonal forms within loess "some decimeters thick" at an altitude of 4050m on the north slopes of the A'nyêmaqen Mountains (34°50'N, 99°33'E), and on the right side of the Khumbu glacier, Qomolongma at an altitude of 5000m.

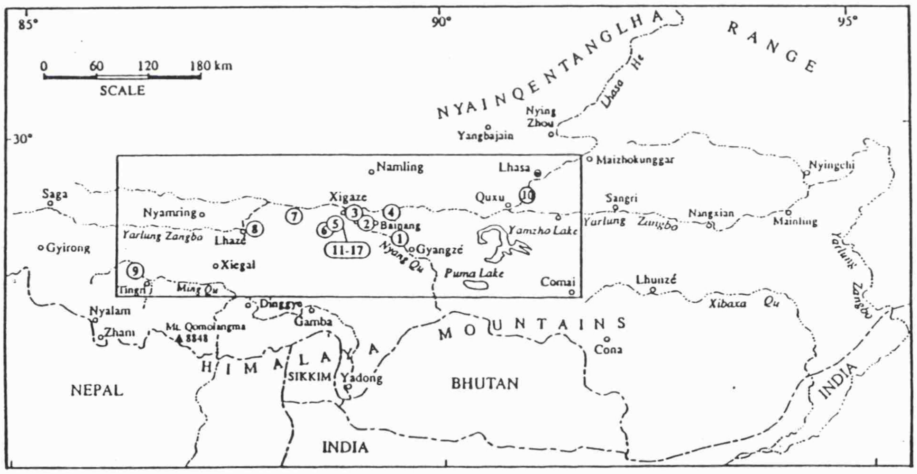

Figure 1.13 Map of south Tibet showing the localities (circled numbers) of loess-like sediment (after Péwé *et.al.*, in press)

2. THE TIBETAN FRONT: SAMPLE ENVIRONMENT AND LOCATION

2.1 Sampling strategy

The majority of research on Chinese loess has been undertaken within the middle reaches of the Yellow River in the central Loess Plateau at sites such as Luochuan and Xifeng (figure 1.1). These sites lie on the lowland plains of central China, in close proximity to the Ordos and Tengger deserts. However, the thickest accumulations of loess in China occur near the city of Lanzhou in the western part of the Loess Plateau. Lanzhou is surrounded by the high mountains which make up the fringes of Tibet to the northwest, west and south. The Loess Plateau extends to the east and the Tengger desert lies to the north.

Both desert and mountain environments have been postulated as source areas for silt production. Bowler et.al. (1987), and more recently Zhang Linyuan *et.al.* (1991), suggest that silt derived from the Kunlun Mountains and Tibetan Plateau contributes to the Lanzhou loess. However, no silt deposits have been described as existing in these mountain environments despite the current presence of glaciers and periglacial environments - the two commonly cited pre-requisites for silt formation. One aim of the project was to sample silt from within the mountains to the west and south of Lanzhou for geochemical fingerprinting (REE) to compare with the work of Wen Qizhong *et.al.*, (1983; 1985) who propose a desert source for Luochuan loess.

2.1.1 The western Loess Plateau

Three regions of the Tibetan Front were chosen for sampling. Two thick (>270m) loess sections were sampled from the Lanzhou Basin. These were the best exposed sedimentary sequences in the area with one situated on the north side of the Yellow River (Jiuzhoutai) and the other lying to the south (Dawan). The top 60 metres at Jiuzhoutai and 40 metres at Dawan were examined in an attempt to isolate the last interglacial palaeosol. The difference in thicknesses examined at the two sites was dictated by the probable level of this palaeosol so that different loess accumulation rates appear to have prevailed at the two sites. Jiuzhoutai lies on the Yellow River whilst Dawan lies on a tributary valley to the southwest. Therefore, the contribution from silt brought down by the Yellow River from Tibet, deposited in the Lanzhou Basin on braided sections of the river at periods of low flow and then deflated would have been greater at Jiuzhoutai than at Dawan.

The Blake magnetic reversal is believed to occur 115-120ka (Tric *et.al.*, 1991) an age which is concurrent with part of oxygen istope stage 5. Thus it is likely that if the Blake Event were recorded it would occur close to the last interglacial palaeosol. At both sections multiple palaeosols were present and these were continuously sampled along with loess above and below them. The presence of multiple palaeosols allows for good comparison of magnetic mineralogy differences between the loess and soils.

One section of loessic alluvium was sampled from Sala Shan near Linxia. This loess was obviously stratified and was used as a control in the fabric experiments. Detailed discussion of sample strategy and sites can be found in section 2.3.

2.1.2 Mountain environment samples

Two sites were selected for sampling within different mountain ranges. The selection of sites was constrained by the political sensitivity of the area. Travels permits are required for Tibet and the routes are strictly controlled. One site was chosen in the mountain range to the south of Lanzhou (A'nyêmaqen Mtns) and a series of sites were located across a transect from the Qaidam Basin and Kunlun Mountains to the Tibetan Plateau. This transect covered the area believed by Bowler *et.al.* (1987) to produce silt which is deflated and carried to the western Loess Plateau.

2.1.2.1 A'nyêmaqen Mountains

Southwest of the Lanzhou Basin loess cover thins and exists only in the form of river terraces, as at Linxia. The northeastern edge of the mountain ranges of Tibet lie south of Linxia in the form of the A'nyêmaqen Mountains. At an altitude of 3000m, within the A'nyêmaqen Mountains, there exists a 60 metre loess terrace which extends southeast from the Tibetan monastery at Labrang. Northwest of Labrang, between the monastery and the Daxia floodplain near Linxia there is no evidence of loess. Thus the Labrang loess is likely to have been formed within the mountain environment and contain cold weathered and/or glacially ground silt. The presence of a thick loess terrace in the mountains provides evidence that silt particles are effectively produced in this environment. Several blocks of consolidated loess were taken in order to compare the Labrang loess with the loess sampled from the Lanzhou Basin in the Chinese Loess Plateau 140km to the northeast.

To further assess the contribution of mountain-derived silt, surface sediment was taken from sites within a transect between the Tibetan Plateau and the Qaidam Basin, from Qumar Heyan to Golmud (figure 2.1) ranging from altitudes of 3000 to 4770m across the Kunlun Mountain range. These samples were analysed for particle size to assess the content of silt-sized particles similar to those resident in the Loess Plateau around Lanzhou, 1100km to the east. The similarity of rare earth element patterns from Tengger desert sand and Luochuan loess have been used to prove the desert origin of the Chinese loess (Wen Qizhong *et.al.*, 1983). For this reason the surface silts from Tibet were used for rare earth element analysis to compare with the loess from Lanzhou and the data of Wen Qizhong for the sand and loess from the central Loess Plateau.

2.2. Physical environment of the Tibetan Front

The following section describes the environment of the areas sampled in this thesis. The 1986 Royal Geographical Society and Mount Everest Foundation 1:3000000 map 'Mountains of Central Asia' provides good coverage of the area studied

2.2.1 The western fringe of the Loess Plateau

The western edge of the loess plateau is situated in a harsh environment of extreme climatic and altitudinal gradients. It is surrounded by "gobi" (stone) and "shamo" (sand) deserts, including the Ordos (also called the Mu Us) and the Tengger desert to the north and north-east; and the Taklamakan and the Qaidam deserts, via the Hexi corridor, to the north-west. In addition to these desert areas, there are mountain chains to the north (Qilian and Altun Shan), and the vast Tibetan Plateau with the Kunlun and A'nyêmaqen mountain ranges to the immediate west (figure 2.1). As outlined in chapter 1, both desert and mountain environments have been postulated as a potential source of loess.

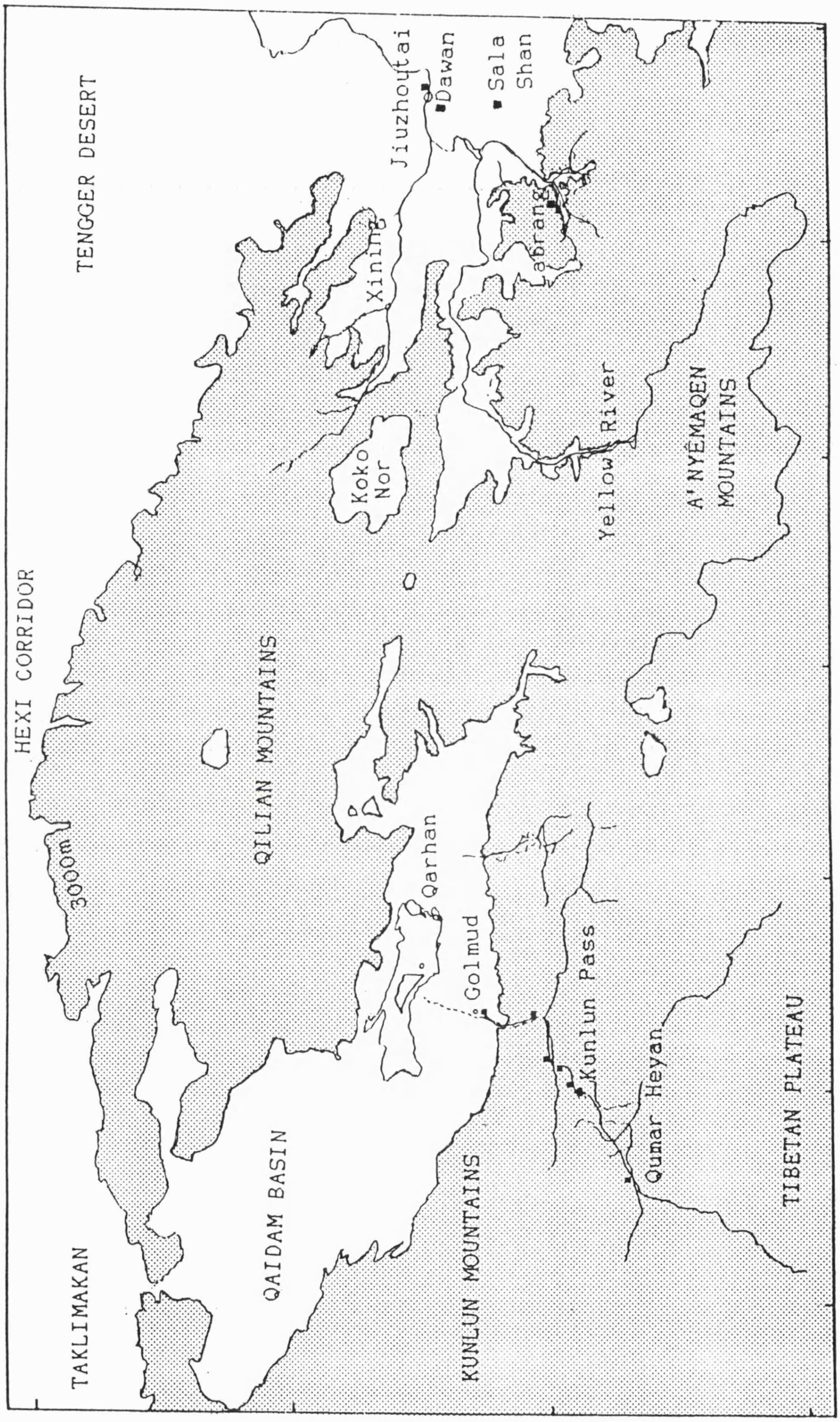

Figure 2.1 Map of the areas studied in this thesis (■ = sample sites).

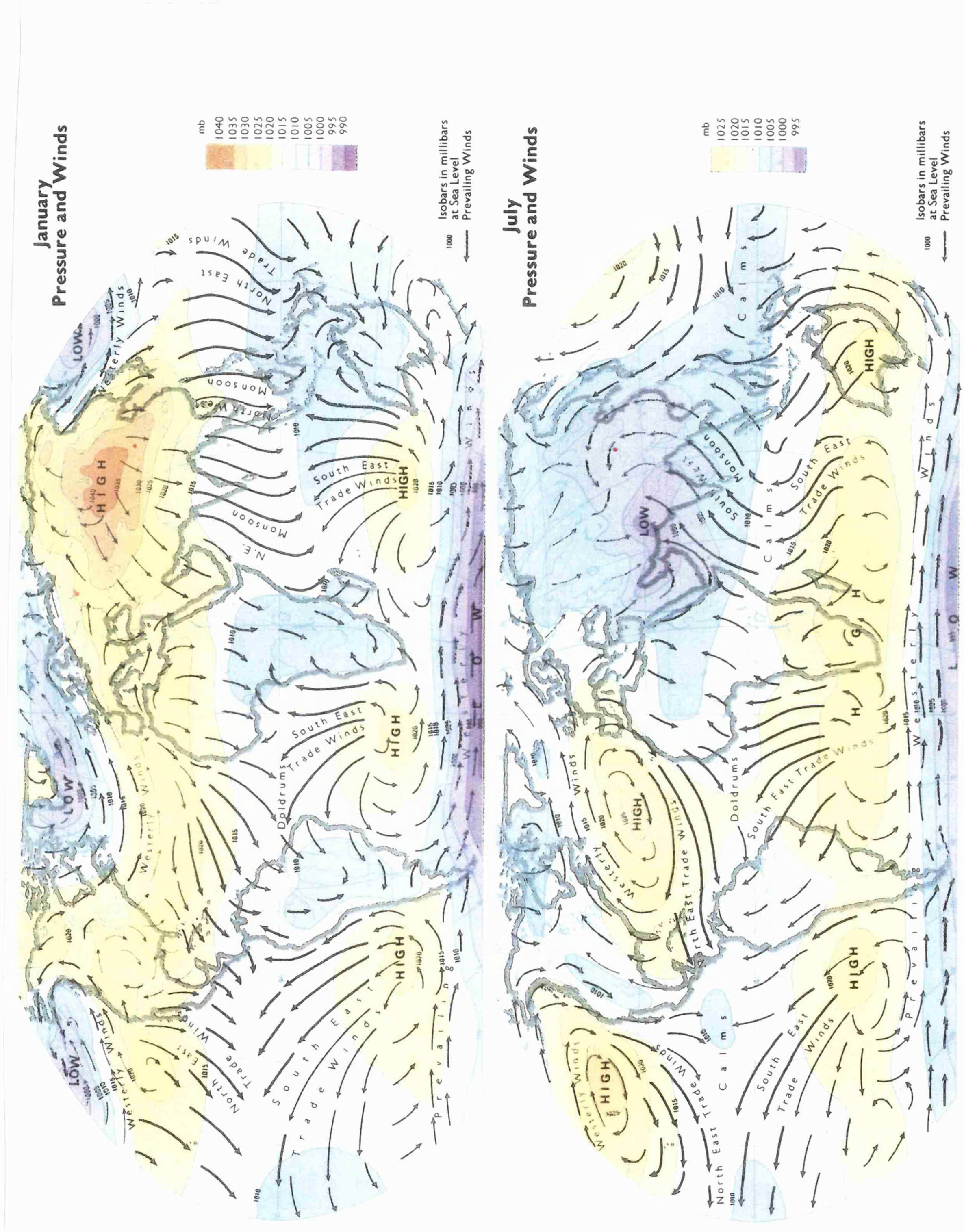

Figure 2.2 World map showing winter dominance of Mongolian-Siberian high pressure system and the summer monsoon winds (Fullard and Darby, 1978). Lanzhou is marked with a red dot in both projections.

Plate 2.1 The western Loess Plateau in the vicinity of Lanzhou

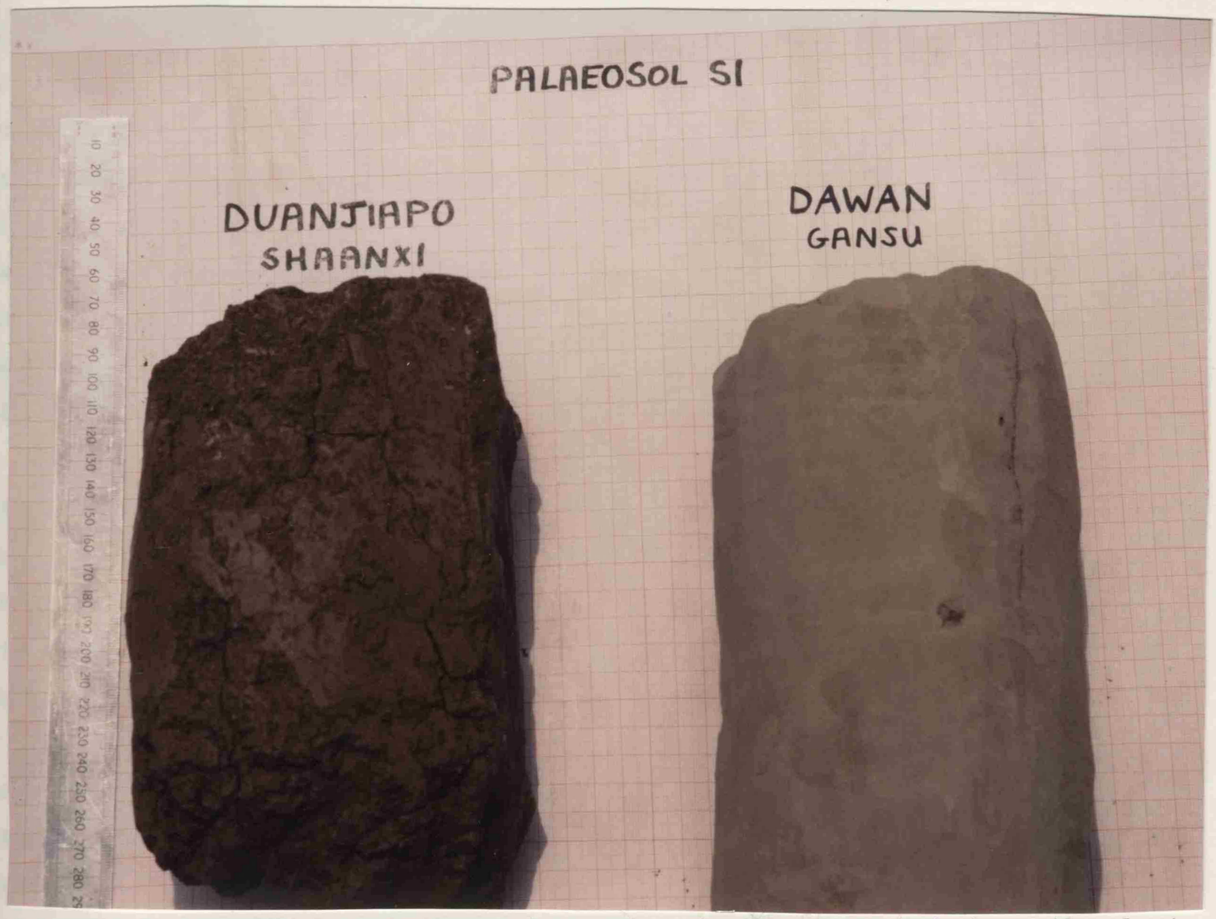

Plate 2.2 A visual comparison of sample blocks excavated from the last interglacial palaeosol horizon (S1) at Dawan, Gansu and Duanjiapo, Shaanxi.

There is a steep climatic gradient between the area affected by the southerly summer monsoon and the arid north west of China. The summer monsoon penetrates north inland as far as the Tibetan front where it impinges on the high mountain areas and meets dry cold air from the Mongolian high pressure system (MHPS) to the north (figure 2.2). The climatic difference between the centre of the loess plateau and the western edge and Tibetan front areas is illustrated in the form of mean annual rainfall in table 2.1.

Table 2.1 Mean annual rainfall for the period between 1951-1970 (Zhao Songqiao, 1986)

City	Region	Rainfall (mm)
Xian	central Loess Plateau	604.2
Lanzhou	western Loess Plateau	331.9
Golmud	Qaidam Basin	38.3

Evaporation potential also increases across this climatic gradient with a mean annual figure greater than 3000mm in the Qaidam Basin (Wang Jingtai *et.al.*, 1986). The difference in texture and degree of weathering between loess sections across this gradient is shown by plate 2.2 which gives a visual comparison between palaeosols assigned to the last interglacial. Duanjiapo (34°12'N, 109°12'E) is situated near the city of Xian overlooking the Ba River, in Shaanxi Province; whereas Dawan (35°54'N, 103°12'E) is located south-west of Lanzhou city on the westernmost fringes of the loess plateau, in the more arid Gansu Province.

The last glacial stage in north China has been subdivided into two cold stages lasting 70-53ka (with mean annual temperatures 10°C colder than present) and 23-11.5ka (12°C colder than present) with an intervening interstadial climate from 53-23ka only 4°C colder than at present (Sun Jianzhong and Li Xingguo, 1986). The authors also report a short stadial cold phase lasting from 36-32ka.

In the western Loess Plateau there are two sites which have been documented as containing Last Glaciation interstadial soils. A recent report by Chen Fahu *et.al.* (1991) contains an illustration of Jiuzhoutai section, near Lanzhou. A triple interstadial soil at a depth of approximately 16-18 metres is shown with associated TL dates of 29.4 ± 1.5ka from loess above the second soil and 74.0 ± 6ka from loess below the bottom soil. A dual palaeosol thought to be representative of the last interglacial (S1) occurs at an approximate depth of 35 metres, some 18 metres below the interstadial soil complex. At Beiyuan, Linxia, southeast of Lanzhou (see figure 2.1), An Zhisheng *et.al.* (1991) report a triple interstadial soil complex dated between 50-30ka. The last interglacial palaeosol appears to be also a triple complex.

2.2.2 The Qaidam Basin

The Qaidam Basin contains the highest sand desert in the world, at an elevation of 2600 - 3000m asl (plate 2.11). It is directly north of the Tibetan Plateau and surrounded by the Qilian and Altun Mountains to the north and the Kunlun Mountains to the south. It consists of shifting and half-fixed sand dunes resting on gravel gobi formed by aeolian erosion of the Tertiary piedmont plain (Zhao Songqiao, 1986). Yardangs are prevalent in the centre and to the northwest of the basin (Zhu Zhenda *et.al.*, 1986) which are indicative of an erosional environment (figure 2.3). The central and lowest part of the Qaidam Basin consists of a series of salt lakes, which are farmed commercially at Qarhan (36°42'N, 95°18'E; plate 2.11). The Qarhan salt flat, which is the largest in the Qaidam Basin, covers an area of 5800km² and represents what remains of a much larger Early-Mid Pleistocene freshwater lake (Chen Kezao and Bowler, 1986). Cores from this and other lakes have been studied by Chen Kezao and Bowler (1986) and Bowler *et.al.* (1986) with a view to interpreting palaeoclimatic change and the onset of salinisation. They report that expanded freshwater or slightly saline water bodies existed in the Qaidam Basin from at least 40ka, based on radiocarbon dating of freshwater clastics and shell deposits. Progressive desiccation, resulting in deposition of halite, occurred from about 25ka until about 9ka, although Bowler *et.al.* (1986) point out that deposition of halite requires more water than is present in the more arid climate of today. Within the 60m thick halite deposits are thin mud layers representing brief humid phases, dated at 20ka, 18ka and 16ka.

The depth of deposit accumulated in the basin during the Quaternary exceeds 2000m (Liu Zechun *et.al.*, 1991). Wang Jingtai *et.al.*, (1986) completed preliminary magnetostratigraphy of a 528m core from Dabusan Lake (37°05'N, 95°25'E). The results show Brunhes age sediments. Samples of negative inclination do occur and these have been tentatively correlated with the Gothenburg, Mono Lake, Blake, Biwa I and Biwa II excursions occurring between 298ka (Biwa II) and 9ka (Gothenburg). Liu Zechun *et. al.* (1991) report a depth of 1460m for the Matuyama-Gauss polarity boundary (2.48 Ma) and 880-710m for the Olduvai polarity excursion (187-167Ma) from boreholes around Dabusan, Taijinaier and Sirlea Lakes.

Chen Kezao and Bowler (1986, p.99) argue that textural analyses of the halite layer confirms the existence of Malan loess components in the evaporites. Bowler *et. al.* (1987) used this evidence, along with the presence of a thin Holocene loess blanket in the Qinghai basin to the immediate east, to explain temporal variation in loess source areas over the Late Pleistocene and Holocene. They argue that silt generated by glacial and periglacial processes at high altitudes is transported to low level fluvial outwash plains, where it is later deflated by strong northwest winds (leaving behind a covering of gobi), and transported southeast to the Loess Plateau. The lakes in the Qaidam Basin, and the large Qinghai Lake (Koko Nor) further east, act as loess traps and record relatively complete sequences of loess input (figure 2.4)

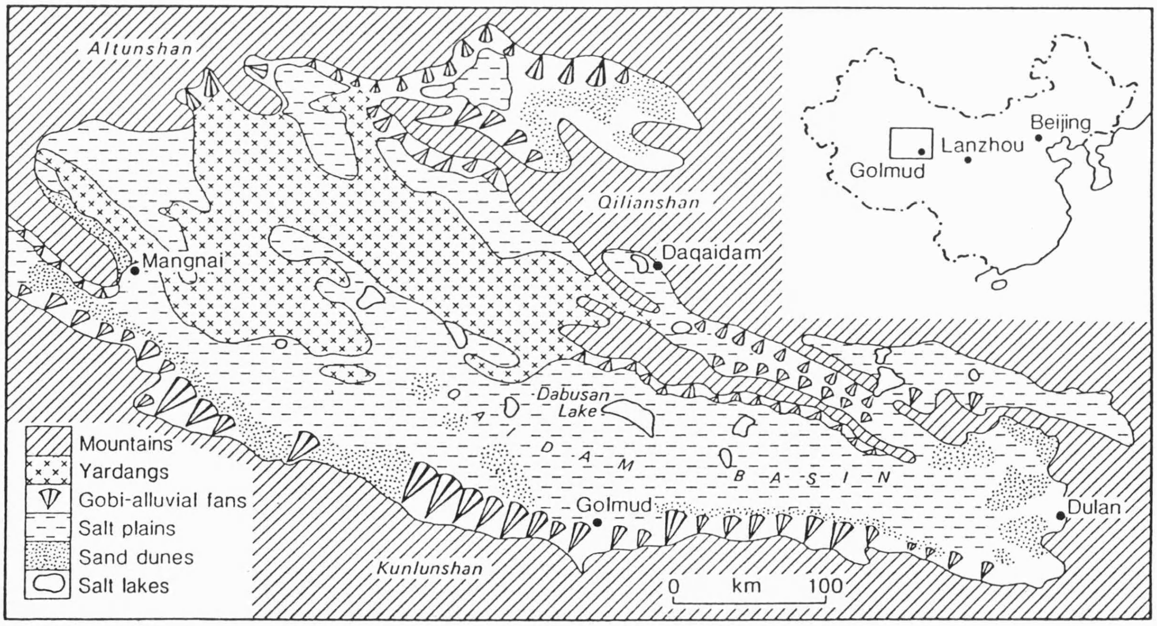

Figure 2.3 Geomorphic map of the Qaidam Basin (Wang Jingtai *et. al.*, 1986).

In addition to the possibility that the Qaidam Basin is a sediment trap for silt produced in the high mountains, the basin itself conforms to the criteria of Pye and Sperling (1983, p.61) who proposed that ..."a particularly favourable environment for silt formation might be expected where alluvial fans extend down from actively rising mountain fronts towards extensive saline basins".

The largest plateau glacier in China, the Dunde glacier, is located within the Qilian Mountains which fringe the northern edge of the Qaidam Basin. The mean annual precipitation of 300mm on the summit (5325m) is sufficient to maintain a positive mass balance, although the extreme low temperature environment (annual air temperature: -12°C to -13°C) means that the glacier is effectively frozen to its bed with negligible sliding and little erosion (Wang and Derbyshire, 1987). However, Wang and Derbyshire (1987) report that frost action is prevalent with accumulation of large volumes of rock debris on the sides of the glacier. A recent study of three cores through the Dunde ice cap by Thompson *et. al.*, (1989) has shown that the climate during the late glacial stage (LGS) was colder, wetter and dustier than during the Holocene with an abrupt change occurring at ~10ka. The increase in dust (particulate matter with diameters <10μm: Smalley and Derbyshire, 1990) and decrease in the $^{18}O/^{16}O$ ratio ($\delta^{18}O$) in the LGS are also observed in ice cores from Greenland, although the mean change in $\delta^{18}O$ is less than that from the polar cores implying that the decrease in temperature during the glacial stage on the Tibetan Plateau was less than that in polar regions (Thompson *et. al.*, 1989).

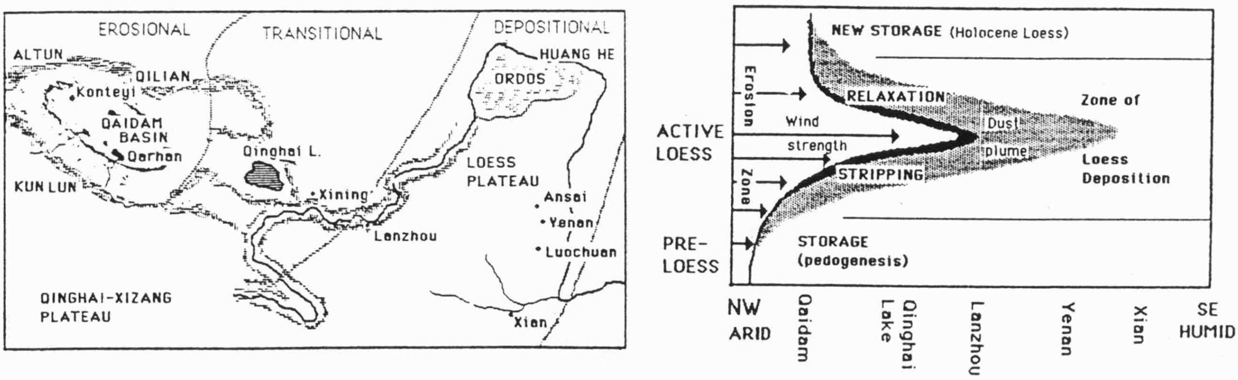

(a) (b)

Figure 2.4 (a) Transition bewteen erosional to depositional environments across the Tibetan Front area and (b) extensions and retreat of the dust plume in response to changing climatic conditions (Bowler *et. al.*, 1987).

Plate 2.3 The surface of the Qaidam Basin. The vegetation matting prevents movement of sand onto the Golmud-Xining railway line.

Plate 2.4 The commercial salt farm at Qarhan playa, Qaidam Basin.

2.2.3 The Kunlun Mountains

Zheng Benxing (1991) has recently summarised the Quaternary stratigraphic sequences found within the Kunlun Mountains, south of the Qaidam Basin. He argues that in the Pliocene the mountains stood at 500-1000m asl, with lakes formed on their southern slopes during the Early Pleistocene. The subsequent low altitude of the Kunlun Mountains during the Early Pleistocene (<<2000m) prevented glaciation, although the mountains were affected by periglaciation. Uplift to 3000m during the Middle Pleistocene (accompanied by the eruption of the Hilonshan volcano at 0.67Ma) allowed widespread piedmont glaciation on the southern slopes although most glaciers did not extend down to the Qaidam or Tarim Basin on the northern slope. Due to increasing aridity, the Late Pleistocene glaciation was less extensive.

Zheng Benxing (1991) lists the sedimentological evidence for this chronology as follows: 536m of Early Pleistocene fluvio-lacustrine sediments (dated 2.7-1.4Ma by palaeomagnetism) outcrop over a layer of sandy gravel thought to be a shore deposit near the Kunlun Pass. Moraine found at 4973m to the west of the Kunlun Pass is correlated with a 1-3km wide, 24km long deeply weathered moraine platform at 4700m in the middle-upper reaches of the Yurunkax River on the north slope of the west Kunlun Mountains, sand from which has been dated by thermoluminescence (TL) at 333 ± 46ka. A further Middle Pleistocene moraine, found beyond the end moraine from the Late Pleistocene, along the Yurunkanx River, has been dated at 206 ± 17ka by TL (Zheng Benxing, 1991). Both of these TL dates are questionable as they give ages substantially beyond the underestimation limits found by Debenham (1985) who obtained TL dates of less than 100ka for samples thought to date from the Brunhes-Matuyama polarity boundary (730ka). Zheng Benxing (1991; p. 399) also uses radiocarbon dates to assign ages to Late Pleistocene moraines stating that "no obvious traces have been found for the early episode of the last glaciation, so far all the ^{14}C datings available about the moraines point to late stage of the last glaciation". This is not entirely surprising as the upper limit of conventional radiocarbon dating is in the order of 40-50ka whilst the climate deteriorated at about 80ka, although the glacial maximum occurred 25-15ka. Loess and aeolian sands from the last glaciation occur over a 65m thickness of alluvial-pluvial gravels near the village of Pulu in the northern slope of the west Kunlun Mountains. Intercalations of loess within the sands have been TL dated at 66.7 ± 3.3 ka for the lowest loess layer and 6.3 ± 3.1ka (Li Baosheng *et. al.*, 1988).

The sequence in the West Kunlun Mountains is summarised by Zheng Benxing and Li Jijun (1981) as follows: the old till plain of the Nieniexongla glaciation is situated at 5200-5300m where it is overlain by the moraine of the Qomolomgma I glaciation, found at 5300-5350m. The end moraine of the Qomolongma II glaciation is located in a U-shaped valley at 5380m, with neoglacial end moraine at 5400m.

Contrary to the evidence of Zheng Benxing and Li Jijun (1981) and Zheng Benxing (1991); Kuhle (1987a) reports a terminal moraine at 3650m on the north slope of the Kunlun mountains, near Nachitai (35°54'N 94°27'E), with apparent glacigenic forms and sediments found down valley as far as 3400m. These, he believes, are of late glacial age.

2.2.4 The Tibetan Plateau

Immediately south of the Kunlun Pass the land becomes level to form the vast high-level Tibetan Plateau, lying at an altitude of 4500-4800m asl, between the Kunlun Mountains and the Gangdisê-Nyainqêntanglha range to the south. Permafrost is continuous with a mean thickness of 80-90m and a seasonal active layer of 1-4m undergoing extensive freeze-thaw (Zhao Youwu, pers. comm). Thickness of permafrost in the study area within the Tibetan Plateau, between the Kunlun and Tanggula Mountains (see section 2.2.5) varies from 40-400m at the Kunlun Pass to 0-40m in the Qumar river basin and 20-300m in the Tanggula Mountains (Tong Boliang, 1981).

There are 123 saline lakes on the Tibetan Plateau containing 40 different salt minerals with the degree of mineralisation decreasing from north to south. Whereas sulphate-chloride type lakes are found in the Qaidam Basin (Chen Kezao and Bowler, 1986), carbonate-sulphate type exist on the northern Tibetan Plateau, with gypsum dominating between the Kunlun and Tanggula Mountains (Chen Kezao *et.al.*, 1981). There have been two main periods of mineralisation, the first during the Pliocene and the second in the Late Pleistocene (figure 2.5) with rock weathering products and saline spring water believed to be the source of the evaporites (Chen Kezao and Xu Zhiqiang, 1991). The existence of Pliocene evaporites upon the Tibetan Plateau indicates that the desert climate of central Asia had an affect upon the area of the Tibetan Plateau north of the Tanggula Range (Chen Kezao *et. al.*, 1981).

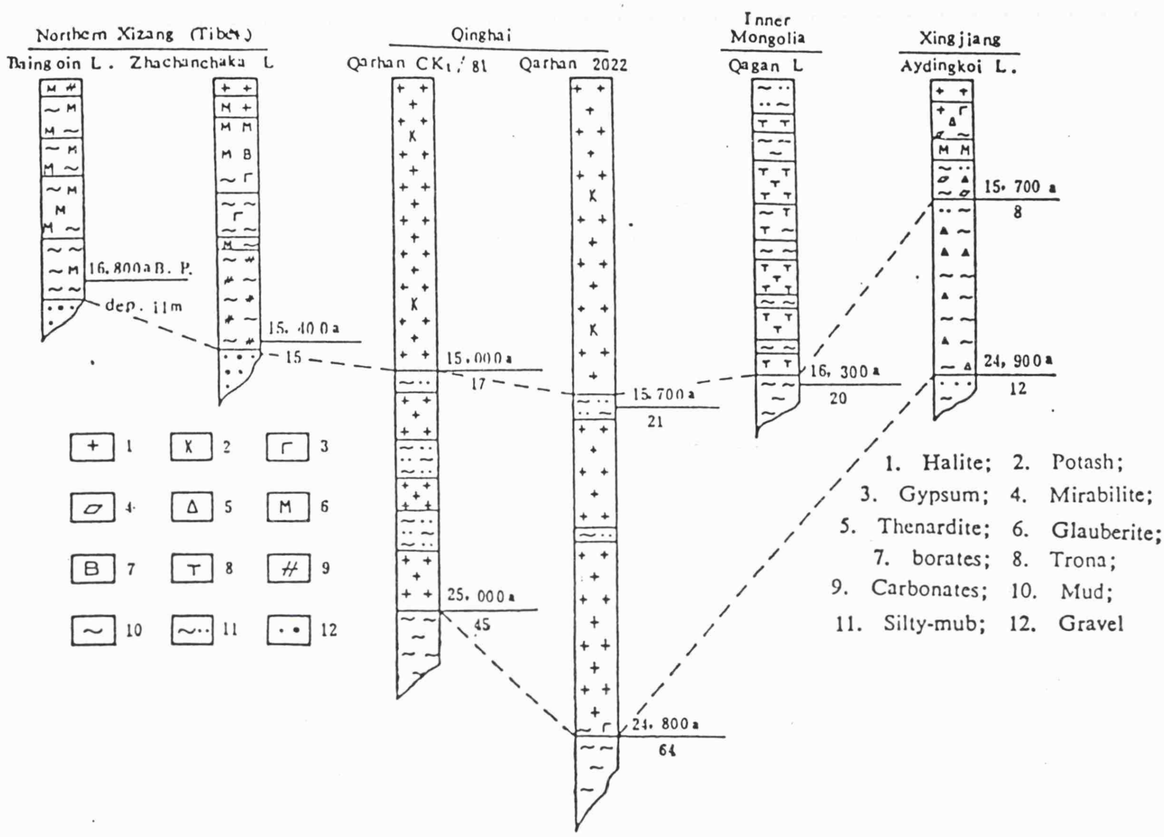

Figure 2.5 Comparison of the ages and salt forming episodes of salt lakes across north China and Tibet (Chen Kezao and Xu Zhiqiang, 1991).

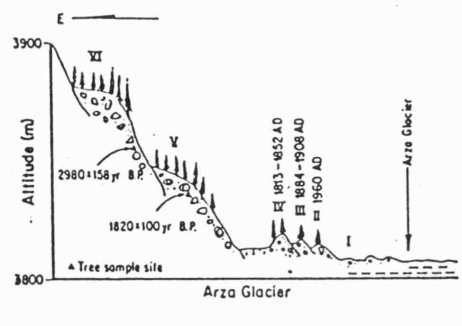

Southern Qinghai-Xizang Plateau

Little Ice Age (dry and cold), 300–0 yr B.P.
Dawelong interval (mild), 1500–300 yr B.P.
Mid-Neoglacial interval
Ice age II (cold), 2000–1500 yr B.P.
(Slightly warm), 2500–2000 yr B.P.
Ice age I (cold), 3000–2500 yr B.P.
Qilongduo interval (Yoli period)
(Warm and moist), 4700–3000 yr B.P.
(Warm but dry), 5500–4700 yr B.P.
(Warm and moist), 7500–5500 yr B.P.
Wumadung interval (slightly cold and dry), 10000–7500 yr B.P.

Figure 2.6 Section through the lateral moraines of the Arza Glacier, showing the location of radiocarbon and dendrochronological age estimates and a table of the relevent Neoglacial stages (Wang and Fan, 1987).

Lake bottom sediments from Siling-co, the second largest freshwater lake on the Tibetan Plateau, have been recently studied to determine climatic fluctuations since the last glacial (Kashiwaya *et. al.*, 1991). Core results from this study suggest that during the LGS, the lake level of Siling-co was low and the climate was arid. An abrupt change occurs ~10ka when the lake level rose rapidly and the climate became more humid, with an intervening marked arid phase 4-2ka. Grain size analysis from the 4-2ka year arid phase sediment shows an increase in fine material "which means that lighter material such as loess accumulated in the lake at this time (Kashiwaya *et. al.*, 1991, p. 1780)". A comparative study by Wang Fubao and Fan (1987) using evidence from lakes, peat layers in sand and gravel, and moraines of the Arza Glacier south of the Tanggula Mountains (table 2.2) suggests that the Tibetan Plateau was cold and dry 10-7.5ka, then underwent a warm interval 7.5-3ka, after which the climate underwent a deterioration 3-1.5ka (correlated with the Siling-Co arid phase) with five glacial advances (figure 2.6).

2.2.5 The A'nyêmaqen Mountains

The A'nyêmaqen Mountains are a NW-SE trending extension of the eastern Kunlun Range located in the northeast of the Tibetan Plateau. The A'nyêmaqen Mountains have been classified as a humid alpine region due to the relatively high precipitation caused by the impinging southeast monsoon: 800mmyr^{-1} falls at the snowline (4950-5000m) and 1200mmyr^{-1} on the mountain summit at 6282m (Wang Jingtai, 1987). Below the snowline, and above 4600m freeze-thaw shattering of rock is common, forming large talus cones. Air temperatures are low but solar radiation is high with rock surface temperatures reaching 30-35°C during the day and falling below freezing at night (Wang Jingtai, 1988). There are two main rivers which rise in the mountains, the Qiemqu and the Qinglong, both of which are tributaries of the Yellow River which takes a southerly then easterly course around the A'nyêmaqen peaks. According to the work of Li Jijun and associates (Shi Yafeng *et. al.*, 1991; Li Jijun *et. al.*, 1991; Derbyshire *et. al.*, 1991) an ice cap between 50000 and 80000km^2 existed in the upper Yellow River around Madoi, leaving behind glacial lake basins, rôches moutonnées, kames and erratic boulders, thus providing geological evidence of a similarly shaped ice sheet to that postulated by Sun and Yang as long ago as 1961. Both Shi Yafeng *et.al.* (1991) and Li Jijun *et.al.* (1991) attribute this ice cap to the penultimate glaciation on unspecified grounds. If they are correct in this assumption, and given the likelihood that an ice sheet of this size and location would have been wet-based, injections of glacial rock flour into the Yellow River system should have been sufficient to contribute to the loess source areas below the Longyang Gorge *i.e.* in the Yellow River system westward (windward) of Lanzhou. Until such a time as the age of this ice sheet is established, however, the significance of this possible input into the Lanzhou loess sequence cannot be tested.

2.3 Site details

The sampling sites were located in three regions of the Tibetan Front: 1. the western Loess Plateau around Lanzhou; 2. Southern Gansu Province - southwest of the Loess Plateau on the edge of the A'nyêmaqen Mountains; and 3. the Qaidam Basin, Kunlun Mountains and the northern Tibetan Plateau. They cover an area extending from 35°00'N to 36°30'N and 93°00'E to 103°45'E. The sites on the western Loess Plateau around Lanzhou consist of thick loess and palaeosol sequences, in excess of 250m, resting on terrace gravels of the Yellow River. The loess of the western Loess Plateau exists as a topographical blanket masking the underlying bedrock, whereas in southern Gansu, it is only present in the form of river terraces, with bedrock clearly visible on the hillsides. The Qaidam Basin, Kunlun Mountains and area of the Tibetan Plateau studied here are situated 800km to the west of Lanzhou.

2.3.1 Lanzhou Area I - Jiuzhoutai (36°00'N, 103°45'E)

Jiuzhoutai is situated on the north bank of the Yellow River overlooking Lanzhou city (figure 2.7). It is the thickest accumulation of loess in the world, with 334m encompassing Wucheng to Holocene loess resting on terrace 6 of the Yellow River (Chen Fahu, 1990). As Jiuzhoutai mountain is steep sided, with slopes of 35° prevalent, actual height measurement is difficult even with the use of electronic distance measuring (EDM) equipment.

The area of loess sampled in this study was chosen with reference to the chronological control in the form of TL dates recently undertaken by Lanzhou University. The lower Malan, last interglacial palaeosol (S1) and

Upper Lishi loess were sampled in an attempt to ascertain changes in palaeoclimate over the last glacial-interglacial cycle. Extensive sampling of the Malan loess was initially envisaged, however, after the first field season it became apparent that its coarse particle size, lack of cementation and resulting friability made it impossible to sample effectively and transport back to Britain in an intact state.

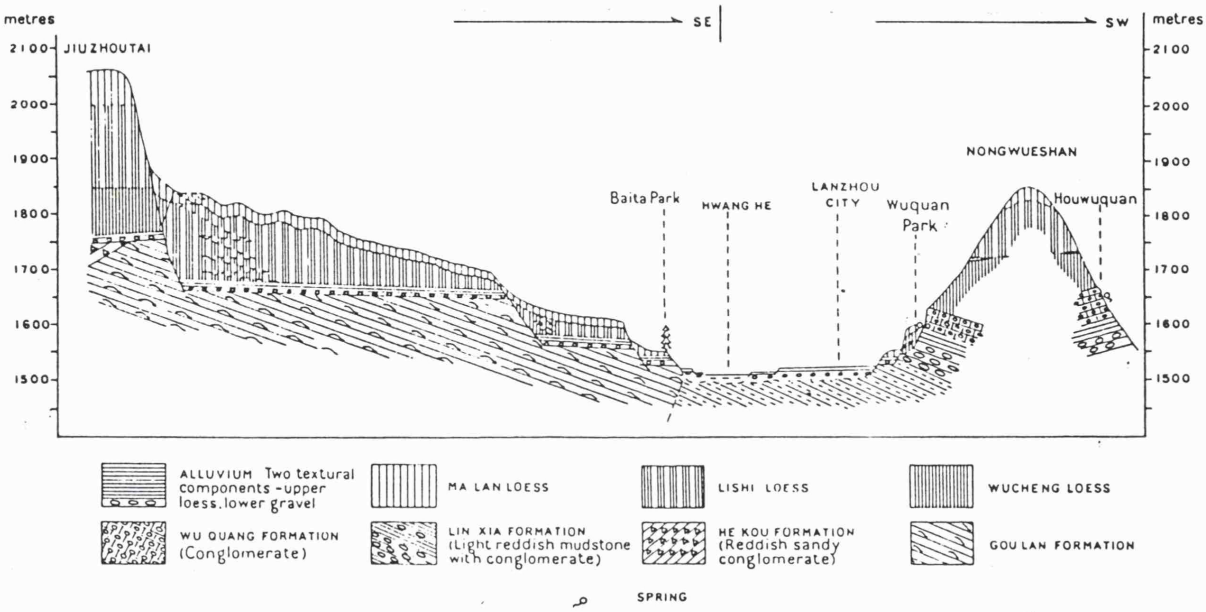

Figure 2.7 Cross section of the succession at Lanzhou (Derbyshire, 1983)

The Malan loess at Jiuzhoutai is believed to be 42m thick preceded by a dual S1 palaeosol and capped with Holocene loess. Lanzhou University have obtained TL dates of 81 $\pm$ 5.9ka for the bottom of the Malan loess; 91.25 $\pm$ 10.9ka for the top of S1 and 123.2 $\pm$ 13.0ka for the top of the Lishi loess from within the Scorpion Pit on Jiuzhoutai. The Scorpion Pit was so called to distinguish it from the main section at Jiuzhoutai which lies 45m to the east of the Scorpion Pit and runs continuously down the mountain in the form of shallow pits 0.5 to 2m in depth. Preliminary investigation of Jiuzhoutai in 1989 showed the main section to be in a poor state for sampling with pits covered in redeposited loess from sheetwash and slurry flow, which are common on slopes of greater than 35°.

Plate 2.5 The Scorpion Pit section at Jiuzhoutai.

Plate 2.6 Dawan section showing the upper cultivated terrace and the rough grassland in which are located the sample pits.

Seven metres of sediment were sampled from the Scorpion Pit after six days of extensive digging to ensure a clean undisturbed section (plate 2.3). The seven metres included the dual S1 palaeosol dated by Lanzhou University. The samples from Jiuzhoutai have been labelled in the form Loess I, Palaeosol I, Loess II, Palaeosol II, Loess III from the topmost stratigraphic unit downwards to avoid repeated use of the Chinese nomenclature which can be very confusing when applied to multiple palaeosols (S1S1; S1L2; S1S2 etc). In this roman script, Loess III corresponds to the Lishi loess of Chen Fahu (1990) and Loess I to the Malan loess. Loess II is the loess deposited between the two palaeosols (figure 2.8).

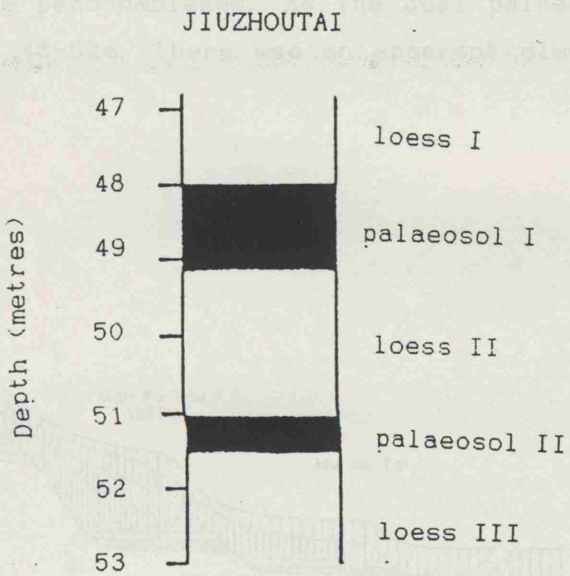

Figure 2.8 Diagrammatic representation of the sediment sampled in the Scorpion Pit, Jiuzhoutai.

2.3.2 Lanzhou Area II - Dawan (35°54'N, 103°12'E)

The 273m section is located on the east side of the Shua Jia valley 250m north of Dawan village (fig 2.9). The Shua Jia is a tributary of the Yellow River whose confluence lies at the west end of the Lanzhou Basin near Xikou. 200m of loess outcrops over terrace 5 of the Yellow River which in turn rests on Pliocene Red Clays. The section is composed of a series of 5-8m deep pits dug into uncultivated rough pasture. The top 20m of the section has been excavated and levelled for cultivation and comprises wheat and potato fields and, as such, is unsuitable for sampling (plate 2.4).

The sampling strategy at Dawan was to identify the last interglacial palaeosol and sample the Malan loess above it and the Lishi loess below it. Previous mapping of the palaeosols at Dawan by the Lanzhou Geological Hazards Research Institute identified a palaeosol at 25m depth with that of the last interglacial. Thus the preceding five metres of loess (Loess I) were sampled along with the palaeosol. However, further investigation of the section over two field seasons identified six palaeosol horizons within ten metres of sediment, from 25-35m down the section, which appeared to be arranged in two triple pedocomplexes. As the dual palaeosol at Jiuzhoutai existed at a depth of 48-52m, there was an apparent discontinuity between Jiuzhoutai and Dawan.

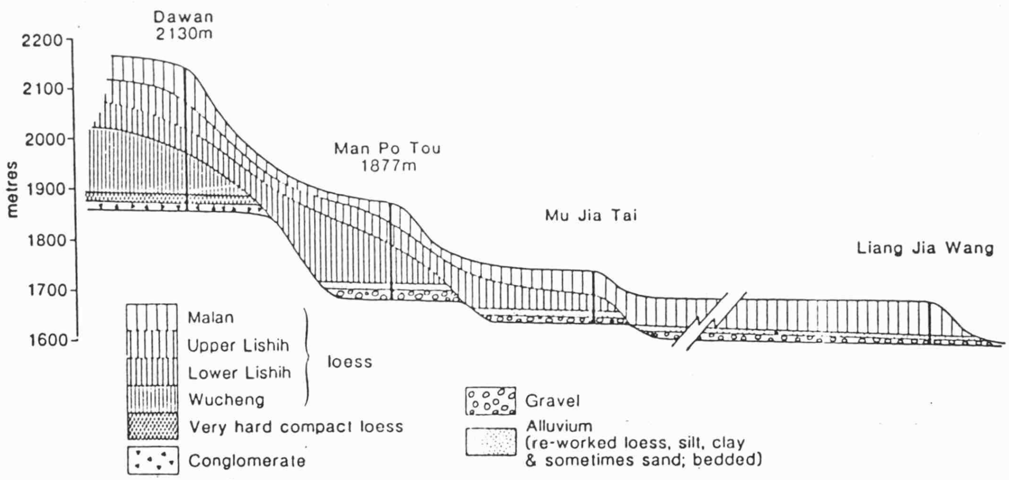

Figure 2.8 Cross section of the locations in the Shua Jia valley.

The roman script labelling was again used here (figure 2.9) as complete lack of chronological control made further estimates of age impossible. The palaeosols are typically 0.5 - 1.0 m thick but only palaeosol III (plate 2.6) and VI were clearly visible as brown horizons (7.5YR 5/4 to 7.5YR 7/3). Loess was typically buff yellow (10YR 7/2 to 10YR 7/3). A speckled horizon was located two metres above palaeosol I at a depth of 23m (plate

2.5). However it was discounted by the Chinese as not being the result of pedogenic processes (Wang Jingtai, pers.comm). Gypsum layers, indicative of the aridity of climate, are common within the Dawan section.

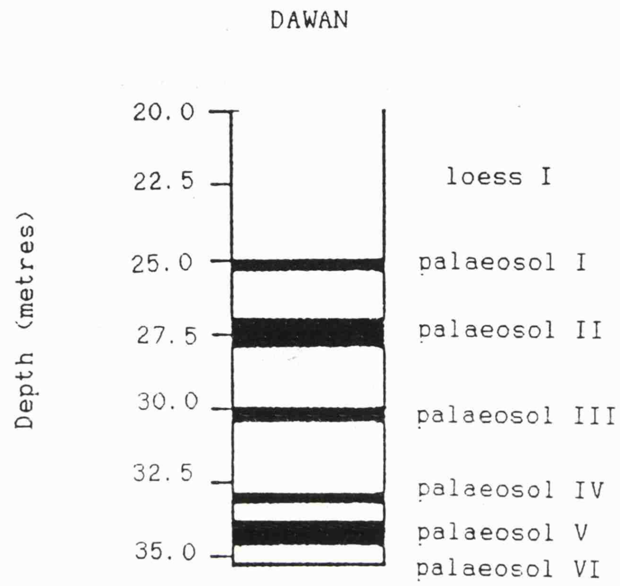

Figure 2.9 Diagrammatic representation of the section sampled at Dawan.

In addition to the fifteen metre continuous section described above, a sample of recent soil from a depth of 1.3 metres was sampled for use in REE geochemistry to compare with surface silts from Tibet and the uncultivated Pleistocene loess from Jiuzhoutai and Dawan.

Plate 2.7 Dawan: strongly developed palaeosol III showing mottling.

Plate 2.8 Dawan: speckled horizon at 23 metres which gave no increased magnetic susceptibility reading.

2.3.3 Southern Gansu I - Sala Shan (35°50'N, 103°00'E)

The site at Sala Shan lies on the Ba Xie river east of the town of Linxia (35°40'N, 103°10'E) and 60km SSW of Lanzhou. The Ba Xie is an east-west running tributary of the Tao River which, in turn, joins the Yellow River at Liujiaxia reservoir (figure 2.10). Sala Shan was the site of a large loess landslide in 1983, which buried 4 villages and killed 227 people in under one minute (Derbyshire *et. al.*, 1991a). Two orientated blocks were taken from fluvially deposited loessic alluvium (plates 2.9; 2.10) to use as a control in fabric analysis (see chapter 8).

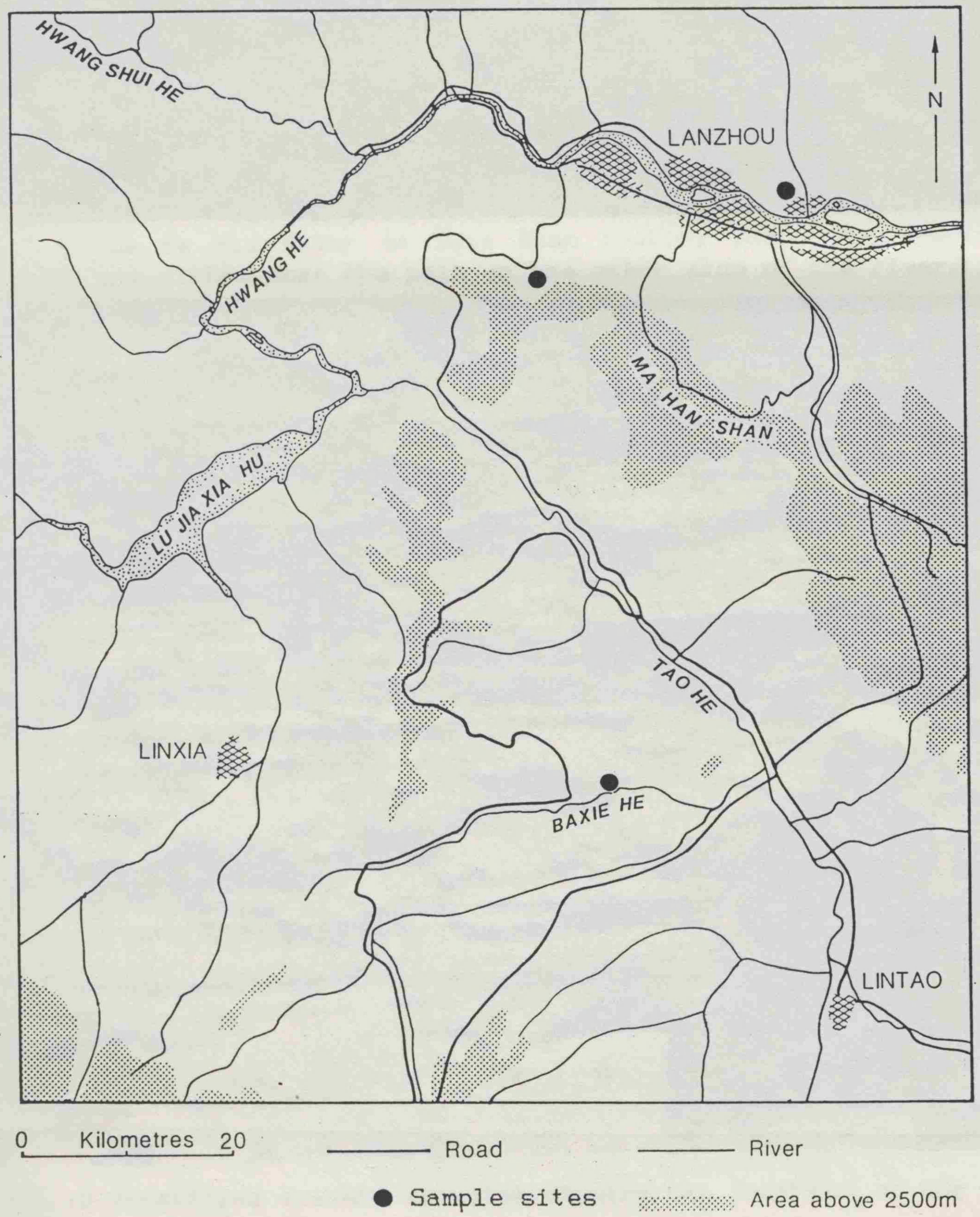

Figure 2.10 Location of Sala Shan in relation to Lanzhou.

Plate 2.9 The Ba Xie River at Sala Shan looking east. The samples were taken from the cliffs near the path on the other side of the river.

Plate 2.10 Stratified loessic alluvium showing the location of the sample.

2.3.4 Southern Gansu II - Labrang (35°20'N, 102°50'E)

The site at Labrang, in the mountains fringing the eastern edge of the Tibetan Plateau, just east of the A'nyêmaqen range, lies south of the Tibetan Monastery on the northern slope of the Daxia River valley. This area of southern Gansu is known as the Grasslands as it lies over 3000m and forms the eastern fringes of Tibetan pastureland. A sixty metre high loess terrace occurs either side of the Daxia River (plate 2.11). The sample blocks were taken from the northern loess terrace 300m east of the Xiahe Binguan (plate 2.12). As there is no chronological control and no published data on the loess near Labrang, two separate sample blocks were taken at a vertical spacing of approximately 12 metres. The upper sample, Labrang B was visibly coarser than the lower sample Labrang A.

2.3.5 Tibetan Plateau, Kunlun Mountains and Qaidam Basin

The Kunlun Mountains and the Tibetan Plateau were visited as part of an expedition run by the Lanzhou Institute of Glaciology and Cryopedology in May 1990, involving scientists from Lanzhou and the Soviet Siberian Permafrost Institute. The expedition started from the town of Golmud (36°12'N, 94°38'E) in the Qaidam Basin. Seven sites along a transect between Golmud and Wudoliang (35°06'N, 93°00'E), an army encampment on the Tibetan Plateau, were visited and samples of sediment collected. Just outside Golmud, desert sands were taken from the Qaidam Basin for comparison with the Kunlun and Tibetan samples. The foot of the Kunlun Mountains, approximately 75km south of Golmud, were snow covered to a depth of a few centimetres. A sample of surface silt (Kunlun A; 10YR 7/3) was taken from below the snow cover, approximately 2 metres above the road level, near kilometre post 2798.

Next to the 1951 bridge over the Kunlun River, at 3400m, where the river cuts steeply through greenish bedrock as a result of neotectonic movement, approximately 10 metres of silt rest on the bedrock which has been gorged by the river. Due to the military sensitivity of the bridge no photographs or samples were allowed. Further upstream, at an altitude of 3600m the downcutting of the river exposes 30 metres of river terrace composed entirely of a succession of sands and gravels (plate 2.13). The sands and gravels appear to be predominantly of glaciofluvial origin (Klimovsky, pers. comm).

Plate 2.11 View of the Daxia Valley looking southeast showing the truncated loess terrace. Photo taken from the terrace surface above the sample sites.

Plate 2.12 Sample sites at Labrang. The partly excavated block in the centre foreground above the grass clumps is Labrang A, with Labrang B situated where Christine Scott is standing, twelve metres above A.

Plate 2.13 Terrace sands and gravels of the Kunlun River.

Plate 2.14 Surface silt at 3400m (Kunlun A)

Buff coloured surface silt (10YR 7/2) was sampled from an altitude of 3800m. The silt was excavated to a depth of 50cm although the total thickness was thought to be in excess of one metre (plate 2.14). Bedrock in this area was visibly frost shattered, see plate 2.14. The sample was labelled Kunlun Glacier because just south of this site was an open area of flat land leading eastwards from the Kunlun River up to a series of glaciers. Plate 2.15 was taken on 2 May 1990 on this expedition, whereas plate 2.16 is a view of the same site taken in August 1984. The marked climatic difference between these two photographs indicates a large seasonal fluctuation in temperature suggesting that cold weathering may play a vital role in the breakdown of bedrock and the formation of fine particles in this mountain environment.

At 4100m, next to the Golmud-Lhasa Highway, there exist four well-developed barchan sand dunes, approximately 8.5-10m in height, which have been evolving here since 1984 (Zhou Youwu, pers. comm) and are probably the highest altitudinal sand dunes in the world (plate 2.17; 2.18). The shape of the dunes indicates a southerly wind eminating from the Tibetan Plateau, bringing sediment down the Kunlun Mountains. Sand was taken from the dunes, bottled and labelled.

Near the Kunlun Pass at 4700m there is a relic pingo (35°35'N, 94°03'E), 20 metres in diameter and 18 metres high (plate 2.19) partially blown up by engineers building the Golmud-Lhasa Highway. The presence of this pingo also testifies to the ongoing prevalence of intense cold weathering in the area. Buff coloured silt samples (10YR 7/2) were taken from the surface of the Kunlun Pass (4767m) and grey coloured silt (2.5GY 6/1) from the ice core of the pingo. Plate 2.20 shows the occurrence of aeolian transport at the Kunlun Pass.

The Tibetan Plateau is sparsely vegetated and covered exensively with silt and sand. At no point between the Kunlun Pass and Wudoliang was bedrock visible. The surface of the plateau was also covered with ice patches (plate 2.21) indicating that moisture is present and suggesting an intensive cold weathering environment. This is also demonstrated by many broken sections of metalled road (plate 2.22). Samples of dull brown to yellow surface silt (2.5YR 7/2) were collected at Qumar Heyan (35°18'N, 93°20'E), near the broken section of the Lhasa Highway shown in plate 2.22 (plate 2.23) at an altitude of 4550m.

Plate 2.15 Glacier in the Kunlun Mountains, in spring (M. Clarke 2/05/90)

Plate 2.16 Glacier in the Kunlun Mountains, in summer (E. Derbyshire 08/84)

Plate 2.17 Close up of one of the barchan dunes found at an altitude of 4100m in the Kunlun Mountains.

Plate 2.18 View of an entire dune showing relative height. Crescent arms point north.

Plate 2.19 The ice core centre of the pingo situated near the Kunlun Pass.

Plate 2.20 Active aeolian transport at the Kunlun Pass (4767 metres asl).

Plate 2.21 The Tibetan Plateau (4550m asl) showing the presence of surface silt and ice patches. The Kunlun Mountains are visible to the north.

Plate 2.22 A broken section of the Golmud-Lhasa Highway at Qumar Heyan indicating an intense freeze-thaw environment.

Plate 2.23 Silt on the surface of the Tibetan Plateau at Qumar Heyan

2.4 Sampling procedure

For the Gansu samples (Jiuzhoutai, Dawan, Labrang and Sala Shan) which were consolidated loess, the following procedure was adopted. The loess face was cleaned and then excavated to form blocks approximately 15cm across and 35cm in depth. The top surface was levelled to horizontal using a small 2 way-spirit level and a north arrow was marked on the level surface before the block was removed from the face. These orientated blocks were then placed into cardboard boxes and insulated with straw to facilitate transport in an intact state to the Geological Hazards Research Institute at Lanzhou. Here they were sub-sampled into cubes and placed in 2.2cm³ perspex boxes prior to being transported back to Britain. At least 2 cubes were prepared from each sample height and the remaining material was stored in plastic bags before being shipped back to Britain as container-ship cargo. The cubes were hand transported by plane.

The samples taken from the Qaidam, Kunlun and Tibetan Plateau were samples of unconsolidated sub-surface sediment and were placed into plastic bottles.

3. SILT PROVENANCE: PHYSIOCHEMICAL PROPERTIES

Bowler *et.al.* (1987), and more recently Zhang Linyuan *et.al.* (1991), have suggested that silt is formed in the mountain environments of the Tibetan Plateau and northwestern (Kunlun) mountains as a result of both glacial grinding and freeze-thaw weathering, and that this silt forms a constituent part of the Loess Plateau. This section describes the particle size, scanning electron microscopy and rare earth geochemistry of silts and desert sand sampled from these mountain environments, and a comparison made with samples obtained from the Loess Plateau.

3.1 Particle size distribution.

Particle size fractionation across the gobi, the sand deserts and the Loess Plateau, linked with predominant winds, has been used to account for a desert source for the Chinese loess (Wang Yongyang, 1983). The occurrence of silt on the Tibetan Plateau and in the Kunlun Mountains testifies to the formation of silt in these high mountain environments. The presence of crescentic dunes indicates aeolian transport down from the Tibetan Plateau and Kunlun Pass. The predominant northwesterly winds of the Siberian-Mongolian high pressure system deflate fines resident in the Qaidam Basin and carry them to the Loess Plateau (Bowler *et.al.*, 1987). The presence of a large silt component in the sediments of Qarhan Lake over the last 40ka has been reported by Chen Kezao and Bowler (1986). They argue that these silts are virtually indistinguishable both texturally and mineralogically fom the Luochuan loess. The particle size of silts from the Tibetan Front has been investigated here.

3.1.1 Measurement of particle size

The particle size of samples collected from all of the sites was measured. The silt grade samples were measured using a Microtechnics model 5100ET SediGraph which determines the concentration of particles remaining at decreasing sedimentation depths as a function of time. Approximately 3 grammes of sample were ground in a pestle and mortar then dispersed in 0.01% calgon prior to being pumped into the measurement cell which is placed in the path of a finely collimated x-ray beam. When the pump is turned off the particles in the cell settle according to Stokes' Law. The intensity of the x-ray beam received from the cell varies with the concentration of particles in its path, which is related to their settling velocity. Thus the difference between intensities of received and emitted x-rays gives a measure of particle size distribution (and settling) over time.

The two sand grade deposits (from the Qaidam Basin and the Barchan dune field in the Kunlun Mountains) which were too coarse to be tested within the SediGraph, were weighed then shaken through a nest of sieves with mesh diameters of: 1000μm (1mm); 500μm; 250μm; 125μm; and 63μm.

3.1.2 Results

The median diameter (d^{50}) was calculated for the silt grade samples and cumulative frequency graphs of particle diameter were plotted. The percentage mass of sediment, arranged into size classes, is presented in tabulated form for each sample. Folk and Ward sorting parameters were not applicable as not all of the samples had a unimodal particle size distribution and this non-normal distribution would make comparisons between samples impossible.

The cumulative frequency curves for Jiuzhoutai loess and palaeosols are illustrated in figure 3.1. The envelope enclosing the curves is narrow, indicating little variation in grain size between the samples or between unweathered loess and weathered palaeosol.

Table 3.1 Percentage mass of sediment in micron diameter size classes for Jiuzhoutai (JL1 = loess I; JP2 = palaeosol II)

diameter (μm)	JL1	JP1	JL2	DP2	JL3
>60	3.1	1.8	0.4	1.1	1.6
50-60	1.1	1.7	2.5	1.6	1.8
40-50	2.4	3.4	4.8	4.3	5.7
30-40	6.6	8.5	8.8	9.9	10.5
20-30	14.5	14.2	13.9	16.6	14.7
10-20	19.4	17.2	17.6	16.6	15.9
2-10	23.5	22.3	23.1	19.9	20.0
0.5-2	10.3	10.1	11.5	10.8	11.6
<0.5	19.1	20.8	17.4	19.2	18.2

Samples from each of the loess and palaeosols from Dawan were analysed, along with two samples of recent soil material from beneath the cultivated surface at the top of the section. The envelope encompassing percentage cumulative frequency against grain diameter for the loess and recent material samples (figure 3.2a) is wider than that at Jiuzhoutai, and covers a larger grain size than that of the Dawan palaeosol samples (figure 3.2 b). The median grain diameters calculated for each of the samples (see table 3.1) confirms that loess I is generally coarser than the other samples, with a median diameter of 17.8μm. Median diameters for the other loess samples range from 14.4μm - 9.1μm, the palaeosols range from 10.8μm - 5.3μm and the recent material samples have median diameters of 15.2μm and 10.0μm.

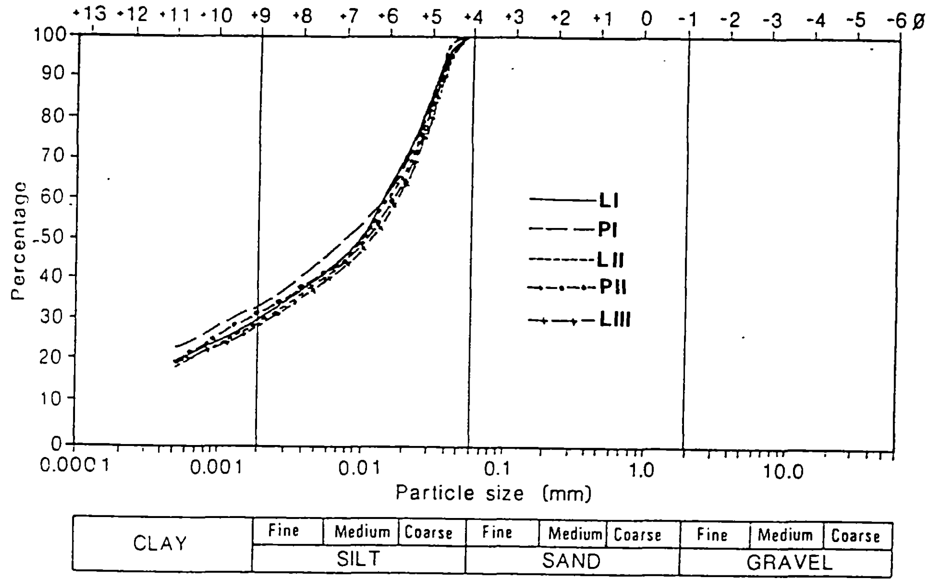

Figure 3.1 Cumulative frequency particle size distribution for loess and palaeosol units from the Scorpion Pit, Jiuzhoutai.

Table 3.2 Percentage mass of sediment in micron diameter size classes for Dawan samples (DL1 = loess I; DP2 = palaeosol II; DH2 = recent material 2).

(μm)	DH1	DH2	DL1	DP1	DL2	DP2	DL3	DP3	DL4	DP4	DL5	DP5	DL6	DP6
>60	3.0	3.0	0.6	0.8	3.4	1.1	1.4	1.8	1.3	0.3	3.7	1.9	3.6	1.0
50-60	2.3	3.9	3.6	2.1	2.0	1.3	3.0	1.4	2.2	2.0	1.7	1.1	3.7	1.1
40-50	4.6	6.8	7.2	4.4	4.3	3.0	3.9	4.4	5.4	4.4	3.7	3.7	5.9	3.1
30-40	9.6	11.2	13.5	8.8	9.5	7.0	7.1	8.8	12.0	8.6	8.7	8.6	10.2	6.7
20-30	13.9	16.9	20.6	15.5	17.0	13.1	14.2	13.4	18.5	15.3	15.8	15.1	15.2	12.2
10-20	16.8	17.3	18.8	20.3	19.2	19.1	18.4	16.4	17.9	20.5	18.5	19.2	15.8	15.4
2-10	23.4	20.5	15.9	24.4	20.5	26.7	25.2	21.0	18.8	25.1	21.5	24.8	23.9	23.2
0.5-2	12.2	8.8	10.2	11.7	10.3	13.6	11.9	15.4	8.4	11.6	10.8	11.7	12.4	16.1
<0.5	14.2	11.6	9.6	12.1	13.8	15.1	14.9	17.4	15.5	12.2	15.6	13.9	9.3	21.2

One sample from each of the blocks taken from the Labrang loess terrace and one sample from the fluvially redeposited Sala Shan silt were analysed and are presented in figure 3.3. The Labrang B sample from the topmost block was considerably coarser than the Labrang A sample taken from 10 metres below it, indicated by the median grain sizes, which were LA d^{50}=13.3μm; LB d^{50}=29.7μm.

Table 3.3 Percentage mass of sediment in micron diameter size classes from Labrang, Sala Shan the Kunlun Mountain and Tibetan Plateau sediment.

diameter (μm)	Lab A	Lab B	Sala	Glac	Pingo	KP	QH
>60	3.4	2.9	1.0	14.8	8.5	14.7	29.1
50-60	3.3	11.7	3.8	11.4	10.7	10.2	5.0
40-50	6.3	16.6	7.0	11.9	13.4	13.4	5.4
30-40	10.5	18.2	13.7	10.6	17.1	12.5	7.3
20-30	15.7	14.7	19.8	9.2	19.0	11.3	6.9
10-20	15.7	8.5	20.6	8.8	16.9	11.2	4.6
2-10	18.7	9.6	16.6	13.0	8.8	14.3	19.5
0.5-2	11.0	5.3	8.0	6.1	2.1	5.7	7.4
<0.5	15.4	12.5	9.5	14.2	3.5	6.7	14.8

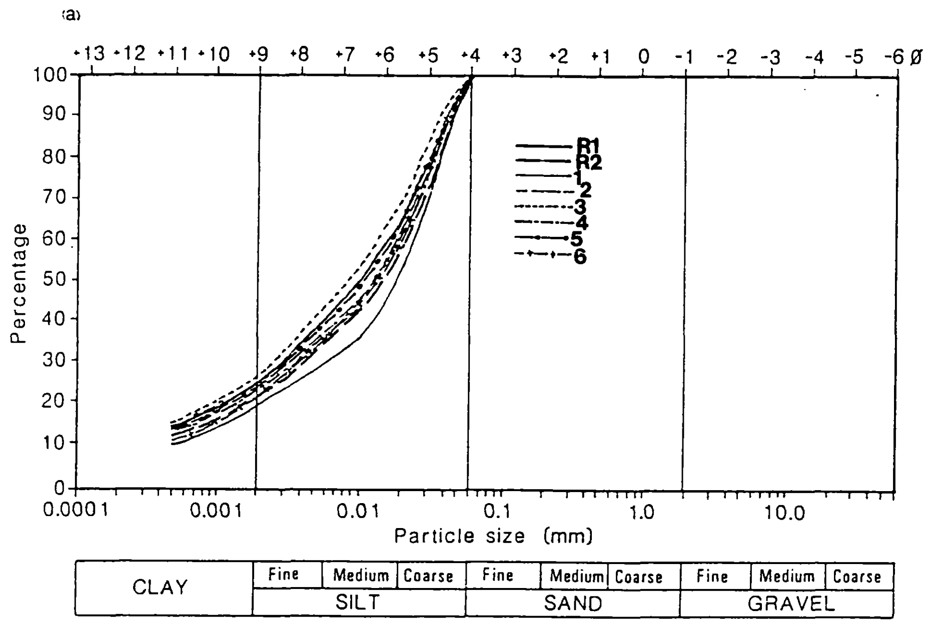

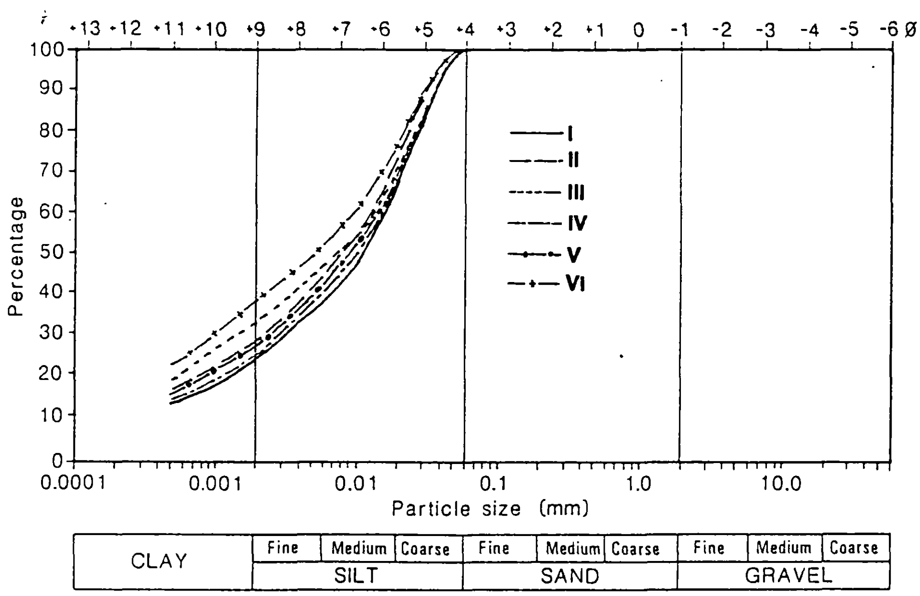

Figure 3.2 Cumulative frequency particle size distributions for (a) loess and recent soil and (b) palaeosols from Dawan.

Both silt and sand samples were tested for particle size from the Qaidam Basin, Kunlun Mountains and the Tibetan Plateau. Figure 3.4 shows the cumulative frequency diagrams against particle diameter for the four silt-sized samples from the Kunlun Mountains and Tibetan Plateau and the two sand grade samples. The median grain diameters for these silt grade samples indicate that they are significantly coarser than the Gansu loess and palaeosol samples, and are illustrated in table 3.1

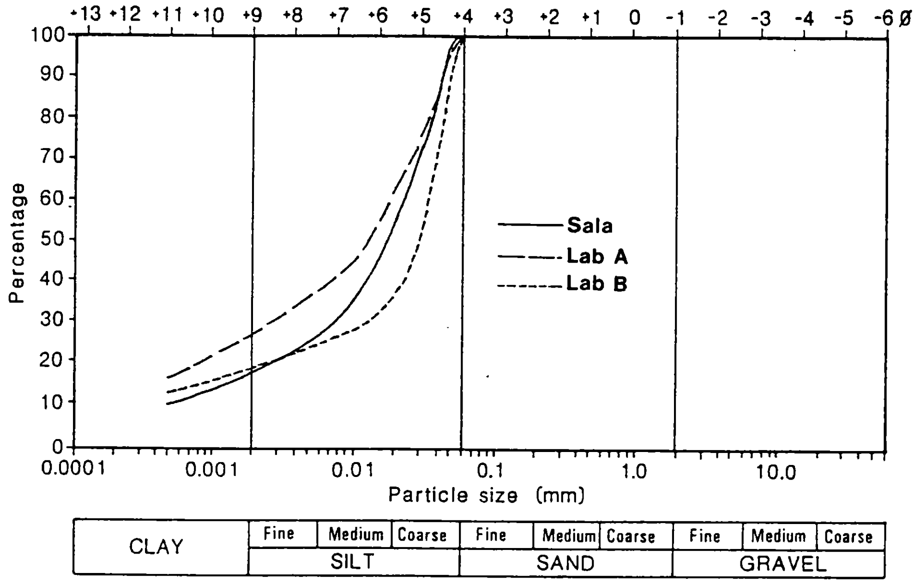

Figure 3.3 Particle size distributions from Labrang and Sala Shan.

The sand grade samples were first weighed, then shaken through a nest of seives with mesh sizes ranging from 63µm to 1000µm (1mm). The sand sample taken from the surface of the Qaidam desert, just outside the town of Golmud, had the majority of grains falling into the 125-250µm class. Both coarse sand (>1000µm diameter) and silt sized (<63µm) grains were present. In contrast, the sand from the barchan dune field, at 4100m in the Kunlun Mountains, had a very narrow size range with the majority of grains falling into the 125-500µm diameter class. No silt grains were present, with only negligible content >500µm.

Table 3.4 Percentage mass of sediment in micron diameter size classes for sand from the Qaidam Basin and Kunlun barchan dunes.

diameter (µm)	Golmud Qaidam Basin	barchan dune Kunlun Mountains
>1000	5.6	0.0
500-1000	3.2	0.2
250-500	28.2	76.3
125-250	33.3	21.8
63-125	23.2	1.7
<63	6.5	0.0

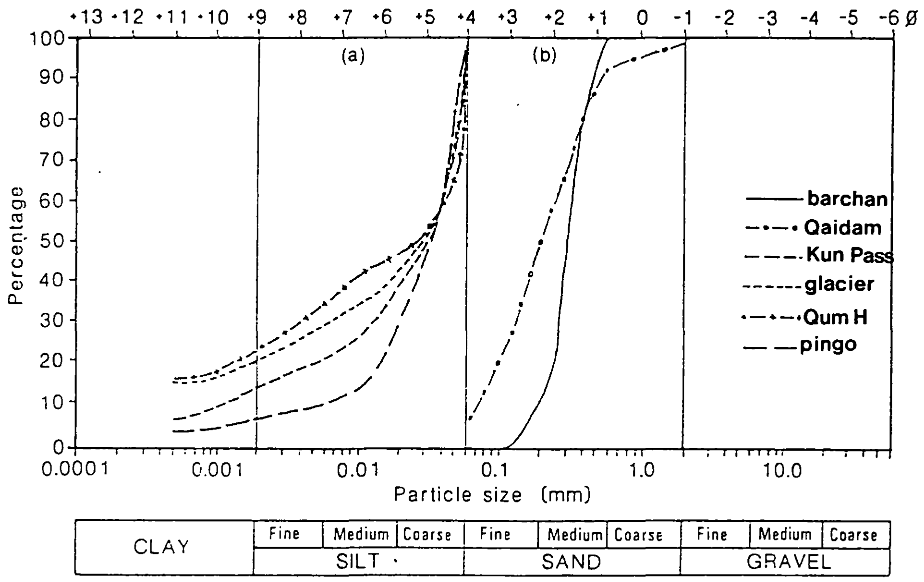

Figure 3.4 Particle size distributions from (a) Kunlun Mountain and Tibetan Plateau silt samples and (b) Qaidam Desert and Kunlun barchan sand.

3.1.3 Summary of particle size distribution

Median diameters derived from the SediGraph (table 3.6) show that the Kunlun (30.6 - 28.7μm), Tibetan (26.1μm) and Labrang (29.6μm) samples are coarser than the loess samples from Dawan (17.8 - 10.4μm), Jiuzhoutai (10.2 - 8.8μm) and Sala Shan (17.0μ). However, fine silts less than 20μm in diameter, which make up the bulk of the Lanzhou loess (table 3.2), constitute between 31% and 46% of the particle size distributions of the Kunlun Mountain and Tibetan Plateau samples. The presence of a barchan dune field at 4100m in the Kunlun Mountains, orientated with the crescent arms pointing down valley towards the Qaidam Basin, indicates that there is an effective aeolian transport system directing fine material from the Kunlun Mountains and the part of the Tibetan Plateau in its immediate vicinity, down into the Qaidam Basin. Fine material resident in the Qaidam Basin may be deflated by very strong frontal winds associated with the Mongolian high pressure system (Chen Kezao and Bowler, 1987).

Table 3.1 Median diameter of silt samples from sites on the Tibetan front

DAWAN

sample	d^{50} (μm)
Recent 1	10.0
Recent 2	15.2
Loess I	17.8
Loess II	12.5
Loess III	9.1
Loess IV	14.4
Loess V	11.1
Loess VI	10.4
Palaeosol I	10.8
Palaeosol II	7.7
Palasosol III	7.8
Palaeosol IV	10.1
Palaeosol V	9.8
Palaeosol VI	5.3

JIUZHOUTAI

sample	d^{50} (μm)
Loess I	8.8
Loess II	8.3
Loess III	10.2
Palaeosol I	8.4
Palaeosol II	10.0

LABRANG

sample	d^{50} (μm)
Labrang B	29.7
Labrang A	13.3

SALA SHAN

sample	d^{50} (μm)
Ba Xie River	17.0

KUNLUN TIBET

sample	d^{50} (μm)
Qumar Heyan	26.1
Kunlun Pass	30.6
Kunlun Pingo	29.8
Kunlun Glacier	28.7

In addition to the tabulated particle size data, scanning electron microscopy (plate 3.11) indicates that fine silt is present in the Kunlun Mountains probably formed by cold weathering and/or glacial grinding. It is also possible that there is some reworking of the thick fluvio-lacustrine sedimentary sequence reported to exist near the Kunlun Pass (Zheng Benxing, 1991).

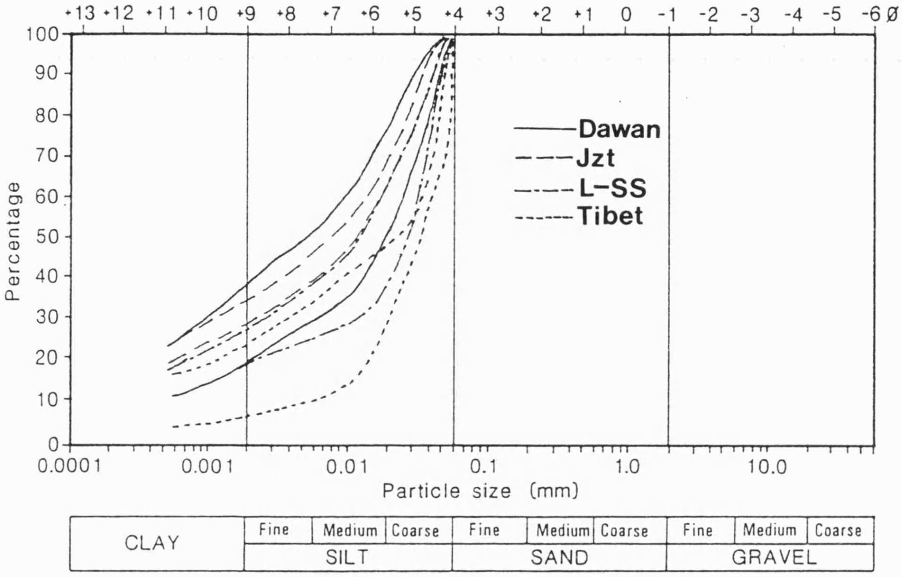

Figure 3.6 Distribution of particle size of silt grade sediments from the Tibetan Front

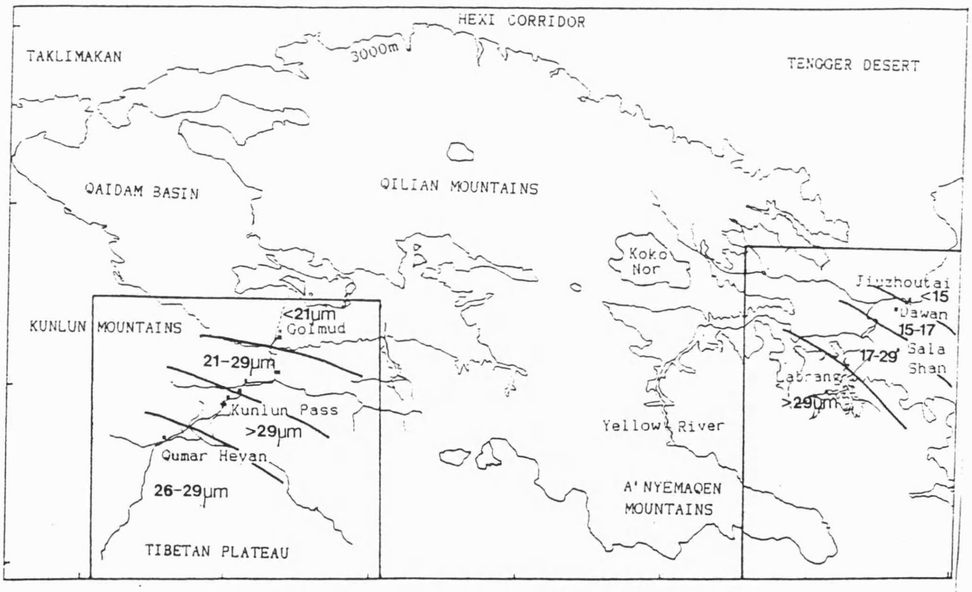

Figure 3.7 Particle size gradation across the areas of the Tibetan Front covered in this thesis.

3.2 Scanning electron microscopy

The particle size and sedimentary fabric of selected samples was investigated at Leicester University using an Hitachi 520 scanning electron microscope. Figure 3.7 is a schematic representation of the scanning electron microscope (SEM). A beam of electrons is emitted from an electron gun which passes through a series of condenser lenses and a scanning raster before impacting upon the sample stub. The reflected electrons are collected and amplified before being displayed on a video screen as a scan of the surface of the sample. A camera is attatched to the SEM for taking black and white still photographs of the scanned image. Both consolidated blocks of sediment and individual grains were viewed.

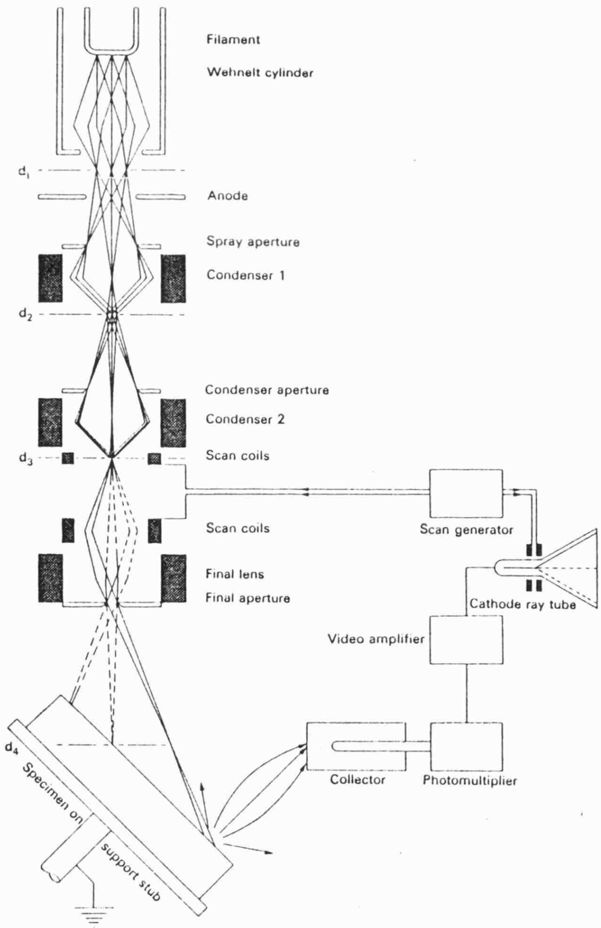

Figure 3.7 Schematic diagram of the Scanning Electron Microscope. (Smart and Tovey, 1982)

Preparation of the consolidated samples was carried out following the procedure of McGown and Derbyshire (1974). Horizontal and vertical undisturbed faces were prepared and mounted on 3cm diameter stubs using 'araldite'. The sides were painted with colloidal silver to enhance conductivity and the entire stub was then sputter coated with 10nm of gold under vacuum to prevent the samples charging when irradiated by the electron beam. Consolidated samples from Dawan, Jiuzhoutai, Labrang and Sala Shan were investigated in the SEM. Individual grains of sand from the Qaidam Basin and Kunlun barchan dunes were viewed along with individual grains of silt from the Tibetan Plateau and Kunlun Mountains. These grains were placed upon 'araldite' coated stubs using an artist's paint brush with all but one of the hairs removed. The stubs were then sputter coated with gold.

The small number of SEM micrographs displayed here were chosen in order to illustrate how the particle sizes demonstrated in section 3.1 are distributed in a range of representative samples.

3.2.1 Results

Black and white photographs of the scanned image of the samples are presented. The magnification is indicated at the bottom of the photograph along with a micron (um) size bar and the voltage of the electron beam (kV).

3.2.1.1 Dawan

Images of undisturbed consolidated sediment from Dawan are shown in plates 3.1 to 3.3. Plate 3.1 is an undisturbed vertical section through a sample of loess I from 20.5 metres, showing poor sorting with large voids ratios and little cementation indicative of the highly friable nature of this loess. A lower magnification photograph (x150 compared with x200 for loess I) of the top of palaeosol III at a depth of 30.0 metres is shown in plate 3.2. This photograph shows the increase in compaction of the sediment with depth down the section and the decrease in voids ratio. The palaeosol contains a larger proportion of finer grains with cementation and clay bridges visible. The finer grains are clearly seen in figure 3.3 (compared with the 43μm size bar) which is a x700 magnification of the centre of figure 3.2.

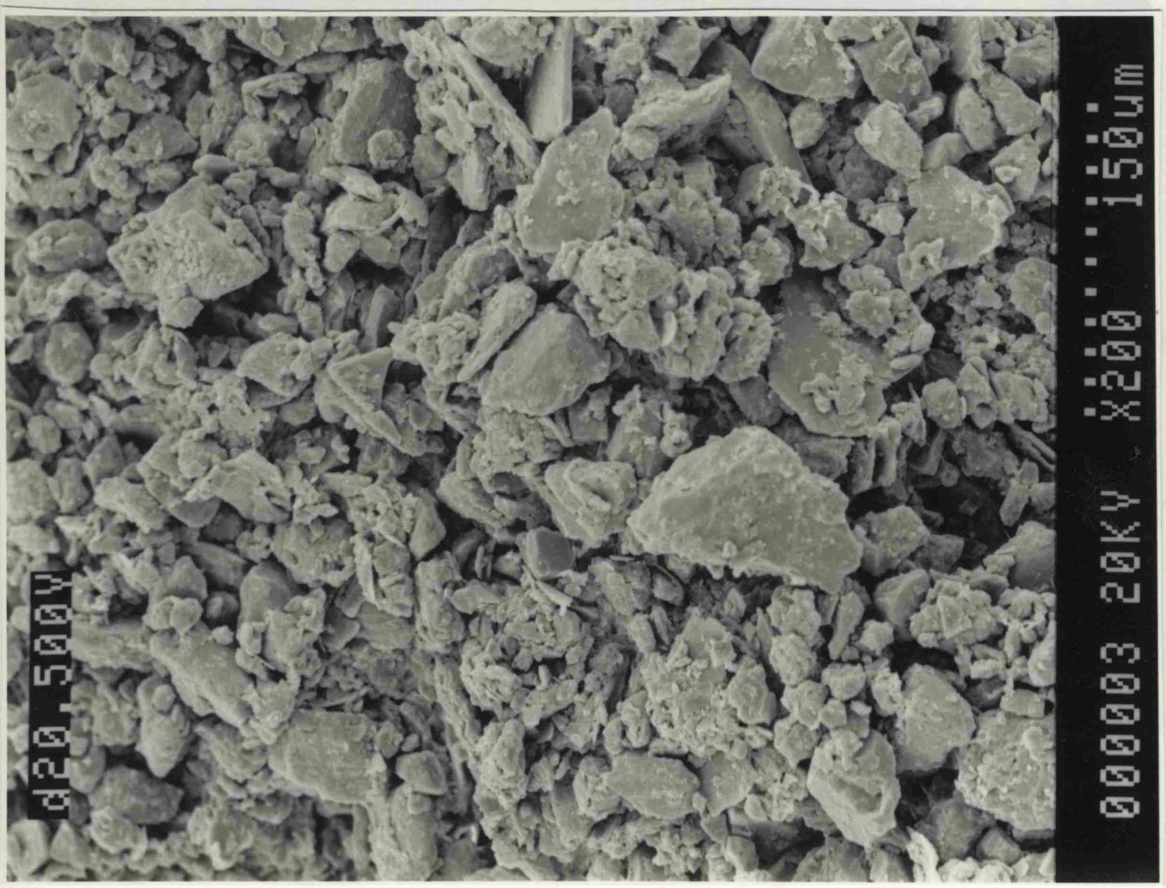

Plate 3.1 Dawan: vertical section through loess I at 20.5m.

Plate 3.2 Dawan: vertical section through the top of palaeosol III at 30m.

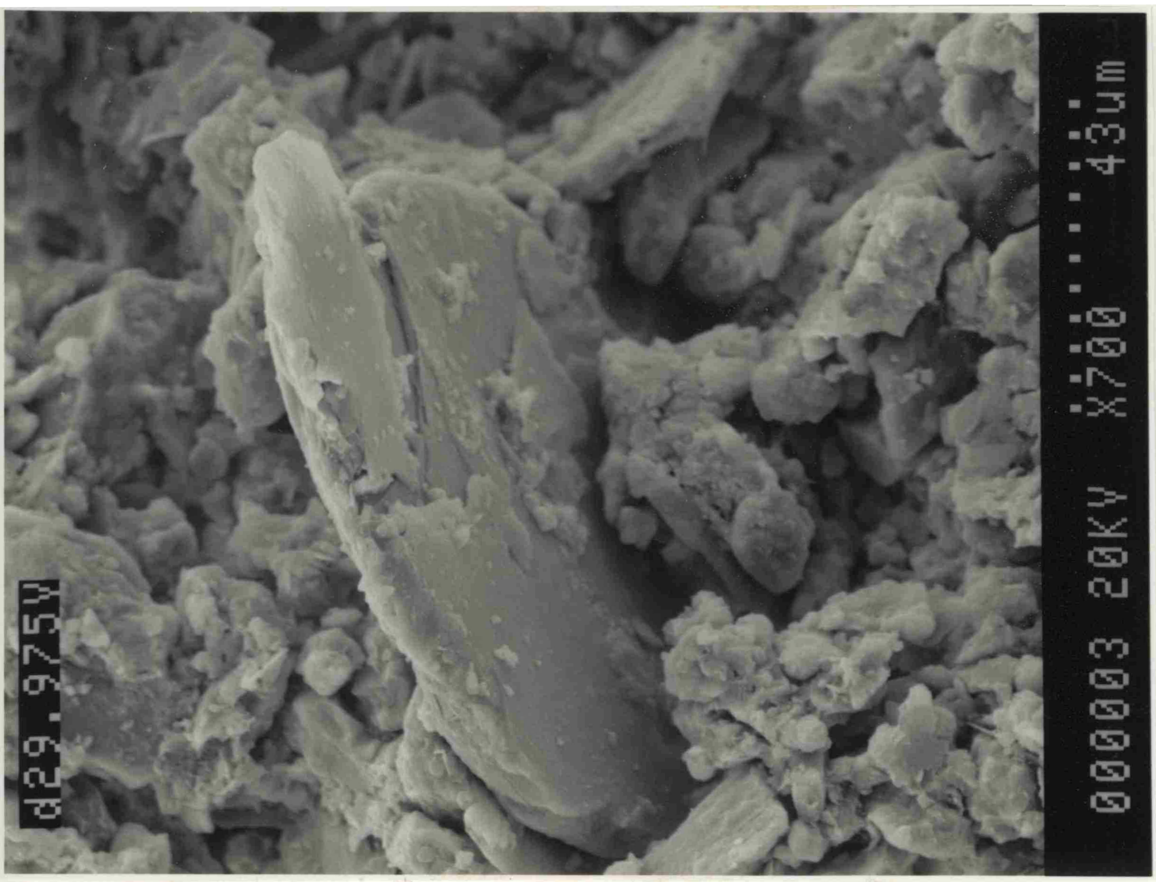

Plate 3.3 High magnification enlargement of plate 3.2 showing large weathered mica surrounded by fine silt and clay particles.

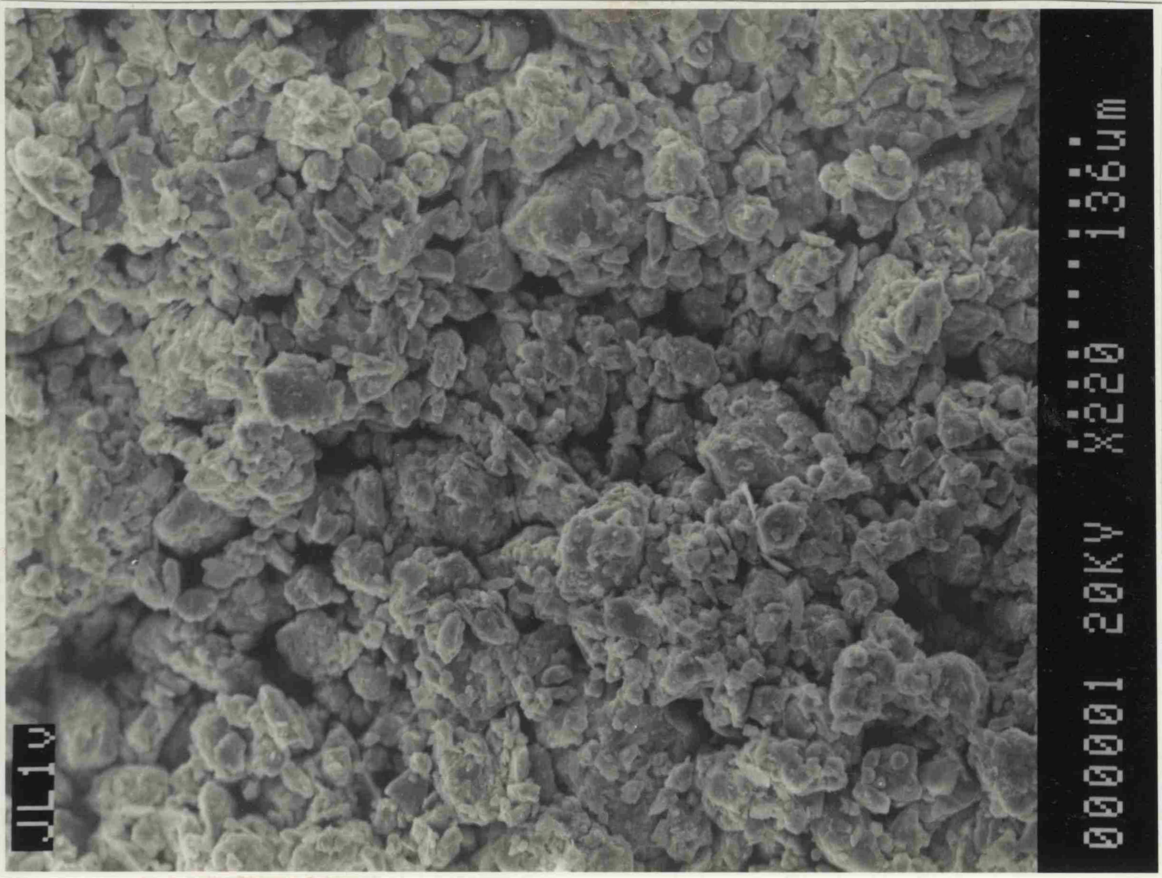

Plate 3.4 Jiuzhoutai: vertical section through loess I from 47.5m.

3.2.1.2 Jiuzhoutai

Plate 3.4 shows a vertical undisturbed section through loess I at Jiuzhoutai which can be compared with figure 3.1 of loess I at Dawan. This sample from Jiuzhoutai, at a depth of 47.5m, is generally finer than loess I from Dawan with fewer void spaces. The surfaces of the larger grains are covered by adhesions of fine silt and clay whereas the loess I sample from Dawan showed a "cleaner", more open fabric.

3.2.1.3 Labrang and Sala Shan

Plates 3.5 and 3.6 are horizontal sections through Labrang A loess at different magnifications. The quality of the Labrang photographs is unfortunately poor due to a problem with the scanning raster in the SEM when the sample was viewed (this is also true of the Sala Shan and Qumar Heyan samples). The fabric shows a large grain-to-void ratio containing a larger proportion of platy grains and widespread cementation.

Figures 3.7 and 3.8 show a vertical section through Sala Shan alluvial loess. These show a marked horizontal stratification with little cementation, low voids ratios and a high proportion of platy grains which is consistent with deposition through a water column.

3.2.1.4 Qaidam Basin, Kunlun Mountains and Tibetan Plateau

Individual sand grains from the Qaidam Desert were photographed (plate 3.9) along with sand grains taken from one of the barchan dunes at 4100m in the Kunlun Mountains (plate 3.10). The micrographs reflect the particle size differences between these sands, as stated in section 3.1. The Qaidam Desert sand (GM5) relects a wide range of particle size and shape whilst the barchan dune sand (BK5/700) is of a remarkably uniform size although shape does vary. This attests to the sorting of sediment grains within the Kunlun Mountains with fine grains deflated downwind to the Qaidam Basin which acts as a sediment trap and thus reflects a larger range of particle size.

Plates 3.11 and 3.12 show high magnification photographs of individual grain clusters from surface sediment at the Kunlun Glacier site (KU1c). Grains of varying sizes adhere together to form clusters 50-200μm in diameter. Clay minerals are prevalent and act as bridges and cements to hold the clusters together. This clustering of grains is also shown by samples from the Kunlun Pass (Plate 3.13: KU1f) and Qumar Heyan (Plates 3.16 and 3.17: QH5). Aggregates of grains 50-200μm in diameter are liable to be deflated and thus very fine grains which would otherwise remain *in situ* are carried into the aeolian transport pathway. In it's dynamic state loessic material is moderately well sorted but when disaggregated in the laboratory for the determination of of particle size curves, most of the aggregates are broken down by the use of dispersants and ultrasonic disaggregation procedures, so that it appears poorly sorted. The sediments from the Kunlun Mountains appear to contain a large proportion of platy minerals including micas, most of which are derived from the highly micaceous grey granites best seen in exposure on the northern flanks of the central Kunlun including the area adjacent to the Kunlun Pass (Derbyshire, *pers. comm.*). In other words, the micas in the Kunlun loessic samples discussed here appear to derive from local source rocks.

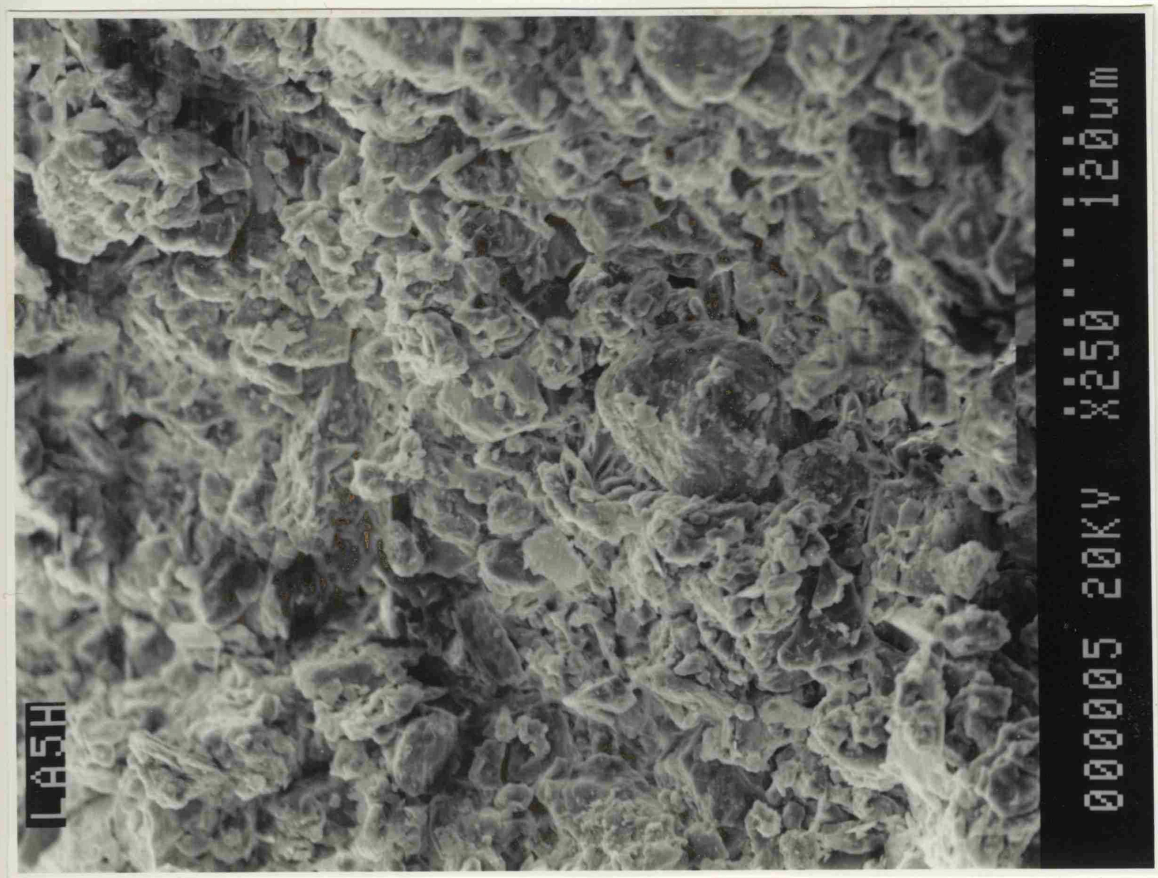

Plate 3.5 Low magnification photomicrograph of loess from Labrang A

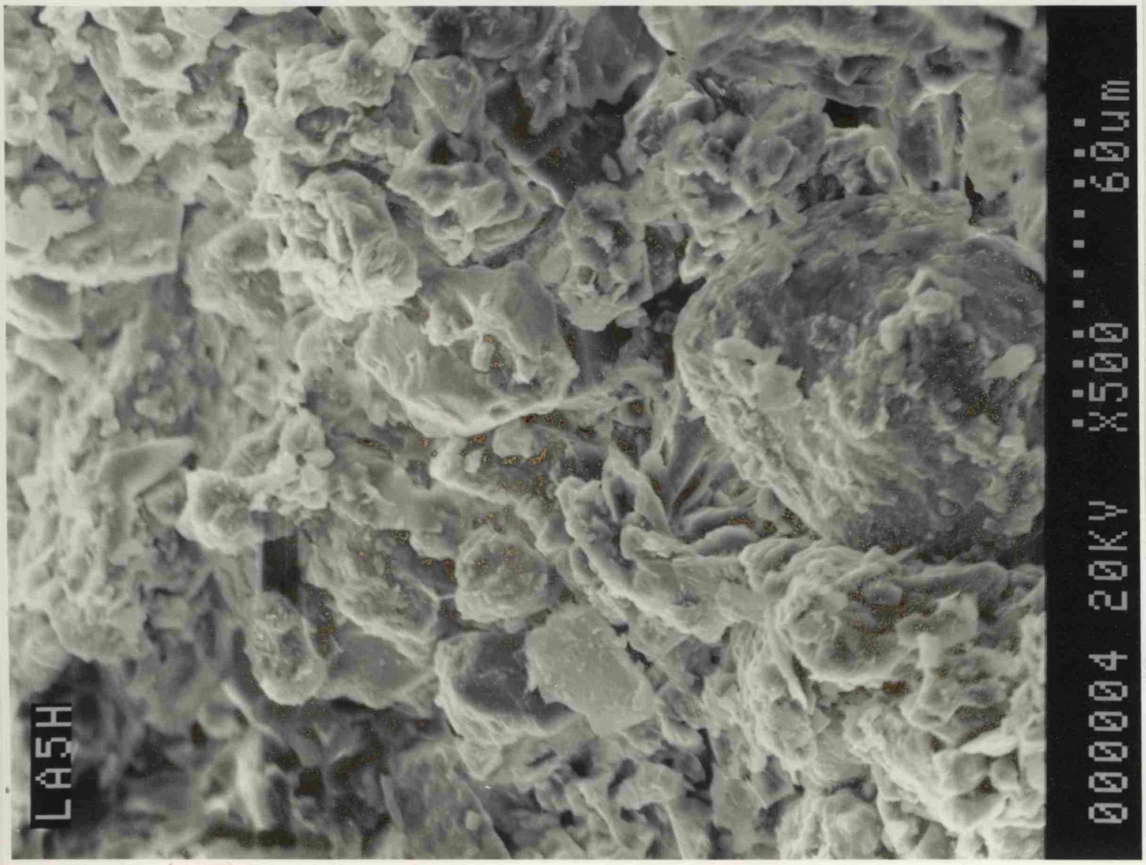

Plate 3.6 Labrang A: higher magnification detail from plate 3.5 showing low voids ratios and high degree of cementation.

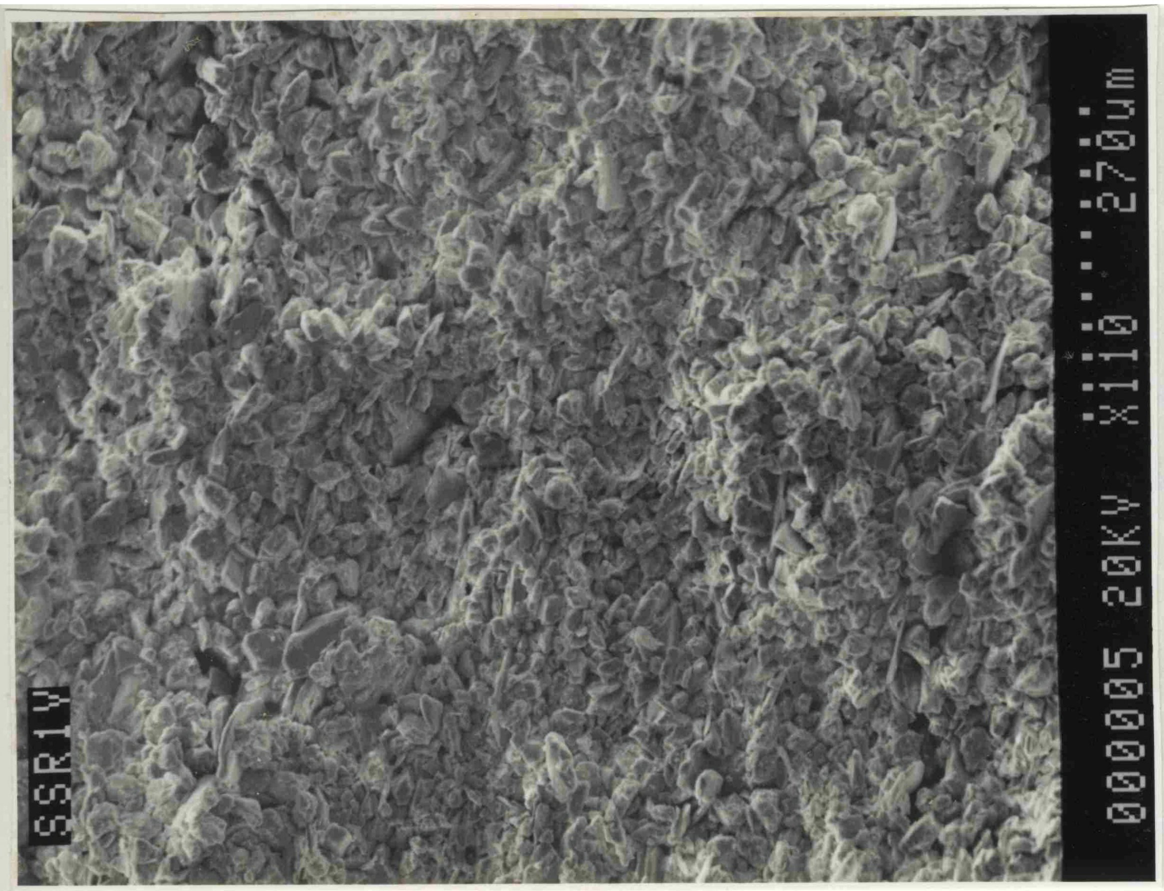

Plate 3.7 Vertical section through stratified loessic alluvium from Sala Shan. The horizontal fabric is clearly visible.

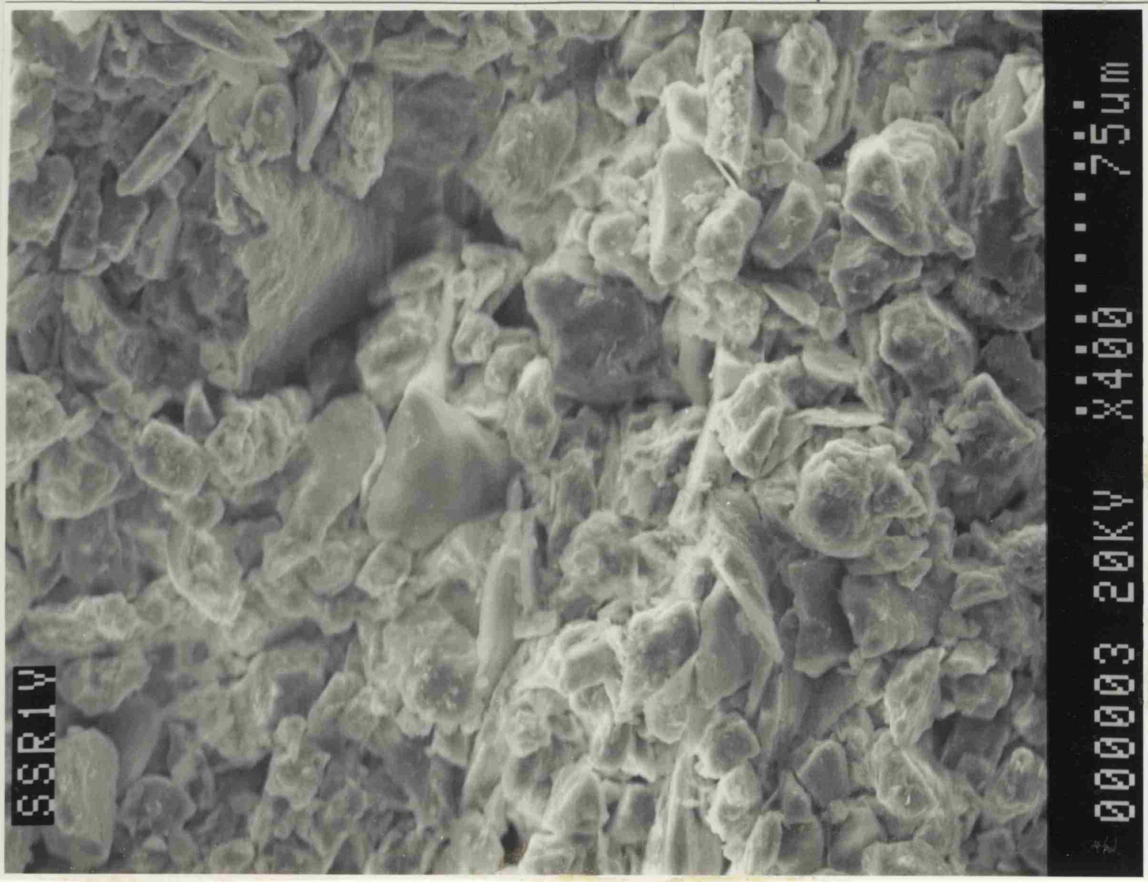

Plate 3.8 Sala Shan: high magnification photo showing very low voids ratios and absence of cementation.

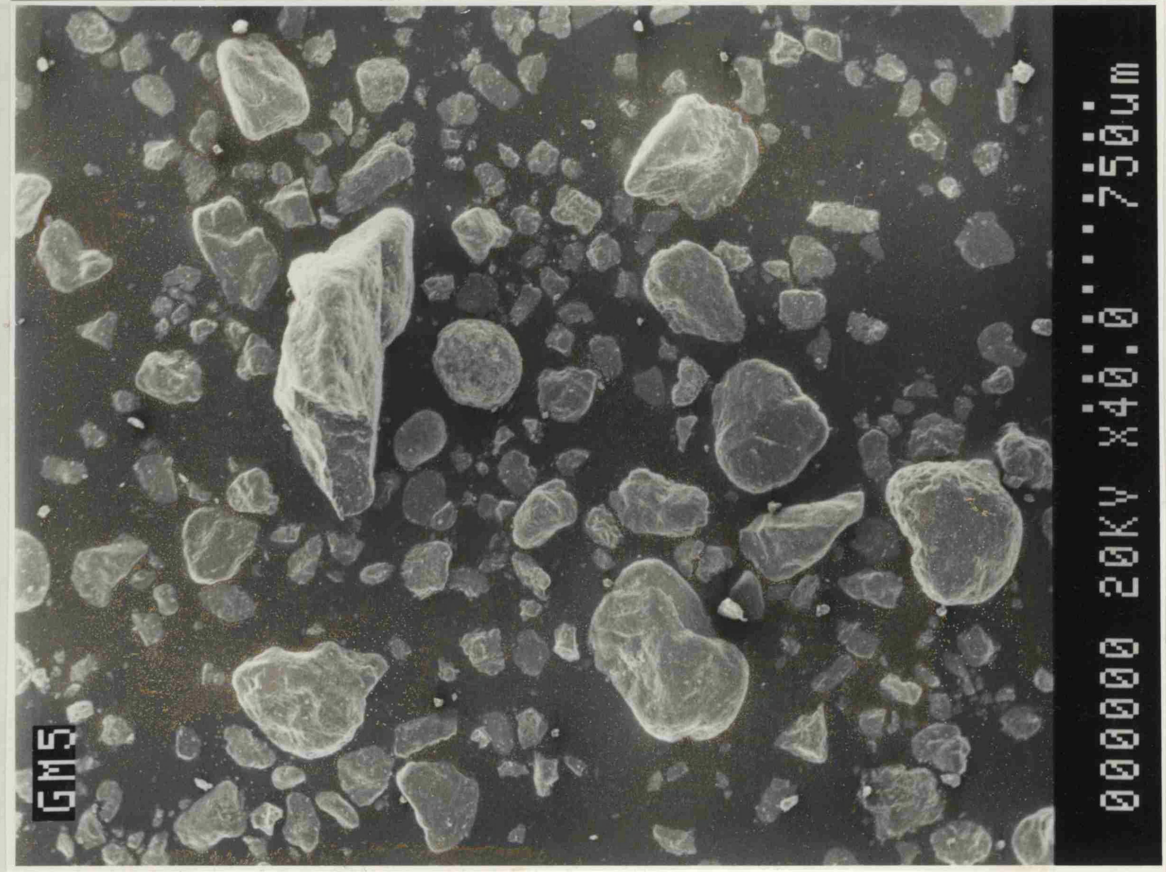

Plate 3.9 Sand grains from the Qaidam Desert near Golmud.

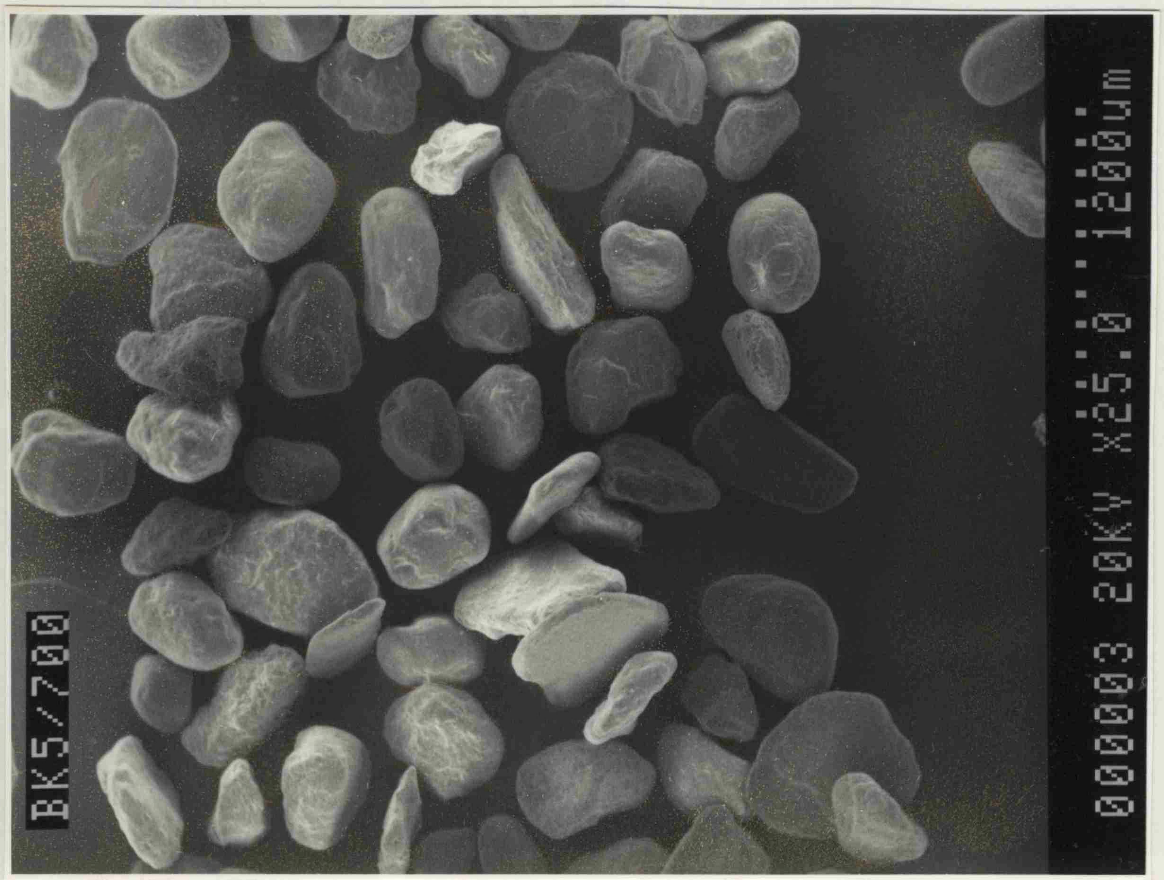

Plate 3.10 Sand grains from the barchan dune field in the Kunlun Mts.

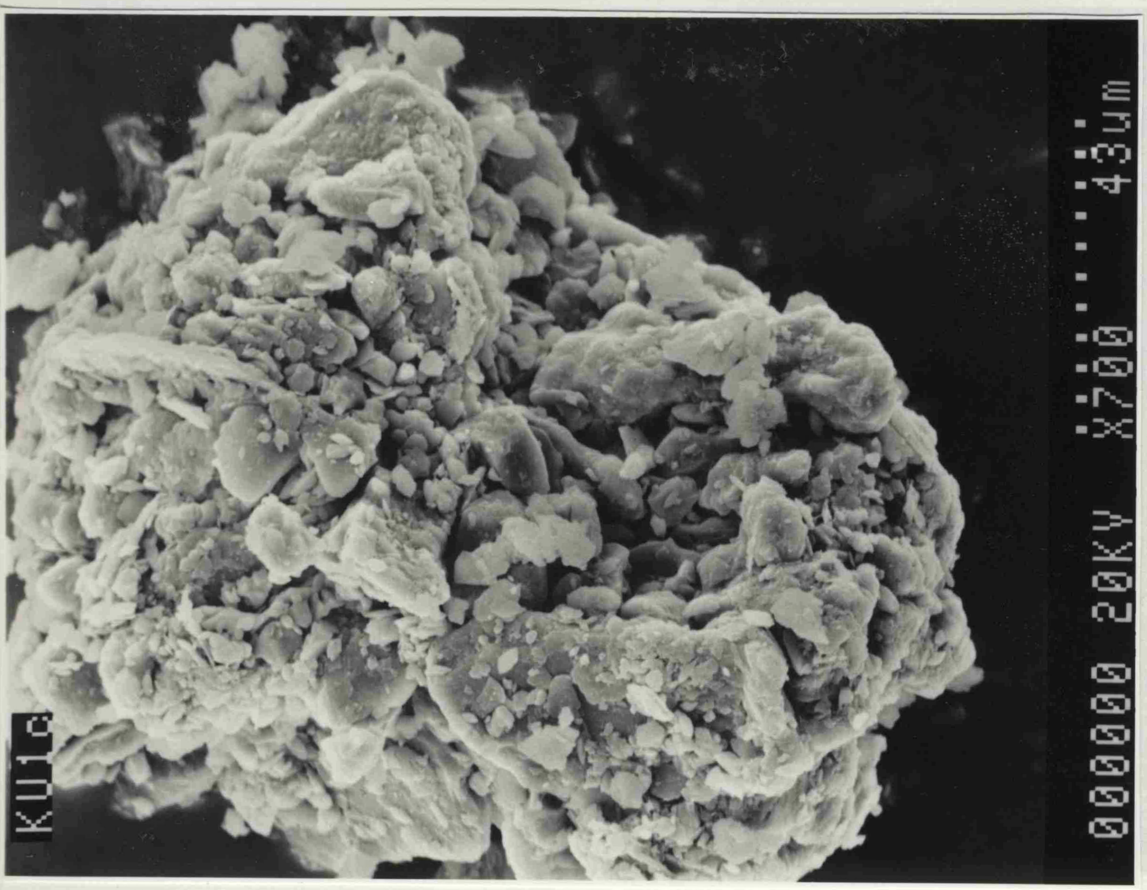

Plate 3.11 Kunlun Glacier: 80µm diameter aggregate of silt and clay size particles from the surface silt in the Kunlun Mtns.

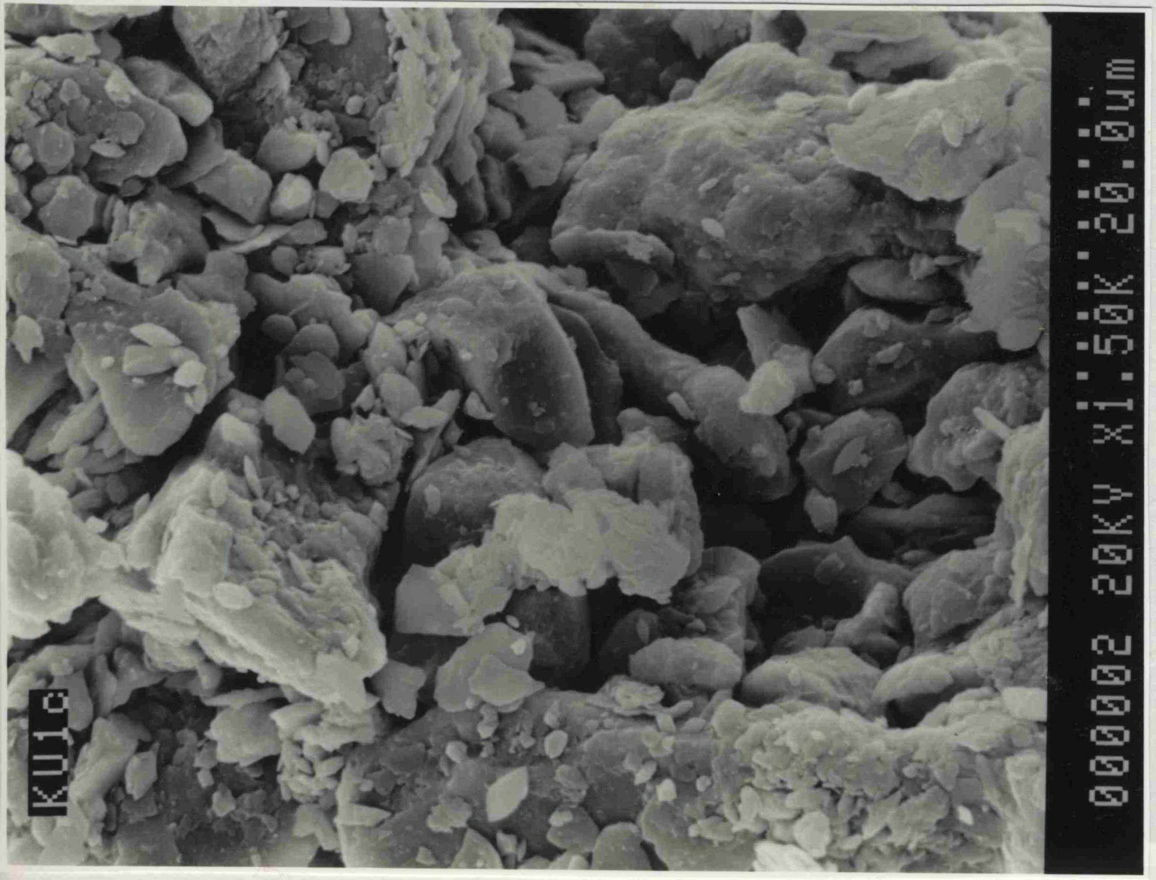

Plate 3.12 High magnification detail from plate 3.11 showing the presence of quartz, platy micas and clay adhesions.

Plate 3.13 Kunlun Pass: 200μm aggregate of silt particles.

Plate 3.14 Kunlun Pass: detail from an aggregate showing a large proportion of fine particles adhering to quartz grains.

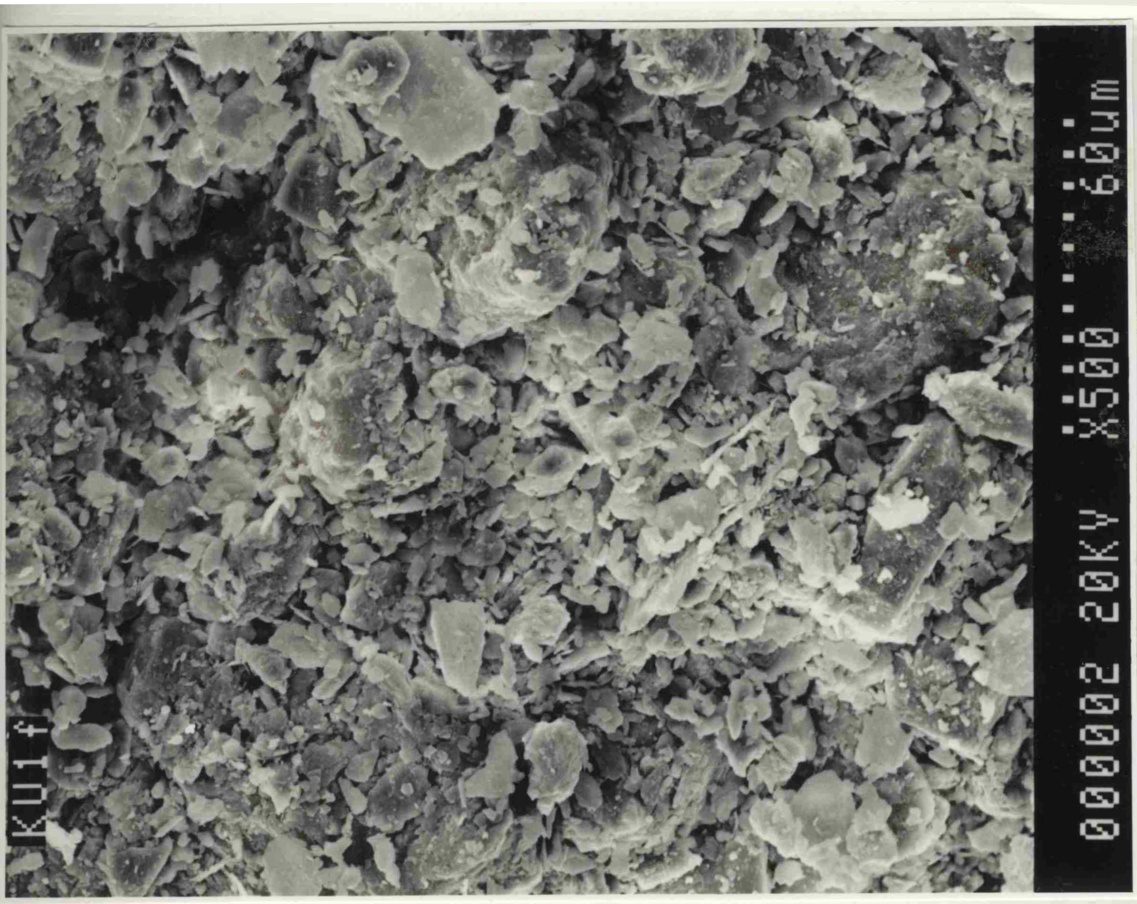

Plate 3.15 Kunlun Pass: detail from another aggregate - the relatively large size of the platy grains suggests that they may be micas.

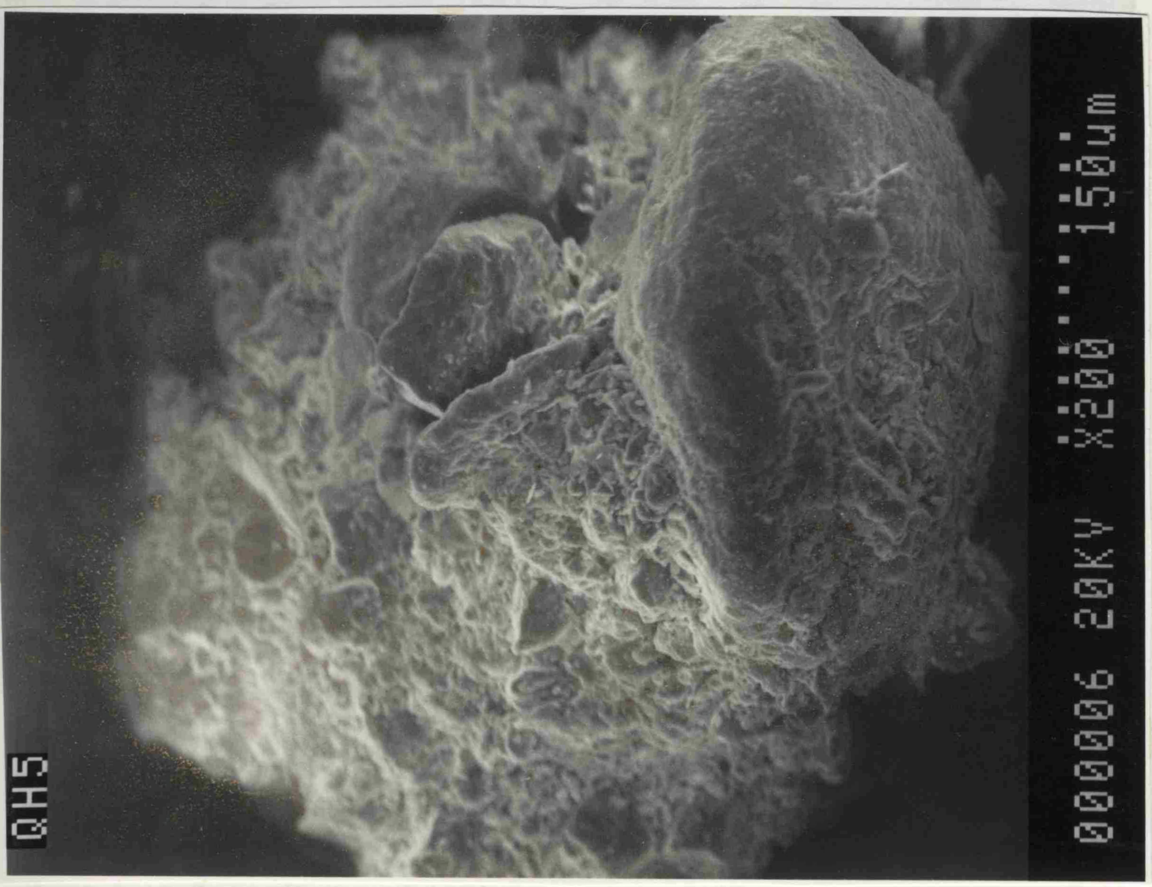

Plate 3.16 Qumar Heyan: 250μm diameter aggregate of fine grains from the surface of the Tibetan Plateau

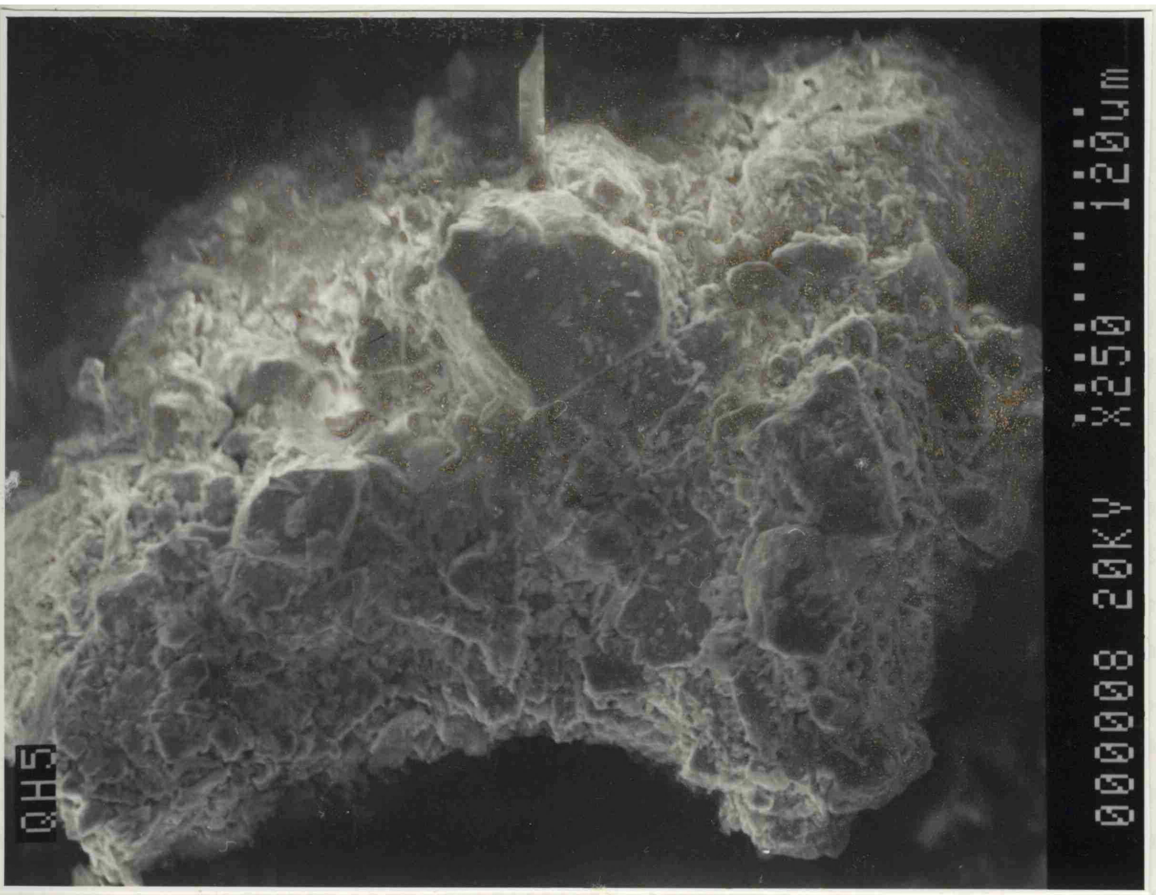

Plate 3.17 Qumar Heyan: 200µm diameter aggregate of fine particles.

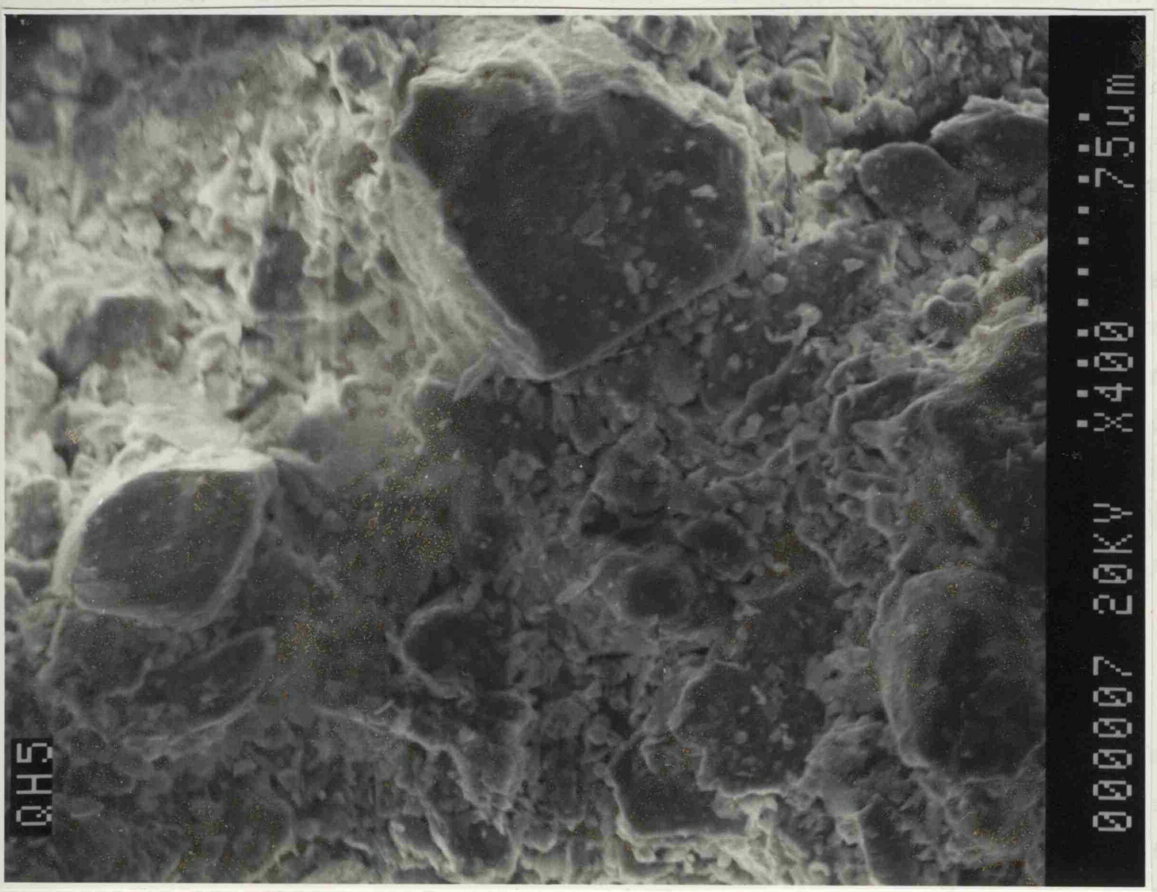

Plate 3.18 Qumar Heyan: detail from plate 3.17 showing large quartz grains and a high proportion of fine material.

3.3. Rare Earth Element Analysis

The abundance of the rare earth elements (REE), otherwise known as the lanthanide series of elements, is related to their atomic number, with rare earth metals with even atomic numbers more prevalent than those with odd atomic numbers. Most rare earth metals exhibit a trivalent state with ionic radii similar to that of Ca^{2+} and thus they replace calcium in a number of minerals *e.g.* apatites (Vinogradov, 1959). Some of the REE exhibit other valency states, for example Eu^{2+} and Ce^{4+}. Although cerium occurs as Ce^{3+} in continental sedimentary and igneous rocks it is apparently oxidised in seawater to Ce^{4+} which is highly insoluble (Piper, 1974) and often incorporated in Mn nodules (Chen *et. al.*, 1990). Thus Ce anomalies are common in marine sediments. Eu may occur as Eu^{2+} or Eu^{3+} in volcanic rocks. Eu^{2+} is relatively stable and resembles Sr^{2+}, thus occurring in strontium-rich plagioclase feldspars (Rankama and Sahama, 1950). However evidence suggests that throughout the sedimentary environment Eu exists predominantly in the trivalent state (Piper, 1974). REE content is higher in acidic rocks than in basic (Vinogradov, 1959).

Rare earth element (REE) analysis has been used as a geochemical fingerprinting technique to ascertain the petrological source of various sediments. For example, it has been applied to the stratigraphical identification of tephra layers found within loess profiles across Alaska and the Yukon Territory, Canada; and used to identify the source of the volcanic eruption (Westgate *et. al.*, 1985). REE geochemistry has been applied to loess deposits from America, China, Europe and New Zealand to show a general unity of composition (Taylor *et. al.*, 1983) and has more been recently applied to Chinese loess specifically to identify the probable source of the loess within the middle reaches of the Yellow River (Wen Qizhong *et. al.*, 1983; Wen Qizhong *et. al.*, 1985).

3.3.1 REE geochemistry of Chinese loess

Wen Qizhong *et. al.* (1983) compared REE concentrations of loess from Luochuan, in the middle Yellow River valley, with alluvium from the Hebei plain and wind-drifted sand from the Tengger desert. The concentration of REE oxides in the desert sand was a factor of 4 or 5 times lower than that of loess (see fig. 3.8) but the distribution patterns were similar and therefore the authors postulated that this was "probably indicative of the cognition of source material (Wen Qizhong *et. al.*, 1983, p. 85)". The alluvium gave anomalous neodymium (Nd) signals and therefore wasn't thought comparable. Following this study Wen Qizhong *et. al.* (1985) compared REE concentrations of loess and palaeosols from Luochuan with: a lacustrine sediment from Luochuan; a modern moraine from Xinjiang; a sample from the East China continental sea shelf; and a sample of oceanic crust. None of these sediments gave patterns similar to that of the loess.

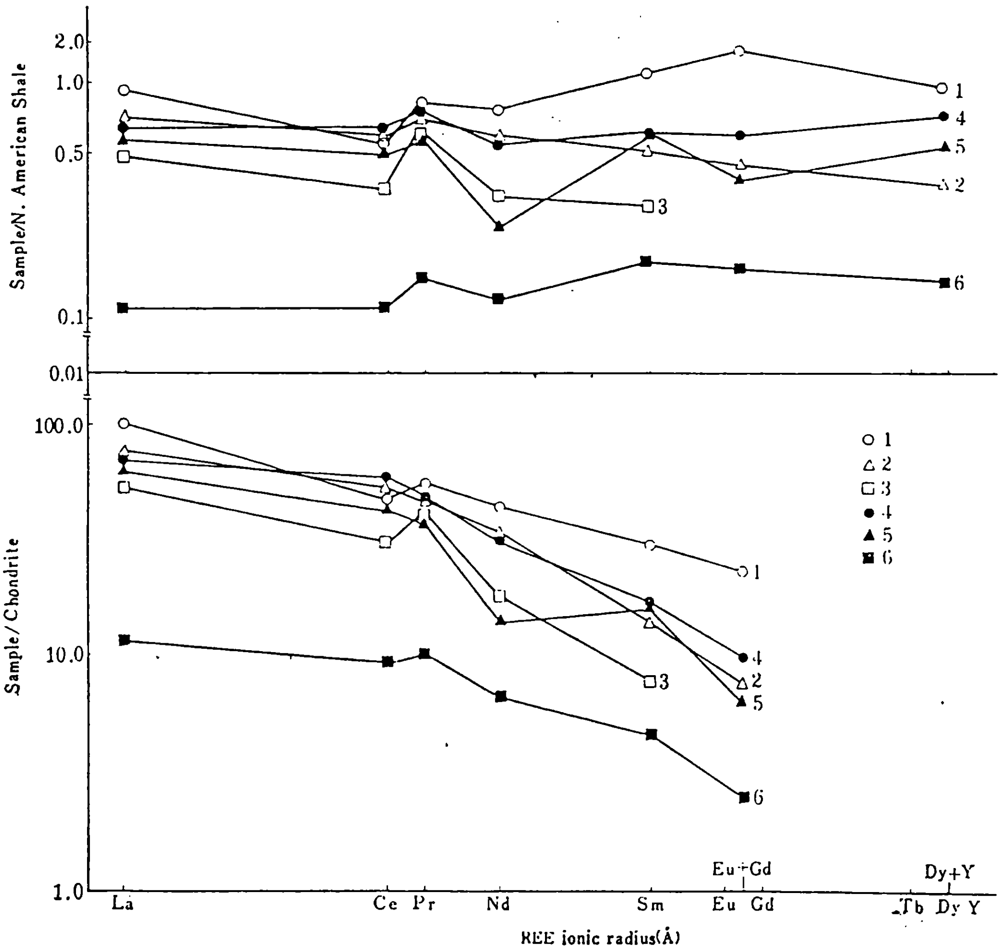

1. Malan loess; 2. Lishi loess; 3. Wucheng loess: 4. Holocene loess; 5. alluvium; 6. sand sample.

Figure 3.8 Rare earth element distribution pattern normalised to chondrite and North American Shale (NAS) for loess and other Chinese sediments. Wen Qizhong *et. al.* (1983).

Both Tian *et.al.* (in press), who studied differences between loess and palaeosols from Xinji section on the southern margin of the Loess Plateau, Shaanxi, and Wen Qizhong *et.al.* (1985) report higher REE abundances (ΣREE) in palaeosols than in loess although the pattern of abundance is similar suggesting that the REE consitituents are not affected by soil formation. The higher abundance of may be explained by the finer particle size of palaeosols than loess. Wen Qizhong *et.al.* (1985) argue that ΣREE is related to particle size, with >63μm fractions containing less ΣREE than finer fractions and with a majority of ΣREE held in particles less than 20μm in diameter. However, REE abundance is also related to mineralogy. Heavy minerals, such as zircon, garnet and apatite, have high REE abundances and extreme HREE enrichment, which may significantly affect the REE patterns in siltstones and sandstones (Taylor and McLennan, 1985). Quartz contains low REE, whereas mica, which contributes to the silt fraction has a higher REE abundance. In sand-size fractions, the presence of heavy minerals will have a marked affect on overall REE abundance: when they are removed the ΣREE decreases but the La/Yb ratios are raised (Taylor and McLennan, 1985).

It is worth noting that the analytical techniques used by Tian *et.al.* (in press) and Wen Qizhong *et.al.* (1982; 1985) to identify the abundance of REE (chromotography and neutron activation analysis) were different from those used in this study (atomic emission spectrometry), although they should give comparable results.

3.3.2 Laboratory procedure

Samples from each of the sites were prepared and run on the inductively-coupled plasma atomic emission spectrometer (ICPAES) in the Department of Geology at Leicester University. The following preparation procedure was adopted: about 0.5g of sample was finely powdered and ignited at 950°C for 1.5 hours to aid digestion. Following heating, the sample was placed into a PTFE beaker and damped down with a few drops of distilled de-ionized water. The damping with water is to prevent spitting when the HF is added. 15 ml of 40% HF (hydrofluoric acid) followed by 4ml of 67-70% $HClO_4$ (perchloric acid) was then added to each beaker and the beakers were placed on a hot plate at 180-200°C. After 3-4 hours, when the samples had been digested and the mixture had evaporated to incipient dryness, another 4ml of perchloric acid was added and the beakers left again to attain incipient dryness. This second stage of digestion ensures that any fluorides produced by the initial digestion are converted to chlorides or perchlorates and that all the HF is driven off (otherwise insoluble fluorides will be later precipitated and these scavenge REE's).

The digestion products are redissolved in 20ml of warmed (40-50°C) 25% HCl (hydrochloric acid) and made up to 50ml with distilled water. The solutions are then transferred to the ion-exchange columns.

For REE analysis strongly acidic cation exchange resins are used. In the Leicester laboratory the resin used is a Dowex AG 50W-X8(H), 200-400 mesh, which is a sulphonated gel-type polystyrene resin cross linked with 8% divinylbenzene. This is a finer grain size than standard resins, which are usually 20-50 mesh, as it allows for both slow flow rates and much cleaner group separations with smaller volumes of resin due to improved exchange kinetics. Dilute hydrochloric acid is used in the exhange column for separation of the REE's from other cations in the loess or sand samples. Using dilute HCl, the REE bearing fraction of the elutant also carries Ba^{2+}, Sr^{2+} and some Ca^{2+} but these can be corrected for relatively easily in the ICP analysis.

The ion exchange columns were topped up with 250ml 1N HCl, then the sample solutions were run through the columns by adding them to the dropping funnels above each column. When only 2-3cm remained above the top of the resin, 450ml of 1.7N HCl was added to the dropping funnel. When only 2-3cm remained 600ml of 4N HCl was added to the dropping funnels and the solution was collected in pyrex beakers which were rinsed with 10% HNO_3 (nitric acid). The solution in the beakers contained the REE from the samples plus Sr, Ba and some Ca. The solutions were then evaporated down to 10-15ml when 2ml concentrated HNO_3 was added. The addition of the nitric acid causes the REE's to precipitate as easily soluble nitrates rather than chlorides.

The samples were run on a Philips PV8050 Emission Spectrometer in batches of six including one standard. Inductively coupled plasma atomic emission spectrometry (ICPAES) is a destructive technique. Its sensitivity is due to the inductively coupled plasma excitation source in which argon gas, carrying the sample material is heated to 8000 K. At these temperatures atomisation occurs in which the atoms become highly excited and partly ionised, emitting a spectrum which is observed just above the plasma (figure 3.9). The REE emit complex spectra in the ICP, concentrated at wavelengths of 340-440nm (Thompson and Walsh, 1983). The large number of spectral lines emitted by the REE are characteristic, although with such an intense pattern problems of spectral overlap may occur. The precision achieved by the ICP analysis of REE is in the order of 1-2% (Thompson and Walsh, 1983).

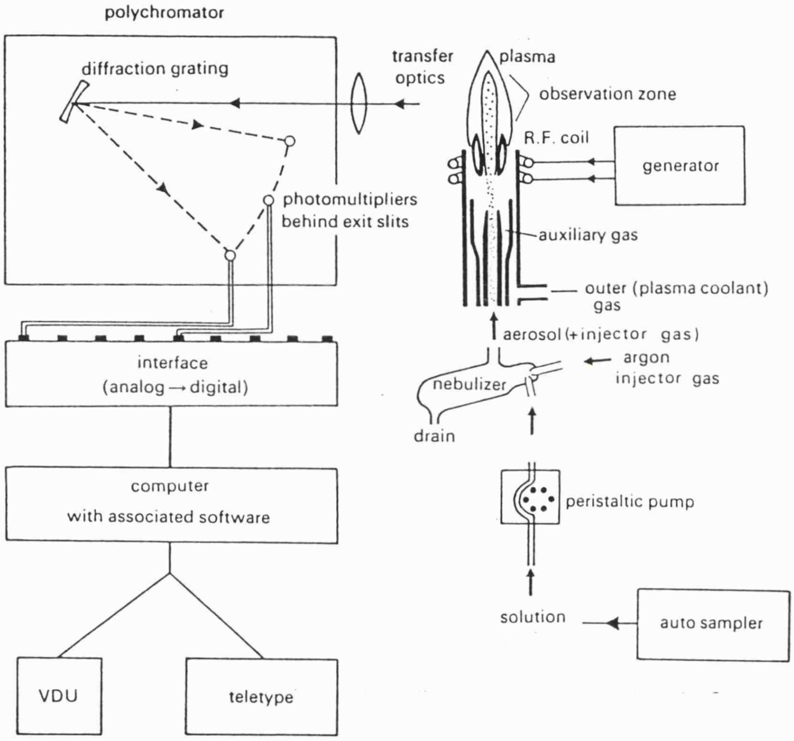

Figure 3.9 Schematic diagram of the ICPAES system (Thompson and Walsh, 1983).

3.3.3 Results

The rare earth elements obtained from the atomic emission spectrometer were run in two batches. Initially a pilot study involving two samples, one of Dawan loess (II) and one of silt from the Kunlun Pass were measured in Spring 1991. The similarity of the results from these samples led to a further nine being submitted for analysis, including samples from Labrang, Sala Shan, the Qaidam Basin and recent soil from 1.3 metres below the cultivated surface of a wheat field at Dawan. The measurement was carried out by Adelaide Holmes and Brian Dickie of the Geology Department of Leicester University.

The abundance of rare earth elements from these samples is presented in table 3.7. A check on the the performance of the atomic emission spectrometer was made by measuring a laboratory standard of known rare earth concentration ('standard' in table 3.7). The results of this standard from each batch of runs are labelled REE chk1 and REE chk2.

Table 3.7 Abundance of rare earth elements (ppm) in samples of silt and sand from the Tibetan Front

Sample	La	Ce	Pr	Nd	Sm	Eu	Gd	Dy	Er	Yb	Lu
Standard	20.0	40.4	4.0	20.2	4.0	2.0	4.0	4.0	4.0	4.0	0.4
REE chk1	21.4	40.9	5.3	19.7	4.3	2.2	4.7	4.0	4.1	4.1	0.4
Dawan	33.3	65.3	9.4	40.4	5.4	1.1	4.9	3.7	1.9	1.5	0.2
Kun Pass	31.4	61.6	9.0	37.4	5.1	1.0	4.7	3.0	1.8	1.2	0.2
REE chk2	20.5	39.5	3.0	9.5	5.8	1.6	-19.4	3.4	3.3	0.3	0.4
Golmud	19.1	35.8	5.3	21.4	2.9	0.9	6.9	2.9	2.5	1.2	0.2
Barchan	19.0	37.4	4.5	20.3	3.0	0.7	4.4	1.7	1.0	0.7	0.1
Glacier	29.0	55.6	7.7	29.3	4.7	1.2	8.8	3.8	3.1	1.6	0.2
Pingo	37.3	75.1	9.3	37.5	5.5	1.4	11.4	3.4	2.4	1.5	0.2
Qumar	20.3	39.9	5.5	21.4	2.9	0.8	6.0	2.3	2.1	0.9	0.1
Sala Shan	33.5	66.0	8.2	33.6	5.2	1.2	7.8	4.0	2.6	2.0	0.3
Labrang	5.8	11.3	1.5	5.8	0.9	0.2	1.8	0.8	0.7	0.3	0.05
Jiuzh'tai	30.6	59.8	7.8	30.8	4.9	1.2	8.1	3.9	2.8	1.8	0.3
Daw rsoil	32.0	63.0	8.0	32.8	4.9	1.2	7.9	4.0	2.8	1.9	0.3
shale†	41.0	83.0	10.3	38.0	7.5	1.61	6.34	5.5	3.75	3.53	0.61
chondrite§	0.33	0.86	0.11	0.63	0.20	0.07	0.27	0.34	0.23	0.22	0.03

† an average concentration of REE (ppm) in shales from North America, Europe and the Soviet Union (Haskin and Haskin, 1966)
§ an average of 10 ordinary chondrites (Nakamura, 1974)

Differences between the two REE runs are evident from the REE standard checks. The first batch of runs gave anomalous Pr results whereas the second batch of runs involving nine samples showed anomalous Pr, Nd, Gd and Yb results, probably a result of spectral interference, and thus these elements were omitted from figures 3.10 to 3.13. As a result of this difference the two batches of runs are plotted separately.

Chondrite normalised REE patterns for Tibetan Front sediments are shown in figure 3.10 and figure 3.11. They are all enriched in LREE (light rare earth elements: La-Sm) and the Dawan loess and Kunlun Pass silt show negative Eu anomalies (Eu/Eu*; table 3.8). No Ce anomalies were observed in these sediments. The LREE of the nine batch run (figure 3.11) appear to be arranged into three groups, with silt from the Kunlun Mountains, Sala Shan, Dawan recent soil and Jiuzhoutai loess II forming one group with high LREE abundances. The sand samples from the Qaidam Desert and the Kunlun barchan dune field form another group with silt from the surface of the Tibetan Plateau at Qumar Heyan. The LREE of this 'sand' group is less abundant than that of the 'silt' group by a factor of 1.5-2. The loess from Labrang is particularly interesting in that although the shape of the REE pattern is consistent with that of the other samples, the concentration of REE is 5.5 to 6 times lower. The HREE (heavy rare earth elements: Gd-Lu) distributions follow similar patterns, with the 'silt' samples retaining a higher elemental abundance than the 'sand' (and Qumar Heyan) samples except for the pingo sample which has similar Er and Yb concentrations to the Qaidam Basin sand sampled from near Golmud. The barchan dune sand shows a low Er concentration. The Dawan loess and Kunlun Pass silt samples (figure 3.10) show REE patterns comparible of the 'silt' group (figure 3.11).

Figure 3.12 and figure 3.13 show REE patterns for the samples normalised to shales which are more indicative of REE abundance from terrestrial sediments. Both Dawan loess II and the Kunlun Pass silt (figure 3.12) show positively sloped REE patterns from Ce-Nd with Dawan loess II showing a positive Nd peak slightly above the shale value. All the other elements show a decreased abundance with respect to that of the shale. The shale-normalised patterns for the other sediments (figure 3.13) reflect the three groupings found with the chondrite-normalised patterns.

All of the samples tested showed a lower REE abundance than that of the shale composite. This 'European' shale composite was used instead of the North American Shale Composite (NASC; Gromet *et.al.*, 1984) or the Post-Archean Average Australian Sedimentary Rock (PAAS; Nance and Taylor, 1976) as it was though to be more representative of the crustal average over China.

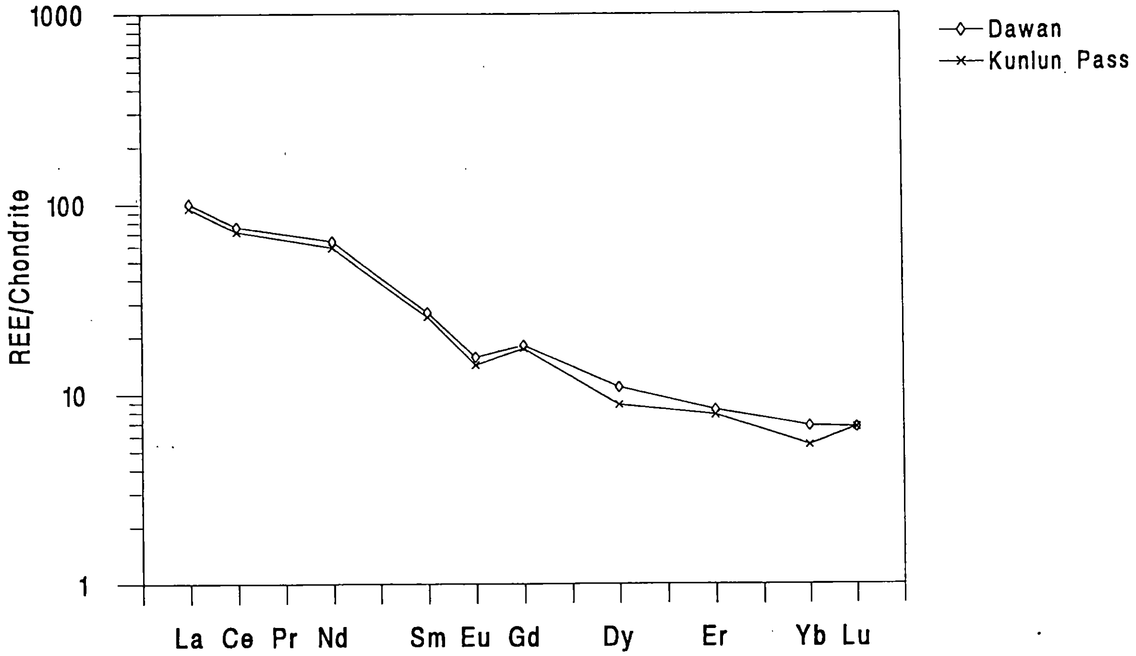

Figure 3.10 Chondrite normalised REE distribution for Dawan loess II and silt from the Kunlun Pass.

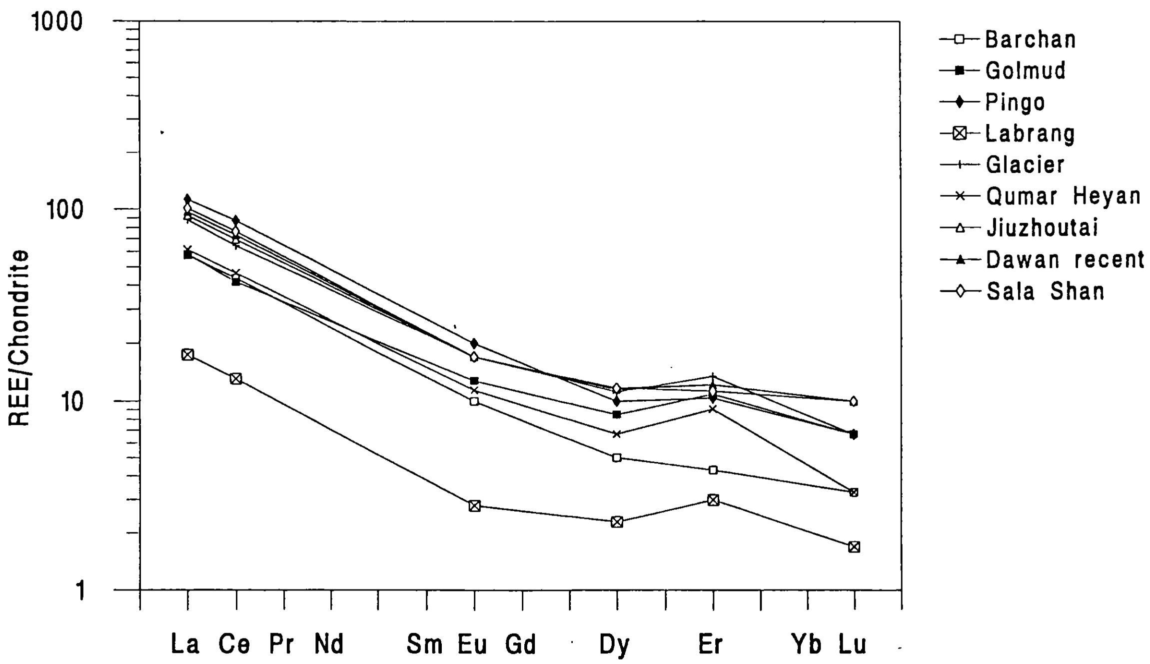

Figure 3.11 Chondrite normalised REE distribution pattern for the other nine sediments from the Tibetan Front.

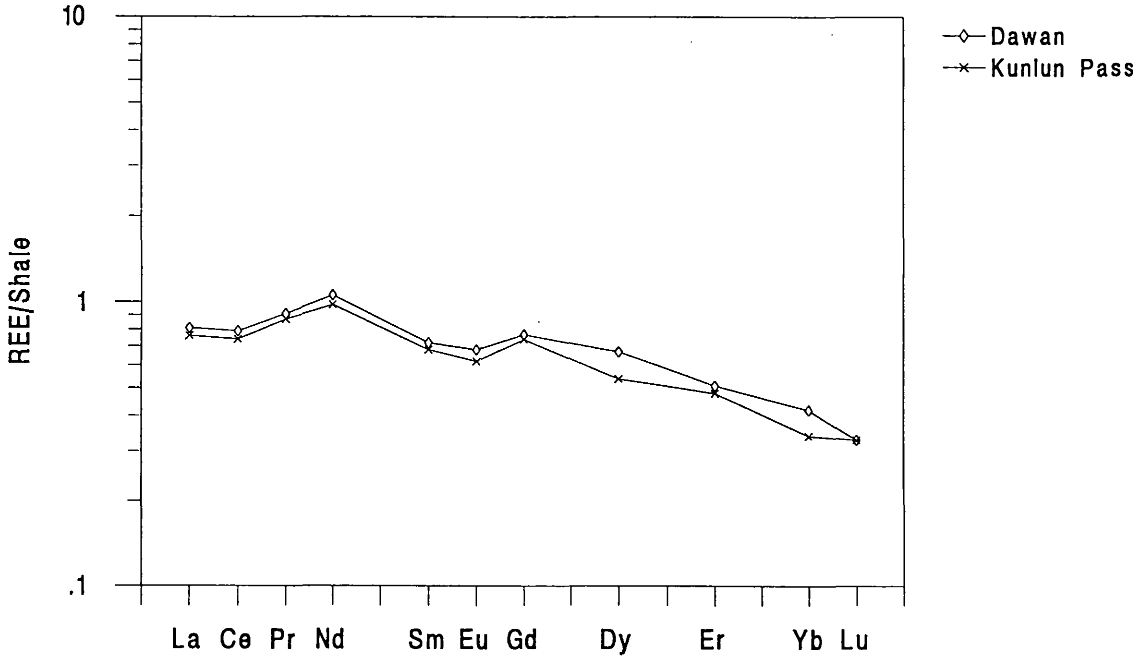

Figure 3.12 Shale normlised REE distribution pattern for Dawan loess II and Kunlun Pass silt.

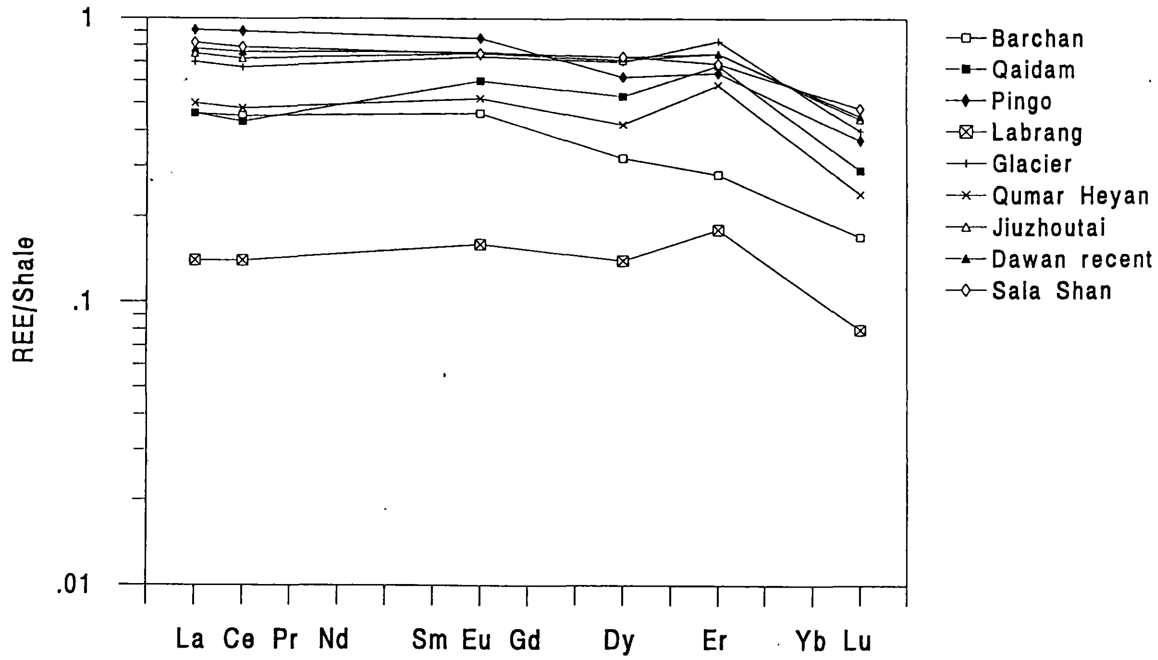

Figure 3.13 Shale normalised REE distribution patterns for the other nine sediments from the Tibetan Front.

3.3.4 Summary of REE

Due to the spectral interference problems associated with the runs, comparison of ΣREE from these Tibetan Front sediments with other published data has not been possible. The standard used here has a ΣREE of 103ppm. Using this batch#1 gave 111ppm and batch#2 67.9ppm. Despite these problems differences in rare earth abundances are still evident (figures 3.11 and 3.13). The lower abundances shown by the sand samples may be explained by the coarser particle size or by differences in mineralogy. Whilst it is theoretically possible to overcome some of this uncertainty by comparing the REE from a set grain size obtained from the Tibetan Front sediment, it ~~is~~ was not undertaken as the particle sizes of the barchan dune sand did not overlap with any of the silt sized samples (see section 3.1 and appendix I).

The uniformity of composition of loesses from different regions of the world has been documented (Taylor *et.al.*, 1983). The presence of mica in the sediments of Qarhan Lake in the Qaidam Basin (Chen and Bowler, 1986) suggests that it may be present in the surrounding mountain environment. Both mica and plagioclase feldspars (containing Eu^{2+}) have been found in Jiuzhoutai loess (Derbyshire *et.al.*, 1987) and scanning electron microscopy carried out here shows that mica is present in Dawan loess (plates 3.2 and 3.3). Zhang Jing *et.al.* (1990) report that, across the Loess Plateau, heavy minerals account for 5-10% of loess, in which zircon and apatite are quite common. Wen Qizhong *et.al.* (1987) found that the majority of heavy minerals in Luochuan loess were concentrated in the silt fraction.

The barchan dune sand is probably depleted in REE due to the complete absence of fine material <63µm. The different particle size characteristics of the Qaidam Desert sand and the barchan dune sand (shown in section 3.1.2.4) probably account for the higher REE abundances in the Qaidam Desert sand, which contains 6.5% of particles <63µm. The sample from Qumar Heyan on the Tibetan Plateau has a lower REE content than those of the Kunlun and Lanzhou silts despite containing 46.3% of particles less than 20µm, therefore it is possible to argue that the source of this silt may be of a lower REE content rock than that of the Kunlun Mountain silt. The extremely low REE content of the Labrang loess could be due to dilution of sedimentary carbonate minerals which have low REE abundances (Chen *et.al.*, 1990) although this is unlikely as the quantities of carbonate needed to dilute the REE at Sala Shan to the level of Labrang REE would be great. Alternatively, the low ΣREE suggests that Labrang loess derives from a different source than the Loess Plateau silt and is most probably formed within the local mountain environment from a low ΣREE content rock. The similarity of the Sala Shan loessic alluvium to the loess from the Lanzhou sites suggests that it derives from the same source.

Eu/Eu* depletion values (where $Eu^* = [(Sm)_N \times (Gd)_N]^{1/2}$ and N stands for chondrite normalised) were available only from the Kunlun Pass (0.68) and Dawan loess (0.71), due to the anomalous Gd signal in the second batch of samples. These results compare favourably with the Eu/Eu* values of 0.63-0.72 derived for loesses from America, Europe, New Zealand and Nanjing (Taylor et.al., 1983). In wet humid environments Eu^{3+} may be reduced to Eu^{2+} which would be leached out in preference to other rare earth elements increasing the Eu depletion, however the similarity of Eu/Eu* in loess and palaeosols suggests that this did not occur on the loess plateau (Wen Qizhong *et.al.*, 1985).

Values of $(La/Yb)_N$ (where $(La/Yb)_N = [(La/Yb)_{sample} / (La/Yb)_{chondrite}]$) were also only available for the Kunlun Pass and Dawan samples. These results, Kunlun Pass = 17.5 and Dawan = 14.8, were significantly higher than those of Taylor *et.al.* (1983) who found $(La/Yb)_N$ = 7.8 to 11.7 for a variety of loesses. They are also higher than the upper crustal average, documented at 9.3 (Taylor and McLennan, 1981). This indicates that the source rocks may have a higher $(La/Yb)_N$ than the crustal average. REE distributions derived from igneous rocks from the Ulugh Muztagh area of northern Tibet (36°28'N, 87°29'E), in the Kunlun Mountains 600km west of the Kunlun Pass, have been found to give high primary $(La/Yb)_N$ ratios of 10.7 to 35.7 (McKenna and Walker, 1990). The shape of the chondrite normalised REE distributions obtained from these rocks were similar to the results obtained here for Tibetan Front sediment. Of particular interest were the results from potassium-poor rocks which gave decreased REE abundances in the order 2.8-3.5 times lower than the extrusive and intrusive igneous rocks, although the distribution pattern remained the same. The sample from Labrang showed a REE pattern consistent with that from the other Tibetan Front samples but 5.5-6 times less abundant.

It is possible to directly compare the REE signature from the Dawan and Kunlun Pass samples with the the results of Wen Qizhong *et.al.* (1983; 1985) and Tian *et.al.* (in press) for loess from Shaanxi Province which encompasses the central Loess Plateau (table 3.9). Luochuan is located north of Xian in the big bend of the Yellow River (see figure 1.6) whereas Xinji lies southwest of Xian in the southern margins of the Loess Plateau. The Kunlun Pass and Dawan samples have been chosen as they pose fewer problems with spectral interference than the other Tibetan Front samples. The Xinji data are an average of seven Malan and Lishi loess samples (Tian *et.al.*, in press) and the Luochuan data are an average of ten Malan, Lishi and Wucheng loess samples (Wen Qizhong *et.al.*, 1985). The LREE of the samples from the Tibetan Front compare favourably with both the Luochuan and Xinji loess with the exception of cerium which is more abundant in the Xinji loess. The distribution of HREE, however, shows a markedly greater abundance in the Luochuan and Xinji loess. Whilst this apparent dissimilarity between the sediments of the Tibetan Front and those of the central Loess Plateau is worth noting, further work is needed before any conclusions may be reached. It is possible that a variation in source area of these sediments may account for the higher HREE abundances in the central Loess Plateau or that there is a greater abundance of heavy minerals such as zircon, garnet and apatite within the central Loess Plateau as they are enriched in HREE (Taylor and McLennan, 1985).

The wind drifted sand sample from the Tengger desert (Wen Qizhong *et.al.*, 1983) showed a very low REE abundance which is considerably lower than that of the sand from the Qaidam Desert and barchan dune field (table 3.7).

Table 3.8 Comparison of REE distribution of samples from Dawan and the Kunlun Pass with published results of REE from Luochuan loess* (Wen Qizhong *et.al.*, 1985), Xinji loess (Tian *et.al.*, in press) and Tengger desert sand† (Wen Qizhong *et.al.*, 1983).

Sample	La	Ce	Pr	Nd	Sm	Eu	Gd	Dy	Er	Yb	Lu
Dawan	33.3	65.3	9.4	40.4	5.4	1.1	4.9	3.7	1.9	1.5	0.2
Kun Pass	31.4	61.6	9.0	37.4	5.1	1.0	4.7	3.0	1.8	1.2	0.2
Luoch*	31.9	62.4	-	41.3	6.2	1.2	-	-	-	2.7	0.5
Xinji	39.0	83.1	-	37.6	6.7	1.3	5.9	-	-	2.7	0.5
Tengger†	3.4	7.7	-	1.2	3.9	-	-	-	-	<1.0	<1.0

3.4 Discussion

Chinese scientists have long believed that the source of the central Chinese loess is the gobi and sand deserts to the north and northwest. The processes by which the constituent silt particles are formed has not been frequently addressed, although Whalley *et.al.* (1982a; 1987) believe that aeolian attrition within desert storms could produce sufficient silt-sized material. Recently Bowler *et.al.* (1987) proposed a mountain source for some of the Chinese loess with silt produced within the Kunlun Mountains deflated from the Qaidam Basin and carried by the dominant northwesterly winds to the western part of the Loess Plateau. The evidence presented here suggests that this is indeed a viable hypothesis. Silt is readily available within the Kunlun Mountain system, formed by both glacial action and freeze thaw processes, and the presence of high altitude aeolian duneforms indicates the necessary transport processes. The presence of a widespread silt cover blanketing the surface of the Tibetan Plateau also testifies to the ongoing prevalence of silt producing mechanisms within this vast region, probably dominated by freeze thaw processes. The Plateau surface may also act as a high altitude sediment trap for silt produced within the mountain ranges rising above the Plateau, such as the Tanggula and A'nyêmaqen ranges, as well as the Kunlun, Karakorum and Himalayan ranges which fringe the Plateau.

The Qaidam Basin, as well as acting as a sediment trap for silt produced in the mountains to the north (Qilian) and south (Kunlun), may itself contribute to silt production by salt weathering processes acting on alluvial fans emanating from the actively rising mountain front, conforming to the favourable conditions proposed by Pye and Sperling (1983). The extensive salt flats of the Qaidam Basin contain mirabilite which, when linked with the large temperature gradient present in the highest sand desert on earth (with a mean January temperature of -10°C; and a July mean of 25°C, Bowler *et.al.* (1986)), would produce an effective environment for salt weathering. Mirabilite is also present in the salt lakes on the northern Tibetan Plateau (see figure 2.5). The Qaidam Basin contains areas of shifting and half-fixed sand dunes resting on gravel gobi (Zhao Songqiao, 1986) which may also contribute to the production of silt via aeolian attrition in desert storms. Thus it is likely that the silt particles which form the loess have been formed by a variety of processes.

REE geochemistry of the samples suggests that there is a relationship between the source rocks of the Kunlun Mountain silt, Lanzhou loess and Sala Shan alluvial loess. The ratios of $(La/Yb)_N$ for the Kunlun Pass silt and Dawan loess samples gave values higher than the crustal average. Rocks of high $(La/Yb)_N$ have also been reported from northern Tibet in the Ulugh Muztagh area of the Kunlun Mountains (McKenna and Walker, 1990).

The Sala Shan site lies in the plains at the foot of the A'nyêmaqen Mountains (which form the edge of the Tibetan Plateau) on the Ba Xie, a second order tributary of the Yellow River. The Yellow River rises near Ngoring Lake on the Tibetan Plateau, an area thought to have been covered at some stage in the Pleistocene by an ice cap at least 50000km² (Shi Yafeng *et.al.*, 1991), and passes to the north of Sala Shan. As stated above, the volume of silt produced by this Yellow River ice sheet is not verifiable at present. The Ba Xie river rises on the piedmont of the A'nyêmaqen foothills and runs into the Tao River just east of Sala Shan. The REE abundance suggests that the loessic alluvium is composed of reworked loess from the western Loess Plateau and is not a result of silt produced from the A'nyêmaqen Mountains. This proposition is based upon the similarity of REE signature to that of the Loess Plateau samples and the disparity between the Sala Shan and Labrang samples.

The silt sample from the surface of the Tibetan Plateau at Qumar Heyan had REE distributions similar to the results obtained from the Loess Plateau and Kunlun Glacier samples: the abundances of each element were lower, although not as low as the Labrang loess which also had a similar distribution pattern.

According to the model of Bowler *et.al.* (1987), silt deflated from the Qaidam Basin is transported to the Loess Plateau by the northwesterly winds eminating from the Mongolian-Siberian high pressure system. However, it is unlikely that the constituent particles which comprise the huge area of loess covering 273,000km² derive from one source alone. Figure 3.14 summarises the various source areas which could contribute silt to the Loess Plateau and the mechanisms of silt formation. Transportation of the silt from its source is discussed by Middleton *et.al.* (1986) who propose a theoretical model of geomorphological environments from which substantial deflation of silt would occur (figure 3.15) many of which are present in this area of the Tibetan Front.

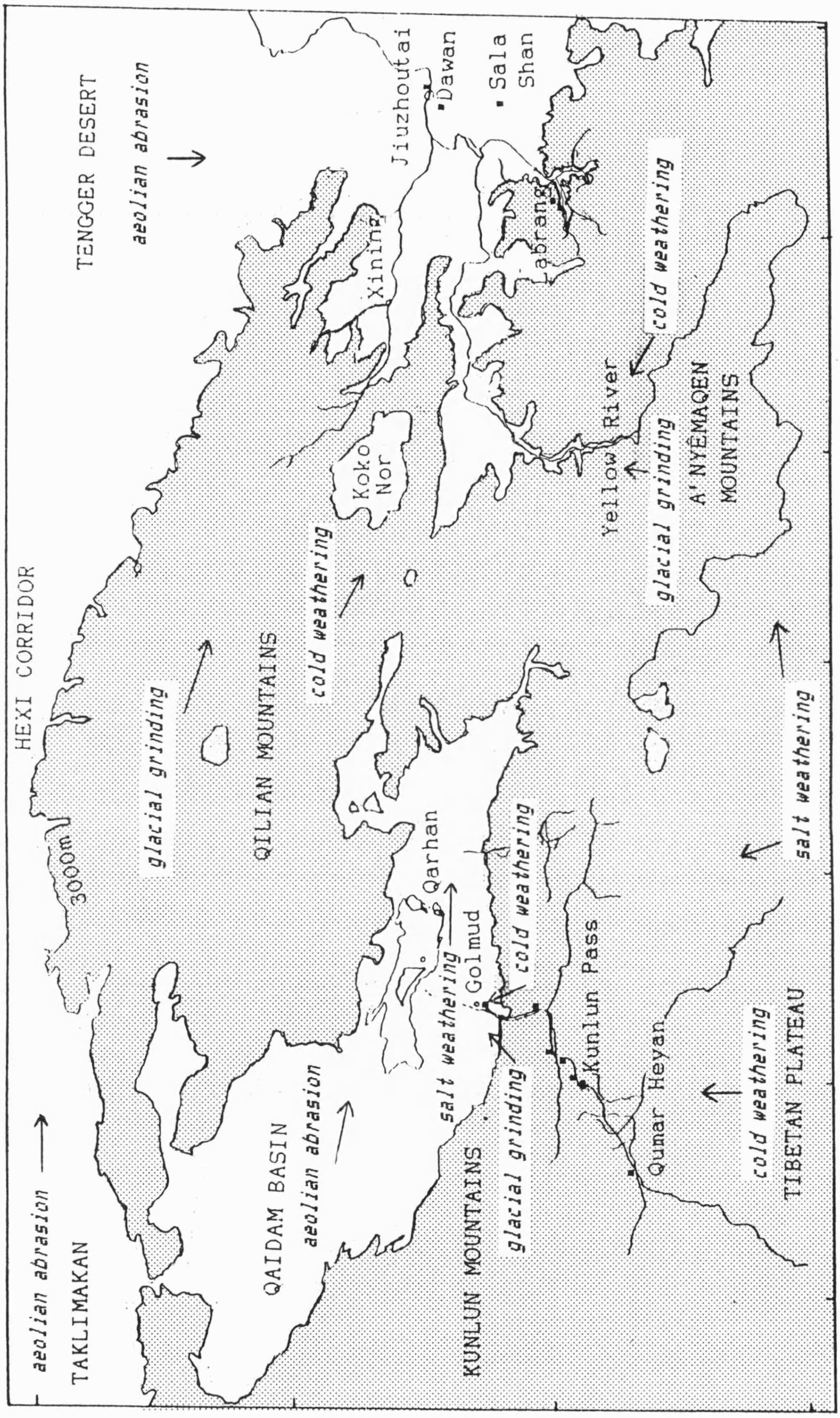

Figure 3.14 Possible mechanisms of silt production across the Tibetan Front

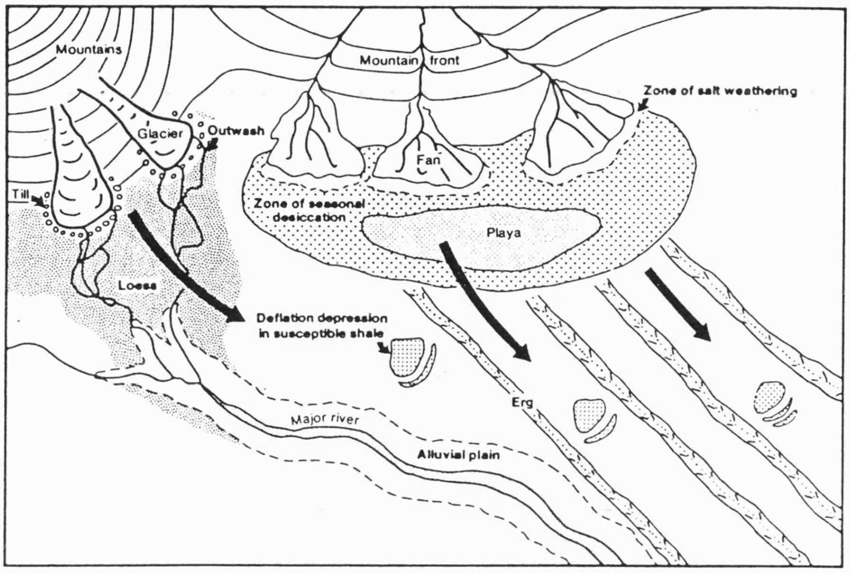

Figure 3.15 A model of geomorphological environments from which substantial deflation occurs (Middleton *et. al.*, 1986).

Sandstorms within the desert regions, which produce aeolian abrasion are frequent. For example, in the south of the Taklimakan Desert, one third of the year is shrouded in dust and sandstorms; and in Minqin, on the margin of the Tengger Desert, dust storms occur 148 days of the year (Zhu Zhenda, *et. al.*, 1986). The sands which make up the Taklimakan and Qaidam Deserts were formed by erosion of alluvial fans eminating from the Kunlun Mountains (Zhu Zhenda *et. al.*, 1986) and are thus liable to contain a REE signature similar to the Qaidam Desert and Kunlun barchan sand, that is the pattern of REE abundance would be similar to the mountain-produced silt but with lower total abundance due to the coarse particle size. As sand contains a lower REE signal than finer particles, silt sized chips produced by aeolian abrasion would also contain a lower REE signal than silt derived directly from the mountain source. Thus it may be possible to assess the contibution of 'primary' mountain silt and 'secondary' sand-derived silt to the loess plateau if it is assumed that the mineralogy between the sites remains constant and that the quantities of micas, in particular, remain fairly low. A predominance of desert sand-chipped silt would lead to a lower ΣREE than a predominance of mountain derived silt. If this is upheld for the Lanzhou loess, the input of Kunlun mountain silt dominates that of Tengger and Taklimakan aeolian abraded silt.

The uplift of the Kunlun Mountains and northern Tibetan Plateau would, by implication, have a direct effect upon the formation of the constituent silt of the Chinese Loess Plateau. According to Zheng Benxing (1991) the Kunlun Mountains were widely glaciated in the Middle Pleistocene with glaciation less extensive in the Late Pleistocene due to increasing aridity. Therefore, if a large proportion of the silt component of the Loess Plateau were formed by glacial processes alone, the Middle Pleistocene Lishi loess would be the most extensive. Early Pleistocene Wucheng loess would not exist in this case, as Zheng Benxing (1991) argues that the low altitude of the mountains at that time (<2000m) inhibited extensive glaciation. The presence of loess within the Kunlun Mountains at Pulu, with associated TL dates suggesting that the deposition began about 70ka (Li Baosheng *et.al.*, 1988), indicates that during the Late Pleistocene substantial quantities of silt were produced in the mountain environment. The present observations of silt blanketing large areas of the northern Tibetan Plateau and Kunlun Mountains, together with the evidence from Pulu, suggests that the highly active geomorphic environment in this region has continued to produce silt throughout the Late Quaternary and Neogene despite the variations in palaeoclimate.

4. MAGNETIC MINERALOGY I : LOW FIELD BEHAVIOUR

4.1 Magnetism

Magnetism is the result of the rotation of electrons about the atomic orbitals of an ion and the spin of the electrons about their own axes. The magnetic behaviour of a substance will depend upon the combination of electrons in its atomic orbitals which, in turn, is a result of crystal shape and the spin state of the electrons.

4.1.1 Types of magnetic behaviour

Materials that can only acquire an induced magnetisation in the presence of an applied field, the magnetisation being lost once the field is removed, are either paramagnetic or diamagnetic. Paramagnetic minerals have unpaired electrons and thus acquire a net magnetisation in the direction of the applied field due to a combination of orbital rotation and unpaired electron spins in the atoms of the material. The intensity of acquired magnetisation is proportional to the strength of the applied field. Common paramagnetic substances include olivine, biotite and clay minerals. Diamagnetic substances, which have no unpaired electrons and therefore no net spin moment, acquire a magnetisation in the opposite direction to the applied field due to the partial alignment of the electron orbits. These include quartz and calcite.

The first transition metal series of elements, which contain unpaired 3d orbital electrons, acquire spontaneous magnetisation due to electron spin coupling performed by exchange reactions between adjacent atoms in molecular crystal lattices. For example, non-metal ions such as oxygen perform exchange reactions between their p-orbitals and the d-orbitals of the metal. Within transition metal complexes, the ligand field within the lattice quenches the orbital motions of electrons leaving the spin moments alone to contribute to the net magnetisation. Transition metal complexes can exhibit ferromagnetism, antiferromagnetism and ferrimagnetism.

Ferromagnetic materials exhibit a spontaneous spin alignment of unpaired electrons producing a high magnetic moment. This strong magnetisation is retained in the absence of an applied field and at temperatures below the specific Curie point of that substance. Above the Curie temperature, thermal agitation causes disordering of the spin alignments and the material becomes paramagnetic, with a subsequent decrease in net magnetisation. Once the temperature has fallen below the Curie temperature the substance reverts to being ferromagnetic.

Antiferromagnetic materials have aligned but antiparallel moments forming layers within the crystal lattice, resulting in a net magnetisation of zero (fig 4.1). Imperfect antiferromagnetism occurs if the antiparallel layers of the lattice are not exactly uniform, due to either lattice distortion, low crystal symmetry, or the presence of defects. The imperfect alignment results in a small net spontaneous magnetisation. Antiferromagnetism is destroyed at the Néel temperature, above which the material behaves paramagnetically.

Ferrimagnetic substances exhibit spontaneous magnetisation as a result of unequal antiparallel aligned spin moments. A common example of a ferrimagnetic substance is one in which two cation valency states occur in unequal proportions.

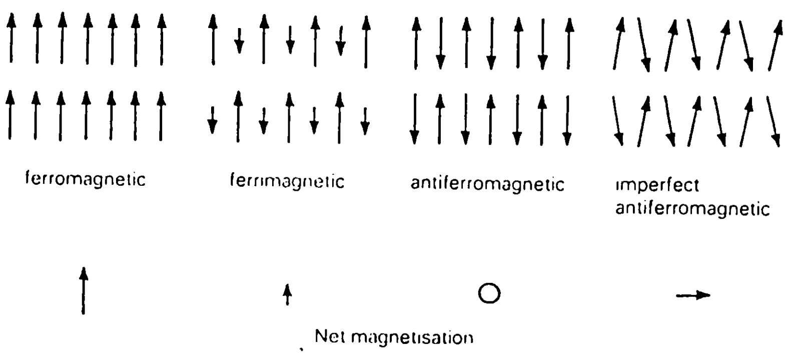

Figure 4.1 Arrangement of magnetic moments in ferromagnetic, ferrimagnetic, antiferromagnetic and imperfect antiferromagnetic materials (Tarling, 1983)

4.1.2 Magnetic anisotropy and domains

Within a crystal lattice there are 'easy' axes along which it is easier for a substance to become magnetised, in either direction, than in others. These different magnetisation axes are a result of magnetocrystalline anisotropy, which varies according to crystal structure and composition.

Although ease of magnetisation differs, the saturation magnetisation is the same for all of the axes. Imperfect antiferromagnetic minerals, such as hæmatite and goethite have high coercivities as a result of their magnetocrystalline anisotropy (Thompson and Oldfield, 1986; coercivity is defined as the field required to reduce the magnetisation of a grain to zero). In small single domain grains, in the presence of an external field the magnetisation of each grain will be along the easy axis that has a component of the applied field along it. As the grain grows, magnetocrystalline anisotropy still operates. However, the grain is also affected by magnetostatic interactions between the poles that form on the surface of the grain. The larger the grain, the greater the magnetostatic interaction. Magnetostatic forces are affected by the shape of the grain. For example, in a needle-shaped grain the 'easy' axis is situated along the needle length so that the surface poles occur at the points of the needle. The magnetic poles are thus further apart in a needle-shaped grain than a cubic one, with a subsequent lower magnetostatic energy. This is known as shape anisotropy. Strain anisotropy is the result of magnetostriction which occurs due to internal strain caused during the application of a magnetic field. The size of the grain alters during magnetostriction.

In a large grain, magnetostatic attraction between the surface poles of a grain becomes so large that the alignment of lattice spins alters to reduce the attraction and thus increase equilibrium and reduce internal energy. Under these conditions a Bloch wall is formed separating two domains of antiparallel spin moments (figure 4.2). The domains become orientated in such a way that the magnetostatic forces on adjacent domains are reduced by mutual interaction (Tarling, 1983). As grain size increases, domains will continue to form until it becomes energetically unfavourable to create a further domain (Bloch) wall. Thus the resulting domain structure represents a balance between magnetostatic energy and the domain wall energy (Halgedahl, 1987). Domain walls are some 0.1µm thick, while the domains may be 0.1-0.05µm in magnetite and up to 1.5µm in hæmatite (Tarling, 1983).

Single domain grains may be subdivided into stable single domain (SSD) and superparamagnetic (SP), where SP grains are single domain grains which are so small that thermal vibrations destroy any spin alignment upon removal from a field. The threshold size between SP/SSD has been documented at 0.035-0.050μm for magnetite (Dunlop, 1973) and 0.03μm for hæmatite (Tarling, 1983). Between SD and multidomain (MD) grain size there is a range of grain sizes where a 'mixed' magnetic behaviour is observed: the pseudo-single domain (PSD) range (Hartstra, 1982). PSD particles are essentially large grains in which lattice defects in the structure act as a trap for domain walls, and thus zones of the grain will behave as if they were SD (Tarling, 1983). For equidimensional magnetite the threshold for the SD-PSD transition is thought to be ~0.1μm and the PSD-MD transition is between 10-20μm (King et.al., 1982).

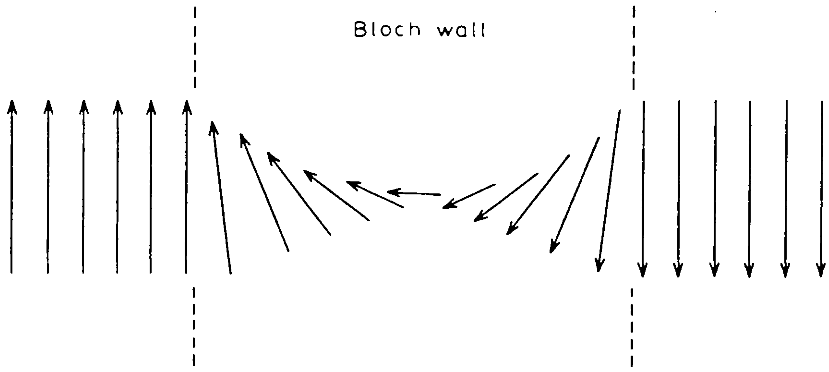

Figure 4.2 Diagram of a domain or Bloch wall showing the canting of spins between two domains of opposite spin alignment (Tarling, 1983).

4.1.3 Magnetic Mineralogy

Naturally occurring remanence bearing minerals present in sediments belong to either the FeO-TiO_2-Fe_2O_3 ternary series (figure 4.3) or to the iron hydroxide, iron carbonate or iron sulphide groups. Within the ternary series the principal minerals can be divided into two groups on the basis of their structure. The magnetite-ulvöspinel solid solution series (including maghæmite) exhibit a cubic spinel structure, whereas the hæmatite-ilmenite solid solution series exhibit a rhombohedral corundum structure and are weaker magnetically.

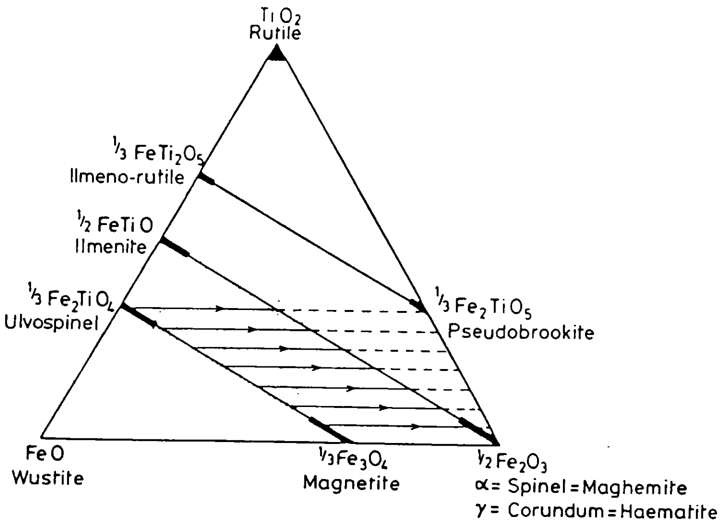

Figure 4.3 Ternary diagram for iron-titanium oxides (Tarling, 1983)

Magnetite (Fe_3O_4) crystallises as an inverse spinel (cubic close-packed face-centred) structure. Fe^{3+} ions occupy tetrahedral holes in the crystal lattice whereas both Fe^{3+} and Fe^{2+} ions occupy octahedral holes. This is because the Fe^{2+} ions are ligand-field stabilised and therefore occupy the higher energy state, to produce maximium stabilisation energy (Jolly, 1984). As the ions in the octahedral holes have their spins aligned in the same direction, the Fe^{3+} ions occupying the octahedral holes have equal and opposite spins to those in the tetrahedral holes and are thus antiferromagnetically coupled with a net spin moment of zero. The magnetic moment of magnetite is a result of the spin of the Fe^{2+} ions and magnetite is therefore ferrimagnetic:

$$\overset{\uparrow}{[Fe^{3+}]}_{tet} \qquad [\overset{\downarrow}{Fe^{3+}} \mid \overset{\uparrow}{Fe^{2+}}]_{oct}\, O_4 \qquad \text{(Jolly, 1984).}$$

Magnetite has a spontaneous (saturation) magnetisation of 92 Am^2kg^{-1} and a Curie temperature of 575°C (Tarling, 1983).

Titanomagnetites are a series of cation substituted spinel structured minerals with the general formula $Fe_{3-x}Ti_xO_4$, ranging from magnetite (Fe_3O_4; where x=0) to ulvöspinel (Fe_2TiO_4; where x=1), which has Fe^{2+} ions occupying tetrahedral sites and Fe^{2+} and Ti^{4+} occupying octahedral sites in the crystal lattice.

Maghæmite (γFe_2O_3) has the same chemical formula as hæmatite but whereas hæmatite has a stable corundum structure, maghæmite has a metastable cation-deficient spinel structure. $Fe^{3+}[Fe^{3+}_{5/3} \mid \square_{1/3}]O_4$ is a possible structural formula (Thompson and Oldfield, 1986) with the tetrahedral sites filled and some vacancies in the octahedral sites. It is formed by either: low temperature (<200°C) oxidation of magnetite during weathering; burning; the dehydration of lepidocrocite ($\gamma FeOOH$); or as a product of pedogenic redox reactions (Mullins, 1977). The temperature at which maghæmite converts to hæmatite ($\gamma Fe_2O_3 \rightarrow \alpha Fe_2O_3$) depends upon the presence of impurities and is the subject of some discussion. Pure maghæmite is believed to have a Curie temperature of about 645°C (Özdemir and Banerjee, 1984) and a spontaneous magnetisation of 70-85 Am^2kg^{-1}.

Hæmatite (αFe_2O_3) is a common mineral in sediments. It may exist either as black particles of specularite >1µm, or as a fine pigment with particles <1µm in diameter which are a distinctive blood-red colour (Dunlop, 1972). It has a corundum structure of hexagonal close-packed lattices with Fe^{3+} ions coupled antiferromagnetically but imperfectly giving rise to a spontaneous magnetisation in the order of 0.4-0.5 Am^2kg^{-1} (Tarling, 1983). Both spin canted and defect-induced imperfect antiferromagnetism occur in hæmatite (Dunlop, 1970).

Goethite ($\alpha FeOOH$) is an orthorhombic yellow-brown iron oxyhydroxide mineral associated with weathered sediments, especially in humid climates. It is uniaxial antiferromagnetic with a weak superimposed ferromagnetism which may be caused by lattice distortions, impurities or vacancies but which has yet to be fully explained (Dekkers, 1989). It has a Néel temperature of between 120°- 130°C and a saturation magnetisation of about 1 Am^2kg^{-1}. At higher temperatures (>300°C) it dehydrates to form hæmatite.

Iron sulphides occur in sediments associated with organic, saline and eutrophic freshwater environments. The presence of the cubic paramagnetic mineral pyrite (FeS_2) has recently been reported in basal grey silts at the Beizhuangcun loess section, central China (King, 1990).

4.1.4 Genesis of magnetic minerals in sediments

Magnetic minerals occur within sediments as a result of either detrital or authigenic processes. Weathering of bedrock can release resistant grains of primary ferrimagnetic magnetite into silt and sand-sized fractions of the soil (Dearing *et.al.*, 1985) from where they may be retransported and incorporated as detrital particles in other sediments. Other sources of detrital magnetic particles include volcanic ash and industrial fall-out. Authigenic magnetic minerals may be formed by biogenic processes, chemical alteration or burning. The action of fire upon soils causes non-ferrimagnetic oxides and oxy-hydroxides to be reduced to magnetite, which may then re-oxidise upon cooling to maghæmite (Dearing *et.al.*, 1985). Biogenic ultrafine grained superparamagnetic and single domain magnetites are produced through the reduction of ferric iron by both extracellular processes in dissimilatory iron-reducing bacteria and intracellular processes in magnetotactic bacteria (Stolz *et.al.*, 1990). Magnetotactic bacteria, which inhabit both aerobic and anaerobic sediments (Sparks *et.al*, 1990), produce intracellular magnetite of a specific morphology and narrow size distribution within membrane-bound magnetosomes (Moskowitz *et.al.*, 1989). The crystals produced by magnetotactic bacteria occur as cubic chains, hexagonal prisms, parallelapiped and teardrop-shapes (Stolz *et.al.*, 1990). A recent comparison between magnetites formed by magnetotactic and dissimilatory iron-reducing bacteria showed that, whereas the crystals produced by magnetotactic bacteria are uniform in size, morphologically specific and of high structural perfection, the crystals formed by the iron-reducing bacteria were irregular in shape, relatively small with a broad size spectrum (5-23nm) and structurally ill-defined, characteristic of rapid uncontrolled growth (Sparks *et.al.*, 1990). Both types of bacterially produced magnetite have been described as substitution-free. An inorganic *in situ* mechanism for production of magnetite has been described by Maher and Taylor (1988) for particles similar to those produced by dissimilatory iron-reducing bacteria.

Whilst the above section describes only the genesis of magnetic minerals it is worth noting that, depending on the substrate conditions, magnetic minerals may undergo diagenesis. For example, Karlin (1990) describes magnetite dissolution and subsequent formation of iron sulphides as a result of redox conditions existing during the decomposition of organic matter. Some examples of diagenesis at high temperature are described in section 5.2.

4.1.5 Relaxation time and remanence

The time taken for the electron spin magnetic moments in a mineral to return to an equilibrium position after aligning themselves to the direction of an imposed external field is termed the relaxation time (τ) of a grain. At saturation magnetisation, thermodynamic energy has been expended to overcome the tendency of spins to align themselves along the easy axis of the crystal lattice and therefore the grain is in a state of high energy non-equilibrium. The relaxation time of any given grain is proportional to the volume of the grain (v) and the temperature of the surrounding environment (T), by:

$$\frac{1}{\tau} = C \exp\left(\frac{-vHcMs}{2kT}\right) \qquad (4.1)$$

where C is a frequency factor ($\approx 10^{10} s^{-1}$); Hc is the coercivity; Ms the saturation magnetisation of the grain; and k is the Boltzmann constant.

The relaxation time of a grain determines its ability to hold a remanent magnetisation (remanence). When the relaxation time of a grain is in the order of a few seconds, a magnetisation is rapidly acquired in the presence of a weak field and also rapidly lost on removal of the field. Although such grains can exhibit an induced magnetisation, they cannot retain a stable remanence and are termed superparamagnetic. The term superparamagnetism is used to describe the behaviour of a grain which exists in an environment higher than its blocking temperature or is below its blocking volume (O'Reilly, 1984). This can be seen in equation 4.1, where either a large T or small v will produce a small relaxation time, τ. Therefore, for a given temperature there is a critical volume (termed the blocking volume, V_B) below which the grains are superparamagnetic, and for a given volume there is a critical blocking temperature (T_B) above which the grains are superparamagnetic. Viscous grains lying at the superparamagnetic/single domain boundary (SP/SDD), spanning grain sizes of 0.035-0.05µm for magnetite (Dunlop, 1973) and ~0.03µm for hæmatite (Tarling, 1983), have a time-dependent magnetisation.

4.2 Low field room temperature susceptibility

The measurement of the low field susceptibilty of loess and palaeosol sequences provides a quick and relatively easy method of studying the variations of magnetic minerals down a section.

4.2.1 Introduction

Magnetic susceptibility provides a measure of the magnetisation induced in a sample by the application of a magnetic field. For a given field, the strength of the induced magnetisation depends on the susceptibility, which itself depends upon the concentration of magnetic minerals, their size, shape and mineralogy, and the temperature. The volume susceptibility (K), which is dimensionless, is defined as:

$$K = M / H \qquad (4.2)$$

where M is the induced magnetisation and H is the intensity of the applied field. Mass specific susceptibility (χ) is a measure of the susceptibility per unit mass of a sample and described in units of m^3kg^{-1}. It is defined as:

$$\chi = K / \rho \qquad (4.3)$$

where ρ is the density of the material. Table 4.1 shows the specific susceptibilities for a variety of minerals.

Table 4.1 Specific susceptibilities of various minerals (Thompson and Oldfield, 1986).

Mineral	susceptibility ($10^{-8}m^3kg^{-1}$)
iron	20000000
magnetite	50000
maghæmite	40000
goethite	70
hæmatite	60
pyrite	30
water	-0.9
halite	-0.9
quartz	-0.6
calcite	-0.5
feldspar	-0.5

Susceptibility varies with the size of the grain. Superparamagnetic grains have a high susceptibility, which increases linearly with their volume. At the superparamagnetic - stable single domain (SP-SSD) boundary the applied field is no longer assisted by thermal agitation and the susceptibility falls by a factor of 25 (O'Reilly, 1984). Susceptibility then remains stable with increasing size until the multidomain threshold is reached. Multidomain grains have a slightly higher susceptibility than single domain grains due to energetically reversible movements of the domain walls in response to the applied field.

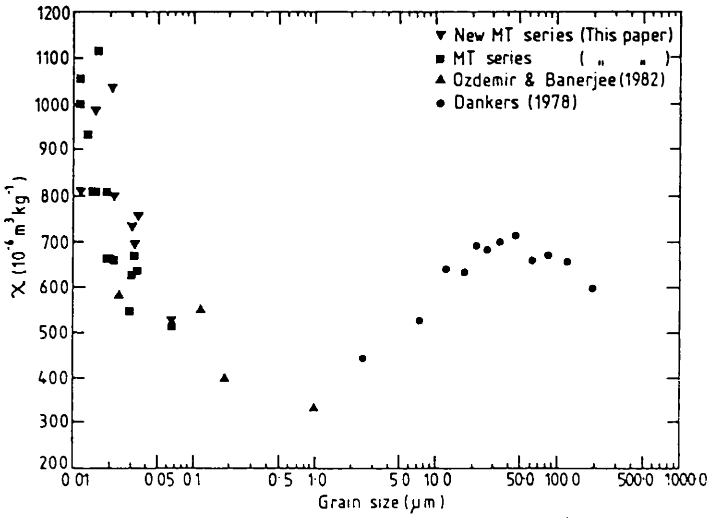

Figure 4.4 The variation of susceptibility with grain size (Maher, 1988)

4.2.2 Magnetic susceptibility of Chinese loess sequences

Heller and Liu Tungsheng (1984) proposed that low field magnetic susceptibility records of Chinese loess-palaeosol sequences could be related to the deep sea oxygen isotope record and, as such, can be used as a proxy indicator of climate change. They reported that the magnetic enhancement of palaeosols, in which susceptibilities were a factor of 2.5 higher than in loess, was mainly controlled by relative enrichment of detrital magnetic minerals in soils and precipitation of iron oxides and hydroxides from unstable iron-bearing minerals. Kukla *et.al.* (1988) further suggested that this method may be used to 'date' loess-palaeosol sequences. Since these early studies, many experiments have been undertaken in this field (Kukla and An, 1989; Hovan *et.al.*, 1989; Kukla *et.al.*, 1990; Wang *et.al.*, 1990; Rutter *et.al.*, 1991; Liu Xiuming *et.al.*, 1992).

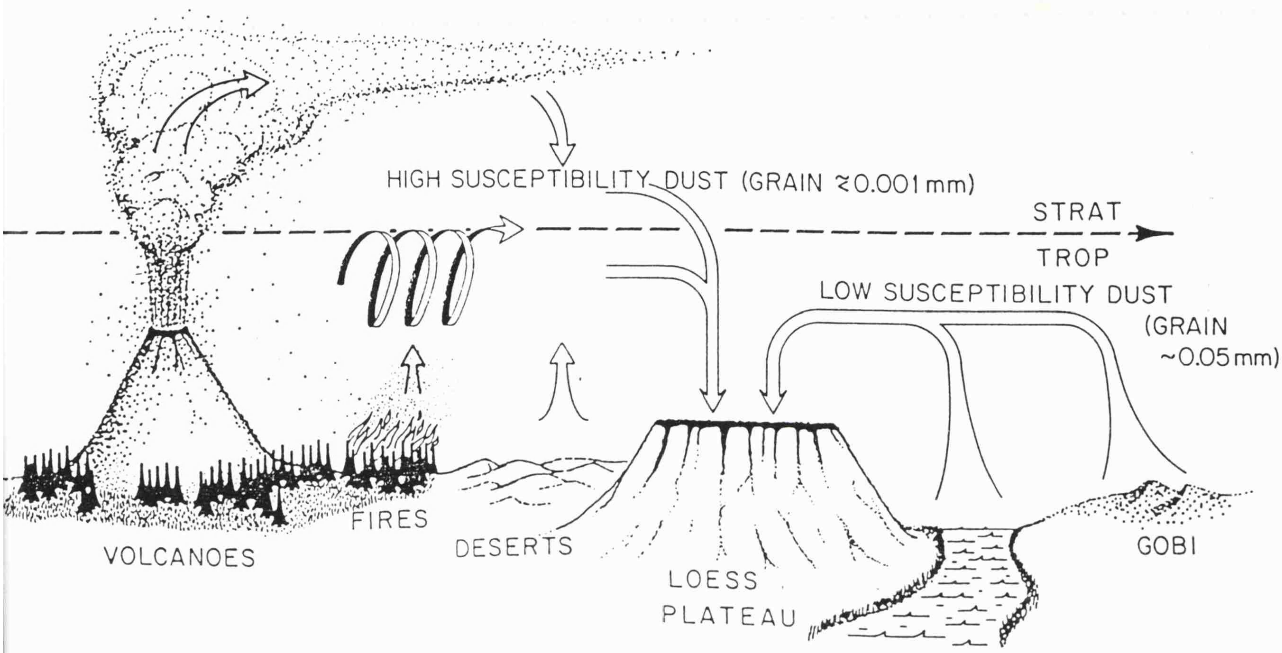

Figure 4.5 Dust deposition in the Chinese Loess Plateau from Kukla (1988).

The low field magnetic susceptibility of a loess or palaeosol will depend upon the type, concentration and size of its constituent magnetic minerals. Interpretations vary as to the genesis of the ferrimagnetic minerals. Kukla (1988) and Kukla *et. al.* (1988) explained the magnetic enhancement within palaeosols as a result of a reduction of the input of non-magnetic minerals, rather than *in situ* pedogenetic enhancement of the magnetic minerals. Figure 4.5 illustrates this theory, which is based upon the contention that throughout the depositional history of the sediment there is a constant influx of natural magnetic dust from the upper atmosphere. The relative increase in magnetic susceptibility in soils is interpreted as resulting from the decrease in sedimentation of non-magnetic material during the interglacial periods. This model has been recently criticised by

Zhou Liping et. al. (1990) and Maher and Thompson (1991) on the grounds that the model discounts any *in situ* formation of magnetite in soils by chemical or biochemical processes.

4.2.3 Measurement of room temperature low field susceptibility

Low field susceptibility is the reversible response to the application of a low field and is independent of the magnitude of the applied field. A Bartington dual frequency MS1 susceptibility bridge was used to study the low field susceptibility at frequencies of 0.47kHz and 4.7kHz, with a noise level in the order of $2 \times 10^{-9} m^3 kg^{-1}$. The samples were tested at both frequencies to ascertain the percentage of superparamagnetic grains contributing to the initial susceptibility. At low frequencies (0.47kHz), superparamagnetic grains flip in phase with the alternating field and make a large contribution to the overall susceptibility (Maher, 1988). However, at high frequencies (4.7kHz) the grains cannot oscillate sufficiently fast to remain in phase with the applied field and there is a subsequent decrease in the overall susceptibility. The difference between the high frequency (χHF) and low frequency (χLF) susceptibility is expressed as a percentage and generally termed the frequency dependent susceptibility ($\chi FD\%$), where:

$$\chi FD\% = \frac{\chi LF - \chi HF}{\chi LF} . 100 \qquad (4.4)$$

Frequency dependent susceptibility has been recently applied to loess sequences in China because of its apparent sensitivity to slight variations in palaeoclimate (Liu Xiuming et. al., 1990). Maher (1988), using synthetic magnetites found that the frequency dependence was affected by the dispersion of grains within the matrix, some SP grains forming aggregated SD-like grains.

4.2.4 Results

Samples were measured from sections at Jiuzhoutai, Dawan and Labrang; and surface sediment from Tibet. All of the magnetic susceptibility results are quoted in mass specific units and normalised to 10 grammes.

4.2.4.1 Jiuzhoutai

The Scorpion Pit section was continuously sampled for 6.30 metres corresponding to a depth of 46.80 - 53.10 metres from the top of the section. Samples were run on the Bartington meter at both frequencies and the frequency dependence (also called frequency effect) was calculated using equation 4.4. The Scorpion Pit was believed to contain a dual palaeosol, and the presence of two soils is clearly reflected in the susceptibility results. Figure 4.6 represents the low frequency, high frequency and percentage frequency dependent results obtained from these samples. In figure 4.6 the % frequency dependence has been smoothed using a ten point moving average. Figure 4.7 shows the % frequency dependence both before and after the smoothing.

The susceptibility curve for the Scorpion Pit suggests two main soil horizons. These represent the palaeosol complex believed by Chen Fahu (1990) to date from the last interglacial. The first climatic amelioration, represented by a soil-forming phase (the lower palaeosol, II), occurs between 51.55 and 51.10 metres, with a maximum low frequency susceptibility value of 49.4 x $10^{-8}m^3kg^{-1}$ at a depth of 51.45m. Just below this soil there is a minor susceptibility peak at 52.15 to 52.0 metres, which reaches a maximum value of 39.4 x $10^{-8}m^3kg^{-1}$.

Table 4.2 Mean mass specific low frequency susceptibility values for Jiuzhoutai loess (x$10^{-8}m^3kg^{-1}$).

unit	mean susceptibility	standard deviation	mean % χFD	sample number
Loess I	28.3	2.1	2.8	45
Loess II	26.2	2.4	2.7	46
Loess III	28.5	3.7	2.6	55

Above this first soil, there seems to be a return to cold climate deposition with 1.65m of loess with low frequency susceptibilities in the order of 24 to 28 x $10^{-8}m^3kg^{-1}$. Above this loess unit (II), between 49.45 and 48.10m there exists a dual peaked soil-forming episode (the upper palaeosol, I) with maximum low frequency values reaching 60.7 x $10^{-8}m^3kg^{-1}$ at 48.32m; and 58.0 x $10^{-8}m^3kg^{-1}$ at 48.82m. This upper soil is capped by loess I.

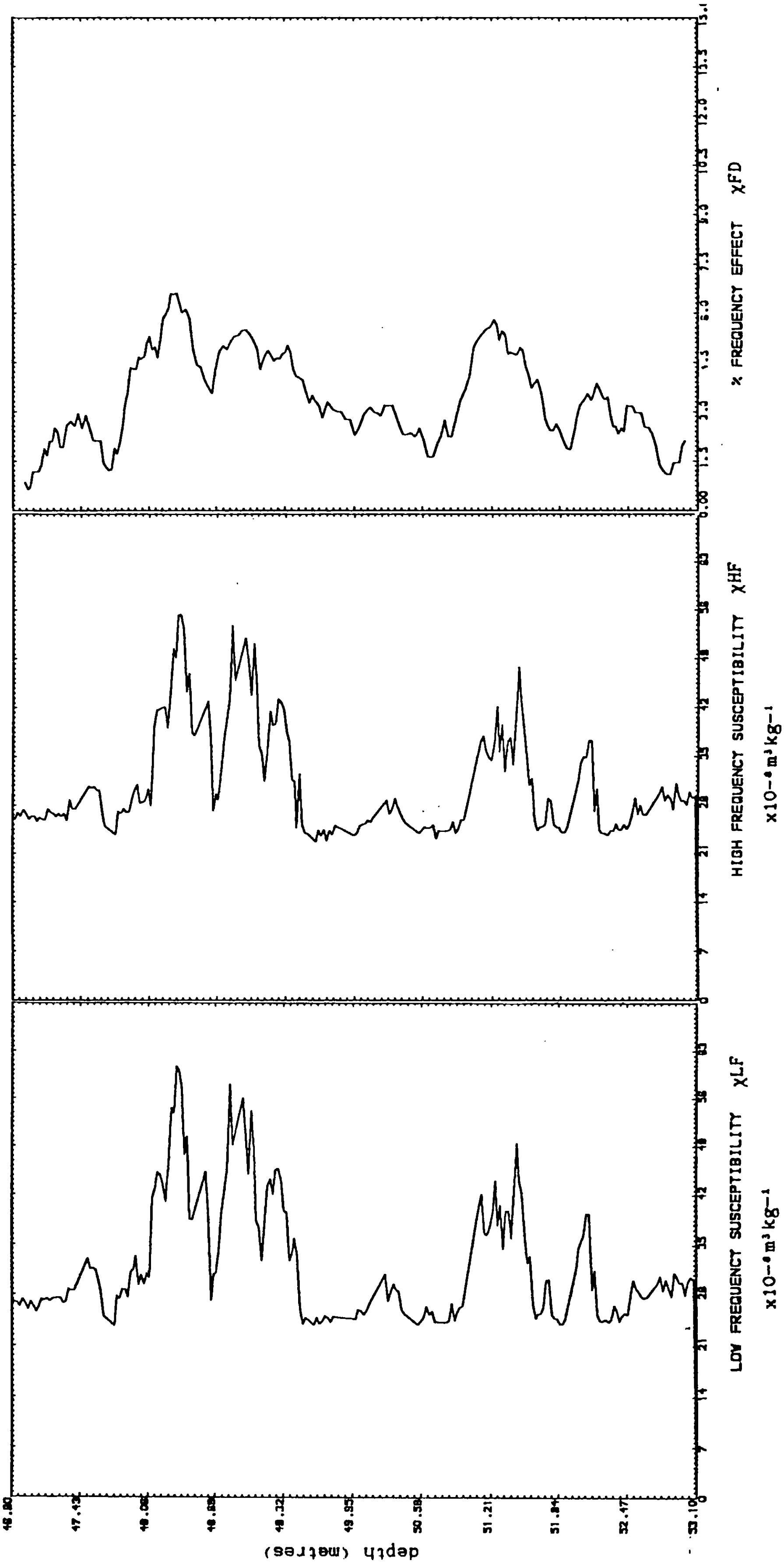

Figure 4.6 Variations in χLF, χHF and $\chi FD\%$ down the Scorpion Pit.

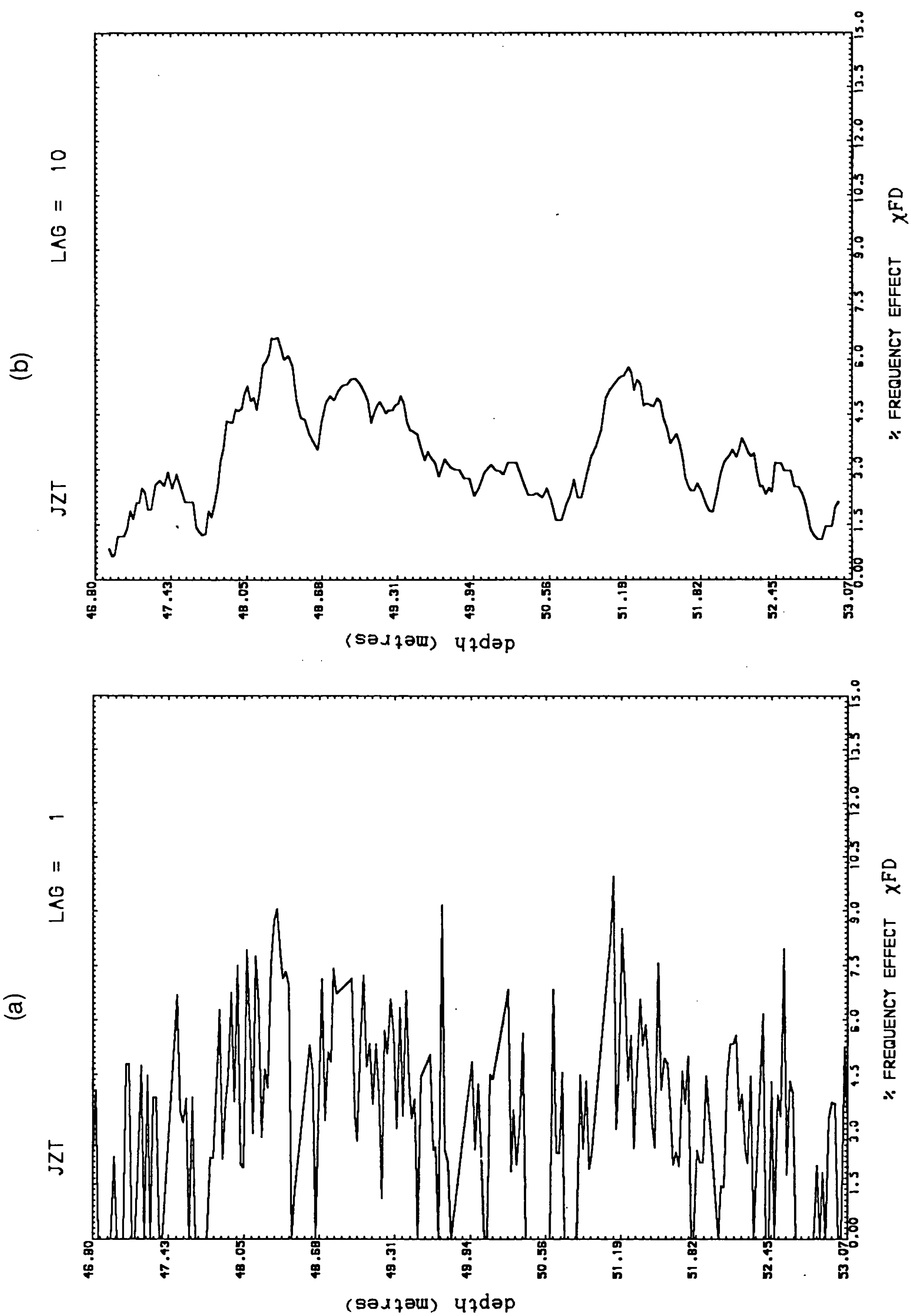

Figure 4.7 (a)Unsmoothed and (b)smoothed χFD% curves for the Scorpion Pit section, Jiuzhoutai.

Both the low frequency and high frequency curves show clear susceptibility peaks associated with these soils. The frequency dependence shows the same peaks with maximum values of 9.06% and 7.56% for the upper and lower palaeosol. However, the peaks are less sharply defined and the curve suggests a more gradual change from cold (glacial) to warm (interglacial) climate, although this may be an artifact of the calculation. The mean $\%\chi FD$ of the loess units at Jiuzhoutai, shown in table 4.2, suggests a small 2-3% content of ultrafine magnetic particles which remains fairly constant throughout the 8 metres of loess studied. One possibility is that the ultrafine particles in the loess may be of detrital origin whereas the higher concentration in the palaeosols may be a result of augmenting this with ultrafine particles produced during pedogenesis.

4.2.4.1.1 Frequency dependence: reduction of noise

As frequency dependence is the only specifically diagnostic mineral magnetic test used in this thesis an attempt was made to reduce the 'noisy' results obtained using the $\%\chi FD$ calculation by using the non-normalised frequency dependence:

$$\chi FD = \chi LF - \chi HF \qquad (4.5)$$

The non-normalised curves are presented next to the normalised percentage curves in figure 4.8. The patterns of the unsmoothed curves (figures 4.8a-b) are similar, with the non-normalised curves more clearly defined. Both of these curves were treated with a ten point moving average (figure 4.8c and 4.8d). The smoothed curves of $\chi FD\%$ and χFD are identical in shape suggesting that the use of non-normalised curves does not significantly reduce the error shown in the non-smoothed curves.

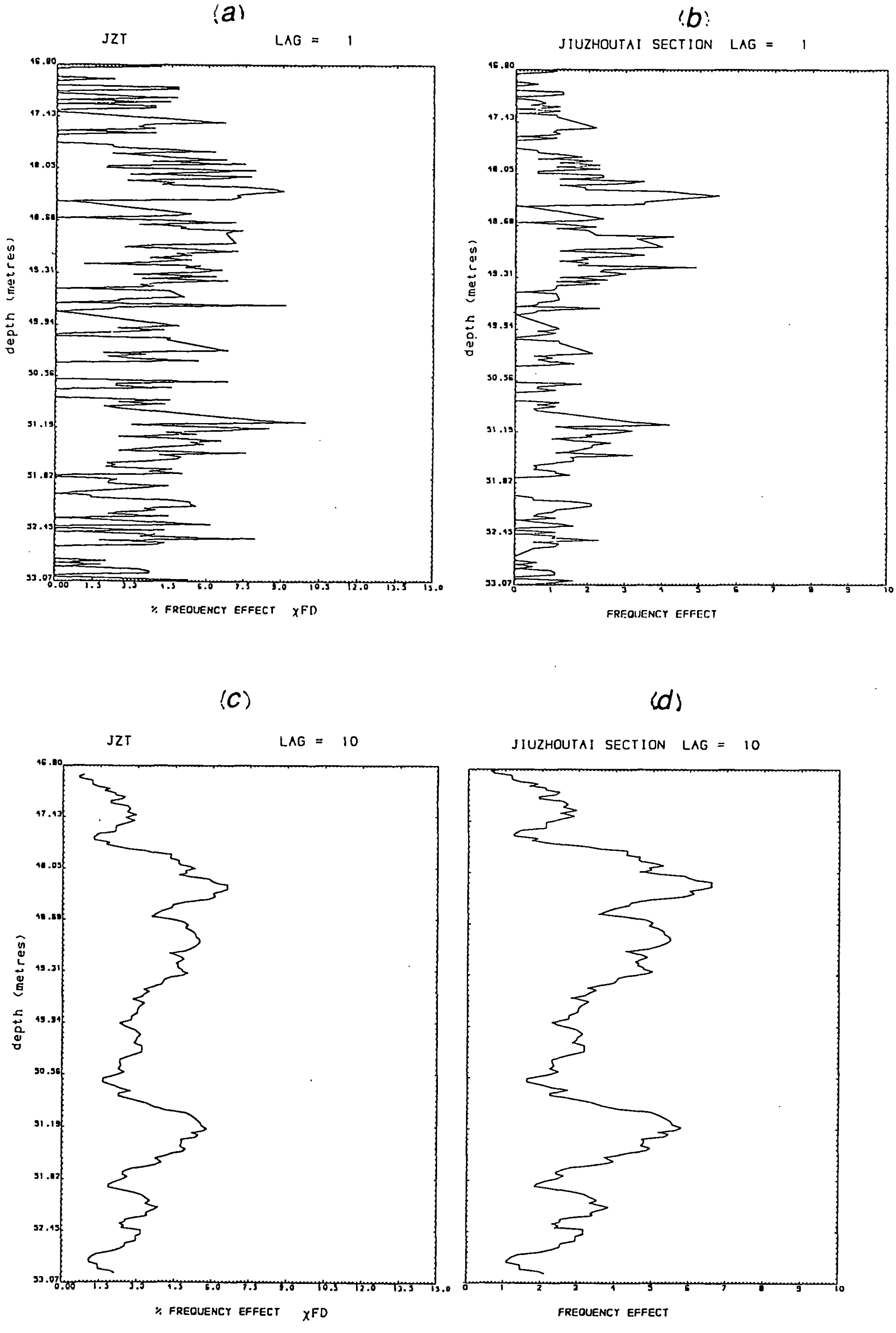

Figure 4.8 Comparison between plots of unsmoothed and smoothed percentage frequency dependence ($\chi FD\% = [(\chi LF - \chi HF)/\chi LF].100$) and non-normalised frequency dependence ($\chi FD = \chi LF - \chi HF$) for Jiuzhoutai. (a) unsmoothed $\chi FD\%$ (b) unsmoothed χFD (c) smoothed $\chi FD\%$ and (d) smoothed χFD.

4.2.4.2 Dawan

The studied section at Dawan consists of 15.3 metres of loess excavated from below uncultivated pasture. The low frequency curve (figure 4.9) clearly shows the presence of two triple palaeosol complexes separated by 2.40 metres of loess (termed loess IV). These soil horizons are each separated by at least 0.8m of loess and are thought to be distinct features based on magnetic fabric results (see chapter 8) which suggest that they are unlikely to have been caused by slumping. They have been labelled from the top, soil I (25m) to soil VI (35.2m). Triplet I-III covers 5 metres of sediment whereas triplet IV-VI covers just 2.2 metres.

Both of the triple soils decrease in susceptibility from the lowermost soil (VI and III) to the uppermost (IV and I). This is also reflected in the visible characteristics of the palaeosols with VI and III being markedly mottled brown horizons (plate 2.6) whilst IV, V, I and II are not noticeably different from the surrounding loess. Maximum low frequency susceptibility values for each soil are illustrated in table 4.3 along with the corresponding %χFD results which range from 4.4% to 8.5% indicating a higher percentage of SP and viscous grains in the palaeosols than in the loess which range from 2.2% to 4.5% (table 4.4).

Table 4.3. Maximum low frequency susceptibility values χ ($\times 10^{8} m^{3} kg^{-1}$) and corresponding %$\chi$FD for Dawan palaeosols.

unit	max. χ	%χFD	depth (metres)
Palaeosol I	53.4	6.2	25.22
Palaeosol II	56.9	7.7	27.27
Palaeosol III	85.0	8.2	30.05
Palaeosol IV	49.2	4.4	33.05
Palaeosol V	54.7	7.3	34.47
Palaeosol VI	80.3	8.5	35.27

The smoothed percentage frequency dependence curve (χFD%), treated with a ten point moving average, shows peaks corresponding to palaesols I, II, III, V and VI. Palaeosol IV shows a small peak, between 2-3% but does not stand out from the surrounding loess as a distinctive increase in content of superparamagnetic grains, as do the other soils. However, as this is a relatively thin soil covering just 40cm, it is likely to be masked more than a thicker soil by the effects of the smoothing. There is also a dual peak around 23 metres, where there is a visible mottled horizon (plate 2.5), although samples from this height did not show obvious peaks in low frequency susceptibility in either laboratory or field measurements. Prior to using the moving average, the noise associated with the frequency dependent curve made it impossible to relate to the low and high frequency curves (figure 4.10). As with the Jiuzhoutai frequency dependent results the $\chi FD\%$ curves were compared with non-normalised χFD (figure 4.11). These curves also do not appear to significantly reduce the noise.

Table 4.4 Mean low frequency susceptibility values for Dawan loess ($\times10^{-8} m^3 kg^{-1}$)

unit	mean χ	standard deviation	mean $\%\chi FD$	sample number
loess I	30.6	2.0	3.0	175
loess II	30.3	4.1	2.7	62
loess III	29.7	4.9	2.8	63
loess IV	28.2	2.9	2.2	85
loess V	26.7	0.6	2.5	17
loess VI	28.4	1.7	4.5	12

4.2.4.3 Sala Shan, Labrang and Tibet

As the samples from Labrang were taken from different parts of the loess terrace a continuous section could not be reconstructed. Mean low frequency susceptibilities from both Labrang and Tibet are shown in table 4.5. None of the Labrang or Tibetan samples showed any frequency effect indicating an absence of SP grains. Conversely the sediment from Sala Shan, on the edge of the Loess Plateau, showed a small frequency effect with a mean of 2%.

Table 4.5 Mean low frequency susceptibility χ ($\times10^{-8} m^3 kg^{-1}$) and $\%\chi FD$ from Labrang and Tibet.

Site	Mean χ	Mean $\%\chi FD$	Sample Number
Sala Shan	27.6	2	10
Labrang	27.5	0	9
Golmud	25.1	0	1
Kunlun A	24.7	0	1
Glacier	27.7	0	1
Barchan	9.0	0	1
Pingo	21.4	0	1
Kunlun Pass	22.9	0	1
Qumar Heyan	8.2	0	1

What happened to the Tibetan sample with a value of 7% ? of χFD

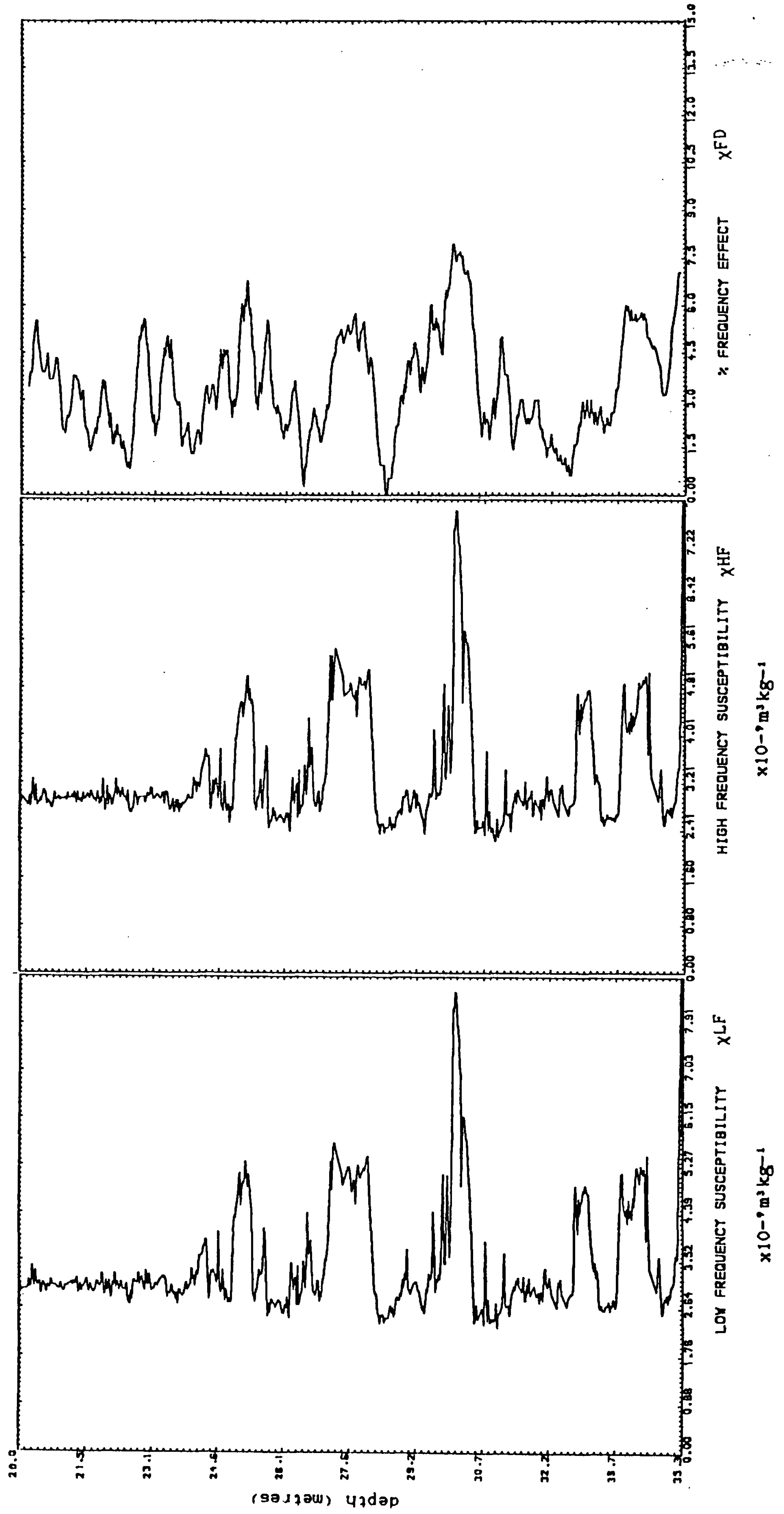

Figure 4.9 Variations in χLF, χHF and χFD% down the Dawan section

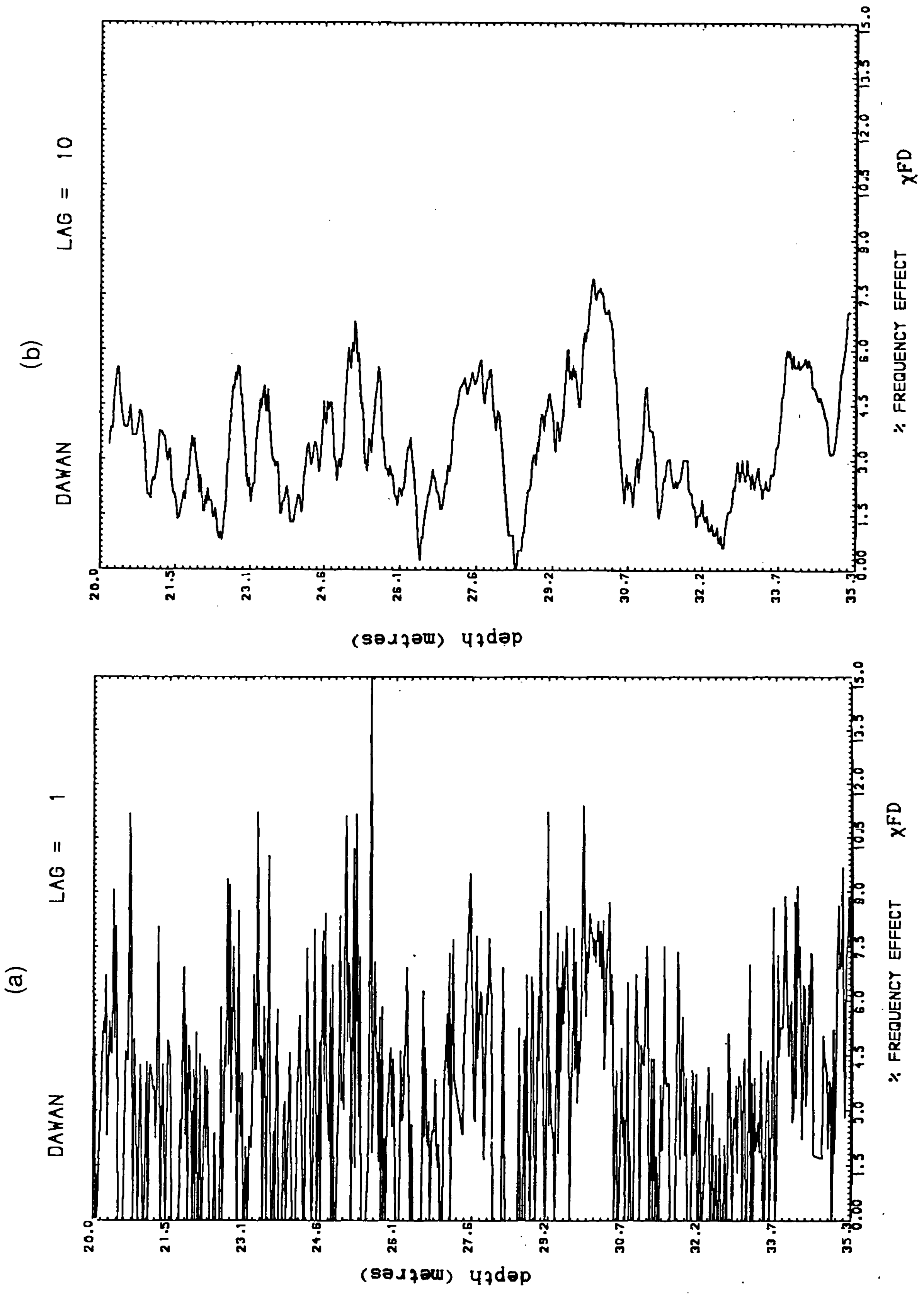

Figure 4.10 (a)Unsmoothed and (b)smoothed $\chi FD\%$ curves for the Dawan section.

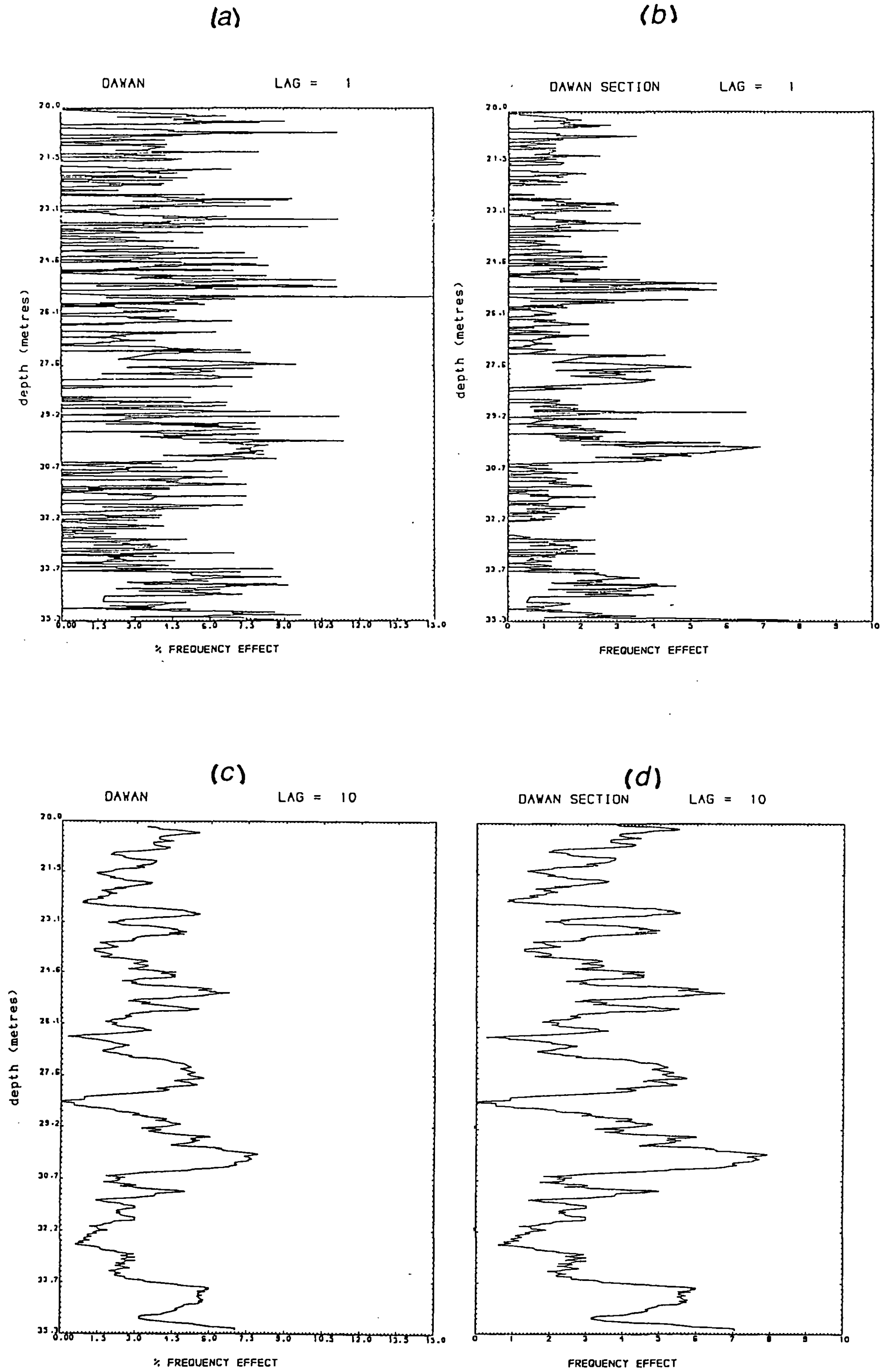

Figure 4.11 Comparison between plots of unsmoothed and smoothed percentage frequency dependence ($\chi FD\% = [(\chi LF-\chi HF)/\chi LF].100$) and non-normalised frequency dependence ($\chi FD = \chi LF-\chi HF$) for Dawan. (a) unsmoothed $\chi FD\%$ (b) unsmoothed χFD (c) smoothed $\chi FD\%$ and (d) smoothed χFD.

4.3 Low Temperature Susceptibility

The temperature dependence of susceptibility differs with mineralogy, shape and grain size. Low field room temperature susceptibility has been described in section 4.2. This section deals with the variations in susceptibility at low temperatures ranging from +20°C down to that of liquid nitrogen, -196°C.

Certain minerals undergo reordering of their crystal structure at low temperatures which affects their susceptibility. At temperatures of about 263°K (-10°C) the canted antiferromagnetism of hæmatite reorders to become near perfect antiferromagnetism as the spin direction changes from perpendicular to the c-axis, to parallel with it (Dekkers and Linssen, 1989). This is known as the Morin transition and is accompanied by a loss of spontaneous magnetisation and a sharp drop in susceptibility. The Verwey transition occurs in multidomain magnetite at temperatures of about 128° to 118°K (-145° to -153°C) depending on cation-substitution. At the Verwey transition ordering occurs in the octohedral sublattice and the crystal structure transforms from cubic to orthorhombic, with a subsequent drop in magnetocrystalline anisotropy (O'Reilly, 1984). This minimum in the magnetocrystalline anisotropy, relates to the anisotropy constant K1, and is accompanied by a maximum susceptibility. This peak in susceptibility in multidomain grains occurs only in MD magnetite because magnetocrystalline anisotropy influences wall positions in MD grains and the decrease in K allows wall movement to occur. Pyrrhotite (FeS_{1+x}), the only ferrimagnetic iron sulphide (Collinson, 1983) undergoes a low temperature transition at 34°K (-293°C) where the domain structure of MD grains changes to SD or PSD (Dekkers et.al., 1989).

The susceptibility of SP grains decreases with temperature until the temperature passes through the specific blocking temperatures of the SP grains. Their relaxation times increase beyond the period of susceptibility measurement (Maher, 1988), and they subsequently behave as SD grains and their susceptibility remains constant. The susceptibility of paramagnetic minerals increases with decreasing temperature according to the Curie Law:

$$K \propto 1/T \qquad (4.6)$$

Observing low-field susceptibilty changes from room temperature (293°K; 20°C) down to liquid nitrogen temperature (78°K; -196°C) is a relatively new technique which has been applied mainly to basalts (Radhakrishnamurty et. al., 1977; Senanayake and McElhinny, 1981; Urrutia-Fucugauchi et. al., 1984; Sherwood, 1988), and more recently to synthetic magnetites (Maher, 1988). Three main types of behaviour have been noted (figure 4.12) although their interpretations differ. These differences are due to varying opinions of magnetic carriers within basalts, and as such may not be relevent to the study of sediments.

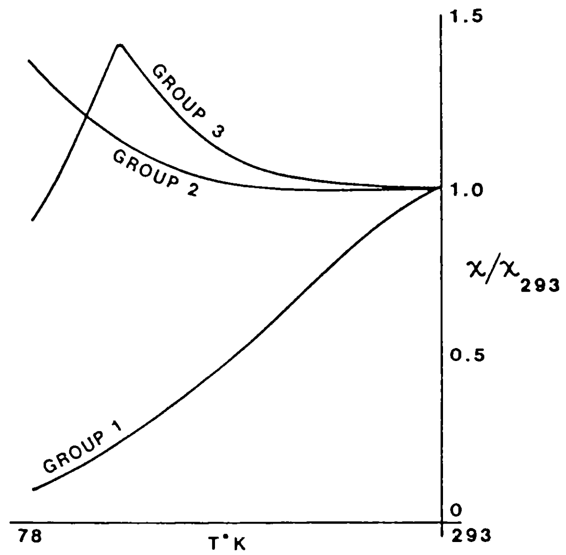

Figure 4.12 The three main groups of low temperature magnetic behaviour (Senanayake and McElhinny, 1981)

Radhakrishnamurty et. al. (1977), who base their interpretations on a purely magnetite mineralogy, believe group 1 behaviour, where the susceptibility decreases with decreasing temperature, to be the result of predominantly single domain (SD) or superparamagnetic (SP) magnetite grains; with Group 2 representing cation-deficient magnetite (or maghæmite); and group 3 as predominantly multidomain (MD) magnetite. Senanayake and McElhinny (1981; 1982) also consider the presence of titanomagnetites and corroborate their interpretations with measurements of synthetic magnetites and titanomagnetites of known grain size. They attribute group 1 behaviour to predominantly MD homogenous titanium-rich (x>0.3) titanomagnetite; group 2 behaviour to titanomagnetite grains with exsolved ilmenite lamellae with the subdivided regions acting as elongated SD grains; and group 3 samples as predominantly MD magnetite or magnetite-rich titanomagnetites (x<0.15). Further to this, Sherwood (1988) found that titanium-rich titanomagnetites which had undergone maghæmitisation gave curves indicative of group 1 behaviour.

Maher (1988) tested ultra-fine grained synthetic magnetites ranging from SP to SD and found that they behaved in a similar manner to group 1.

4.3.1 Measurement

The measurement of low temperature susceptibility was conducted using a Bartington MS2 susceptibility meter attached to a BBC microcomputer. A small hole was drilled into the centre of approximately $2cm^3$ samples of consolidated loess and palaeosol and a thermocouple was inserted. The sample and thermocouple were then encased in a plasticine ball which was immersed into liquid nitrogen and left to cool. After sufficient time for the sample to stabilise at -196°C (77°K) the plasticine ball containing the sample was removed and placed into a susceptibility bridge and the susceptibility was measured as the sample slowly warmed up to room temperature. The BBC programme accounts for external drift in the susceptibility meter before plotting the graph of change in susceptibility with temperature.

4.3.2 Results

Only samples of consolidated material, chosen to be representative of both loess and palaeosols, were tested from Dawan and Jiuzhoutai. Values of percentage difference from the room temperature susceptibility are quoted. It is difficult to assess the contribution of SD grains to the results; they define an effective 'base line' due to their stability. Whilst a levelling off of the susceptibility may be due to SD grains, it may also be the result of balancing curves of decreasing SP and increasing paramagnetic components. However, a large SD content would cause SP and paramagnetic components to appear less important. This is because, in this case, they would have a smaller percentage of the total susceptibility. Interpretation of low susceptibility behaviour is therefore highly complex.

4.5.3.1 Jiuzhoutai

Three samples were tested, two loesses and a palaeosol. The loesses, from depths of 46.65m (loess I) and 52.45m (loess III), both showed initial decreases in susceptibility. Loess I showed a decrease of 25% from room temperature to -60°C. Between -60°C and -196°C the susceptibility then increased to a value 40% above that at room temperature (figure 4.13a). This curve may be interpreted as a combination of SP magnetite (the decrease in room temperature to -60°C) and paramagnetic clay. The presence of SD magnetite is difficult to ascertain due to the temperature stability of its susceptibility.

Loess III behaved slightly differently (figure 4.13b). There was an initial decrease in magnetisation of 20% from room temperature down to -30°C after which the curve flattened off showing a very slight increase of 1% between -30°C and -60°C. Between -60°C and -105°C the susceptibility increased slightly; then from -105°C to -163°C the susceptibility remained the same value, with possibly a small decrease towards -160°C, and finally increased by 15% from -163°C to -196°C to end 10% above the value at room temperature. This curve of initial decrease, then stepwise increase in susceptibility suggests the presence of SP and SD grains of magnetite or maghæmite together with paramagnetic clay. There is some evidence of a 'hump' in the curve centred at -125°C, and this probably reflects the presence of MD magnetite. This MD peak is almost obscured by the strong paramagnetic signal. The apparently high temperature (-125°C) of this peak is a common phenomenon with large samples. It is unlikely to be an artifact of the meaurement procedure as the thermocouple is measuring the temperature in the centre of the sample whilst the susceptibility meter is measuring the whole sample; thus the outside of the sample warms up before the middle (giving a too low temperature as the thermocouple lags the sample on heating).

The palaeosol sample was taken from a depth of 51.45m from the horizon labelled palaeosol II. As with the loess samples, the susceptibility of the palaeosol initially fell 19% from room temperature to -50°C, where the curve then stabilised from -50°C to -120°C. Between -120°C and -196°C the susceptibility increased by 13%. At -196°C the susceptibility was 4% lower than that at room temperature. This curve seems to imply an initial dominance of SP grains, which 'block in' at about -50°C and then behave as SD grains with a consequent levelling off of susceptibility. The increase below -120°C is due to the increasing influence of the paramagnetic component.

There is some similarity in the susceptibility behaviour of Loess III and palaeosol II, both of which show an initial decrease driven by the 'blocking in' of SP grains and then show the increasing influence of the paramagnetic component affecting the susceptibility at temperatures below 120°C. The palaeosol sample comes from 51.45m, which is only 10cm above the loess III/palaeosol II transition.

Loess I seems to be dominated by paramagnetic material but with a small amount of SP behaviour. The dominance of the paramagnetic component probably reflects a relative paucity of ferrimagnetic material rather than an increase in paramagnetic clay. We might expect a greater clay content in the palaeosol but this is more than balanced by a greatly enhanced SP content. As the susceptibility of paramagnetic materials behaves linearly with temperature a future improvement of this technique would be to model the paramagnetic curve and subtract it from the sample curve. In this way it may be possible to observe the MD peak which is at present likely to be masked by the paramagnetic component.

4.5.3.3 Dawan

Four samples from Dawan were tested: one from loess and three from palaeosols. The loess sample was taken from a depth of 26.45m and corresponds to Dawan loess II (figure 4.14a). The susceptibility decreased initially some 16% from room temperature to -30°C where it then levelled off to -75°C. Below -75°C the susceptibility increased slightly at first and then more steeply to -196°C. At -196°C the susceptibility was 29% above that at room temperature. This curve is very similar to that of the Jiuzhoutai loess sample, being dominated initially by SP grains which block-in at temperatures of around -50°C. Below -75°C, the susceptibility behaviour is dominated by the increasing signal from the paramagnetic component.

The three palaeosol samples (fig 4.14b-4.14d) show an initial decrease in susceptibility above -50°C due to the higher susceptibility of SP grains. The signal from the paramagnetic minerals appears to contribute most strongly to the sample from the top of palaeosol IV at 32.82m below a temperature of -100°C. The sample from 32.82m showed a slight increase of 8% at -196°C, whilst the other two samples (28.02m and 33.12m) showed a slight decrease of 5% and 1%.

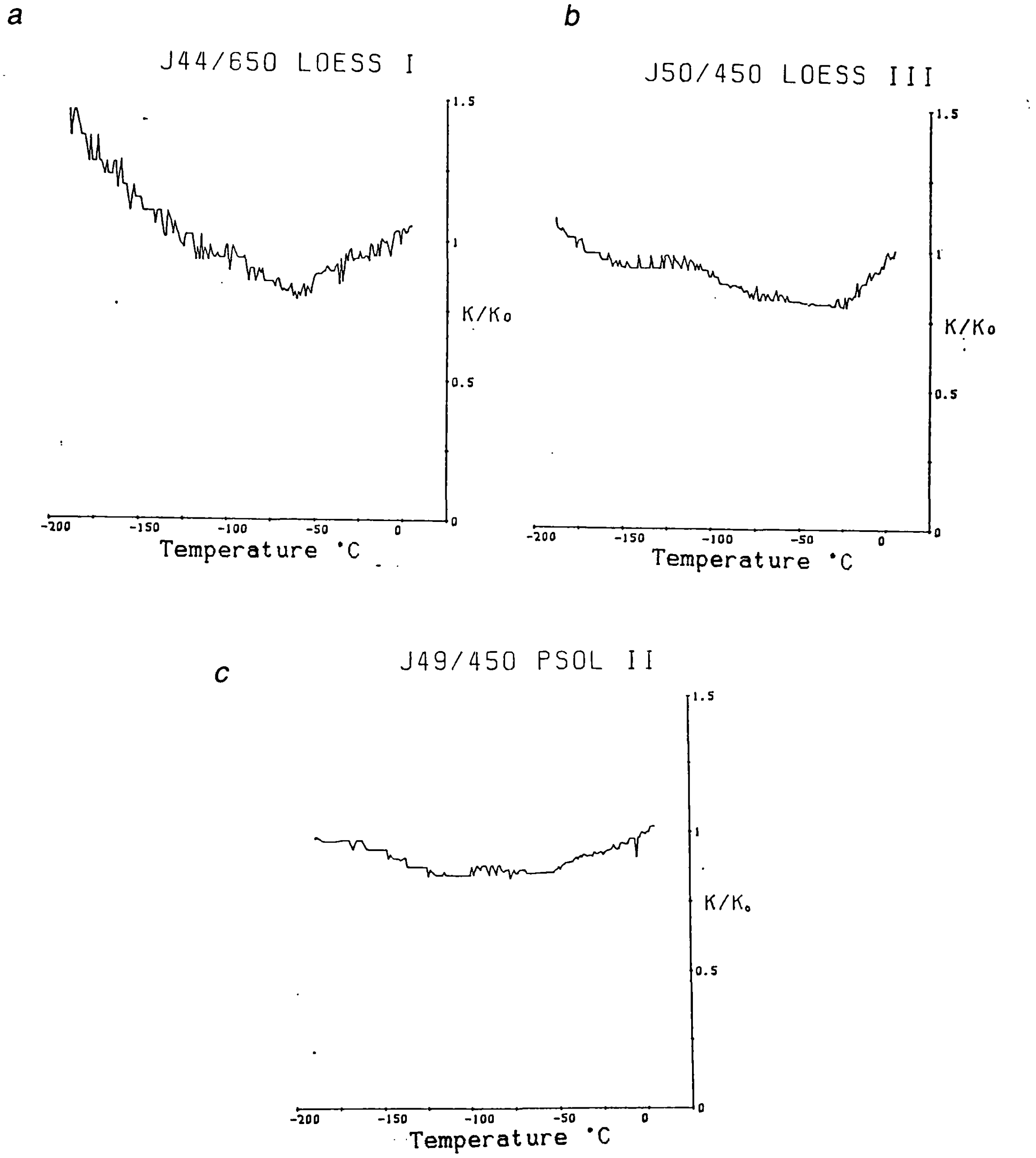

Figure 4.13 Variations in susceptibility with low temperature for samples of (a) Loess I (b) Loess III and (c) Palaeosol II from Jiuzhoutai.

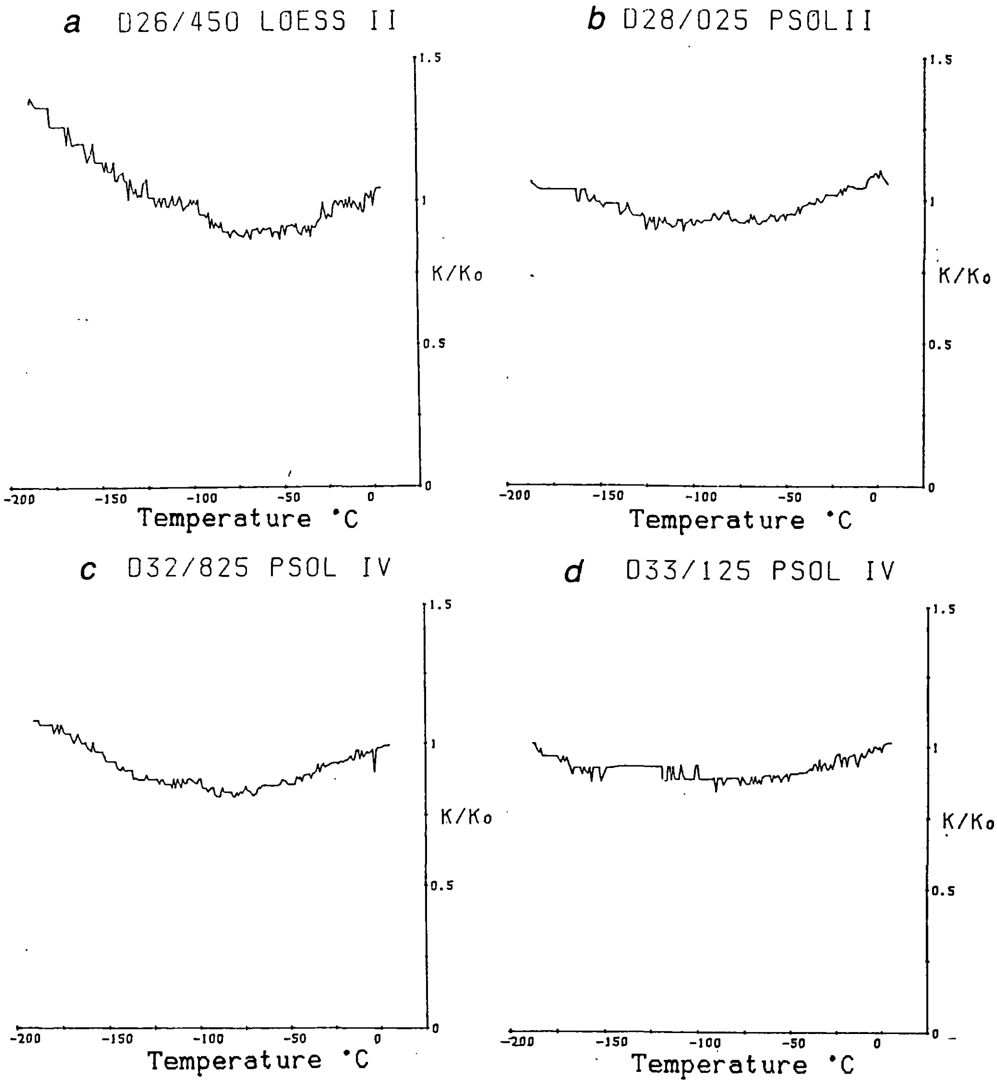

Figure 4.14 Variations in susceptibility with low temperature for Dawan samples of (a) loess II; (b) palaeosol II; (c) palaeosol IV at 32.8m; (d) palaeosol IV at 33.1m

The three palaeosol samples (fig 4.14b-4.14d) seem dominated by SD grains with an initial decrease in susceptibility at temperatures above -50°C due to the higher susceptibility of SP grains. The signal from the paramagnetic minerals dominate the sample from the top of palaeosol IV at 32.82m below -100°C. The sample from 32.82m showed a slight increase of 8% at -196°C whilst the other two samples (28.02m and 33.12m) showed slight decreases of 5% and 1%.

Table 4.7 Susceptibility values measured at -196°C expressed as a percentage of the room temperature [% change = (χ^{-196}/χ^{+20}) x 100]

Site	Depth	Unit	% change
Jiuzhoutai	46.65	Loess I	140
"	51.45	Palaeosol II	96
"	52.45	Loess III	110
Dawan	26.45	Loess II	129
"	28.02	Palaeosol II	95
"	32.82	Palaeosol IV	108
"	33.12	"	99

5. MAGNETIC MINERALOGY II: HIGH FIELD BEHAVIOUR

5.1 Magnetic hysteresis

When a field of increasing magnitude is applied to a magnetic mineral, the non-reversible induced magnetisation lags behind the field, producing an hysteresis effect (figure 5.1). Initially, when low fields are applied and then removed, the magnetisation returns to zero without any hysteresis i.e. the process is reversible. However, beyond a critical field, the reaction becomes irreversible and upon removal of the field the mineral retains a remanent magnetisation. The application of a field in the reverse direction will reduce the remanent magnetisation towards zero. The field required to reduce the magnetisation (Mrs) to zero is termed the coercivity (Hc).

When high fields are applied to a magnetic mineral the magnetisation acquired tends to saturation. Upon removal of the field this saturation magnetisation (Ms) is reduced to the saturation remanent magnetisation (Mrs).

Hysteresis properties vary with grain size and mineralogy. The magnetisation of paramagnetic and diamagnetic substances does not exhibit hysteresis but shows a reversible linear response to applied fields.

5.1.1 Hysteresis parameters

Saturation magnetisation (Ms) values depend upon magnetic mineralogy and lattice cation substitution. Ms values for common minerals range from 92 Am^2kg^{-1} for pure magnetite, with Ms decreasing with increasing titanium substitution (O'Reilly, 1984); 70-85 Am^2kg^{-1} for maghæmite and 0.4-0.5 Am^2kg^{-1} for hæmatite (Tarling, 1983); to ≤ 1 Am^2kg^{-1} for goethite (Dekkers, 1989).

The intensity of the saturation remanent magnetisation (Mrs) for magnetite is strongly dependent on grain size, with values ranging from 45 Am^2kg^{-1} for SD grains to 0.64 Am^2kg^{-1} for MD grains of 150-250µm (Dankers, 1981). Mrs values for goethite vary between 0.015 Am^2kg^{-1} and 0.1 Am^2kg^{-1} and show a tendency to decrease with increasing grain size (Dekkers, 1989). The range of Mrs values for hæmatite are in the order of 0.2 Am^2kg^{-1} for grains varying from 250µm to less than 5µm, although the finer grains have a slightly higher Mrs (0.261 Am^2kg^{-1}) than the coarser grains (where Mrs = 0.219 Am^2kg^{-1}) (Dankers, 1981).

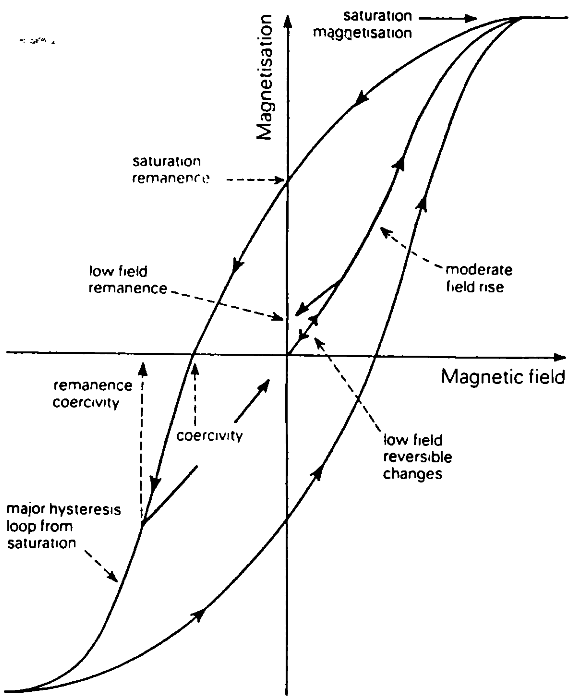

Figure 5.1 Magnetic hysteresis loop and initial magnetisation curve (Thompson and Oldfield, 1986)

Mrs/Ms ratios are used to infer domain structure. Mrs/Ms ratios decrease with increasing grain size from a theoretical ratio of Mrs/Ms = 0.5 for random dispersions of SD grains dominated by shape anisotropy (Dunlop, 1987), to values less than 0.05 which characterise large MD grains whose domain wall displacements are limited by the internal demagnetising field (Argyle and Dunlop, 1990). However, Mrs/Ms values can exceed 0.5 when crystalline anisotropy dominates (Dunlop, 1987). For magnetite, MD values of Mrs/Ms typically fall in the range 0.01-0.03 (Dunlop, 1986). Argyle and Dunlop (1990) report PSD behaviour in fine magnetite grains with ratios of Mrs/Ms = 0.059 for 0.54µm diameter grains and Mrs/Ms = 0.093 for 0.39µm diameter magnetite grains. Mrs/Ms ratios can be used to distinguish between goethite and hæmatite. This is because both large single crystals and fine-grained powders of hæmatite have Mrs/Ms ratios ~ 0.5, whereas Mrs/Ms ratios of goethite show a tendency to decrease with grain size and generally range between 0.2 and 0.35 for 250µm down to <5µm (Dekkers, 1989). Monoclinic pyrrhotite has been shown to give values in excess of 0.5 for SD grains (0.58 for 7um grains) due to its crystalline anisotropy, with values of 0.2 obtained for 83µm MD grains (Clark, 1984). The presence of superparamagnetic grains will decrease the Mrs/Ms value because they contribute to the saturation magnetisation (Ms) but do not hold a remanence and therefore do not contribute to Mrs.

For grains in excess of one micron, the coercivity of magnetite decreases with increasing grain size (Harstra, 1982) and increases with cation substitutions (O'Reilly, 1984). The coercivity for 0.1µm magnetite has been estimated at 1×10^4 Am^{-1}, ranging to 500 Am^{-1} for large multidomain grains where Mrs/Ms ~ 0.01 (O'Reilly, 1984). For sub-micron size magnetite grains the coercivity decreases with grain size. The coercivity of MD magnetite is likely to be controlled by magnetostriction through internal stresses opposing domain wall movement (Hodych, 1986). The coercivity of hæmatite ranges from 10^2-10^4 Am^{-1} for large grains to a maximum of 1.4×10^5 Am^{-1} for 5-10µm (O'Reilly, 1984). Goethite coercivities vary between 2-25 x 10^4 Am^{-1} and contrary to other minerals, tend to decrease with decreasing crystalline size (Dekkers, 1989).

5.1.2 The Vibrating Sample Magnetometer

About 0.8 gramme samples of gently powdered and disaggregated loess and palaeosol were run on a Molyneux Vibrating Sample Magnetometer (VSM) at Liverpool University. The sample was placed in a plastic tube situated between four pick-up coils and vibrated at a frequency of 50Hz. An electromagnet within the magnetometer cycles automatically between fields of 1000mT (1 Tesla) to -1000mT, and magnetisation induced in the sample creates a voltage within the pickup coils. Samples are calibrated against copper sulphate of known mass and susceptibility. The sensitivity of the detection system is approximately 4×10^{-5} Am^2.

As magnetite saturates in a field of about 300mT, with a saturation magnetisation (Ms) of 92 Am^2kg^{-1}, it is possible to estimate the mass of magnetite within the sample by dividing the experimental Ms value by 92. However, this calculation is an approximation because it presumes that magnetite is the only magnetic mineral present. 1 tesla fields are insufficient to saturate hæmatite or goethite.

5.1.3 Results

Hysteresis parameters have been calculated for all of the sites visited within this study and the figures are presented in Appendix I.

5.1.3.1 Jiuzhoutai

Hysteresis curves obtained from the VSM for a loess and palaeosol from Jiuzhoutai are illustrated in figure 5.2. Hysteresis parameters are plotted in figure 5.3 (see Appendix I for the data). Stratigraphic logs and mass specific low frequency susceptibility (χ) are plotted to give an indication of the relationship of hysteresis parameters to the presence of palaeosols. Ms values vary down the section reflecting variations in concentration of magnetic minerals. Assuming that magnetite dominates the mineralogy, the Ms values correspond to magnetite concentrations varying from 0.01% to 0.03%. Mrs/Ms ratios are higher in the palaesols than in the loess indicating a higher concentration of SD and viscous grains (which hold a remanence and thus have a high Mrs/Ms) within the palaeosols (table 5.1). An increase in concentration of viscous grains spanning the SP/SSD boundary would account for the decreasing coercivities within the palaeosols and contribute to the increased values of mass specific susceptibility (χ). Frequency dependence results from section 4.1 suggest that palaeosols contain an increased concentration of SP grains compared with the loess. Therefore combining the $\%\chi FD$ and hysteresis results for Jiuzhoutai implies that the magnetic assemblage within the loess is characterised by multidomain ferrimagnets whereas the palaeosols are characterised by an increasing concentration of SP/SSD ferrimagnets.

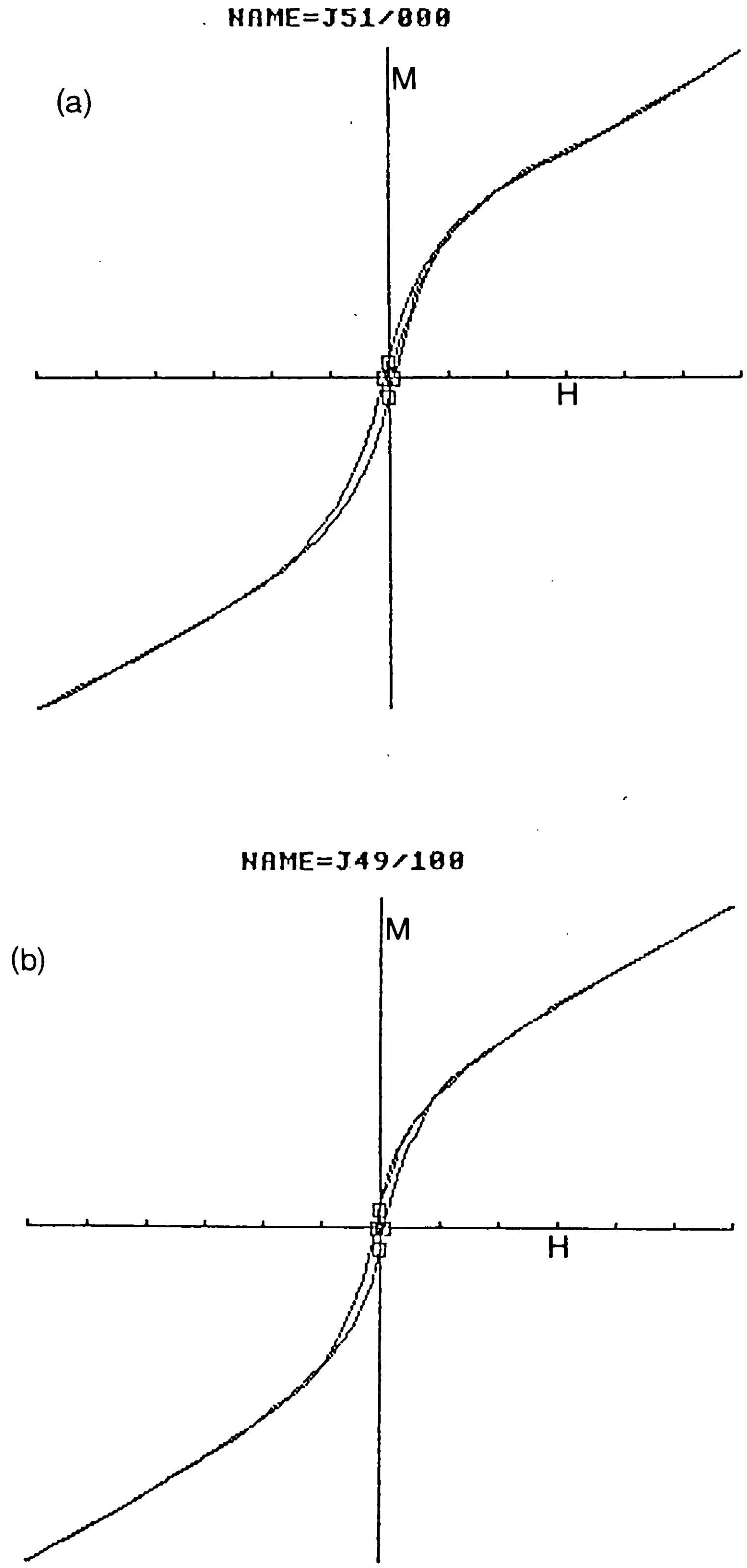

Figure 5.2 Hysteresis curves for Jiuzhoutai (a) loess III and (b) palaeosol II

Table 5.1 Variation in mean Mrs/Ms and Hc ($x10^3 Am^{-1}$) within the loess and palaeosols in the Scorpion Pit, Jiuzhoutai.

Unit	Mrs/Ms mean	standard deviation	Hc mean	standard deviation	samples tested
Loess I	0.132	0.009	9.81	3.09	2
Palaeosol I	0.153	0.005	8.49	0.98	4
Loess II	0.138	0.003	10.67	0.32	3
Palaeosol II	0.156	0.005	8.82	0.63	2
Loess III	0.125	0.011	9.89	0.16	2

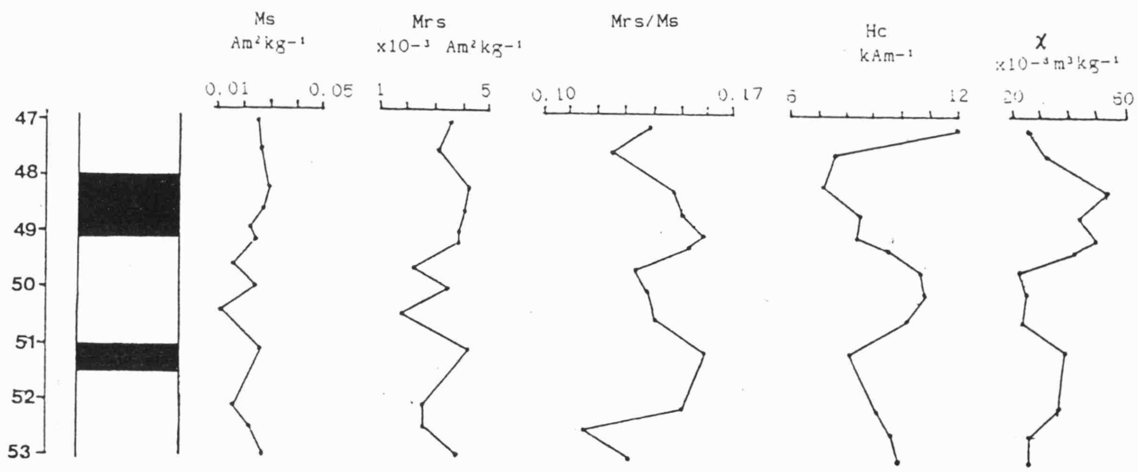

Figure 5.3 The change in hysteresis parameters down the Scorpion Pit, Jiuzhoutai.

5.1.3.2 Dawan

The loess-palaeosol sequence was tested in the VSM using at least one sample per metre down the section (see figure 5.4). Hysteresis curves are presented in figure 5.5. Ms and Mrs values appear to behave in a similiar way down the section, with a large dual-peaked increase in both parameters at a depth of 30.0 to 31.5 metres, suggesting two layers of increased concentration of magnetic minerals. Estimated magnetite concentrations are similar to Jiuzhoutai, ranging from 0.01% - 0.04%.

Table 5.2 Variation in Mrs/Ms ratios with depth at Dawan section.

depth (metres)	mean	standard deviation	sample number
20.0 - 24.5	0.118	0.0079	11
24.8 - 35.3	0.143	0.0132	31

Mrs/Ms ratios increase significantly below 24.5 metres (table 5.2), implying either an increase in the proportion of SD magnetic material or a decrease in MD or SP grains. Average %χFD values of 3.1 for loess above 24.5m compared to %χFD results of 2.2 to 4.5% for the other Dawan loesses suggests that a change in concentration of SP or viscous grains on the SP/SSD boundary is not the cause. The sharp fall of Mrs/Ms and Hc above 24.5m therefore indicates a large increase in concentration of multidomain magnetite within the upper part of loess I. The finer magnetic assemblage at the base of loess I may be due to intermixing with the underlying palaeosol.

With the exception of palaeosols I and V, the palaeosols at Dawan show lower coercivities than the surrounding loess. Palaeosol I at 25 metres, has a high coercivity (Hc = 11.4 Am^{-1}) and large Mrs/Ms, indicating a high concentration of SD grains. Ms values also shows a large increase suggesting a higher concentration of magnetic material in the soil than the surrounding loess. The high coercivity most likely reflects the increase in SD grains although the presence of a harder magnetic mineral cannot be discounted.

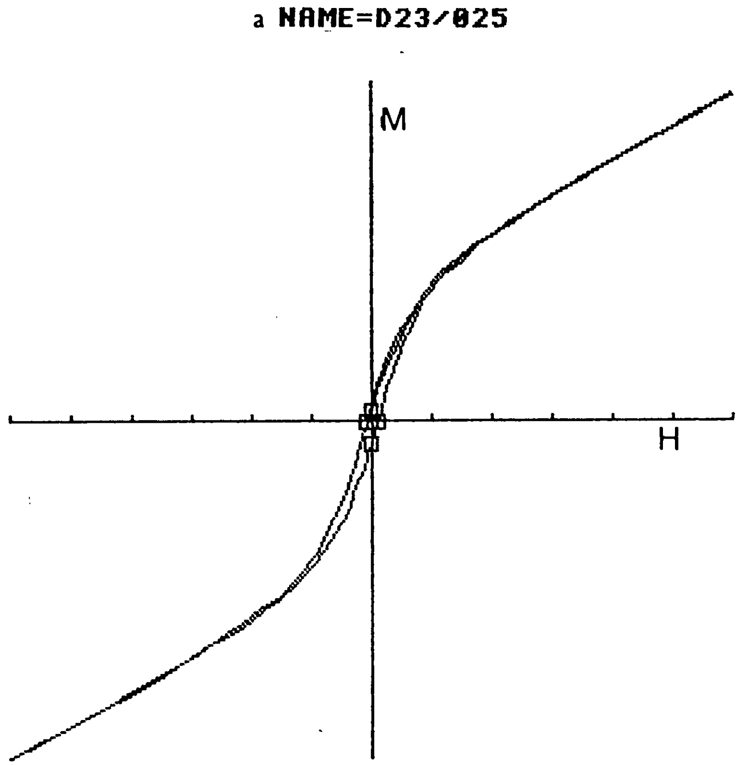

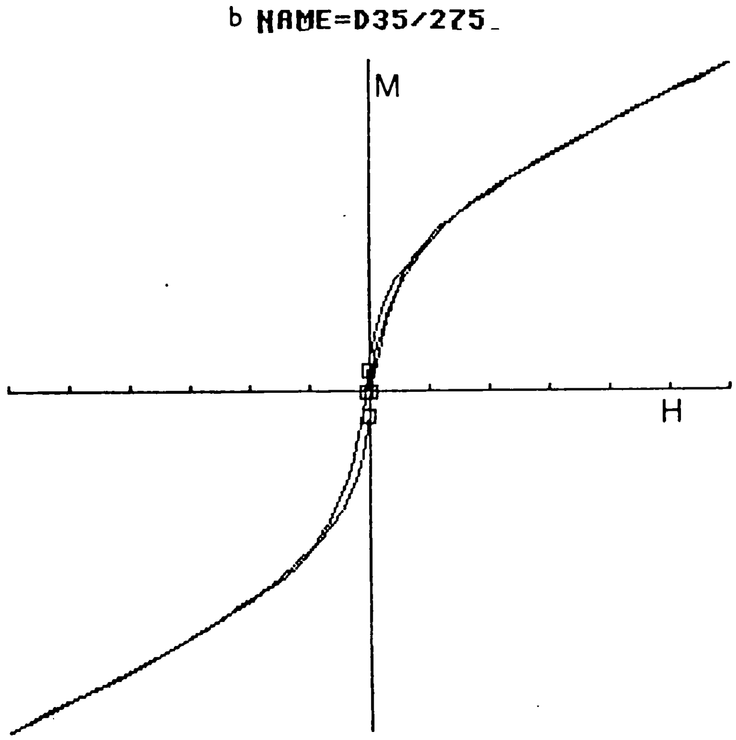

Figure 5.4 Hysteresis curves for Dawan (a) loess I (b) palaeosol VI

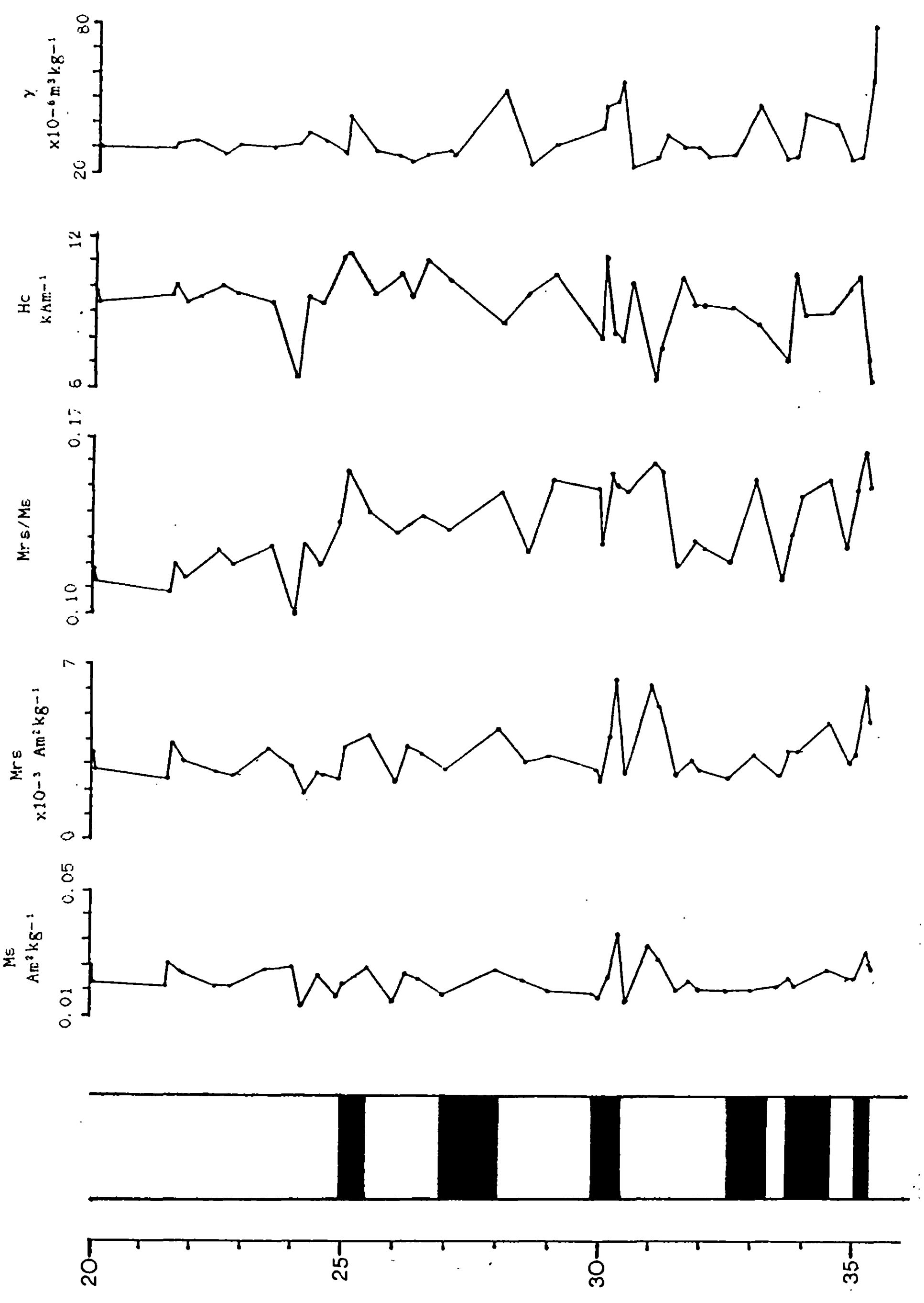

Figure 5.5 Variation in hysteresis parameters with depth down the Dawan section

Table 5.3 Variation in mean Mrs/Ms and Hc ($x10^3 Am^{-1}$) within the loess and palaeosols at Dawan.

Unit	Mrs/Ms mean	standard deviation	Hc mean	standard deviation	samples tested	unit %χFD mean
Loess I	0.119	0.009	9.57	1.01	12	3.2
Palaeosol I	0.157	-	11.40	-	1	6.2
Loess II	0.137	0.002	10.40	0.50	6	2.7
Palaeosol II	0.150	-	8.75	-	1	3.9
Loess III	0.141	0.019	10.29	0.57	2	2.8
Palaeosol III	0.148	0.013	9.00	1.60	4	7.9
Loess IV	0.140	0.018	9.12	1.43	7	2.2
Palaeosol IV	0.155	-	8.73	-	1	3.7
Loess V	0.125	0.012	9.17	2.29	2	2.5
Palaeosol V	0.151	0.002	9.29	0.02	2	7.3
Loess IV	0.141	0.015	10.40	0.28	2	4.5
Palaeosol IV	0.160	0.009	7.04	0.66	2	8.5

Mrs/Ms values are consistently higher in the palaeosols indicating that there is a larger proportion of single domain grains in the palaeosols than in the loess. This was also the case at Jiuzhoutai. The lower coercivities in the palaeosols II, III, IV and VI suggest in increase in proportion of sub-micron viscous magnetite grains spanning the SP/SSD boundary.

Comparing the hysteresis results with %χFD and susceptibility results from chapter 4.1 it is possible to conclude that the palaeosols at Dawan are characterised by SP/SSD grains whereas the loesses contain a higher proportion of MD grains. Loess I shows a coarser magnetic assemblage than the other loess units.

5.1.3.3 Southern Gansu: Labrang and Sala Shan

Hysteresis curves for Labrang and Sala Shan are presented in Figure 5.6. Eight samples from Labrang were tested in the VSM, but only one from Sala Shan due to a scarcity of material. Ms results from Sala Shan estimate a low magnetite concentration of 0.01%, which is the smallest of the samples tested. The magnetite concentration in the Labrang samples ranged between 0.02% to 0.03%. Mrs/Ms ratios used in conjuction with %χFD results show that the magnetic assemblage in Labrang loess is dominated by multidomain grains. Conversely the Sala Shan loessic alluvium appears to be dominated by a finer assemblage implying a greater propoertion of SD grains. Coercivity results from both sites suggested low coercivity "soft" minerals are dominant. At Labrang these are MD grains whereas in Sala Shan they are more likely to be viscous grains on the SP/SSD boundary. This is confirmed by the presence of a 2% frequency dependence in Sala Shan sediment whereas none of the Labrang samples showed any frequency dependence.

Table 5.4 Hysteresis parameters from Southern Gansu
(Ms (Am^2kg^{-1}), Mrs ($x10^{-3}Am^2kg^{-1}$), Hc (kAm^{-1});
(n is number of samples tested).

site	Ms		Mrs		Mrs/Ms		Hc		χFD%	n
	mean	SD	mean	SD	mean	SD	mean	SD		
Sala Shan	0.013	-	1.78	-	0.134	-	7.61	-	2	1
Labrang	0.024	0.004	2.64	0.54	0.107	0.014	8.08	0.35	0	8

5.1.3.4 Tibet, Kunlun Mountains and Qaidam Basin.

Both surface silts from the Tibetan Plateau and Kunlun Mountains and sand from the Qaidam Basin and Kunlun barchan dúnes were tested (table 5.5). Hysteresis curves for the samples are shown in figure 5.7. Ms values for the silt samples decrease with height up the Kunlun Mountains from the foothills (Kun1A; 3400m) to the Kunlun Pass at 4767m suggesting that the concentration of magnetic minerals increases towards the Qaidam Basin. The sample from Qumar Heyan on the Tibetan Plateau was the exception to this trend exhibiting a high Ms value similar to the values for the Ms peaks at Dawan. Mrs/Ms and coercivity values for the silt samples generally decreased with altitude down the Kunlun Mountains indicating that, with the exception of the barchan dune sand, the magnetic grain size is coarser in the Qaidam Basin than in the mountains. The absence of ultrafine magnetic particles is indicated by the lack of frequency dependence in any of the samples. Although trends may be inferred from these samples, there is no bedrock information available in this area and therefore direct comparison between the samples is unwise.

Table 5.5 Hysteresis parameters for Tibet, the Kunlun Mountains and the Qaidam Basin.

Location	Ms (Am^2kg^{-1})	Mrs ($x10^{-3}Am^3kg^{-1}$)	Mrs/Ms	Hc (kAm^{-1})	% χFD
Golmud	0.025	1.13	0.044	2.35	0
Kunlun A	0.022	1.38	0.061	3.09	0
Glacier	0.018	1.77	0.094	7.43	0
Barchan	0.040	0.07	0.019	0.72	0
Pingo	0.017	4.51	0.260	20.50	0
Kun Pass	0.017	1.88	0.108	8.09	0
Qumar Hey	0.039	0.47	0.120	8.47	0

The surface silt from the Tibetan Plateau at Qumar Heyan has Ms, Mrs/Ms and Hc values that compare well with the Lanzhou loess samples. However, the Mrs value is considerably lower than the loess implying a lower concentration of remanence bearing minerals. As %χFD results show that there is no SP material in the Tibetan silt it is likely that the predominant magnetic mineral is not ferrimagnetic but an antiferromagnet such as hæmatite or goethite of MD size.

The silt taken from the exposed ice core of the erupted pingo appears to contain a very high proportion of SD grains (Mrs/Ms = 0.26) with a very high coercivity (Hc = 20.5 kAm^{-1}). Although the pingo is situated at the Kunlun Pass hysteresis parameters from the pingo silt differ from the Kunlun Pass surface silt (Mrs/Ms = 0.11 and Hc = 8.1 kAm^{-1}). The difference in magnetic assemblage between the two samples and the high proportion of SD grains in the pingo maybe the result of the intense freeze-thaw environment present during pingo formation.

The barchan dune sand, taken from 4100m in the Kunlun Mountains, had a high Ms value indicating a large concentration of magnetic material within the sand. Conversely, the Mrs and Hc values were very low, which along with a very low Mrs/Ms ratio indicates that the hysteresis parameters are dominated by very large low coercivity MD grains.

Qaidam Basin sands from the vicinity of Golmud seem to contain very low coercivity, soft grains with a large proportion of multidomain grains. Ms values are similar to those of loess. The relatively low Mrs values reflect the soft MD of the magnetic mineralogy. The Kunlun A silt sample from the foothills of the Kunlun Mountains also contains a high proportion of magnetically soft multidomain grains verified by the zero frequency dependence and low Mrs/Ms and coercivity.

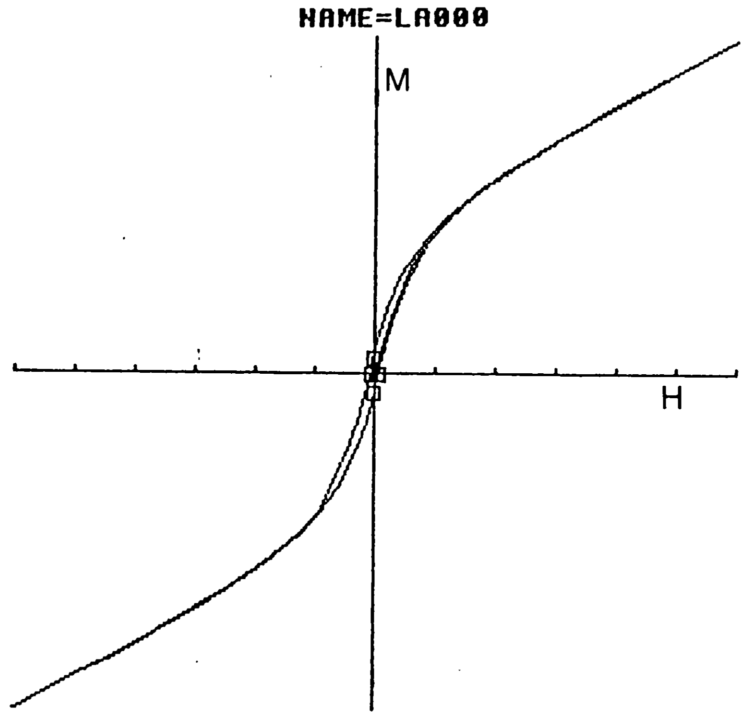

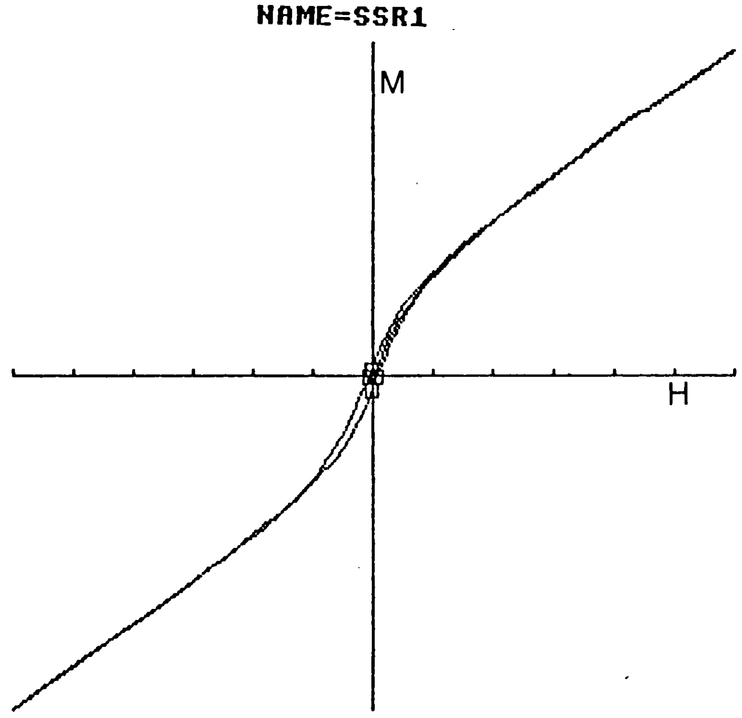

Figure 5.6 Hysteresis curves for Labrang and Sala Shan

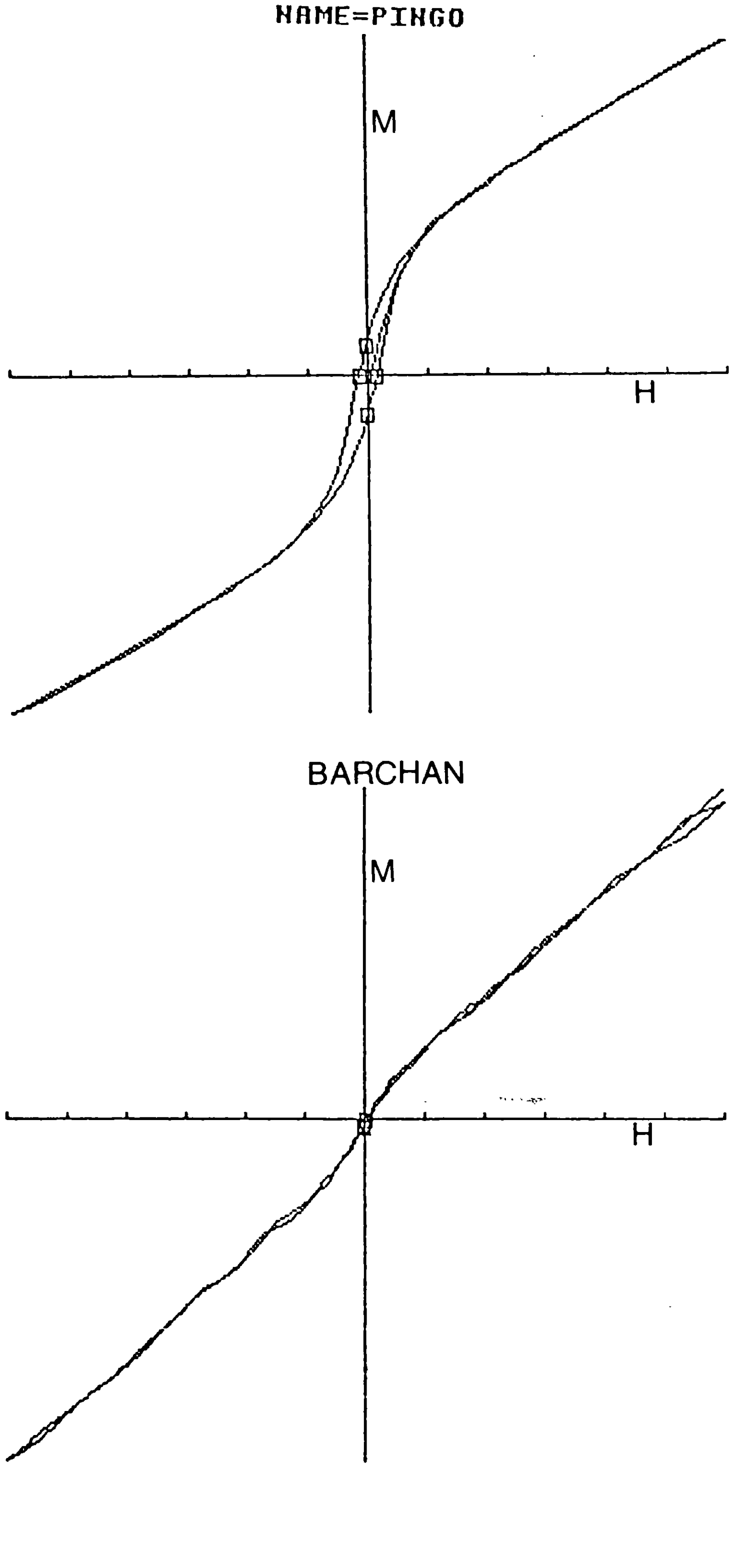

Figure 5.7 Hysteresis curves for Tibetan sediment.

5.2 Thermomagnetic behaviour

For a given crystal, the change in magnetisation with temperature is characteristic of its mineralogy. Ferromagnetic and ferrimagnetic minerals lose their spontaneous magnetisation at their specific Curie temperature (Tc), at which thermal agitation causes disordering of the spin alignments and the material becomes paramagnetic. Antiferromagnetic minerals lose their spontaneous magnetisation at the Néel temperature. Curie temperatures are affected by cation substitutions and deficiencies and are therefore a function of the structural composition of the mineral.

Curie temperatures provide a useful diagnostic tool, the thermomagnetic curves for samples indicating their magnetic mineralogy. For example, 680°C is the Curie temperature for hæmatite (Dunlop, 1970) and 575°C for pure magnetite (O'Reilly, 1984). Özdemir and Banerjee (1984) found that synthetic monodomain maghæmite (γFe_2O_3) was stable with respect to hæmatite (αFe_2O_3) at temperatures as high as 500°C, inverting to hæmatite between 510-660°C. From this they infer that the Curie point of pure maghæmite is around 645°C. Goethite has Tc values between 55-130°C depending upon crystallinity, isomorphous substitution and water content (Dekkers, 1989). For certain temperature ranges, Curie temperatures may indicate a number of magnetic minerals, for example a Curie point of 300°C could indicate a titanomagnetite (where x ~ 0.4), a titanomaghæmite, monoclinic pyrrhotite or a hæmatite-ilmenite solid solution member (O'Reilly, 1984). Titanomagnetites have a range of Curie temperatures from 575°C to -153°C depending on the degree of titanium substitution (O'Reilly, 1984). Paramagnetic minerals have temperature dependent magnetisation and obey the Curie Law giving concave curves. However magnetite and hæmatite give steep convex curves as little magnetisation is lost at low temperatures, the magnetic ordering breaking down only near the Curie points (figure 5.8).

The effect of temperature upon a sample may induce chemical changes in its structure leading to the destruction and formation of some minerals at certain temperatures. For example: lepidocrocite ($\gamma FeOOH$), which is paramagnetic, dehydrates to maghæmite (γFe_2O_3) at 230-270°C involving a strong increase in magnetisation, and, with a further increase in temperature, will invert to hæmatite (αFe_2O_3) above 350°C with a subsequent loss of magnetisation (see table 5.6).

Table 5.6 Thermochemical reactions of some magnetic minerals common in sediments (Tarling, 1983 unless stated).

Mineral	Temperature°C	Alteration product
Magnetite	>500	Hæmatite
Goethite	200-400	Hæmatite
Maghæmite	350-450	Hæmatite (Tarling, 1983)
"	510-660	" (Özdemir & Banerjee, 1984)
Hæmatite	>550	Magnetite
Pyrite	350-500	Magnetite
Pyrrhotite	>500	Magnetite (Dekkers, 1990)
Lepidocrocite	220-270	Maghæmite

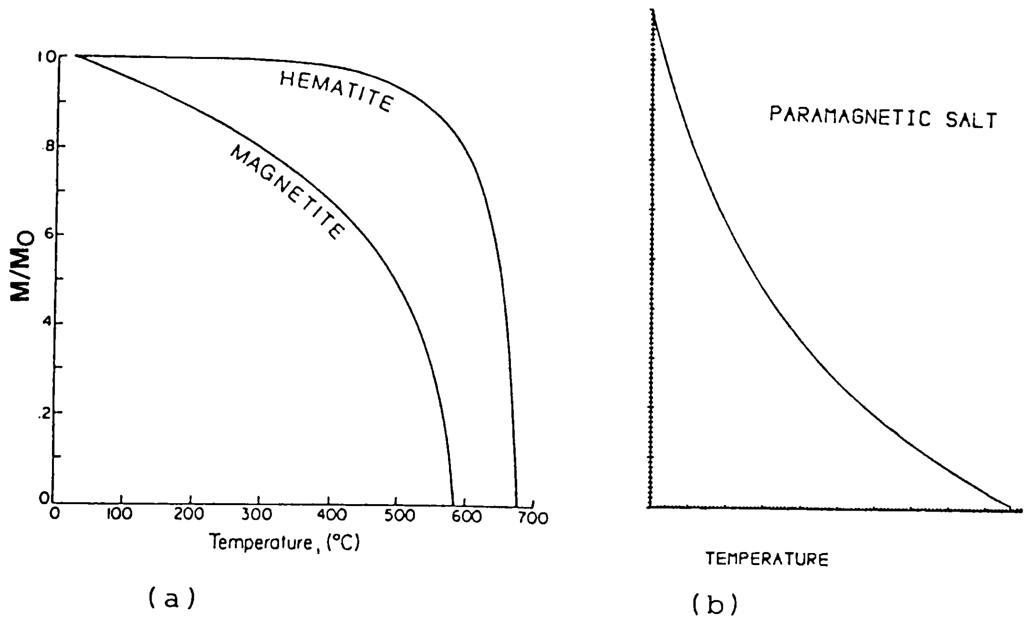

Figure 5.8 Thermomagnetic curves for (a) magnetite and hæmatite and (b) a paramagnetic salt (after Pullaiah *et. al.*, 1975 and King, 1990).

5.2.1 The Curie Balance

Powdered samples weighing approximately 2 grammes were analysed using a microprocessor controlled horizontal translation force Curie balance situated in the Geomagnetism Laboratory of Liverpool University. The samples were placed into a non-magnetic quartz cup which was suspended within an oven between the poles of a large electromagnet. The sample cup was connected to a suspended non-magnetic rod which passes through a feedback coil around a small magnet attatched to the rod, an oil bath to damp the movement and a transducer. As the sample was heated in a non-uniform strong magnetic field the magnetisation induced by this field within the sample altered, as thermal fluctuation caused breakdown in the magnetic ordering of constituent crystals. Changes in the induced magnetisation were identified by changes in the horizontal force on the sample cup and rod which caused a voltage change in the feedback coil in order to maintain the position of the sample. The change in transducer voltage with temperature gave a measure of the change in magnetisation of the sample over the temperature range 25°C to 700°C. A pure magnetite standard was used to calibrate the temperature of the Curie Balance.

5.2.2 Results

The Curie balance was attached to a BBC microcomputer which stored the data and produced plotted output at the end of each run. The Curie points were calculated using the extrapolation method of Grommé et.al. (1969) which adjusts for the contribution from the paramagnetic component. The percentage difference in magnetisation between the heating and cooling curves at 100°C was also calculated. Thermal hysteresis, in which the sample temperature lags behind the thermocouple, may cause the Curie temperature on heating to be higher than that on cooling. However, this may also be due to alteration of the magnetic minerals at high temperatures.

5.2.2.1 Jiuzhoutai

Curie curves derived from Jiuzhoutai loess and palaeosols are illustrated in figure 5.9. Curie points (Tc) obtained from these curves are presented in table 5.7. The average Tc on heating was 624.5°C which is considerably higher than the Curie Point of magnetite (575°C) and lower than that of maghæmite (645°C) and hæmatite (680°C). If both magnetite and maghæmite were present there would be an inflection in the curve indicating two Curie temperatures: one for magnetite and one for maghæmite. The existence of only one Curie point suggests that the mineral is an intermediary state: CD magnetite. The shape of the curves suggests a combination of CD magnetite and a paramagnetic component. On cooling the Tc was always lower than the heating Tc, with an average of 610.5°C. The decrease in Curie temperature on cooling may be due to thermal hysteresis, but may also be explained by reduction of a proportion of the the CD magnetite to magnetite due to the presence of organic matter in the samples. Whilst it is possible that the grains are entirely CD magnetite, the existence of an oxidised outer layer of CD magnetite surrounding a pure magnetite core is also possible.

The shape of the thermomagnetic curves (with the exception of one sample from palaeosol II) showed a decrease in overall magnetisation upon cooling. This may be due to inversion of CD magnetite to hæmatite which has a lower spontaneous magnetisation than magnetite and maghæmite. Conversion of a proportion of the CD magnetite to hæmatite would leave the unaltered magnetite dominating the Curie curve and thus the Curie point would be lowered. The loess samples and one of the palaeosol samples showed a decrease in spontaneous magnetisation upon cooling of between 24 - 42%.

Table 5.7 Curie points and percentage alteration derived from Scorpion Pit loess and palaeosols, Jiuzhoutai.

unit	depth (metres)	Tc heating (°C)	Tc cooling (°C)	% alteration at 100°C.
Loess I	47.0	625	605	-42
"	47.5	625	610	-41
Palaeosol I	48.3	623	610	-31
Loess II	50.0	628	612	-34
"	50.4	615	615	-31
Palaeosol II	51.1	630	605	+210
Loess III	52.5	625	615	-29
"	53.0	625	612	-24

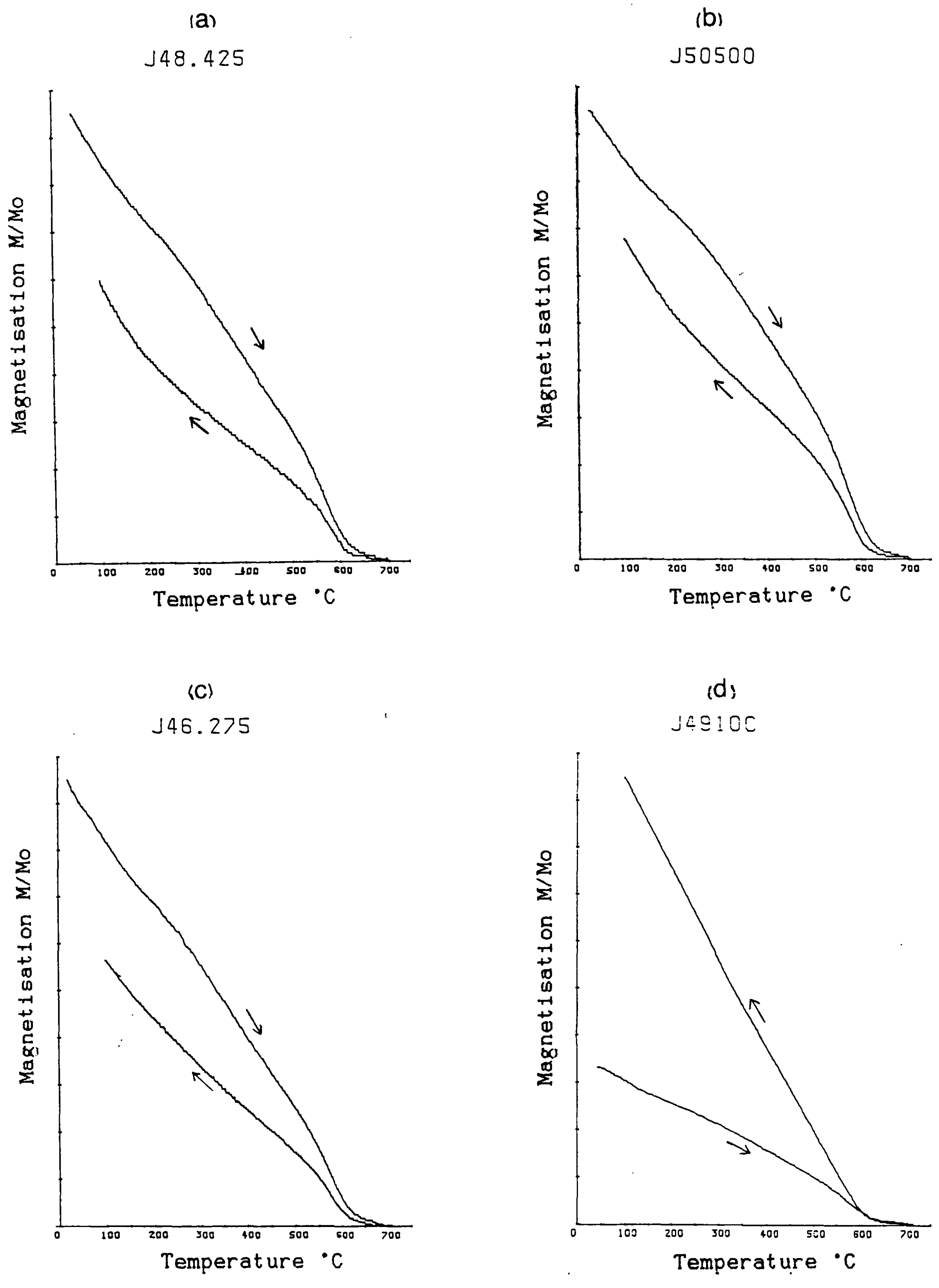

Figure 5.9 Thermomagnetic curves from Jiuzhoutai (a) Loess II (b) Loess III (c) Palaeosol I (d) Palaeosol II

The sample from palaeosol II gave similar Curie temperatures to the other samples, but, on cooling the magnetisation increased to a value of 210% that of the initial (heating) curve (figure 5.9d), indicating that heating to 700°C has formed magnetite, thus increasing the overall magnetite concentration. Alteration of a magnetic mineral with a Curie point <500°C is unlikely as such alteration is usually indicated by a change in slope of the heating curve as the mineral decomposes. However one possible explanation is that iron-rich clays which may be present in the palaeosols along with organic matter convert to magnetite by about 500°C which may not be seen at the Curie Point but are clearly visible upon cooling with a subsequent increase in magnetisation. Particle size analysis (section 3.1) indicates that 30-40% of the palaeosol at both Jiuzhoutai and Dawan are composed of clay-sized material of less than 2µm diameter. Another possibility is that the presence of organic material within the palaeosol would, upon heating, produce a reducing atmosphere which could facilitate reduction of hæmatite or an oxy-hydroxide to magnetite.

From the previous sections (4.1, 4.2 and 5.1) it is inferred that palaeosols contain fine-grained magnetite. This would be expected to oxidise to hæmatite above 500°C, the efficiency of this process depending upon the lag effects from heating of the sample in the cup and surface area open to oxidation from the bulk sample. However the presence of organic matter leading to a reducing environment upon heating would prevent oxidation.

5.2.2.2 Dawan

Thirty eight samples of loess and palaeosol were measured from the uncultivated pasture at Dawan, betweeen the depths of 20 and 35.3 metres (table 5.8). The samples of loess and palaeosol from Dawan had heating Curie temperatures ranging from 610°C to 630°C, with values of 605°C to 615°C obtained from the cooling curves. These Curie temperatures are indicative of CD magnetite. There was no particular difference between the loess and palaeosols, with only palaeosol VI exhibiting reversible Curie points. Percentage change of magnetisation between the heating and cooling curves typically ranged from -29% to -49% (fig. 5.10), with the exception of palaeosols I, III, IV and VI. These samples showed a greater degree of reversibility, with palaeosol IV only showing a reduction of 18% and the top of palaeosol VI (35.225m) giving a small decrease of 7% (figure 5.11). It has been inferred in chapter 4 and 5.1 that palaeosols have a finer magnetic assemblage than loesses. Therefore, due to increased surface area to volume ratios, the finer grains would be expected to oxidise upon heating to hæmatite. However, the samples show a greater reversibility than the loesses. This may be due to increased packing density and lag effects caused by the sample cup and use of bulk samples. An improvement of this method would be to use magnetic separates.

Five samples overall gave increased magnetisations upon cooling indicating the formation of magnetite. These samples were from palaeosols III and VI, which were the strongest developed soils in the section studied, along with one sample from palaeosol I (see fig 5.12). The increase in magnetisation within some of the palaeosols reflects the behaviour of palaeosol II at Jiuzhoutai. As the Curie points do not significantly differ from those of the surrounding loess, it is likely that the initial magnetic composition is similar. Due to the absence of inflection points on the heating curves, it is unlikely that dehydration of an iron oxyhydroxide or conversion of an iron sulphide is the cause of the magnetite formation. It is possible that, as with Jiuzhoutai, it may be caused by reduction of hæmatite or that the soils contain a high concentration of organic matter and iron-rich clays. These clays would convert to magnetite above 500°C causing no change in Curie point but an increase in magnetisation upon cooling.

Table 5.8 Curie points and percentage change in magnetisation of loess and palaeosol samples from Dawan.

Unit	depth (metres)	Tc (°C) heating	Tc (°C) cooling	% change
Loess I	20.000	625	615	-34
	20.500	625	610	-32
	21.000	625	610	-44
	21.500	620	615	-43
	22.025	615	610	-46
	22.800	625	615	-31
	23.500	625	610	-38
	24.000	620	610	-41
	24.500	625	615	-35
	24.875	630	615	-35
Palaeosol I	25.000	625	605	+51
	25.025	615	610	-32
Loess II	25.500	625	610	-33
	26.500	625	610	-49
	27.000	630	605	-41
Palaeosol II	27.750	623	605	-43
	27.875	625	615	-42
	28.000	620	610	-36
Loess III	28.500	620	610	-36
	29.000	625	610	-34
Palaeosol III	29.975	625	610	-35
	30.200	625	610	+18
	30.350	630	610	+57
Loess IV	30.500	620	610	-36
	30.525	620	610	-35
	31.000	615	612	-29
	31.500	630	615	-34
	32.500	625	605	-47
Palaeosol IV	33.000	630	610	-18
Loess V	33.500	625	615	-38
Palaeosol V	34.000	620	605	-40
	34.500	620	610	-39
Loess VI	34.750	620	615	-35
	34.800	615	610	-42
	35.000	620	615	-45
Palaeosol VI	35.225	610	610	-7
	35.250	610	610	+81
	35.275	610	610	+118

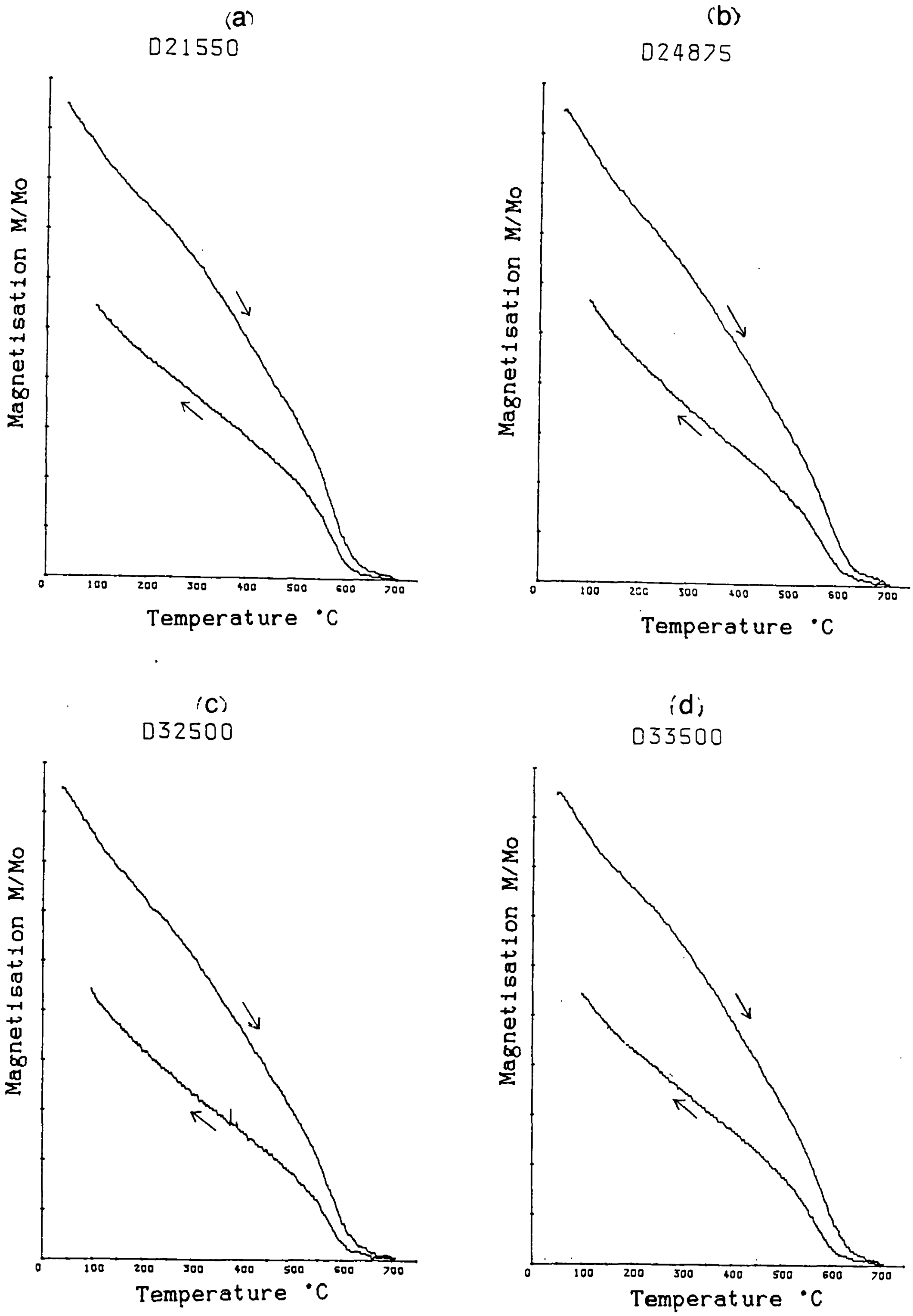

Figure 5.10 Thermomagnetic curves for Dawan loess: (a) Loess I; (b) Loess I, 12cm above palaeosol I; (c) Loess IV; (d) Loess V.

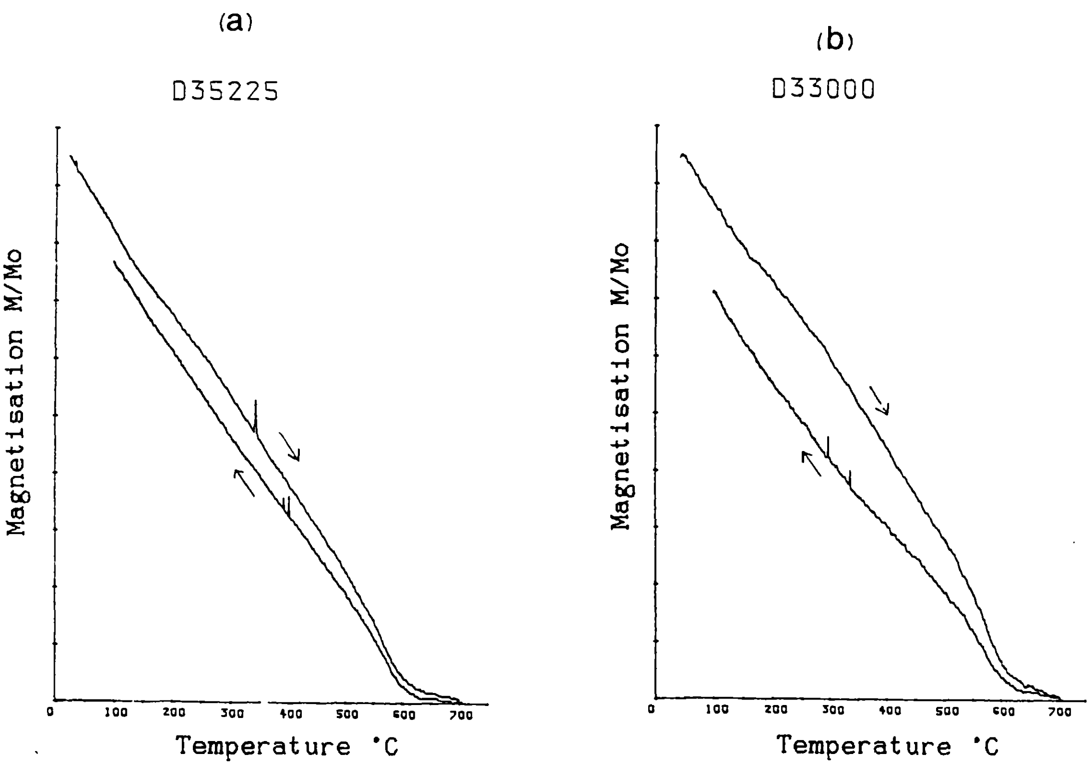

Figure 5.11 Near reversibility of thermomagnetic curves from (a) the top of Palaeosol VI; (b) Palaeosol IV.

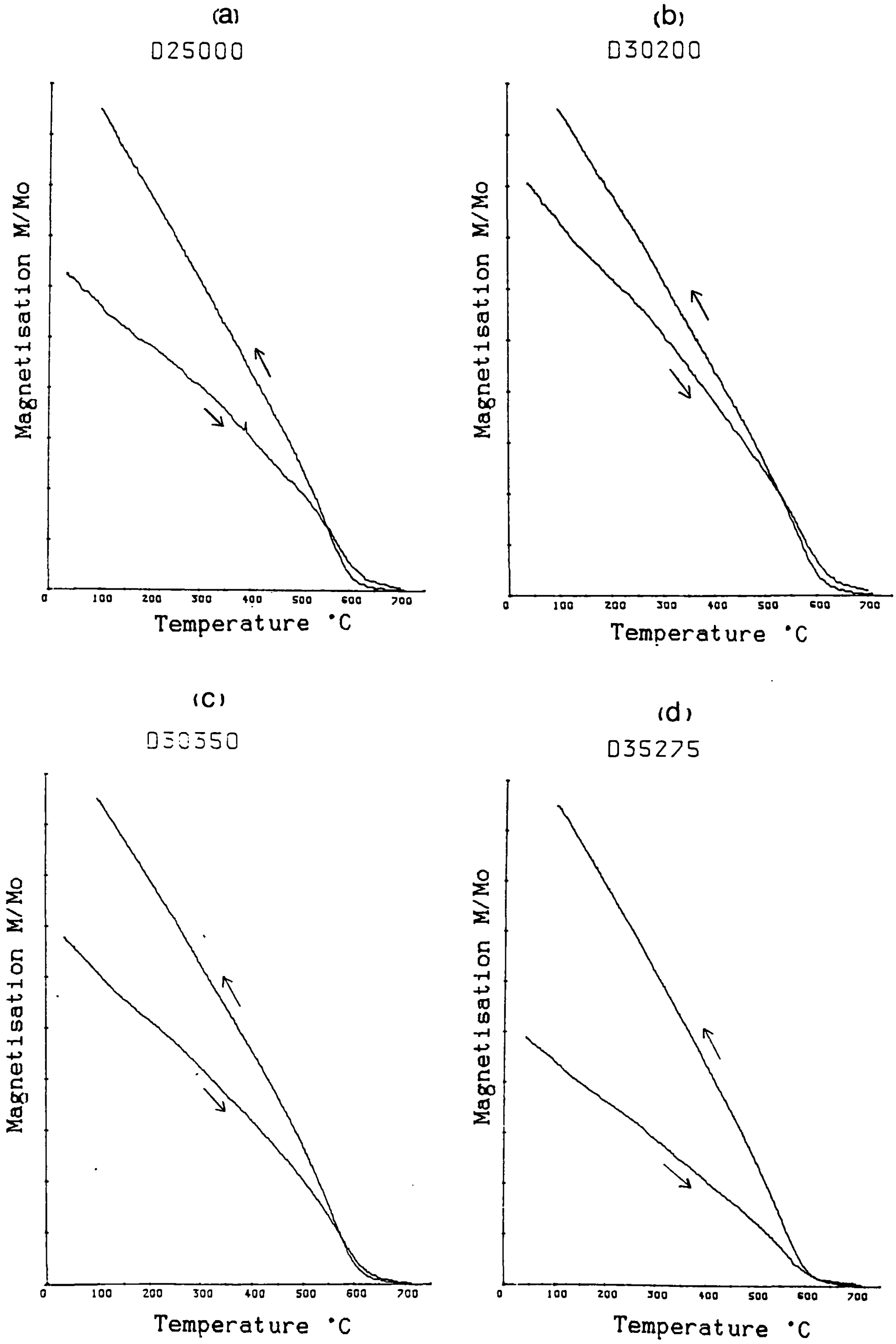

Figure 5.12 Thermomagnetic curves which display increasing magnetisation upon cooling from 700°C; (a) Palaeosol I; (b) Palaeosol III; (c) Palaeosol III; (d) Palaeosol VI

5.2.2.3 Southern Gansu: Sala Shan and Labrang

The two thermomagnetic curves derived from Sala Shan loessic alluvium on the Ba Xie river are dominated by paramagnetic material but show inflection points in their curves giving Curie temperatures indicative of CD magnetite.

Table 5.9 Curie points and percentage alteration at 100°C for Sala Shan loessic alluvium and Labrang loess.

Sample	Tc heating (°C)	Tc cooling (°C)	% alteration
SSR1	632	615	-45
SSM1	625	620	-40
LBA000	620	610	-37
LBA025	620	610	-18
LBA050	618	612	-24
LBA075	620	605	-22
LBA100	625	612	-26
LBB000	620	610	-33
LBB025	620	615	-28
LBB050	625	605	-34
LBB075	615	605	-31

The thermomagnetic curves from the Labrang loess show clear changes in slope so that Curie points can be more easily estimated (table 5.9). These ranged from 615°C to 625°C for the heating cycle and 605°C to 615°C for the cooling curves. The shape of the curves is consistent with those of Jiuzhoutai and Dawan loess, suggesting that all of the loess of the Tibetan front is dominated by the same combination of magnetic minerals, namely cation-deficient magnetite along with some hæmatite and a paramagnetic component. All of the samples showed a reduction in magnetisation upon cooling (figures 5.13).

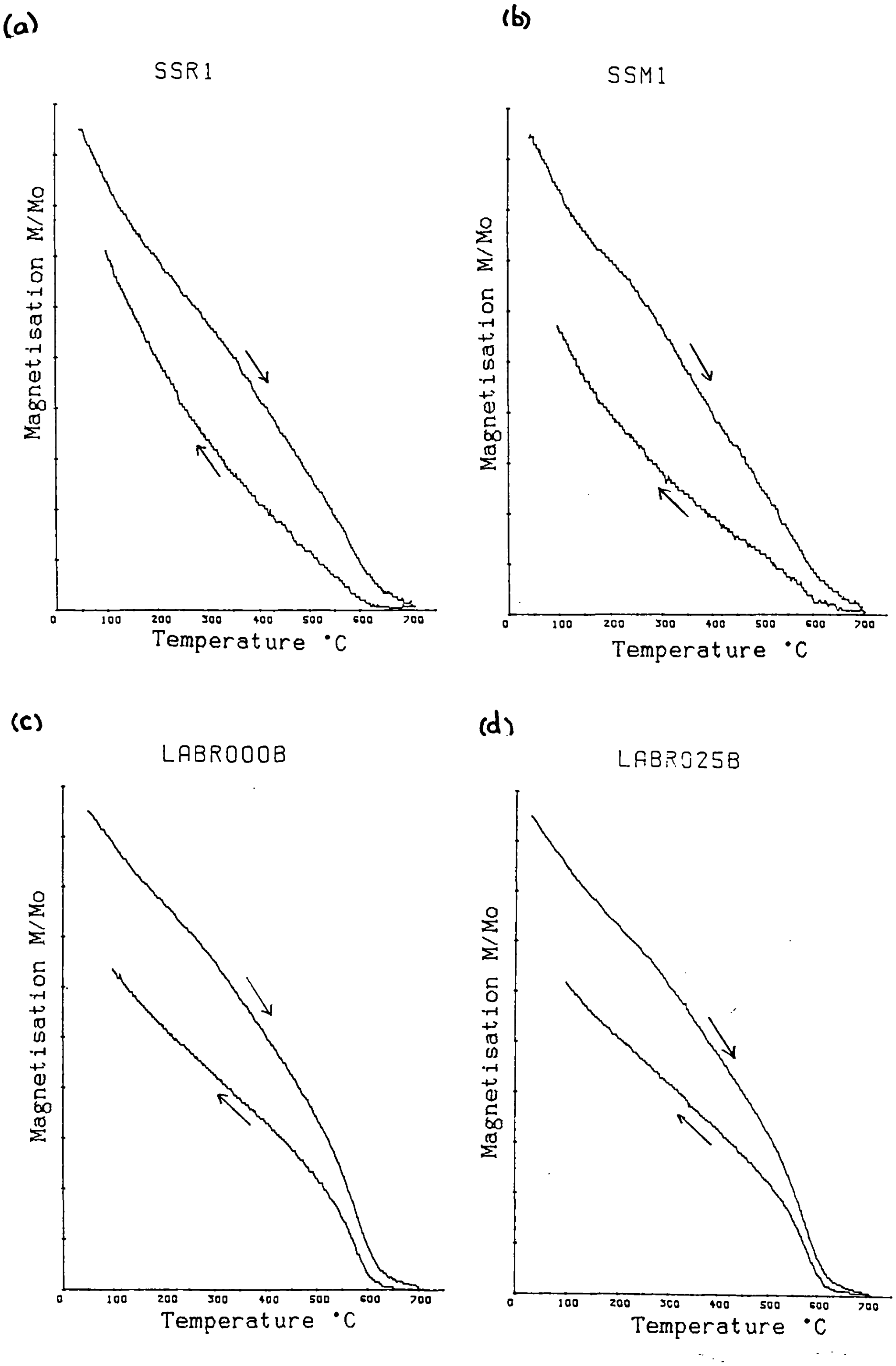

Figure 5.13 Thermomagnetic curves for loessic alluvium from Sala Shan (a-b) and loess from Labrang (c-d).

5.2.2.4 Qaidam Basin, Kunlun Mountains and Tibet

The silt samples from the Kunlun Mountains and Tibetan Plateau have Curie curves similar to those of the loess and palaeosols of Gansu. Curie temperatures of the heating curves range from 600°C - 625°C indicating the dominance of CD magnetite. Cooling curves gave Curie points lower than those of the heating curves, ranging from 585°C - 610°C, which conform to the temperatures expected from an increasing dominance of magnetite over cation-deficient magnetite. Figure 5.14 and 5.15 show the thermomagnetic curves derived from the Kunlun and Tibetan silt samples. The sample from the Kunlun A site gave a thermomagnetic curve similar to those of the Gansu loess with the cooling curve showing a decrease in magnetisation of 17% indicating that some inversion of maghæmite (or CD magnetite) to hæmatite may have occurred. The silt sample taken from the glacier showed an intial decrease of magnetisation upon cooling from 700°C - 235°C after which the magnetisation increased to 26% above that of the heating curve. This behaviour was also found in the sample from the exposed ice core of the pingo which showed an initial decrease in magnetisation on cooling from 700°C - 150°C after which the magnetisation increased to 10% above that of the heating curve.

The silt samples from the Kunlun Pass and Qumar Heyan (on the Tibetan Plateau) gave thermomagnetic curves (figure 5.15) similar to those of some of the palaeosols from the Lanzhou sections. On cooling the magnetisation increases above that of the heating curve by 40% in the Kunlun Pass sample and 660% at Qumar Heyan (measured at 100°C). After cooling both of these samples were immediately retested to ascertain the nature of the product material (figs. 5.15b and 5.15d). Both reheated curves were indicative of magnetite with Curie points of 615°C and 600°C upon heating with 605°C and 585°C derived from the cooling curves. The progressive decrease in Curie points suggests that upon each heating cycle magnetite becomes progressively more dominant as increasing amounts of CD magnetite invert to hæmatite. The presence of maghæmite after the initial thermomagnetic cycle to 700°C, when maghæmite is believed to invert at temperatures of 510°C to 660°C, may be explained by the fact that the thermocouple within the sample cup is placed near the bottom whereas the cup is totally filled with sample. Thus it is possible that although the grains around the edges of the cup reach 700°C, thermal lagging effect and the volume of material may account for grains in the centre of the cup not attaining 700°C. It is also possible that some maghæmite remains stable at these high temperatures. Indeed, Özdemir and Banerjee (1984) found 65% of synthetic maghæmite unchanged at a temperature of 660°C. A change in the lattice structure of cation-deficient magnetite could also explain the decrease in magnetisation upon cooling, if it oxidised to hæmatite.

Table 5.10 Curie points and percentage alteration for samples from Tibet. (temp¹ denotes the Tc of the first mineral; temp² the secondary mineral)

Site	altitude (metres)	Tc heating (°C)		Tc cooling (°C)		% alteration at 100°C
Golmud	2850	635		590		+3
Kunlun A	3600	625		610		-17
Kunlun Glacier	3800	625		595		+26
Barchan	4100	595¹		615¹	365²	+270
Barchan reheat	"	390¹	610²	360¹	610²	+2
Pingo	4700	625		610		+10
Kunlun Pass	4767	620		610		+40
Kunlun P reheat	"	615		605		-10
Qumar Heyan	4550	625		605		+660
Qumar H reheat	"	600		585		-22

Thermomagnetic curves of the sand samples from the Qaidam Basin near Golmud and the barchan dune field in the Kunlun Mountains are presented in figure 5.16. The sand from the Qaidam Desert around Golmud showed steep thermomagnetic curves. The heating Curie temperature of 635°C suggests a prevalence of maghæmite which may have been formed in the oxidising environment within the Qaidam Basin. The cooling curve indicates that heating has inverted the maghæmite to hæmatite leaving magnetite with a Curie temperature of 590°C to dominate the thermomagnetic cooling curve. The magnetisation of the cooling curve increases above that of the heating curve below 150°C in a similar manner to the behaviour of the Kunlun pingo and glacier silts.

The sand from the barchan dunes was unusual in that upon heating the Curie temperature of 595°C suggested a dominance of magnetite combined with paramagnetic material. Upon cooling the magnetisation decreased by some 23% until 380°C whereupon the shape of the curve changed and the magnetisation increased markedly to a total of 270% above that of the heating curve at 100°C. The inflection of this curve gave a secondary Curie point of 365°C, which indicates that heating the sand to 700°C has formed a magnetic mineral of greater magnetisation (or a greater amount of mineral with a similar/smaller magnetisation) than the original sample. To study this product further the sample was immediately rerun, which produced an almost reversible thermomagnetic curve with the Curie points of the new mineral easily identifiable at 390°C on heating and 360°C on cooling. The original mineral is also present, but considerably weaker and, as such, its Curie points are difficult to determine, but seem to be about 610°C. Minerals with a Curie point around 360°C to 390°C include a titanium-poor titanomagnetite, an ilmenohæmatite and greigite (Tc = 333°C). The mineral formed is unlikely to be greigite (Fe_3S_4) as it is thermodynamically unstable with respect to pyrrhotite (Spender et.al., 1972) which alters to magnetite above 500°C. Nickel has a Curie temperature of 357°C and a saturation magnetisation of 57 Am^2kg^{-1} but is extremely rare and usually only found in extraterrestrial material (Tarling, 1983). Therefore, the mineral formed is likely to be a titanomagnetite or an ilmenohæmatite.

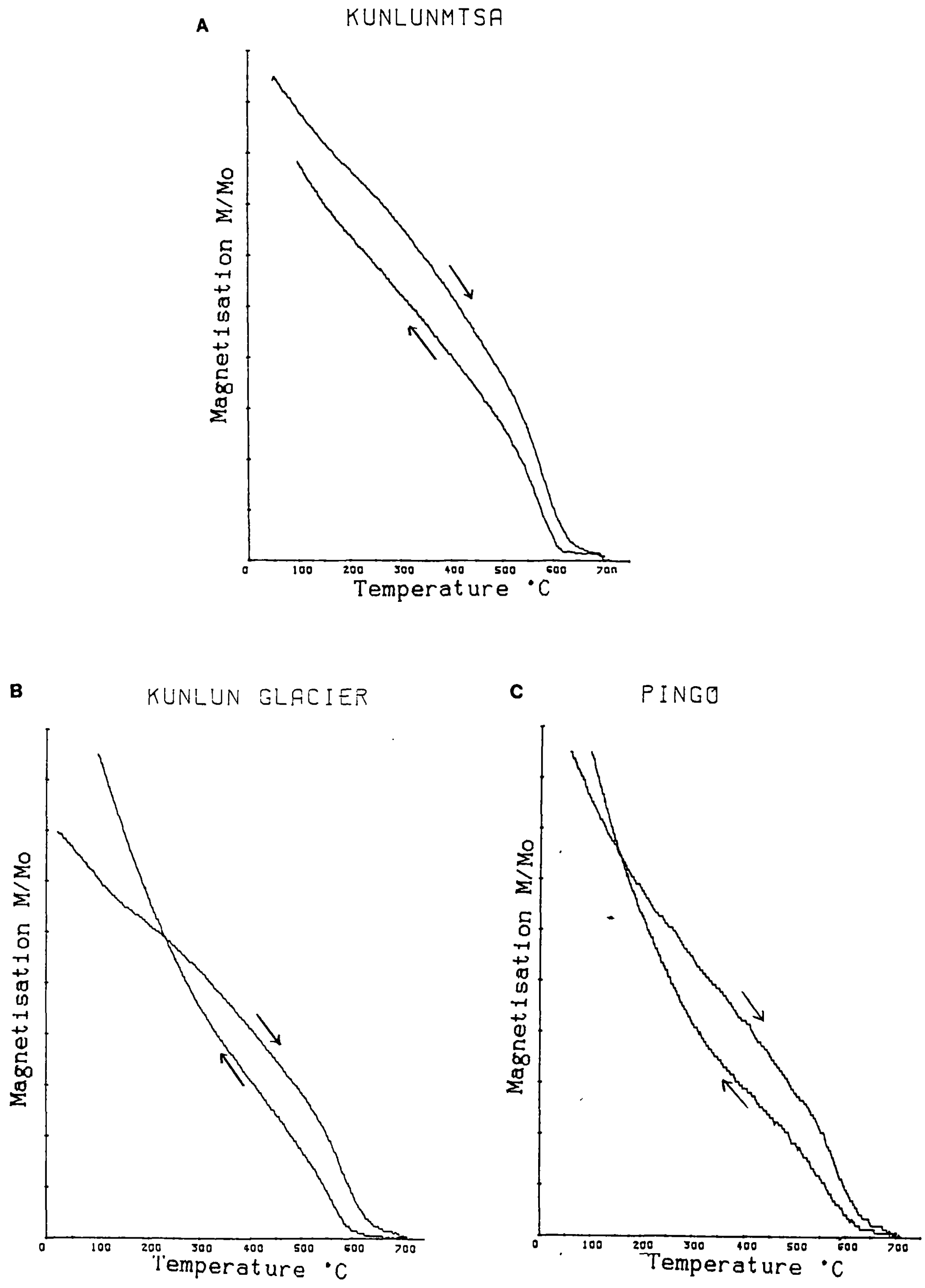

Figure 5.14 Thermomagnetic curves from (a) Kunlun A (b) Glacier and (c) Pingo sediment samples.

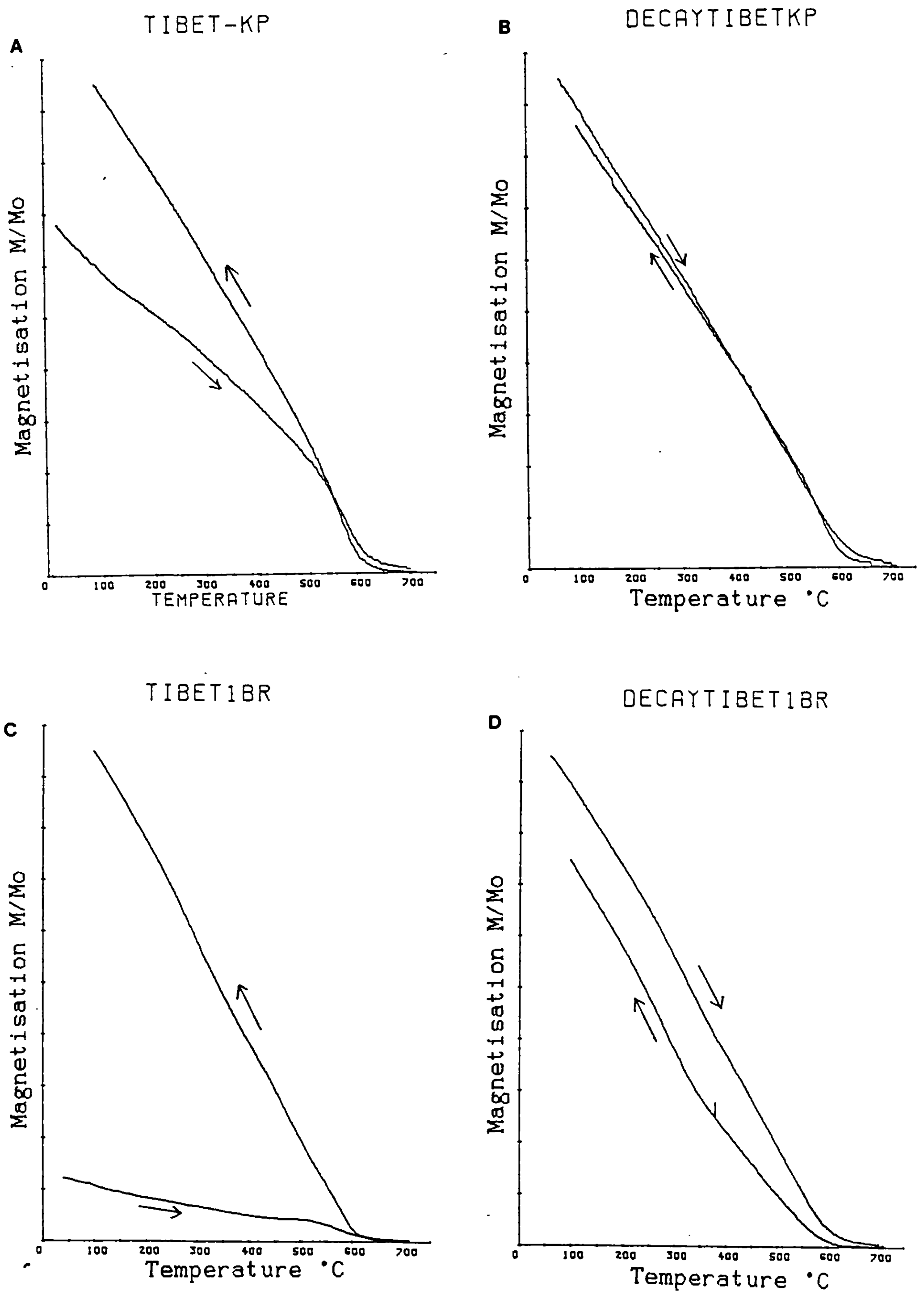

Figure 5.15 Thermomagnetic curves for (a) Kunlun Pass (b) Kunlun Pass immediately reheated (c) Qumar Heyan (d) Qumar Heyan sample reheated.

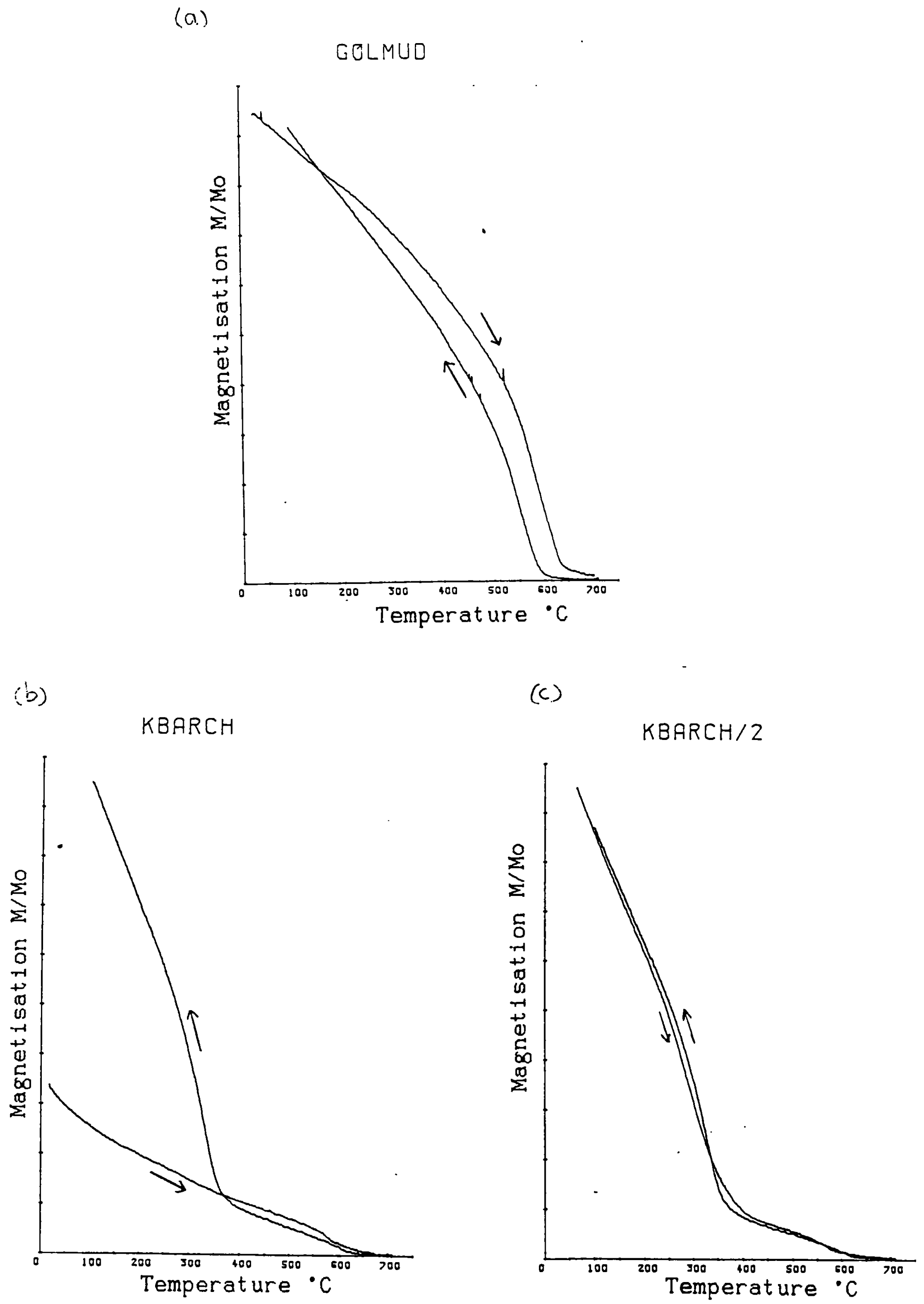

Figure 5.16 Thermomagnetic curves from (a) Qaidam Desert sand (b) Kunlun barchan dune sand (c) barchan sand immediately reheated.

5.3 Isothermal remanence

This technique has been used here to determine whether there is a high coercivity antiferromagnetic component of magnetisation, for example, hæmatite or goethite, present within the sediments. The other techniques used in this thesis, susceptibility, hysteresis and thermomagnetic behaviour are biased towards the ferrimagnetic minerals, as they have a stronger spontaneous magnetisation and swamp the antiferromagnetic components.

Isothermal remanence (IRM) is the remanence acquired by a sample at the ambient temperature upon the application of a strong magnetic field. The field at which saturation isothermal remanence (Mrs) is reached depends upon the coercivity spectrum of the constituent minerals. The difference in coercivity spectra of magnetite/maghæmite and hæmatite means that this technique may be effectively applied to distinguish between the different components of magnetisation (figure 5.17). The majority of magnetite and maghæmite grains saturate in fields of 10-100mT, with a maximum theoretical coercivity of 300mT. Hæmatite does not saturate until fields of betweeen 1000-6500mT (1-6.5T), depending upon particle size (Tarling, 1983). Although pure goethite does not acquire an isothermal remanence until fields exceed 4000mT (Rochette and Fillion, 1989), defect goethite can acquire remanence below 4000mT.

5.3.1 Measurement

IRM acquisition was carried out in the Department of Geography at Liverpool University. Stepwise fields of 10-300mT were applied using a Molspin Pulse Magnetiser and a Trilec Pulse Magnetiser was used for larger fields of 400mT - 4000mT. The remanent magnetisation of each sample was measured on a Molspin spinner magnetometer immediately after removal from the field.

5.3.2 Results

IRM acquisition curves were obtained from all of the Gansu loess sites. The percentage of total magnetisation acquired at fields of 30, 100, 300 and 1000mT was calculated along with the saturating field (table 5.11). The IRM acquisition curves for all of the samples were similar to figure 5.18b indicating the presence of a large 'soft', low coercivity component (10-300mT); a small intermediate coercivity component (300-1000mT); and small high coercivity, 'hard' component (>1000mT).

The palaeosol samples from both Jiuzhoutai (figure 5.18) and Dawan (figure 5.19) show a larger percentage magnetisation acquired in fields of 30mT and 100mT than the loesses indicating that, as with the hysteresis results, the palaeosols contain a larger proportion of soft coercivity minerals. The fraction <30mT is likely to be held by both multidomain magnetite and viscous grains on the SP/SSD boundary, with PSD-SD magnetites saturating between 30-100mT. The strongest developed palaeosols (JPI; DPIII; DPVI) show the largest percentage acquisition of magnetisation at the lower fields due to the higher concentration of viscous ultrafine magnetites. Both the Labrang and Sala Shan samples (figure 5.20) behave similarly to the loess suggesting a predominance of a harder magnetic component in these and the loess samples than in the palaeosols.

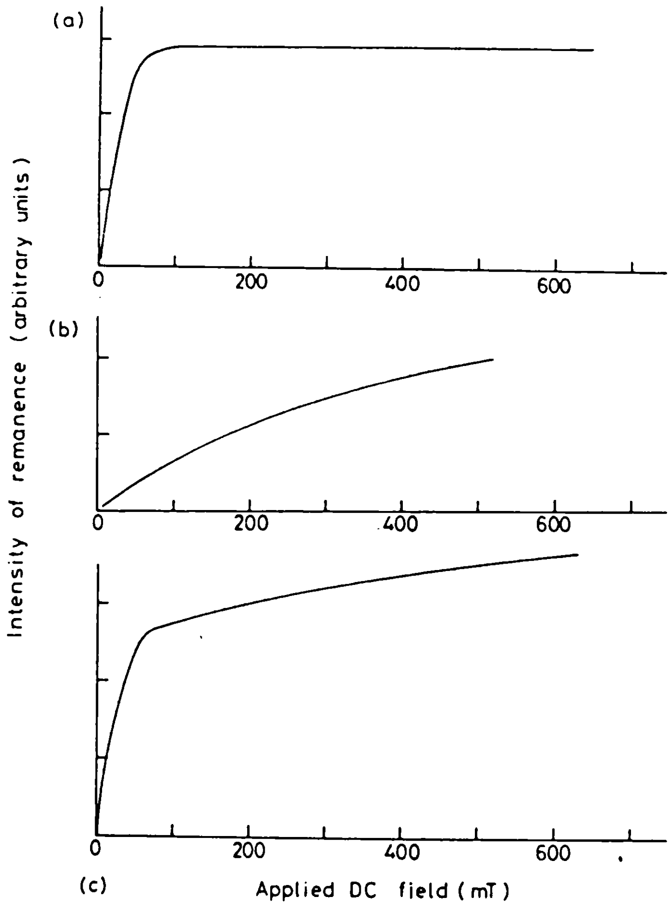

Figure 5.17 IRM curves for magnetite and hæmatite (a) magnetite saturates in weaker fields than (b) hæmatite. When both minerals are present (c) the observed curve is a summation of the two curves, dominated at low fields by magnetite.

The samples acquired 5-10% of their total magnetisation at fields above 300mT, indicating the presence of a magnetically harder fraction which is probably hæmatite. The Sala Shan sample was the only exception, acquiring 17% of its magnetisation above 300mT and 7% above 1000mT (1T) indicating that it contains a larger concentration of high coercivity ('hard') minerals than the other samples.

In conclusion, the samples are dominated by a magnetite/maghæmite mineralogy which contributes up to 90% (except for the Sala Shan sample) of the remanence bearing grains. The remaining 5-17% of the remanence is held by a higher coercivity phase which is likely to be either hæmatite or defect goethite. However the absence of evidence of goethite from the Curie curves (section 5.2) suggest that it is more probably hæmatite.

Table 5.11 Percentage of the total magnetisation acquired in fields of 30mT, 100mT, 300 and 1000mT and the saturating field for loess samples from Gansu.

Site	Sample	Unit	% total magnetisation acquired at: 30mT	100mT	300mT	1000mT	saturating field(mT)
Labrang	A0.100	LA	16	54	90	99	>4000
Sala Shan			11	47	83	93	>4000
Jiuzhoutai	46.575	LI	15	55	91	97	1500
	48.975	PI	23	62	93	97	>4000
	50.400	LII	15	57	92	99	1500
	51.225	PII	21	61	91	99	>4000
Dawan	21.825	LI	15	58	93	97	3000
	25.025	PI	22	61	93	99	3000
	26.550	LII	14	50	91	97	>4000
	27.875	PII	21	55	93	99	3000
	30.000	PIII	33	65	93	100	1000
	30.875	LIV	15	43	90	99	1500
	32.500	LIV	16	43	93	100	1000
	33.025	PIV	23	52	92	99	1500
	33.525	LV	13	55	90	96	3000
	34.025	PV	20	59	93	99	2000
	35.275	PVI	33	70	92	100	1000

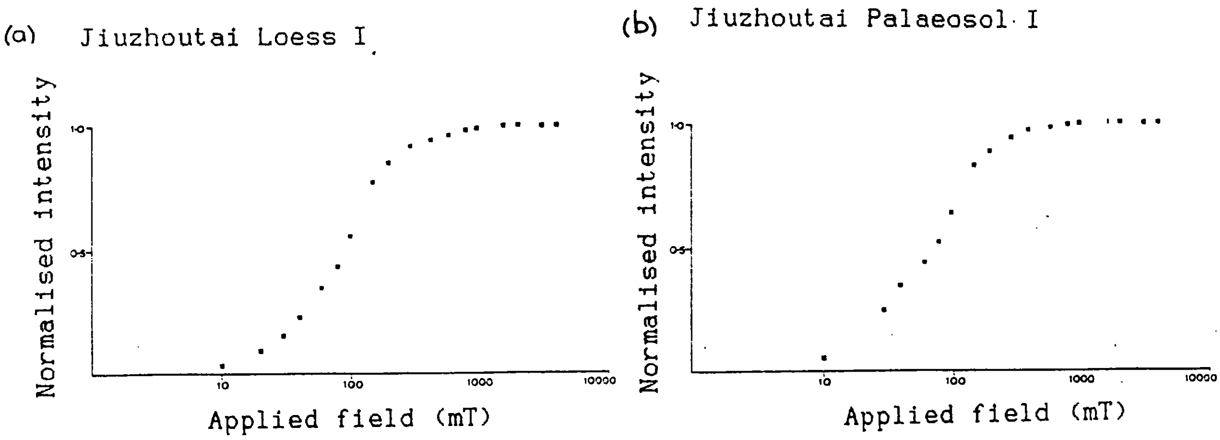

Figure 5.18 IRM acquisition curves for Jiuzhoutai (a) loess I and (b) palaeosol I.

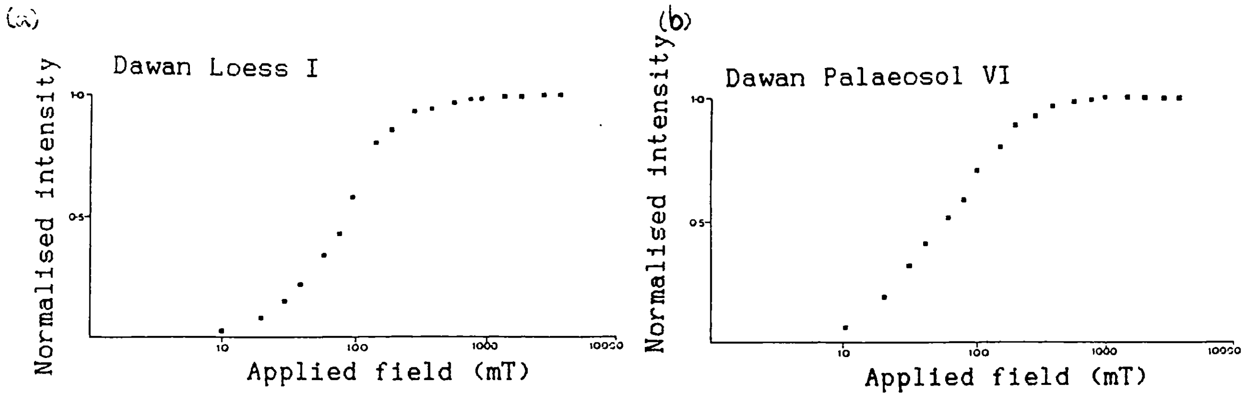

Figure 5.19 IRM acquisition curves for Dawan (a) loess I and (b) palaeosol VI.

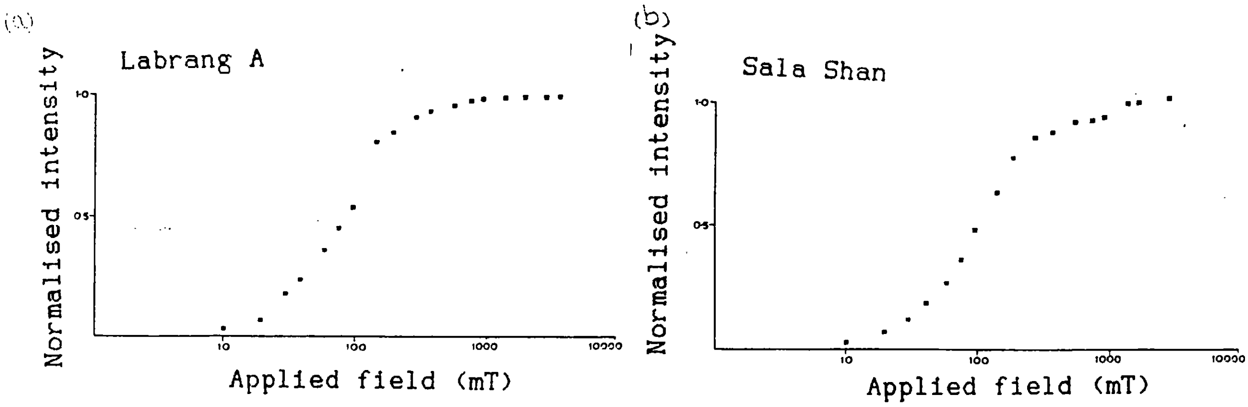

Figure 5.20 IRM acquisition curves for (a) Labrang loess and (b) Sala shan loessic alluvium.

6. SUMMARY OF MAGNETIC MINERALOGY

6.1 Loess and palaeosol sequences from Lanzhou

Both low field and high field tests were carried out to assess the variation in magnetic mineralogy down two loess profiles and across the area of the Tibetan Front. Magnetic minerals originate within loess either as a result of detrital aeolian input or *in situ* chemical or bio-chemical formation. Some measure of the detrital input may be gained from the study of modern dust storms. Liu Tungsheng *et. al.* (1981) collected dust that settled on the roof of the Academia Sinica building in north Beijing during a storm in April 1980. This dust originated 1500km away in the northwest of China, beyond the Hexi Corridor. Mineralogical analysis of the dust taken at the beginning of the storm prior to any mixing and addition of local material, indicated the presence of quartz and feldspars (usually coated with a film of carbonates and iron oxides) as well as hæmatite, magnetite and limonite. King (1990) has recently used this evidence to infer a detrital origin for the magnetite and hæmatite at Jiuzhoutai and a subsequent primary remanence for the hæmatite. The dust in this 1980 storm was apparently carried at high altitude by the strong west wind associated with the Mongolian high pressure system, from the northwest of the Hexi Corridor and western Inner Mongolia "which is the arid desert and gobi area adjacent to the loess plateau and has long been postulated as the provenance of the loess (Liu Tungsheng *et. al.*, 1981, p. 155)". However there is no evidence that the dust did not contain reworked loess from the vast Loess Plateau over which the storm had previously travelled. Ideally dust should be collected from storms at sites to the west of the Loess Plateau so that interaction with existing loess deposits is minimised.

6.1.1 Jiuzhoutai

The variation in magnetic mineralogy throughout the section at Jiuzhoutai reflects the different magnetic assemblages present in loess and palaeosols. The palaeosols are dominated by ultrafine single domain and superparamagnetic magnetite or CD magnetite, including viscous grains which span the SP/SSD boundary and show a time-dependent magnetisation. The magnetic assemblage of loess is characterised by coarser-grained MD and SD magnetite.

Thermomagnetic curves for Jiuzhoutai (figure 5.9) suggest the presence of cation-deficient magnetite within the loess and palaeosol horizons. One of the palaeosol samples showed increased magnetisation after heating (figure 5.9d) which may be the result of the reducing environment created by heating in the presence of organic carbon within the soil which would cause the reduction of hæmatite to magnetite, or possibly the conversion of some clay minerals to magnetite. IRM acquisition and hysteresis showed the presence of a high coercivity component which is most likely to be hæmatite or defect goethite.

Frequency dependent susceptibility shows a higher proportion of superparamagnetic grains within palaeosols consistent with the proposal of Liu Xiuming *et.al.* (1990) that frequency dependence is sensitive to palaeoclimatic variations. The susceptibility behaviour of loess and palaeosols at low temperature (section 4.2) is interpreted as resulting from the combination of a paramagnetic component and an opposing SP component, with SD grains showing little variance with temperature and thus forming a 'baseline'.

Hysteresis parameters were derived from samples taken at intervals throughout the Jiuzhoutai section (section 5.1). Ms values vary down the section in conjuction with Mrs reflecting a variation in degree of pedogenesis related to the *in situ* production of magnetic minerals. These variations contradict the magnetic susceptibility dating hypothesis proposed by Kukla *et.al.* (1988) and Kukla and An (1989) who proposed that magnetic enhancement of palaeosols was the result of constant sedimentation of ferrimagnetic minerals combined with a decreased sedimentation of diluting quartz and feldspars. Mrs/Ms ratios confirm that the palaeosols are dominated by a finer magnetic component than the loesses in agreement with the low temperature susceptibility behaviour. Coercivities decrease within the palaeosols indicating a higher percentage of 'soft' minerals, such as viscous grains at the SP/SSD boundary.

6.1.2 Dawan

Thermomagnetic curves for Dawan loess are similar to those of Jiuzhoutai loess, indicating the presence of CD magnetite, in an intermediate oxidation state between magnetite and maghæmite (figs 5.10-5.12). Curves from three of the palaeosol samples (figure 5.12) gave increased magnetisations upon cooling possibly indicating the reduction of hæmatite to magnetite in the presence of organic carbon, or the conversion of clay minerals to magnetite. Two of these palaeosols were the most strongly developed soils (III and VI) studied in this thesis.

Low field susceptibility indicates the presence of six palaeosols apparently arranged into two triple pedocomplexes. Frequency dependent susceptibility shows some relationship to these climatic fluctuations although they cannot explain all of the peaks in the frequency dependence. The noise level, in which an error of one unit may give a χFD of 5% may have contributed to some of the variation.

Ms and Mrs values appear to behave synchronously down the section, as in Jiuzhoutai, reflecting changes in concentration of magnetic minerals. Both Ms and Mrs suggest that there were two phases of increased magnetic concentration between 30.0 and 31.5 metres. The χFD curves (figure 4.8) suggest that this is due to an increase in pedogenesis. Mrs/Ms ratios increase significantly below a depth of 24.5m metres (0.5 metres above palaeosol I) implying that loess I contains a coarser magnetic component, with a greater proportion of MD magnetite or maghæmite, than the older loesses (II-VI). The concentration of SP/SSD grains within the loess indicated by χFD% appears to remain fairly stable both above and below this depth. The increase in the proportion of SD grains in the lowermost 0.5m of loess I may be due to intermixing of the upper palaeosol layer and the overlying loess. Mrs/Ms values are higher in the palaeosols than in the loess indicating a larger proportion of SD grains within the palaeosols. As with the Jiuzhoutai results, hysteresis coercivities and IRM acquisition point to an increase in SP/SSD magnetite within the soils. The IRM acquisition curves also point to the presence of a high coercivity mineral component, which is most likely to be either hæmatite or defect goethite.

6.2 Southern Gansu loess

The Labrang loess gave mean low field susceptibility (χ) results (27.5 x 10^{-8}kg^{-1}) similar to the results obtained from loess units at Jiuzhoutai (26.2-28.5x10^{-8}kg^{-1}) and Dawan (26.7-30.6x10^{-8}kg^{-1}). None of the Labrang samples showed any frequency dependence (χFD%) indicating an absence of superparamagnetic grains within the size range affected by the test. Hysteresis parameters derived from a sample of Sala Shan loessic alluvium gave comparatively low Ms values indicating a relative paucity of ferrimagnetic minerals within the sample. Mrs/Ms ratios for the sites showed that the Labrang loess was dominated by coarser grained multidomain magnetite than the Sala Shan loessic alluvium and both the loess and palaeosol units from around Lanzhou. Thermomagnetic curves from Labrang indicate cation-deficient magnetite. Coercivities derived from IRM acquisition suggest that there is a hard component, which may be hæmatite or goethite and is proportionally more abundant in the Sala Shan loess ic alluvium. In addition to this hard antiferromagnetic component there is also a softer magnetite component.

6.3 Qaidam Basin, Kunlun Mountains and Tibetan Plateau

Thermomagnetic curves of the sediments from this high altitude mountain dominated environment indicate that CD magnetite dominates the magnetic component. This is most likely explained by a CD surface coating surrounding the magnetite grains. Hysteresis results indicate soft coercivity minerals, which with Mrs/Ms ratios and χFD% suggests a large proportion of multidomain magnetite. The grey silt sample taken from the ice core of the pingo shows a high Mrs/Ms with a high coercivity indicating a large proportion of SD magnetite. Magnetic grains size appears to become coarser toward the Qaidam Basin although in the absence of bedrock information no inferences can be derived from this apparent trend. IRM acquisition curves were not obtained for these samples due to a paucity of material and thus the definite presence or absence of a harder magnetic component *e.g.* hæmatite or goethite, cannot be ascertained.

6.4 Summary of the magnetic mineralogy of Tibetan Front sediments

Thermomagnetic curves show that a combination of CD magnetite and magnetite dominates the magnetic mineralogy of Tibetan Front sediments and is likely to be a detrital component of the Lanzhou loess. The oxidising environment of the Loess Plateau and Tibetan Front region may be the cause of the cation-deficiency causing the formation of a CD coating around magnetite grains.

Mrs/Ms ratios showed an increase in proportion of coarse grain magnetic component from the Tibetan Plateau to the Qaidam Basin sediment, which is dominated by MD grains (table 6.1). No ultrafine magnetites were found within the Tibetan or Labrang silts.

Table 6.1 Mrs/Ms values for the Tibetan Front sediments.

Area	**Site**	**Mrs/Ms**	**mean %χFD**
Tibetan Plateau	Qumar Heyan	0.120	0
Kunlun Mtns	Kunlun Pass	0.108	0
	Kunlun Glacier	0.094	0
	Kunlun A	0.061	0
Qaidam Basin	Qaidam Desert	0.044	0
A'nyêmaqen Mtns	Labrang	0.107	0
Southern Gansu	Sala Shan	0.134	2
Loess Plateau	Dawan loess	0.119 - 0.141	2.2-4.5
	Dawan palaeosol	0.148 - 0.160	4.4-8.5
	Jiuzhoutai loess	0.125 - 0.138	2.6-2.8
	Jiuzhoutai palaeosol	0.153 - 0.156	4.0-7.4

Table 6.1 shows that the Loess Plateau silts (including Sala Shan which is situated at the extreme edge of the Loess Plateau in southern Gansu) contain a finer grained magnetic mineralogy than the sediments of the surrounding mountain and desert environments.

7. MAGNETOSTRATIGRAPHY

7.1 The Earth's Magnetic field

The Geomagnetic field is thought to be generated by the movement of electrical currents in the Earth's molten core. It is described by a vector whose components, inclination (I), declination (D) and intensity (F) are used to define the field at any point on the Earth's surface (figure 6.1). Inclination is the angle of dip of the field below the horizontal plane, varying from near 0° at the equator to near 90° at the poles. Declination is the angle between the horizontal component of the field and the true geographical north. The vertical and horizontal components of the intensity F are denoted by z and H (which can be further resolved into x and y which correspond to north and east orthogonal components).

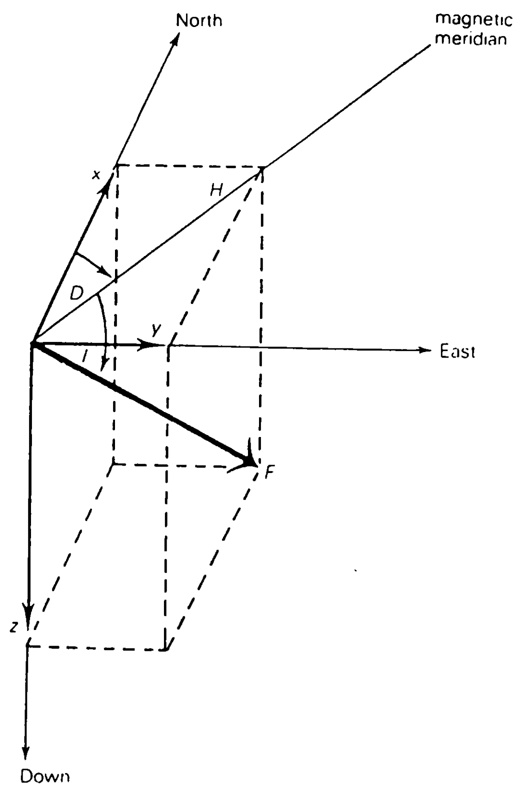

Figure 7.1 The relationship between the components of the magnetic field. (Thompson and Oldfield, 1986)

The Earth's magnetic field is considered to be made up of a dipole and non-dipole field. The primary component, the dipole field, is fairly stable and accounts for about 90% of the Earth's field. The dipole field that best fits the actual field of the Earth today has its poles at 11.5° from the geographic poles (Thompson and Oldfield, 1986). The secondary non-dipole field component comprises the remaining ~10% of the field and is more variable. Major changes in the Earth's magnetic field are the result of changes in the dipole field with minor variations due to non-dipole factors.

The changes in the Earth's magnetic field over time can be studied due to the fact that rocks and sediments record the position of the field at the time of their formation or deposition. Examination of these materials has shown that the field has reversed polarity, by swinging through 180°, many times in the past. For example, over the last 3.6Ma there have been four major reversed and normal polarity chrons (Jacobs, 1984). Within these chrons there have been documented magnetic excursions, or subchrons, with a duration of about 10ka (figure 7.2). The study of rocks with a high deposition rate may also yield records of palaeosecular variation.

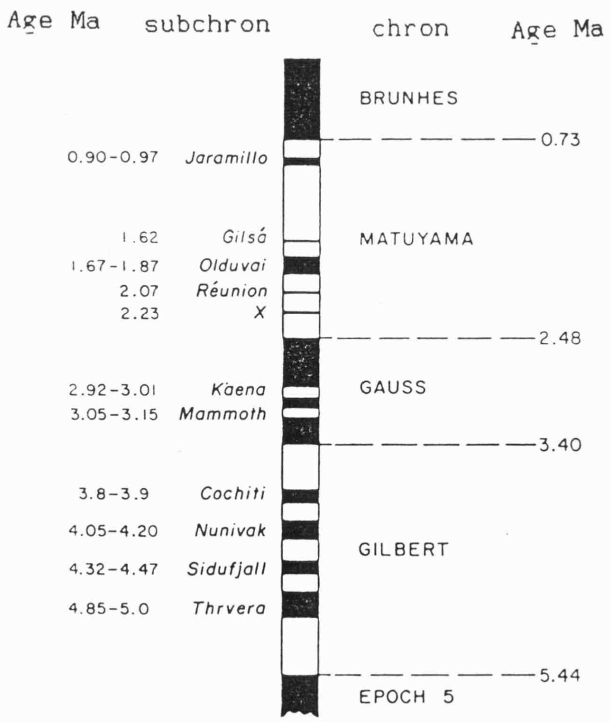

Figure 7.2 Polarity timescale for the last 5 million years. Normal polarity periods are coloured in black (from Bradley, 1985).

7.2 Remanence acquisition in sediments

There are essentially three methods of remanence acquisition pertinent to the study of sediments. These are depositional (detrital and post-depositional) remanence, chemical remanence and viscous remanence. Thermoremanence, caused by the cooling of a substance through its critical blocking temperature, is of more relevance to the study of igneous and metamorphic rocks.

7.2.1 Detrital and Post-Depositional Remanent Magnetisation

An air fall deposit such as loess will acquire a detrital remanence (DRM) upon deposition. As the grains fall through the air column and are distributed by wind they carry a previously acquired magnetic moment which, if positioned in a medium free of external forces, would align to the direction of the Earth's magnetic field. However, upon deposition, the alignment of the grains is affected by the wind direction, the shape and size of the grain and how it fits into the surface texture of the deposit. For example, a small round grain will fall or roll into a hole provided between larger grains on the surface of the deposit. Loess fabric has been described as random and isotropic (Derbyshire *et. al.*, 1988), however, preferential orientation of grains can be attained by the realigning of grain long axes to an imposed flow direction by wind or water (see chapter 8). Once the grain is surrounded by other grains such that it is trapped within the sediment, due to consolidation, the magnetisation is "blocked" in. Subsequent realignment, caused by processes such as bioturbation, salt crystallisation, mass wasting or rotation of particles in water-filled interstices, would lead to the formation of a post-depositional remanent magnetisation (PDRM).

Laboratory redeposition experiments have been widely used to study detrital remanence, although these have been mainly concerned with deposition through a water matrix. In these experiments the detrital remanent magnetisation has been shown to correctly record the declination component of the applied field, however the inclination record is problematic and often too shallow (King, 1955). The cause of the inclination error has been attributed to either bedding error (King and Rees, 1966), where as the grain rolls down an inclined bed it tends to settle on a slight plateau, or berm, leading to a more horizontal inclination than that of the applied field; or as the result of particle shape and settling within the sediment matrix provided by the sediment (Griffiths et.al., 1960). A more recent study (Levi and Banerjee, 1990) suggested that the size of the grain is also relevant, large multidomain grains being more affected by gravity and the surrounding matrix than small relatively strongly magnetised single domains which will be more likely to orient towards the field. However, as most laboratory experiments greatly increase natural deposition and consolidation rates, the inclination error in such studies may be a result of experimental design (Barton et.al., 1980).

7.2.2 Chemical Remanent Magnetisation

A chemical remanent magnetisation (CRM) is formed when the growth of a new magnetic mineral causes it to exceed its critical blocking volume (V_B); or when alteration of an existing magnetic mineral causes the formation of a new magnetic mineral at a temperature below its critical blocking temperature (T_B). A CRM may be formed as a result of chemical changes in detrital magnetic minerals or the production of new magnetic minerals from iron-containing compounds. Weathering and diagenesis of iron-bearing minerals, such as olivines, pyroxenes and amphiboles, releases highly mobile Fe ions, which then undergo a series of reactions, hydrating to form iron hydroxides such as goethite and lepidocrocite (Tarling, 1983).

Chemical alteration of detrital magnetic minerals includes: inversion of maghæmite to hæmatite ($\gamma Fe_2O_3 \rightarrow \alpha Fe_2O_3$); reduction of hæmatite to magnetite ($\alpha Fe_2O_3 \rightarrow Fe_3O_4$); or oxidation of magnetite to hæmatite ($Fe_3O_4 \rightarrow \alpha Fe_2O_3$). Heider and Dunlop (1987) found that when acicular SD magnetite underwent oxidation to a cation-deficient spinel (maghæmite), the CRM preserved the primary NRM direction. However, when the SD magnetite was further oxidised to hæmatite and maghæmite (100% $Fe_3O_4 \rightarrow \alpha Fe_2O_3$ was never achieved), involving a change in lattice structure, the resultant CRM did not refelect the primary NRM direction or the geomagnetic field during oxidation.

7.2.3 Viscous Remanent Magnetisation

When a magnetic material is exposed to a magnetic field it will slowly acquire a magnetisation in the direction of the field. The rate of acquisition of a viscous remanent magnetisation (VRM) depends upon the ambient temperature, grain size and spectrum of relaxation times. VRM is most rapidly acquired by grains of low blocking temperature or coercivity.

7.3 Measurement of remanence

The remanence of samples from Dawan, Jiuzhoutai and Labrang were measured on a Minispin spinner magnetometer before and after stepwise thermal demagnetisation in the Geomagnetism Laboratory at the University of Liverpool. The magnetometer and oven were situated inside a low field cage (a set of Rubens coils), with a field inside the cage of less than 4% of the Earth's field, so that the samples were protected from acquiring a viscous remanence when transferring between the oven and the magnetometer. The magnetometer has a noise level of approximately $0.05 \times 10^{-5} Am^2 kg^{-1}$.

7.3.1 Demagnetisation of loess and palaeosols

Thermal demagnetisation was utilised in this study instead of alternating field demagnetisation (A.F.). In A.F. demagnetisation, the rock or sediment sample is placed in a zero direct current magnetic field and then subjected to cycles of alternating fields of increasing then decreasing strength with the effect that the magnetic minerals in the sample are forced through a series of hysteresis loops. All magnetic domains of coercivity less than the peak alternating field strength will follow the direction of the field as it alternates. When the field falls below the coercivity of a grain, the spin orientation of the domain becomes realigned. MD grains are effectively demagnetised by this method as the magnetic moments from the domains are left with an equal contribution in each of the two antiparallel preferred orientations and therefore cancel each other out. However, individual SD grains are not effectively demagnetised by this method, due to the dominance of their shape anisotropy. However, providing that there is no preferred alignment of the SD grains, then the moments will become randomised and they will cancel each other out, thereby reducing the total SD remanence to (almost) zero. The peak fields attainable in the AF equipment are also not sufficient to demagnetise hæmatite or goethite which have high coercivities.

Thermal demagnetisation involves subjecting the sample to progressive heating and cooling cycles in zero field, using succesively higher temperatures, with the remanence measured after each cycle. As the temperature increases, the relaxation time (τ) of the constituent magnetic grains exponentially decreases, according to equation 4.1 (see section 4.1.4). When the temperature passes through the specific blocking temperature of a particular grain (T_B), the relaxation time (τ) is reduced to a few seconds and the remanence is 'unblocked', with the grain thus behaving superparamagnetically. Once randomised the magnetisation returns to the 'easy' axes of the particle, which in a random isotropic assemblage of grains would lead to a net remanence of zero. Progressive stepwise heating and cooling gives a measure of the blocking temperature spectrum of the sample. Grains with the shortest relaxation times (and lowest T_B) are thermodynamically most susceptible to acquiring a secondary magnetisation over time, 'overprinting' the original remanence. Such secondary components are removed first upon thermal demagnetisation, leaving the thermally harder primary magnetisation at higher temperatures.

The main problem with thermal demagnetisation is that increasing temperature can lead to chemical alteration of magnetic minerals and such alteration may lead to a large increase in sample susceptibility with an increased potential for contamination by a laboratory viscous remanence.

7.3.2 Statistical analysis and data presentation

Orthogonal vector plots were used to assess the demagnetisation behaviour of the samples, within the vertical (denoted +) and horizontal planes (denoted x) - see figure 7.6. For each sample the component of magnetisation was defined using more than three points (see Appendix II) forming a vector converging on the origin. The direction of each component of magnetisation was calculated using principal component analysis with determination of the maximum angle of deviation (MAD) (Kirschvink, 1980).

7.4 Results

Secular variation plots were derived for Jiuzhoutai and Dawan. The expected average primary remanence direction for Lanzhou, predicted using the geocentric axial dipole is inclination: 54.1°; declination: 0°.

7.4.1 Jiuzhoutai

Samples to be measured were taken with approximately a ten centimetre interval down the section. Initial NRM varies from 0.28 - 0.81 x 10^{-6}

Am^2kg^{-1} in loess to 0.77 - 1.77 x 10^{-6} Am^2kg^{-1} in the palaeosols. The primary vectors obtained from the samples gave results indicative of stable conditions of the Earth's magnetic field. The secular variation curve of change in inclination and declination with depth is presented in figure 7.5. No evidence of a magnetic excursion was found. The deposition rate in the upper part of Jiuzhoutai section has been estimated at 26cm per 1000 years (Rolph *et.al.*, 1989) and thus an excursion with a duration of 1000 years would be identified in two consecutive samples. The Blake Event, believed to occur within the last interglacial has been documented as lasting at least 6000 years (Tucholka *et.al.*, 1987) and would therefore be observed in at least 15 samples. The magnetic fabric results (chapter 8) from this site suggest that reworking due to slope processes has occurred which may explain the absence of the Blake Event.

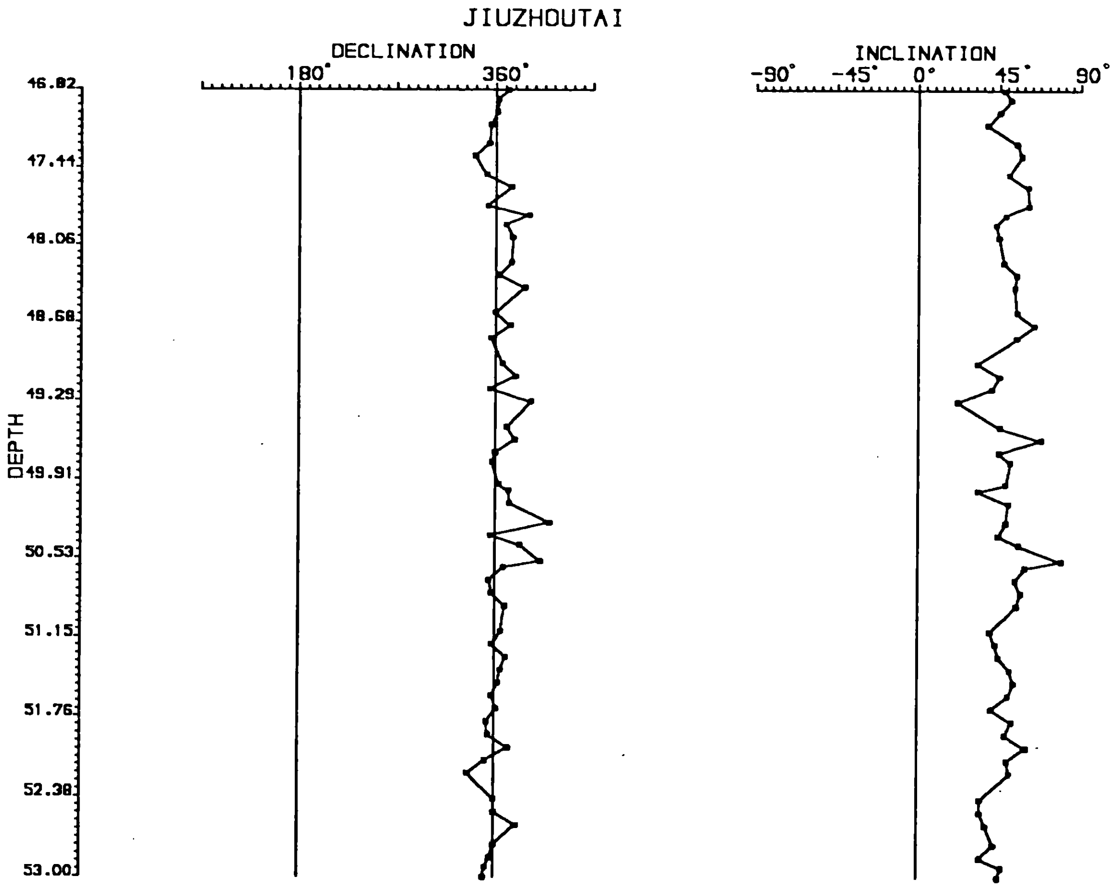

Figure 7.3 Variation in inclination and declination through seven metres of sediment at the Scorpion Pit, Jiuzhoutai.

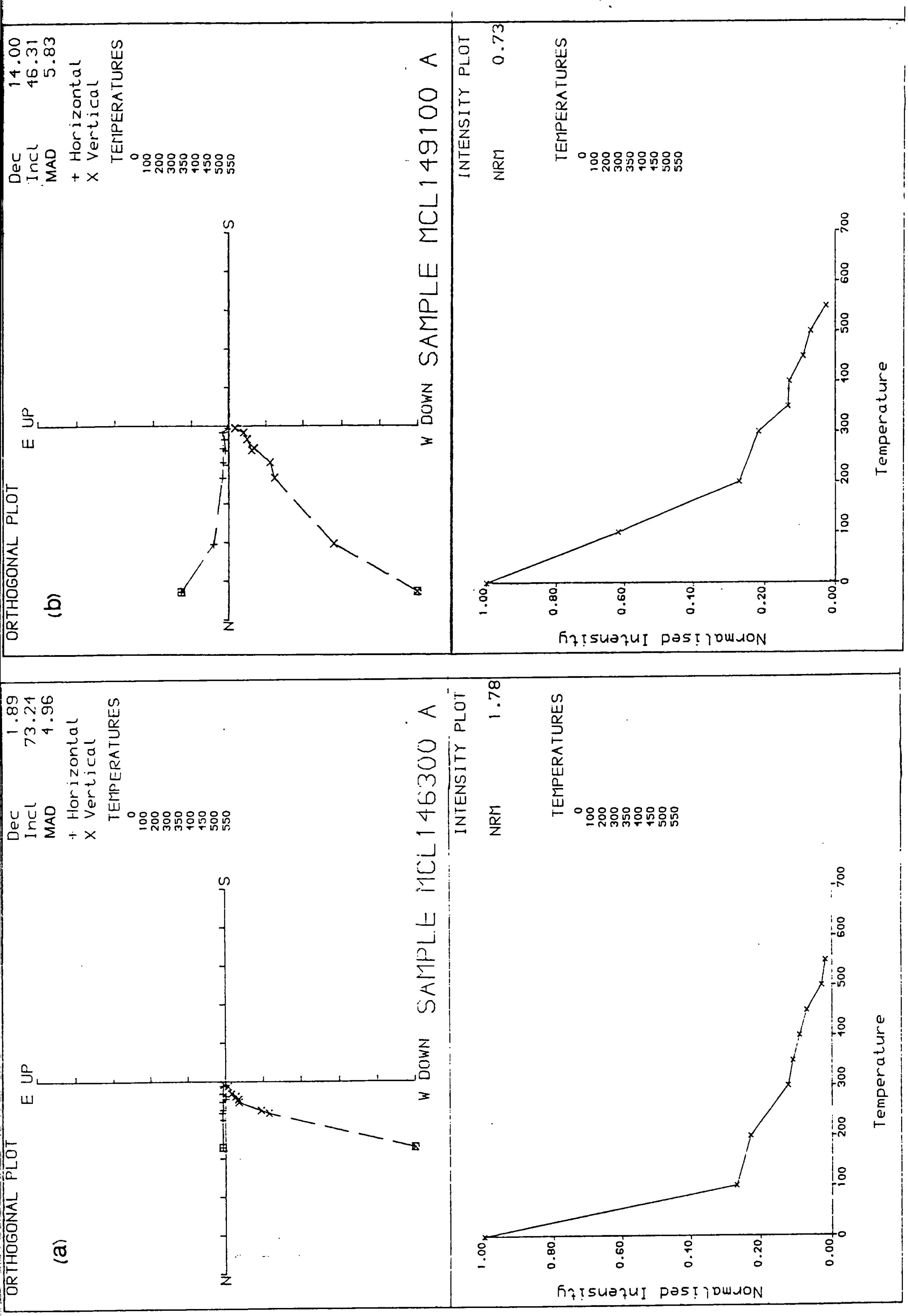

Figure 7.4 Orthogonal vector plots of samples of Jiuzhoutai (a) loess I and (b) palaeosol II.

The demagnetisation characteristics of the samples give a measure of their blocking temperature spectra. Loss of NRM with temperature has been calculated and is presented in Appendix II (table II.2). The results suggest that the remanence holding magnetic grains within the palaeosols have a lower blocking temperature spectrum than those of the loess. This is probably due to the higher concentration of ultrafine magnetic minerals in the palaeosols, as for single domain grains blocking temperatures depend upon grain size.

7.4.2 Dawan

The sample spacing at Dawan was also ten centimetres although as the depth of section covered was fifteen metres, compared with the seven metres at Jiuzhoutai, a more comprehensive secular variation curve was obtained (figure 7.5). Initial NRM intensities in loess varied from 0.21 to 1.61 x $10^{-6}Am^2kg^{-1}$ and from 1.45 to 3.09 x $10^{-6}Am^2kg^{-1}$ in the strongest developed palaeosols. Declination varies around a 0-10° throughout the section however the variation in inclination is more complex. At the base of the section, between 35 and 32 metres inclination varies about 20-30° before increasing to about 55° where it remains stable for the next 10 metres until at 22 metres it again dips rapidly by about 30° before increasing rapidly to 78° at 20.2m. The change in inclination above 22 metres is a rapid one, whereas between 35 to 32 metres the increase is more gradual. These changes in inclination are not mirrored in the declination record suggesting that inclination errors or post-depositional alteration may be the cause. Repeatability of measurement is demonstrated in figure 7.6 where two samples from the same height have been tested. 79% of all Dawan samples gave well defined vectors with MAD values below 10°.

Using an estimated deposition rate of 21cm per 1000yr (obtained by altering the deposition of Rolph *et.al.*, (1989) to the thickness of loess at Dawan) an excursion of 1000 years would be present in two consecutive samples and the Blake Event in fifteen samples.

Demagnetisation characteristics were calculated and are presented in Appendix II, table II.4. As with the Jiuzhoutai results, the blocking temperature spectra of the palaeosols are lower than those of the surrounding loess, probably due to the finer magnetic mineralogy.

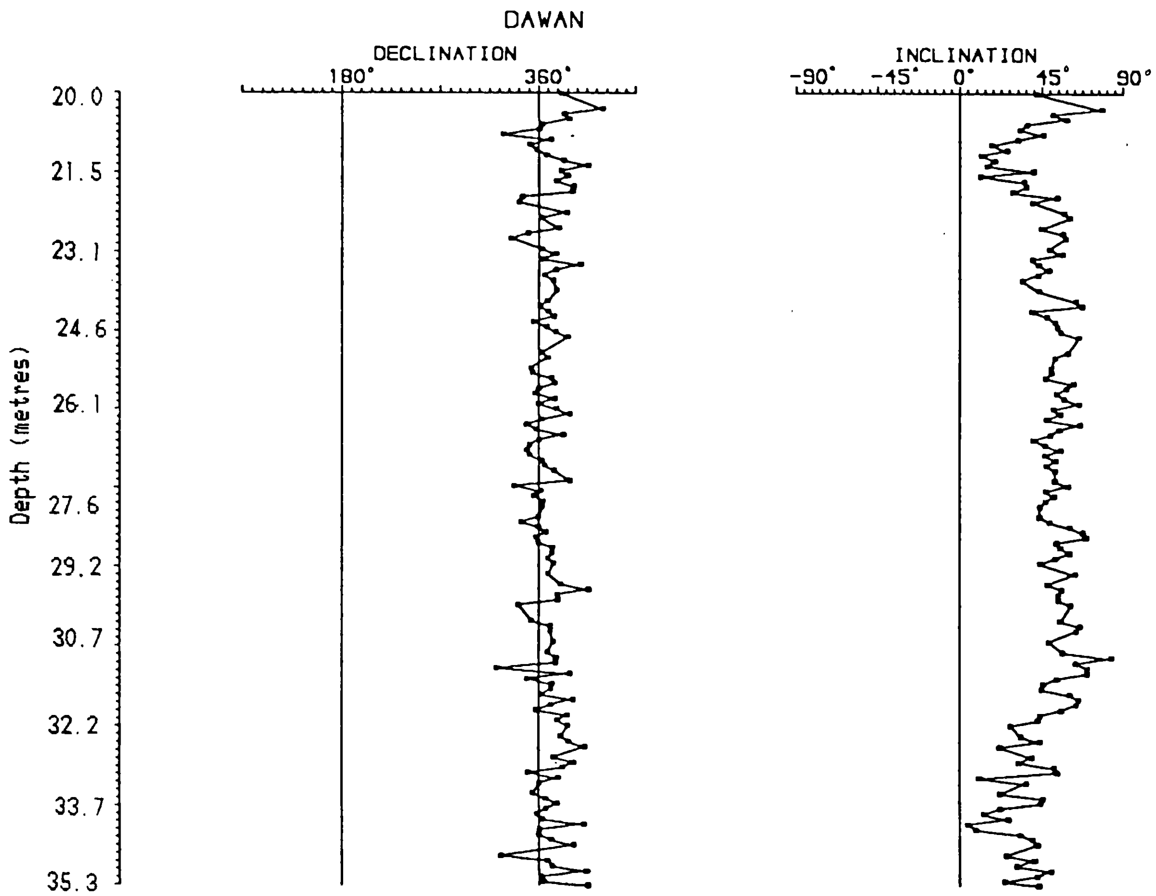

Figure 7.5 Variation in inclination and declination through fifteen metres of Dawan sediment

7.4.3 Labrang

Nine samples from the site at Labrang were measured (table 7.1). NRM intensities are lower for Labrang B than Labrang A, which was sampled 12 metres below B, although both are low and compare with initial NRM of loesses from the other sites. Both declination and inclination are in the range expected for a normal polarity sample from Gansu and the variation with depth is probably as much a result of computational errors as secular variation. Labrang A, which has average inclination values of I = 48.6°, shows an inclination shallowing of 5.5°. Labrang B, which is visibly coarser and less compacted, has an average inclination of 56.4°, which is

2.3° steeper than the average predicted by the geocentric axial dipole. The demagnetisation characteristics are listed in Appendix II, table II.5.

Table 7.1 Declination, inclination and initial NRM intensities derived from thermal demagnetisation of Labrang loess. The number in brackets indicates the number of points used in calcualtion of the MAD.

<u>Sample</u>	<u>MAD</u>	<u>dec</u>	<u>inc</u>	<u>NRM</u>
Labrang B				($Am^2kg \times 10^{-6}$)
0.000	3.5 (5)	351.1	58.6	0.396
0.025	4.9 (4)	4.9	54.6	0.290
0.050	4.4 (5)	346.1	50.7	0.306
0.075	9.1 (5)	1.9	61.7	0.261
Labrang A				
0.000	2.6 (5)	356.2	50.4	0.456
0.025	6.9 (6)	342.8	46.2	0.350
0.050	6.4 (5)	351.8	48.1	0.378
0.075	4.7 (5)	356.7	54.0	0.467
0.100	3.2 (5)	354.2	44.5	0.407

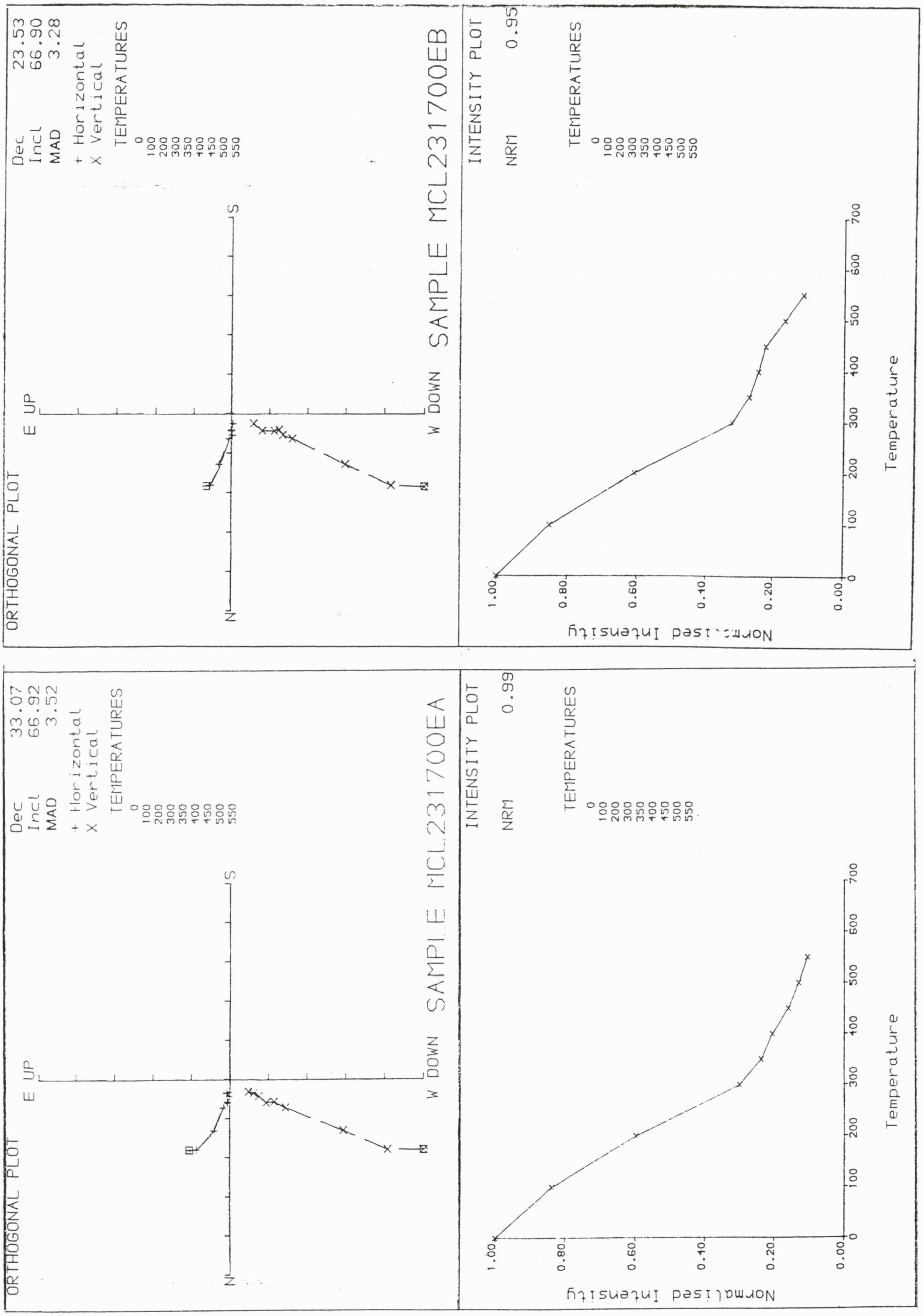

Figure 7.6 A comparison of orthogonal vector plots between two Dawan samples from the same horizon at 31.7 metres depth in loess IV.

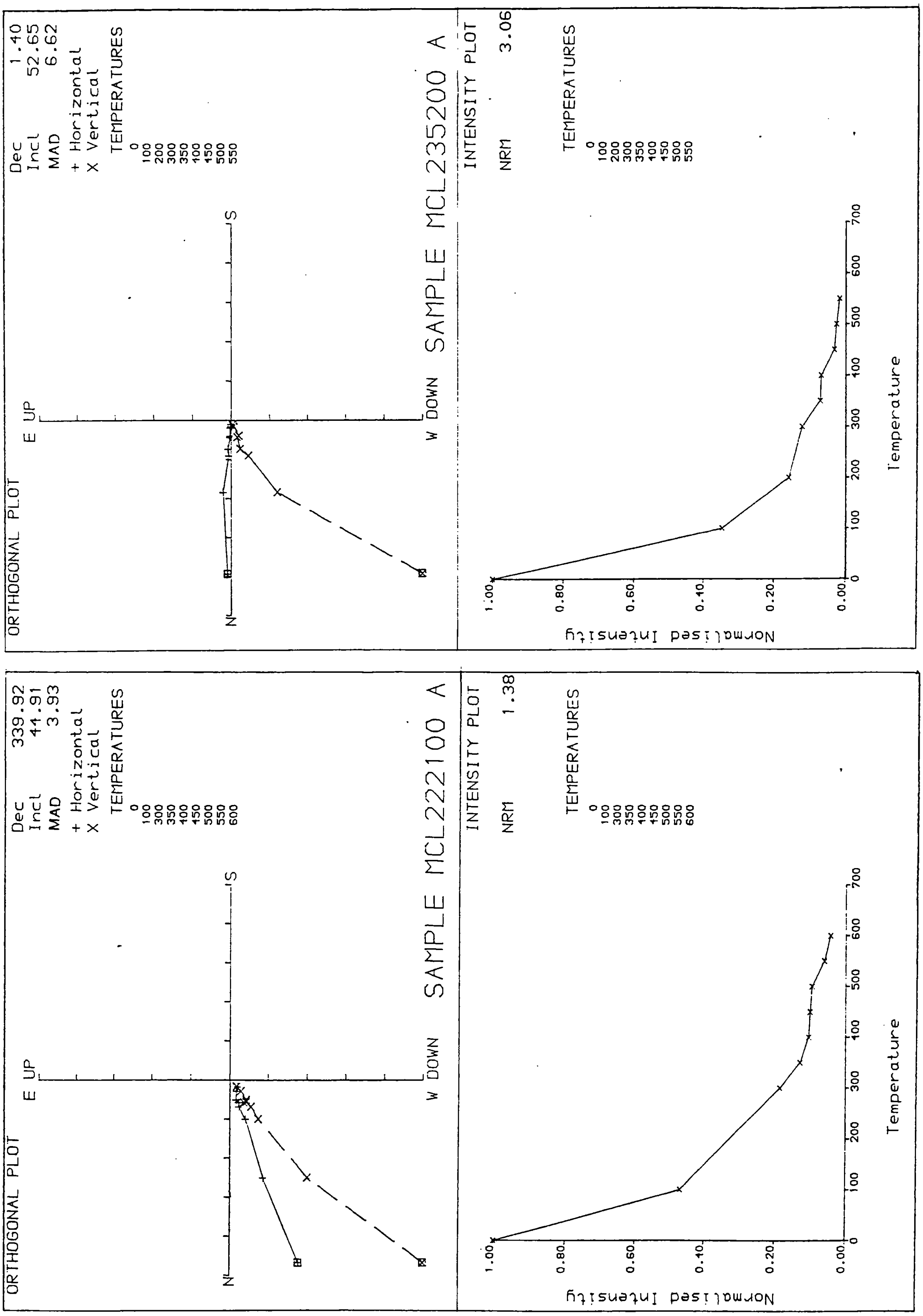

Figure 7.7 Orthogonal vector plots of a sample of Dawan
(a) loess I and (b) palaeosol VI

7.5 Summary of remanence and directional results

Heller and Liu Tungsheng (1982; 1984) undertook the first comprehensive study of the magnetism of Chinese loess, based upon the Luochuan section in Shaanxi Province. They describe hæmatite, of chemical origin, as the primary remanence carrier, with a strong secondary component of viscous origin along the present geomagnetic field which resides largely in magnetite, and is removed by thermal cleaning.

The CD magnetite and hæmatite present in the samples may be either detrital, holding a primary remanence, or formed by post-depositional chemical alteration, and thus hold a secondary chemical remanence. The presence of CD magnetite in the Tibetan Plateau and Kunlun Mountain sediments suggests that some of the CD magnetite found in the Lanzhou loess and palaeosols is of detrital origin. However, the presence of pedogenetically produced CD magnetite holding a CRM would not necessarily affect the remanence as Heider *et.al.* (1987) have found that the chemical remanence (CRM) formed during maghæmitisation of magnetite holds the same direction as the primary NRM.

The demagnetistion characteristics of the samples (appendix II) shows that often over 50% of the magnetisation is lost after heating to 250°C. Thus it is possible that up to 50% of the magnetisation of any sample is held by a secondary viscous component in low T_B magnetite. The temperatures at which 90% of the NRM is lost suggests that in the loesses, more of the NRM is held by a grains with high T_B. The palaeosol samples tend to demagnetise at lower temperatures than the loess units. As the present field holds the same direction as the field during the Brunhes Chron it is difficult to distinguish between a secondary viscous component and a primary direction.

The lack of excursions in the Jiuzhoutai and Dawan deposits suggests that, if they do represent sediments deposited during the last interglacial, these sediments have failed to record the Blake Event which is documented as having occurred 115-120ka (Tric *et.al.*, 1991), although estimates of its exact age and duration vary. The Blake Event has been reported from marine cores in the Caribbean Sea (Denham, 1976; Denham et.al., 1977), the Mediterranean Sea (Tucholka *et.al.*, 1987; Tric *et.al.*, 1991), marine deposits from Italy (Creer *et.al.*, 1980) as well as in loess from Poland (Tucholka, 1977) and Alaska (Wintle and Westgate, 1986).

Continental records of the Blake Event in the eastern hemisphere have come from Japan (Yaskawa *et.al.*, 1973; Yaskawa, 1974; Manabe, 1977) and Indonesia (Sasajima *et.al.*, 1984). However, a comprehensive record of the Blake Event has not been documented in Chinese loess although many authors have tentatively correlated spurious magnetic directions with it (Liu Chun *et.al.*, 1983; Wang Jingtai *et.al.*, 1986; Rolph et.al., 1989). The absence of a magnetic excursion may be due to a sedimentary hiatus or incorrect stratigraphical interpretation. The dual palaeosol at Jiuzhoutai has been dated as covering the period from 81 to 123ka (Chen Fahu, 1990). As there is no chronological control at Dawan, it is not possible to refine the stratigraphical interpretation further. The sediments are of normal polarity and thus are likely to be representative of the Brunhes Chron.

The magnetic fabric results from Jiuzhoutai (chapter 8) suggest that slope reworking has occurred, although the primary fabric has not been entirely destroyed. This reworking brings into doubt the magnetostratigraphy obtained from Jiuzhoutai as much of the remanence is likely to have been affected by the slope processes resulting in acquisition of a secondary remanence. It is impossible to ascertain the age of these slope processes although as the position of the field has remained the same over the time of loess deposition it is unlikely that the remanence acquired by redeposition could be isolated from that acquired at initial deposition.

In contrast, the fabric results from Dawan (chapter 8.2) indicate no substantial post-depositional effects, although the primary fabric becomes more disrupted at the base of the section. The magnetostratigraphy is therefore considered a more accurate representation of the field during sediment deposition and remanence acquisition. The variation in inclination at the top of the section may represent a precursor to an excursion which would have been present in the overlying sediment prior to cultivation. Alternatively it may be the result of secular variation. The inclination shallowing towards the base of the section, where the fabric is more disturbed, may be the result of weathering of the sediment or compaction, but may also be a realistic representation of past field variations.

Both Lanzhou sections show some inclination shallowing, with average inclinations ranging from 5.4° below the geocentric axial dipole inclination at Jiuzhoutai, to 7.9° at Dawan. The large inclination error at

Dawan is probably due to including the field swings found between 32 and 35 metres and again from 20 to 22 metres.

8. DEPOSITIONAL HISTORY: FABRIC

8.1 Introduction

Since Ising (1942) first coined the term anisotropy of magnetic susceptibility (AMS) to explain the preferred orientation of Swedish varved silts, magnetic fabric studies have been successfully applied to igneous, metamorphic and sedimentary sequences. AMS of sediments has been used to establish the depositional environment of the magnetic grains found within the sediment matrix, and thus of the sediment as a whole. Recent studies have included determination of the palaeocurrent directions in laminated cave sediments (Noel, 1983; 1986) and shales (Schreiber and Ellwood, 1988), the latter of which have also been used to assess compaction (Jackson et.al., 1989), and to the identification of areas of deformation and bottom current erosion in deep-sea cores (Løvlie et.al., 1971; de Menocal et.al., 1988). Fabric studies of Chinese loess are comparatively few and are discussed in detail in section 8.1.2.

The orientation of magnetic minerals within a sediment is affected by gravity, the topography of the depositional surface, the aligning forces of current and in small particles, the geomagnetic field. Loess is an air fall deposit, particles of which will be affected by gravity, but may also undergo orientation by wind currents as well as by water (in the form of rainsplash or slurry flow) prior to being incorporated within the surrounding sediment matrix. The orientation of grain long axes depends upon the dominant force operating on the grain. On a slope, gravity may dominate, with the orientation dependent upon slope angle: on steep slopes the long axis will lie parallel to the dip direction, whilst on shallow slopes the grain may roll and lie parallel to the contour line and normal to the slope. Current has an opposite affect upon the grain with the long axes orientating to the current direction, unless the current is strong whereby some grains may roll with their long axes transverse to the current direction (Hrouda, 1982). Grain short axes will invariably lie normal to the bedding direction.

AMS has been used in this study to ascertain the depositional history of the sediment with particular regard to the possibility of reworking by post-depositional slope processes which would affect the remanence. This was deemed a necessity as the section at Dawan lies across the Shua Jia valley from a large landslide, at Tawa, which was triggered by an earthquake in 1125. Some parts of the slide mass are still active, 867 years later, due to shifting of the displaced river which is undercutting the toe of the slide.

8.1.1 Magnetic fabric parameters

Magnetic fabric is usually defined in terms of the principal components of the susceptibility ellipsoid, which is a summation of the susceptibility of all individual magnetic grains within the sediment. Kmax is defined as the axis of maximum susceptibility, Kint is the intermediate and Kmin is the minimum susceptibility axis. If all three axes were equal, Kmax=Kint=Kmin, then the sample would correspond to an average spherical shape for all the grains in the sample, and the sample would be isotropic. An anisotropic fabric would suggest the relative absence of spherical grains and the presence of predominantly oblate or prolate grains (figure 8.1a). Prolate grains are cylindrical or cigar-shaped (figure 8.1b) and characterised by axes Kmax > Kint ≅ Kmin. Oblate grains are disc or pancake-shaped (figure 8.1c) and are characterised by axes Kmax ≅ Kint > Kmin. Using this notation, the parameters most useful in discussing magnetic fabric can then be defined:

mean or bulk susceptibility:

$$\bar{K} = (Kmax + Kint + Kmin)/3 \qquad (8.1)$$

lineation and foliation:

$$l = (Kmax - Kint)/\bar{K} \qquad (8.2)$$

$$f = (Kint - Kmin)/\bar{K} \qquad (8.3)$$

total anisotropy:

$$H = (Kmax - Kmin)/\bar{K} \qquad (8.4)$$

These difference parameters were used instead of ratio parameters, for example L = Kmax/Kint, as they are more precise for use with spinner magnetometers because they measure the differences in the ellipsoid axes with an independently measured bulk susceptibility magnititude, therefore including errors in the initial susceptibility measurement within the calculated ratios (Ellwood et.al., 1988).

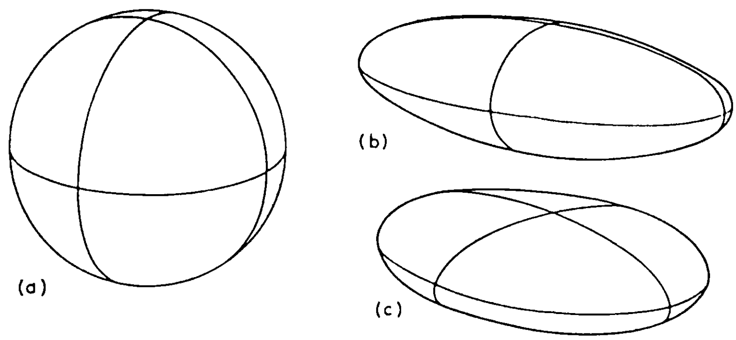

Figure 8.1 (a) spherical (b) prolate and (c) oblate susceptibility ellipsoids; q values derived for the prolate and oblate ellipsoids are (b) 1.98 (c) 0.29 (Tarling, 1983).

The parameter q, the azimuthal anisotropy quotient, reflects the relative importance of lineation and foliation within the fabric, varying from 0 in pure foliar fabrics to 2 indicative of pure lineation, with the change from foliation to lineation occuring at 0.67 (Hamilton and Rees, 1970).

azimuthal anisotropy quotient:

$$q = (K_{max} - K_{int})/[(K_{max} + K_{int})/2 - K_{min}] \qquad (8.5)$$

Hamilton and Rees (1970) found that for sediments composed of 10μm silt the magnetic field was found to be an important factor in determining the fabric orientation, with the effects declining for 25-50μm. Hrouda (1982) argues that the geomagnetic field only influences grains smaller than 30μm, with the orientation of larger grains controlled by hydrodynamic factors. The samples used in this study were of varying particle size with median diameters ranging from 5.3μm to 29.7μm.

Recent research by Potter and Stephenson (1988) has suggested that anisotropy of susceptibility may be dependent upon particle size. They found that multidomain magnetite exhibits a maximum susceptibilty parallel to its easy axis whilst unaxial single domain particles exhibit a maximum susceptibility perpendicular to its easy axis.

8.1.2 Previous fabric studies on Chinese loess

Both magnetic and optical studies have been applied to loess from China. Derbyshire et.al. (1988) used scanning electron microscopy (SEM) and image processing as well as magnetic measurement on loesses from Jiuzhoutai, near Lanzhou in the western fringe of the Loess Plateau. From their measurements they conclude that the Late Pleistocene Malan loess has an unreworked primary isotropic fabric. Magnetic fabric was used on Upper, Middle and Lower Pleistocene loesses from Jiuzhoutai, although only Kmin axes were plotted (figure 8.2). They conclude that there is no evidence of a preferred grain orientation related to wind direction (as found by Matalluci et.al. (1969) in the Vicksberg loess, USA) and that the results suggest that the primary aeolian fabric is an isotropic one with other fabrics the result of reworking by slope and alluvial processes.

More comprehensive magnetic fabric studies have been carried out in the central Loess Plateau at Xifeng (Liu Xiuming et.al. 1988b) and Liujiapo (Thistlewood and Sun Jianzhong, 1991). Liu Xiuming et.al. (1988b) studied the magnetic fabric of loess, palaeosols and redeposited alluvial loess from Xifeng in the central Chinese Loess Plateau. All of the samples showed a nearly horizontal foliation with an oblate susceptibility ellipsoid. They found that the redeposited waterlain alluvial loess fabric differed from the windblown loess fabric by having a stronger developed foliation (figure 8.3) and a strong correlation between foliation and degree of anisotropy. Redeposited alluvial loess gave clearly foliar fabrics with the minimum axes perpendicular to the bedding axis, with very weak lineation and q values less than 0.7. Recently, Thistlewood and Sun (1991) examined the magnetic fabric at Liujiapo just east of the city of Xian and found a weak sub-horizontal fabric with a WNW-ESE orientation of Kmax axes (figure 8.4) which they suggest broadly coincides with the sediment transport direction.

This chapter represents a comprehensive study of loess fabric from the Tibetan front, using magnetic techniques.

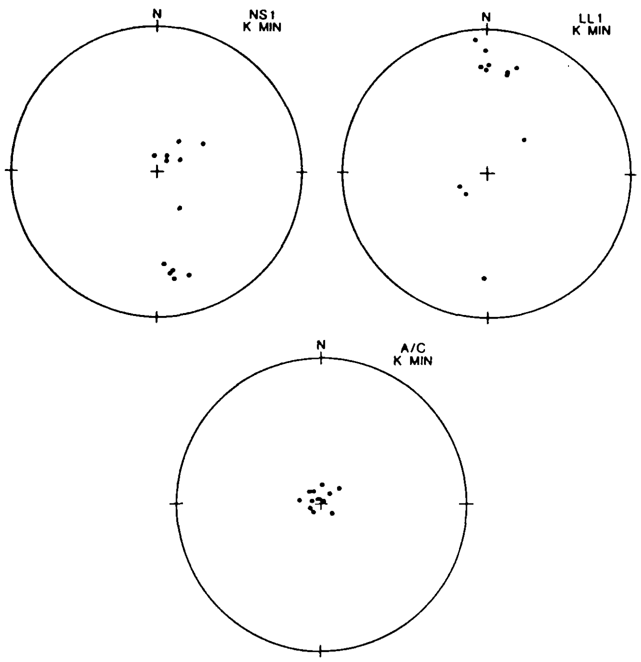

Figure 8.2 Kmin plots for Lanzhou loess: NS1 is Malan, LL1 is Lishi and A/C is Wucheng loessic alluvium (Derbyshire *et. al.*, 1988).

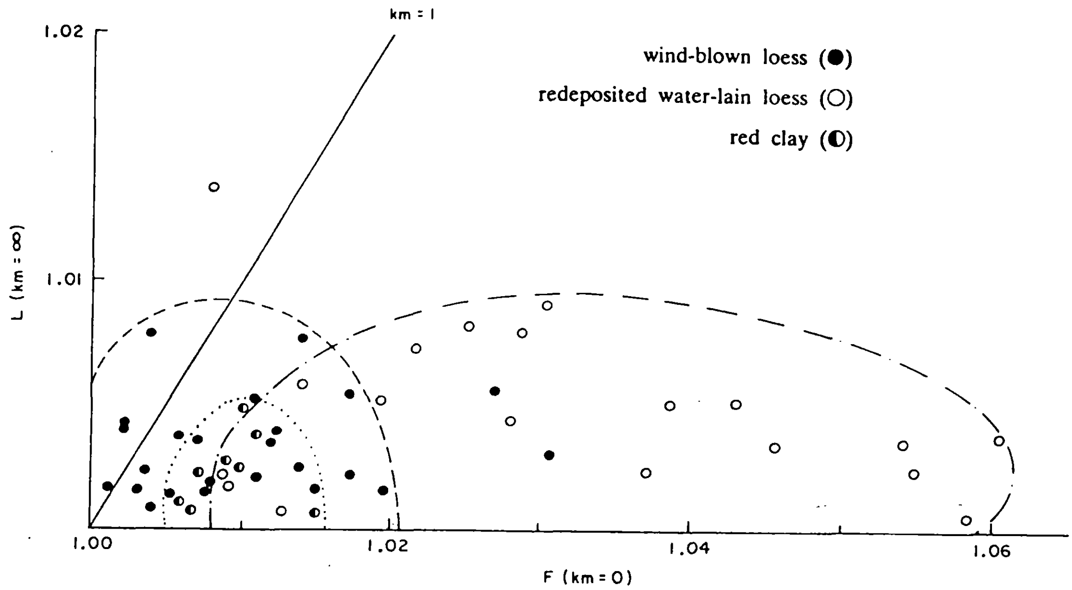

Figure 8.3 Lineation versus foliation for aeolian loess, redeposited water-lain loess and red clay (Liu Xiuming *et. al.* 1988b).

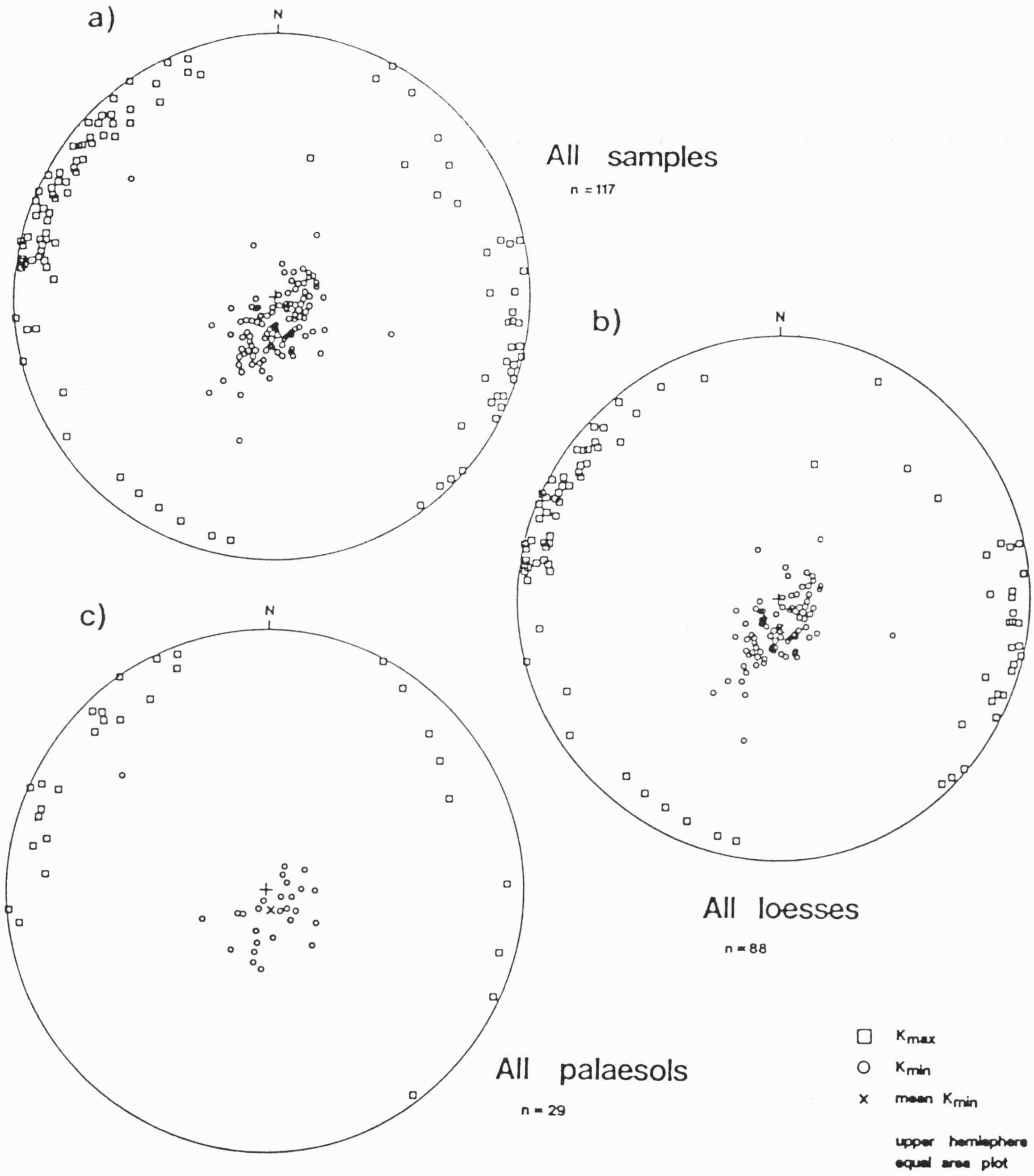

Figure 8.4 Upper hemisphere kmax and kmin plots for Liujiapo loess
(Thistlewood and Sun, 1991)

8.2 Measurement of AMS using a Minisep Delineator

Measurement of AMS was carried out on a Molspin Minisep anisotropy delineator, with bulk susceptibility measured on a Minisep bridge at Leicester University. 2.2cm perspex cubes containing the loess samples were spun at a frequency of 6Hz about a vertical axis within two orthogonal sets of Helmholtz coils. One set of coils produces a field in the order of 0.7 mT while the other set detects a field produced by the sample which varies with twice the rotation frequency. The magnitude of the detected field is proportional to the sample AMS about the axis of rotation. The sample is then rotated about three orthogonal axes which derive the intensity, declination and inclination of the three principal axes of susceptibilty of the sample. The accuracy of the reading is approximately +/- 5%. Each sample measurement was repeated three times and the average declination and inclination were calculated using a dispersal on a sphere statistics programme (Fisher, 1953) to reduce the error due to noise and reject data with high dispersions of axes as a result of noise. The volume susceptibility of the samples ranged from 11×10^{-5} to 42×10^{-5} SI.

The data are presented following the standardisation suggested by Ellwood et.al. (1988) with the use of the symbols: □ to represent the maximum axis; Δ for the intermediate; and o for the minimum axis, plotted on lower hemisphere equal-area projections. Lineation and foliation parameters, degree of anisotropy and q value were derived using programmes on the Liverpool University IBM mainframe computer. Plots of lineation against foliation and foliation against total anisotropy are also presented.

8.2.1. Jiuzhoutai

A total of 399 cubes were measured from Jiuzhoutai. These have been arranged into stratigraphic groups on the basis of their low field susceptibility. The three loesses and two palaeosols are labelled simply loess I; palaeosol I; loess II etc. because of the lack of sufficient geochronological framework to identify them further.

The fabric from the loess samples shows a developed foliation with a slightly weaker developed lineation, reflected in the q values close to the 0.67 foliar-linear boundary, ranging from 0.525 to 0.681 (table 8.2). Total anisotropy (H) varies from 0.037-0.040. The palaeosol samples both show different fabrics to those of the loess. Palaeosol I shows a developed lineation with mean q value of 0.753 and mean lineation greater than the mean foliation. However the total anisotropy is lower than that of the loess indicating that the palaeosol has a weaker fabric. Palaeosol II is dominated by a weak foliation with a mean q of 0.267 and a very weak mean lineation of 0.0033. The mean total anisotropy of 0.0151 is also lower than the anisotropy of the loess. The weaker fabric of the palaeosol samples is most probably due to the disrupting effects of bioturbation and weathering. Figures 8.5 and 8.6 show graphs of lineation-foliation and foliation-total anisotropy for the loess and palaeosol units.

Table 8.2 Mean lineation, foliation and total anisotropy parameters, with standard deviations (SD), for the loess and palaeosol units at Jiuzhoutai. The numbers of samples (n) correspond to the number of cubes measured per unit.

unit	lineation		foliation		total anisotropy		q		n
	mean	SD	mean	SD	mean	SD	mean	SD	
Loess I	0.0154	0.0083	0.0244	0.0138	0.0387	0.0178	0.525	0.305	103
Palaeosol I	0.0139	0.0092	0.0125	0.0079	0.0264	0.0134	0.753	0.380	83
Loess II	0.0181	0.0128	0.0209	0.0132	0.0400	0.0204	0.681	0.366	78
Palaeosol II	0.0033	0.0029	0.0118	0.0089	0.0151	0.0106	0.267	0.159	32
Loess III	0.0178	0.0147	0.0193	0.0131	0.0371	0.0215	0.613	0.393	103

The stereographic projection of principal axes for loess I samples is presented in figure 8.7. The sample long axes (Kmax), presented in the form of red squares, form a distinct pattern of groupings. A proportion of the long axes are clustered on a plane orientated 140°-170°/320°-350° with dip angles of less than 50° but predominantly less than 20°. There is also a wider distribution of maximum and intermediate axes orthogonal to this plane around 240°-280°. The minimum axes are distributed along declination of 40-70° with varying dip angles ranging from 3° to 87°. The scatter of the minimum axes suggests that the grains are not lying on a horizontal bedding plane but are distributed on a slope of varying angle. The dip angles are indicative of some sort of slope movement. This is born out by the wide angle of maximum (long) axes, of which some are clustered about declinations of 140-170°, but many are widely scattered from 170° to 350°. Angles of dip (inclination) are generally less than 50°. The intermediate axes are also scattered about declinations of 170° to 350°, with the apparent reversibility of Kmax and Kmin axes indicative of the oblate nature of the ellipsoid.

The slope at the Scorpion Pit is steep, with a dip angle of approximately 35°, falling off in a easterly direction (110°) to the Yellow River floodplain. The minimum axes for loess I suggest a northeasterly downslope direction with the low total anisotropy indicating that current flow was not a dominant factor in deposition. Therefore it is likely that the loess was affected by powder flows. Thermoluminescence dates from the Scorpion Pit at Jiuzhoutai show that the sediment dates from 50-80ka (Chen Fahu *et.al.*, 1991; Musson unpub. data) thus it is likely that these were active at this time and are Pleistocene events. The downslope direction indicated by the fabric could be the result of a different topographic palaeoslope than that of the present.

In the palaeosol I samples (figure 8.8) some of the maximum axes are closely clustered about 35°-70° with low dip angles less than 30°, with orthogonal intermediate axes and sub-vertical minimum axes, indicating a sub-horizontal fabric, with a dip of approximately 15° bearing 230° southwest. In addition to this fabric component there is a more randomly orientated component with minimum axes of less than 70° some of which are arranged in an easterly direction, with maximum axes arranged orthogonally in a plane about 150°-180°/330°-360°. The fabric appears to reflect a dual component combination of a sub-horizontal fabric with a slope component. Bioturbation and weathering are likely within a palaeosol, which would randomise any anisotropic component and breakdown the fabric, which is weaker than that of the surrounding loesses I and II. This may account for some of the slope fabric. The fabric appears both weakly linear and foliar.

Loess II fabric is illustrated in figure 8.9, which indicates the dominance of a sub-horizontal southwest orientated fabric with the maximum axes clustered about 40°-70° with dip angles of less than 30° and the minumum axes tending towards the vertical with angles of 60°-88°. The intermediate axes of this component are clustered about an orthogonal plane of 130°-170°/320°-360°. In addition to this there is a component similar to that of loess I which was probably caused by easterly oriented slope processes. The minimum axes of this component have variable dip angles and declination, predominantly within 340-110°.

Palaeosol II gave a horizontal foliar fabric indicating the absence of post-depositional slope processes (figure 8.10). Minimum axes are clustered around the vertical, with maximum axes ranged about 350°-90° with dips of less than 10°. The distribution of the maximum and intermediate axes suggest a grain orientation predominantly NE-SW although this is unlikely to be due to deposition in a flowing water medium due to the absence of strong lineation.

The fabric from loess III (figure 8.11), as with that of loess II, suggests a primary horizontal foliar fabric overlain by a secondary slope fabric. The maximum axes and intermediate axes of the primary fabric appear interchangeable suggesting a dominance of oblate grains.

8.2.1.1 **Summary of Jiuzhoutai fabric results**

The fabrics from Jiuzhoutai loess and palaeosols are foliar with a linear component demonstrated by the lineation-foliation graphs in figure 8.5 and 8.6. The palaeosol samples have weaker anisotropy (1.5% and 2%) than the loess (3.7% to 4%) due to weathering effects disrupting the fabric. The total anisotropy appears well correlated with the foliation. The foliation results are weaker than those found from redeposited alluvial loess at Xifeng (Liu Xiuming et.al., 1988) suggesting that the primary foliar fabric, indicating a palaeocurrent direction predominantly NE-SW, is unlikely to be the result of deposition by water.

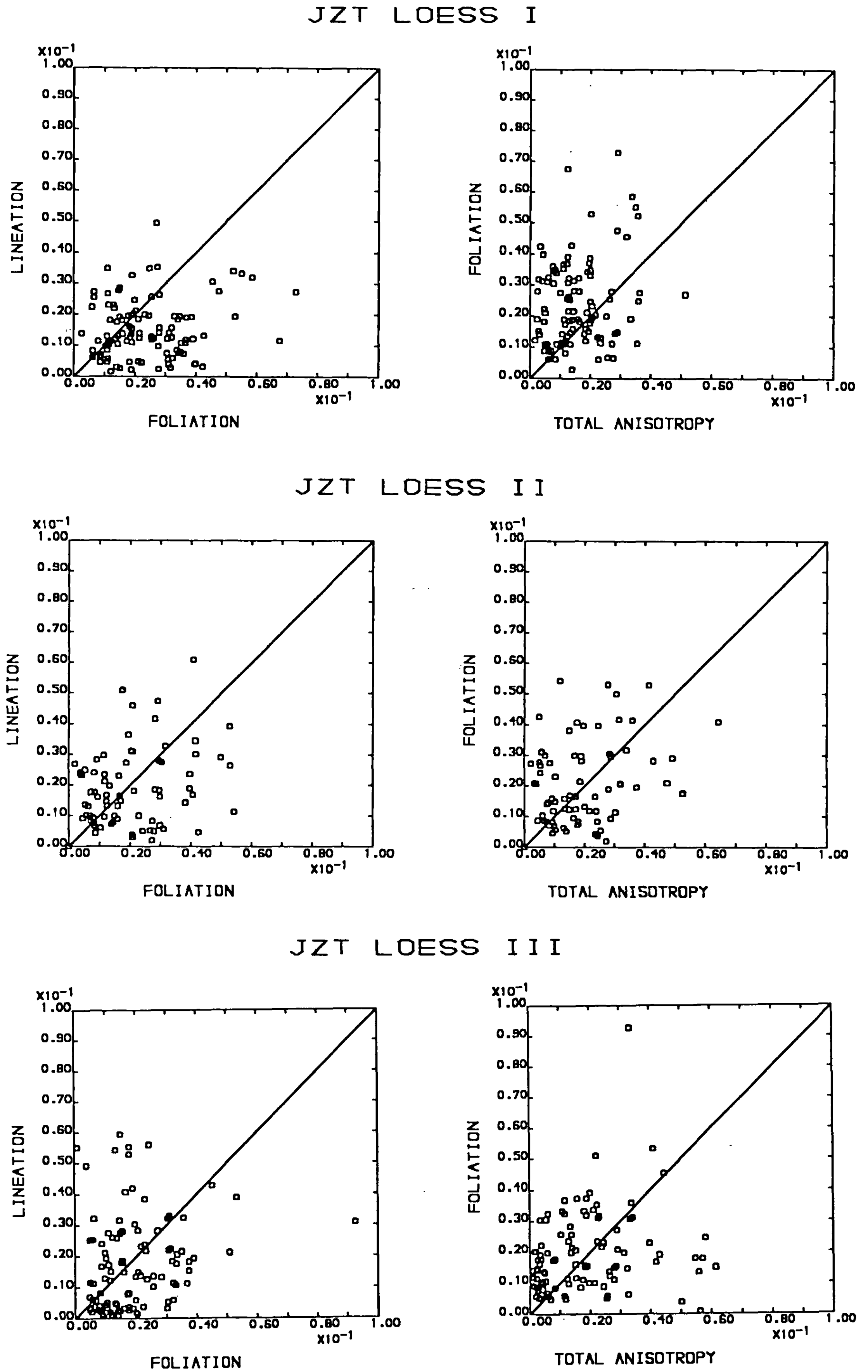

Figure 8.5 Plots of lineation versus foliation and foliation versus total anisotropy plots for Jiuzhoutai loess units.

JZT PALAEOSOL I

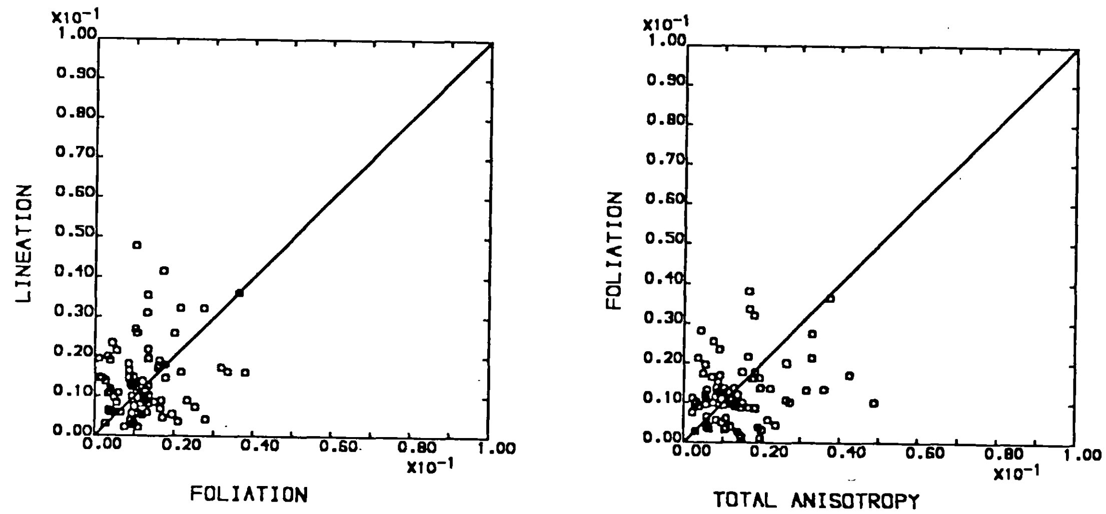

JZT PALAEOSOL II

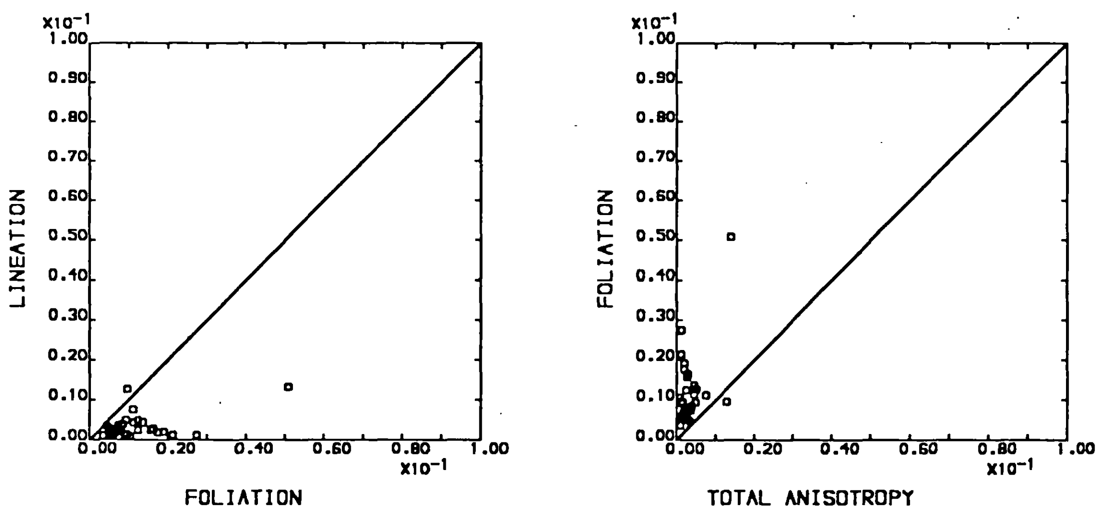

Figure 8.6 Plots of lineation versus foliation and foliation versdus total anisotropy plots for Jiuzhoutai palaeosol units.

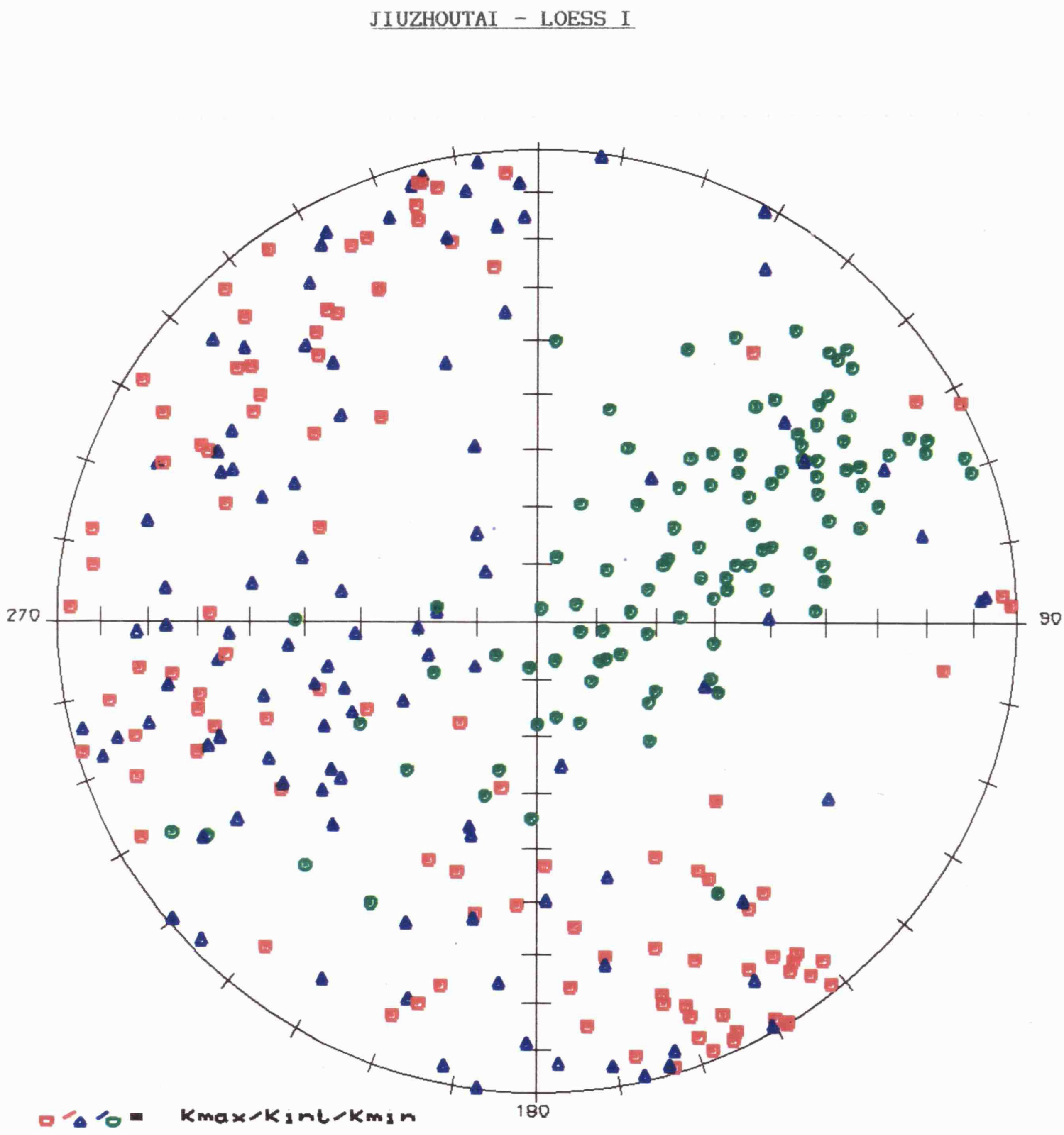

Figure 8.7 Lower hemisphere equal area plot of the principal axes of susceptibility for Jiuzhoutai loess I.

JIUZHOUTAI - PALAEOSOL I

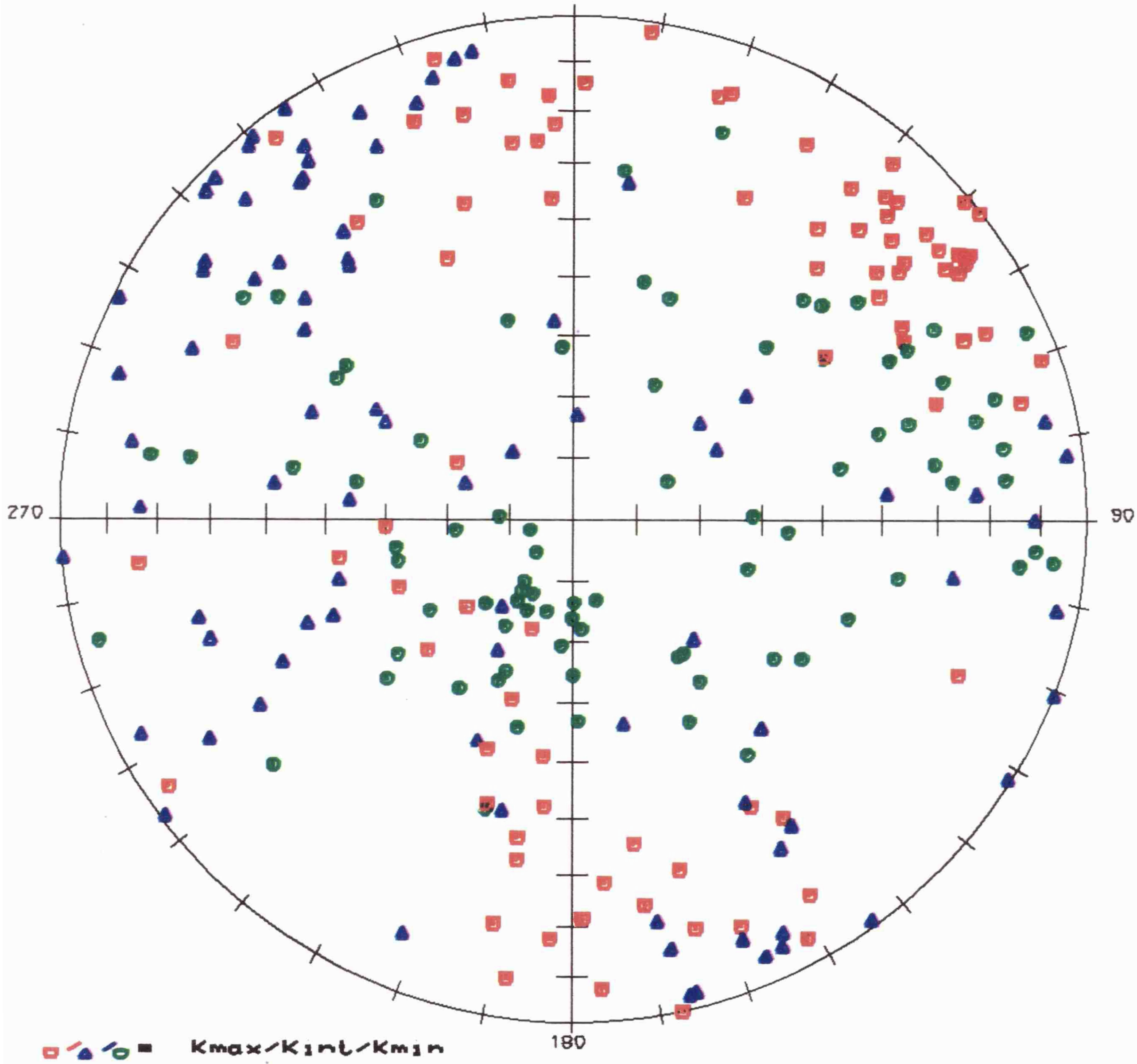

Figure 8.8 Lower hemisphere equal area plot of the principal axes of susceptibility for Jiuzhoutai palaeosol I.

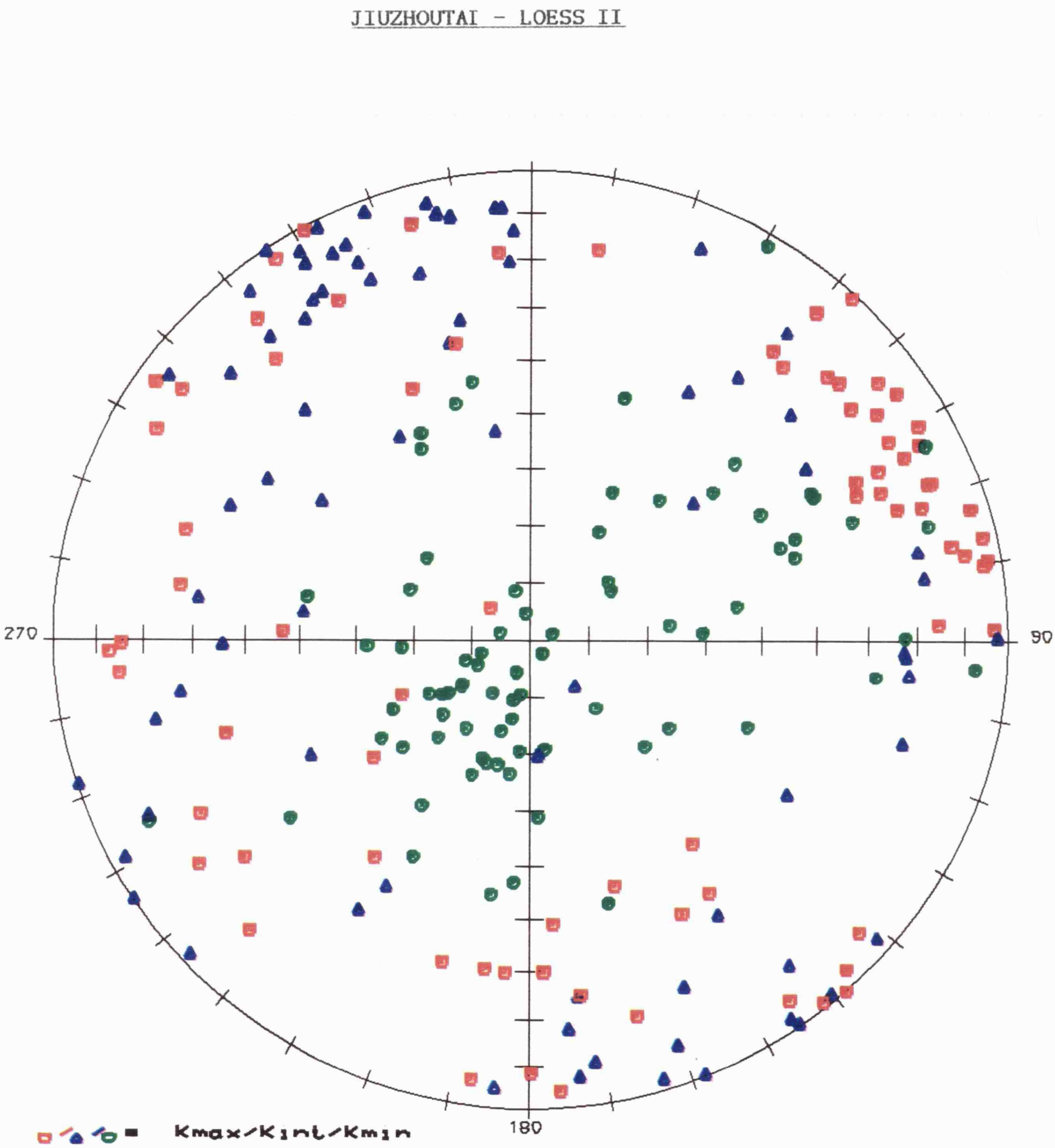

Figure 8.9 Lower hemisphere equal area plot of the principal axes of susceptibility for Jiuzhoutai loess II.

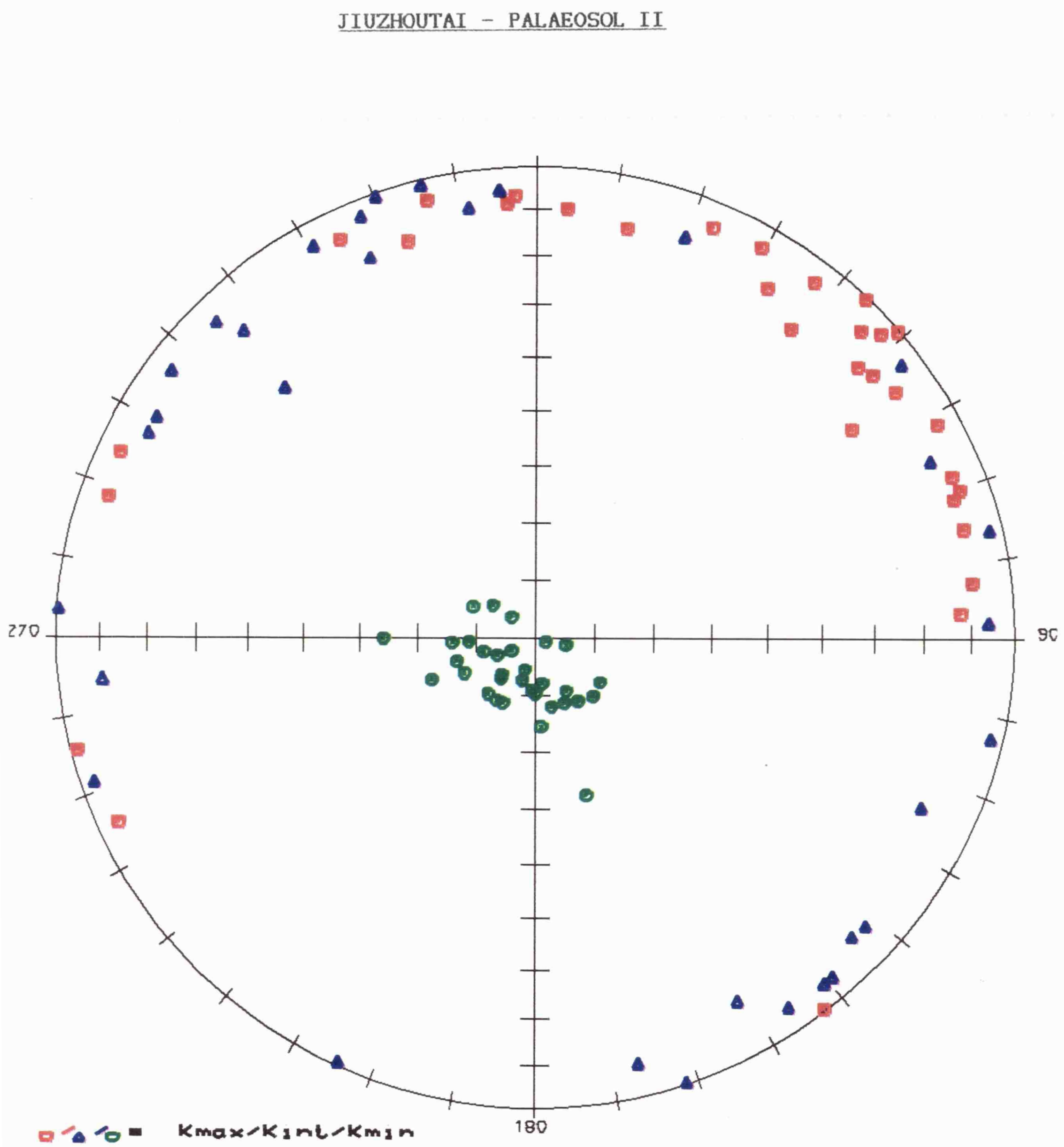

Figure 8.10 Lower hemisphere equal area plot of the principal axes of susceptibility for Jiuzhoutai palaeosol II.

JIUZHOUTAI - LOESS III

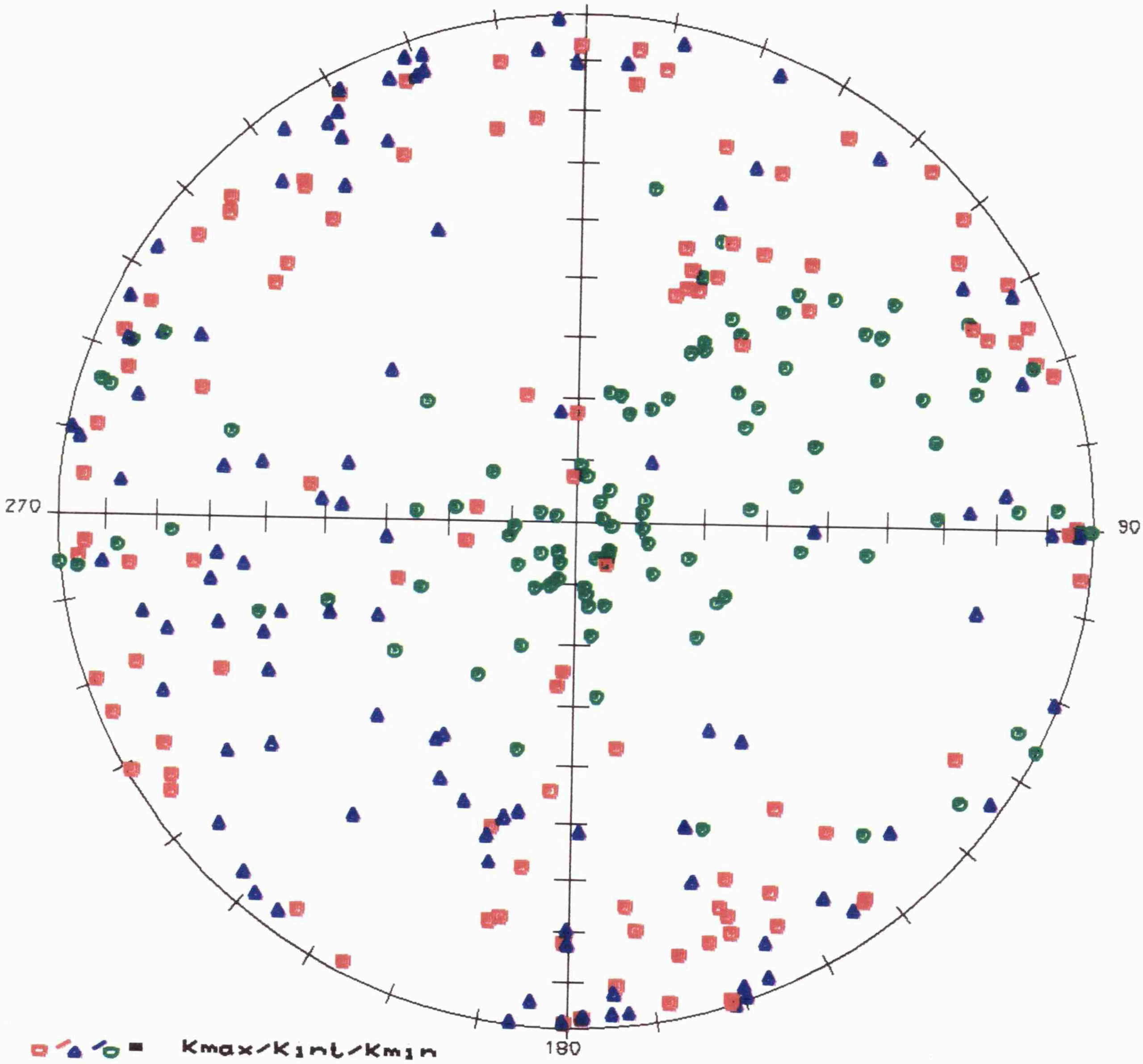

Figure 8.11 Lower hemisphere equal area plot of the principal axes of susceptibility for Jiuzhoutai loess III.

8.2.2 Dawan

1024 samples were measured from 12 stratigraphic units at Dawan, from loess I to palaeosol VI. These were excavated from five sample pits, each of which had a different orientation. The downslope direction is WNW 290° with a slope angle of approximately 35°.

Table 8.3 Mean lineation, foliation, total anisotropy, and q shape parameter, with standard deviations (SD), for the loess and palaeosol units at Dawan. n stands for the number of samples measured per unit.

unit	lineation		foliation		total anisotropy		q		n
	mean	SD	mean	SD	mean	SD	mean	SD	
Loess I	0.0078	0.0063	0.0188	0.0063	0.0266	0.0085	0.345	0.199	326
Palaeosol I	0.0055	0.0037	0.0087	0.0048	0.0142	0.0068	0.534	0.271	48
Loess II	0.0074	0.0043	0.0175	0.0082	0.0248	0.0108	0.386	0.252	128
Palaeosol II	0.0100	0.0053	0.0176	0.0082	0.0276	0.0088	0.472	0.273	44
Loess III	0.0187	0.0125	0.0266	0.0143	0.0453	0.0188	0.561	0.349	125
Palaeosol III	0.0041	0.0017	0.0126	0.0046	0.0167	0.0053	0.320	0.231	36
Loess IV	0.0186	0.0126	0.0301	0.0182	0.0488	0.0254	0.527	0.299	154
Palaeosol IV	0.0259	0.0119	0.0236	0.0084	0.0495	0.0156	0.706	0.255	40
Loess V	0.0337	0.0082	0.0305	0.0110	0.0642	0.0144	0.740	0.235	36
Palaeosol V	0.0143	0.0147	0.0218	0.0172	0.0361	0.0281	0.461	0.296	56
Loess VI	0.0135	0.0071	0.0378	0.0428	0.0514	0.0482	0.343	0.107	24
Palaeosol VI	0.0067	0.0020	0.0168	0.0057	0.0236	0.0074	0.338	0.115	7

The loesses, with exception of loess V, show a weak fabric with developed foliation and mean q values ranging from 0.343 to 0.561. The exception, loess V, is more strongly anisotropic with a developed lineation dominating over a developed foliation. The mean q value for loess V is 0.740 suggesting a relative dominance of prolate susceptibility ellipsoid. The strength of the fabric and the dominance of lineation and does not conform to the strongly foliar fabric found in alluvially redeposited loess from Xifeng (Liu Xiuming et.al., 1988b). Total anisotropy increases from 0.027 and 0.025 in loess I and II to 0.45 and 0.49 in loess III and loess IV. Loess V shows the strongest anisotropy of 0.64 with loess VI: 0.51. The total anisotropy generally decreases up the section. Plots of lineation-foliation and foliation-total anisotropy for Dawan loesses are presented in figure 8.12.

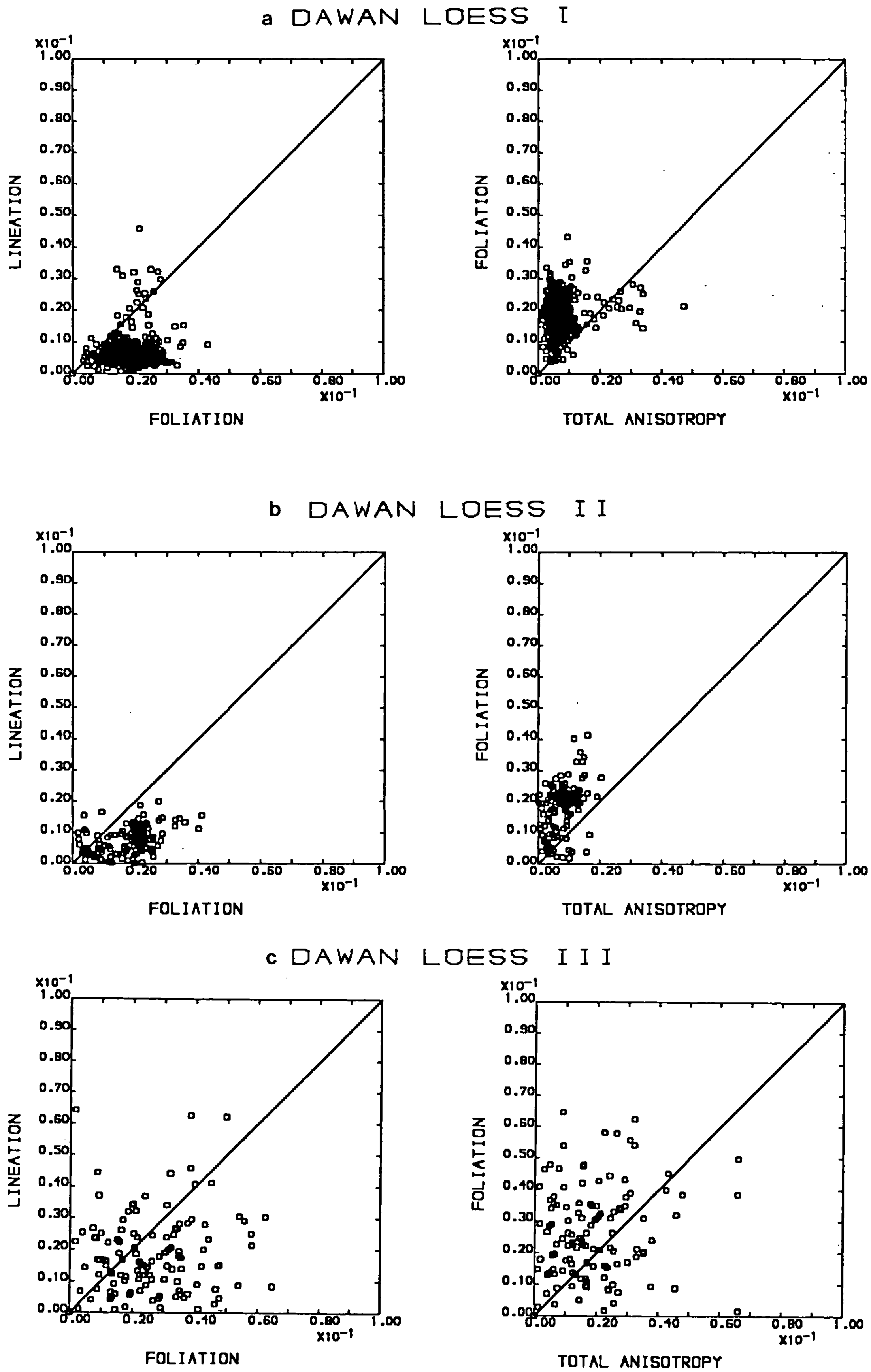

Figure 8.12a-8.12c. Lineation-foliation and foliation-total anisotropy plots for Dawan loess: (a) loess I (b) loess II (c) loess III

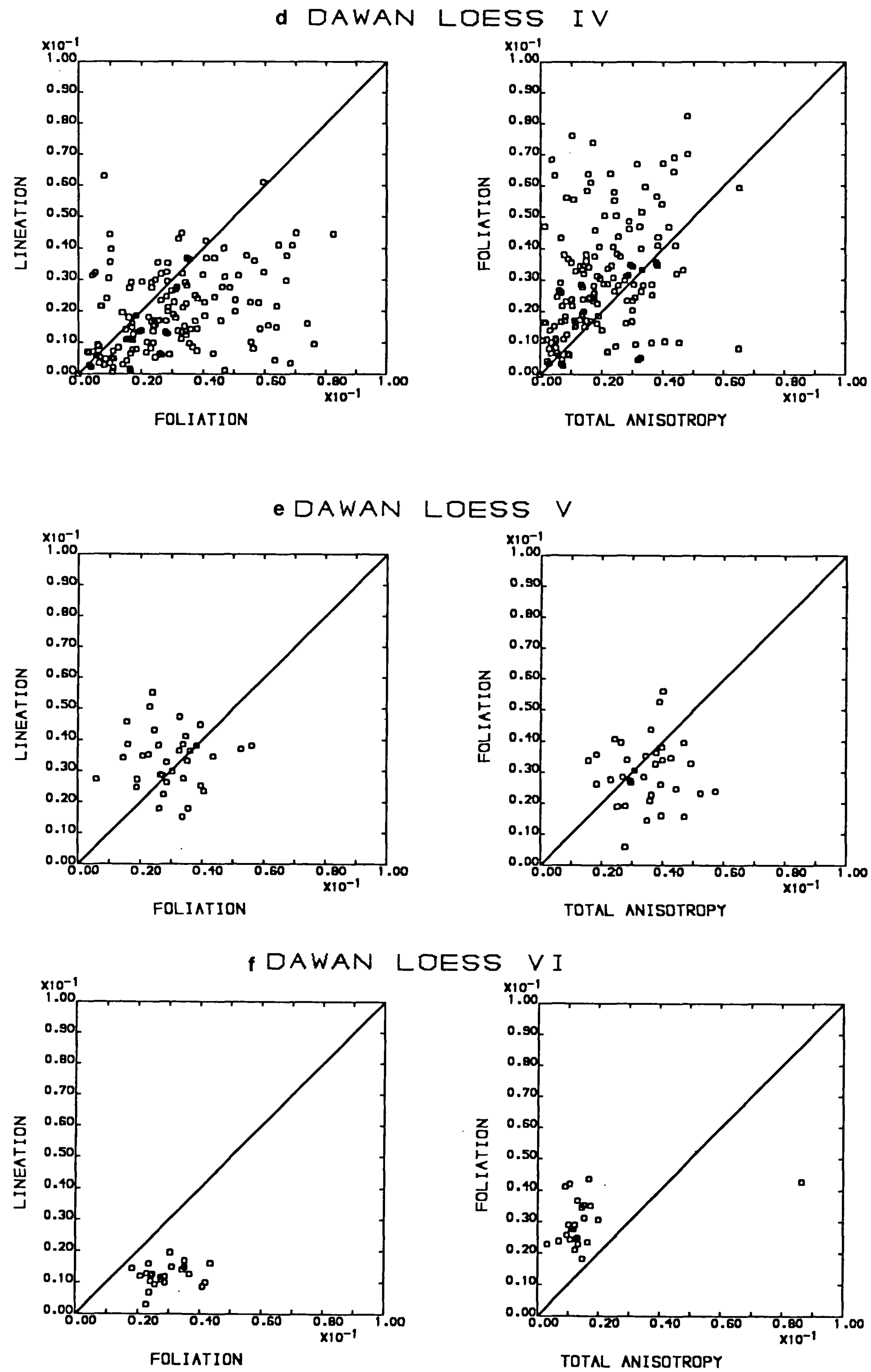

Figure 8.12d-8.12f. Lineation-foliation and foliation-total anisotropy plots for Dawan loess (d) loess IV (e) loess V (f) loess VI

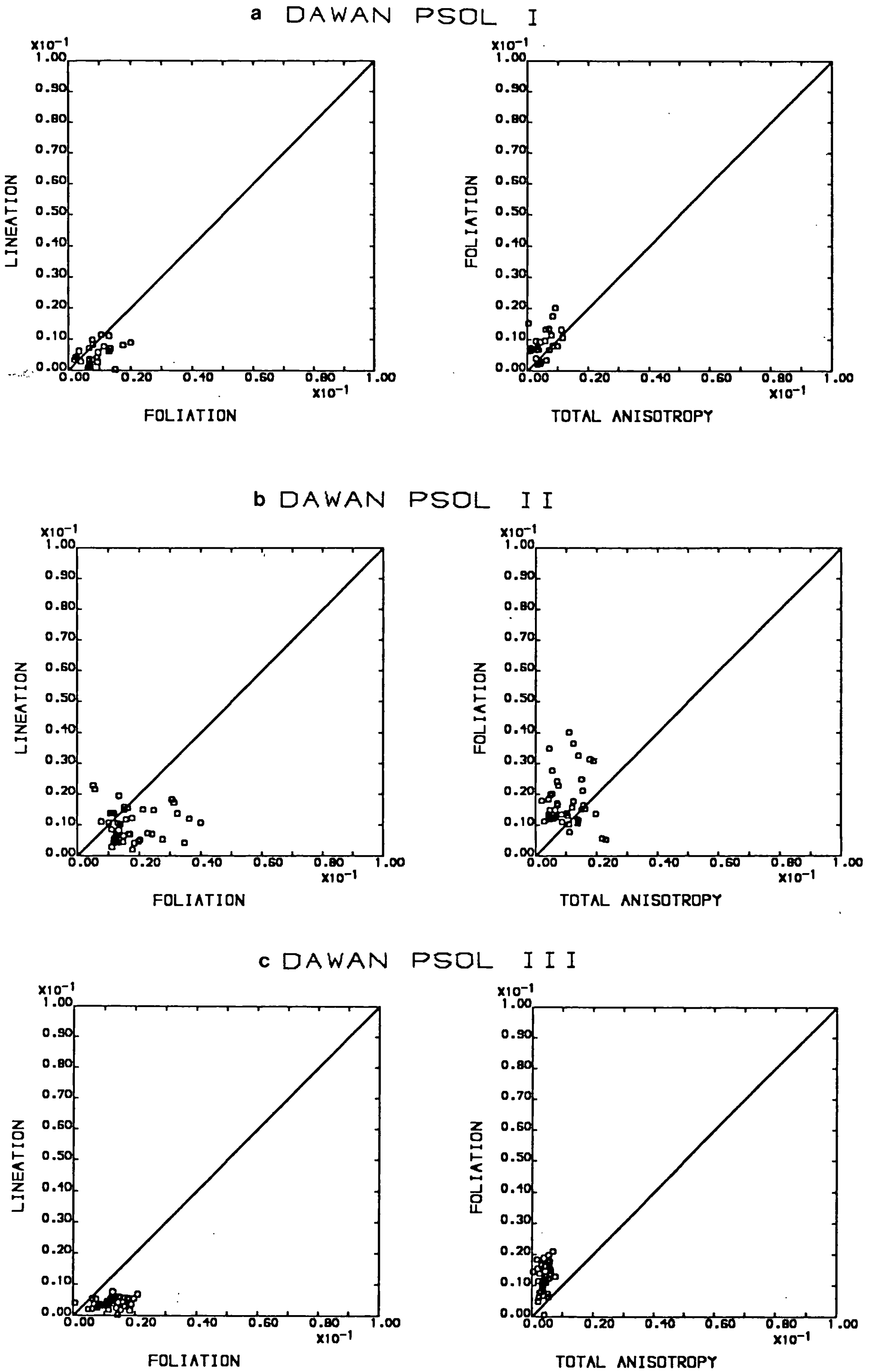

Figure 8.13a-8.13c. Lineation-foliation and foliation-total anisotropy plots for Dawan palaeosols: (a) p'sol I (b) p'sol II (c) p'sol III

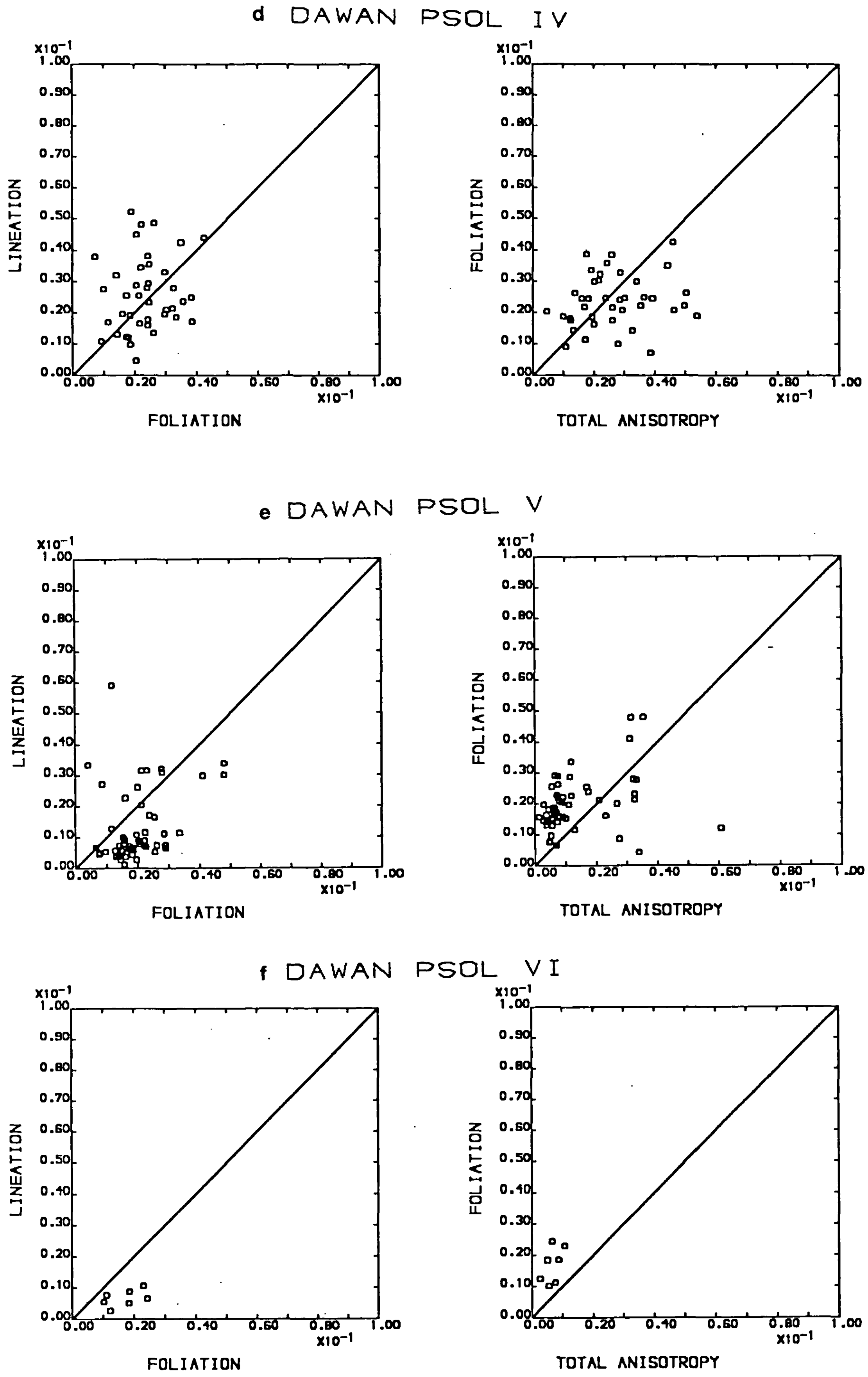

Figure 8.13d-8.13f. Lineation-foliation and foliation-total anisotropy plots for Dawan palaeosols (d) p'sol IV (e) p'sol V (f) p'sol VI

The paleosols from the Dawan section with the exception of palaeosol IV show weakly foliar fabrics with some lineation. The mean q values range from 0.32 to 0.53 with only palaeosol IV giving a mean q value above 0.67 indicative of lineation. The dominance of lineation in palaeosol IV, like loess V beneath it, suggests that the fabric may be a result of an increase in proportion of linear grains or perhaps a relative increase in proportion of hæmatite or a change in deposition mechanism. However, the total anisotropy is weaker than that of loess V indicating that weathering and/or bioturbation has disturbed the fabric.

The 326 samples representing 5 metres of loess I gave constitent results — indicating a horizontal foliar ENE-WSW trending fabric (figure 8.14) with the mean grain direction oriented about 70°/250°. This fabric is apparent throughout all of the Dawan samples, although loess III and loess IV fabrics have subsequently been affected by post-depositional processes (figure 8.18 and 8.20). Loess II and palaeosol II show horizontal ENE-WSW fabrics with a superimposed fabric dipping in a NE direction with minimum axes showing inclinations as large as 20° from the horizontal. This dipping fabric is orientated about 40° in loess II and therefore has a strike some 30° north of that of the horizontal fabric and into the face of the slope. The downslope direction is WNW.

Loess III and loess IV both show the primary foliar horizontal fabric orienated ENE-WSW although this fabric has been disturbed showing a tilt to the NE. Interestingly this superimposed tilt fabric is similar that at Jiuzhoutai, some 75km east on the north bank of the Yellow River, which was tentatively interpreted as a slope fabric.

The loess and palaeosols below loess IV (33-35.2m) gave ENE-WSW trending fabrics with palaeosol IV and loess V showing a 15° dip to the WSW (figure 8.21 & 8.22). Below loess V the fabric returned to being horizontal.

The plots of lineation and foliation indicate that the fabric was not a result of deposition by water and thus is most probably the result of orientation by wind. Northwesterly winds from the Hexi Corridor are thought to have been predominant in the Quaternary, however the southerly monsoon may have also had an effect (see section 8.3).

DAWAN - LOESS I

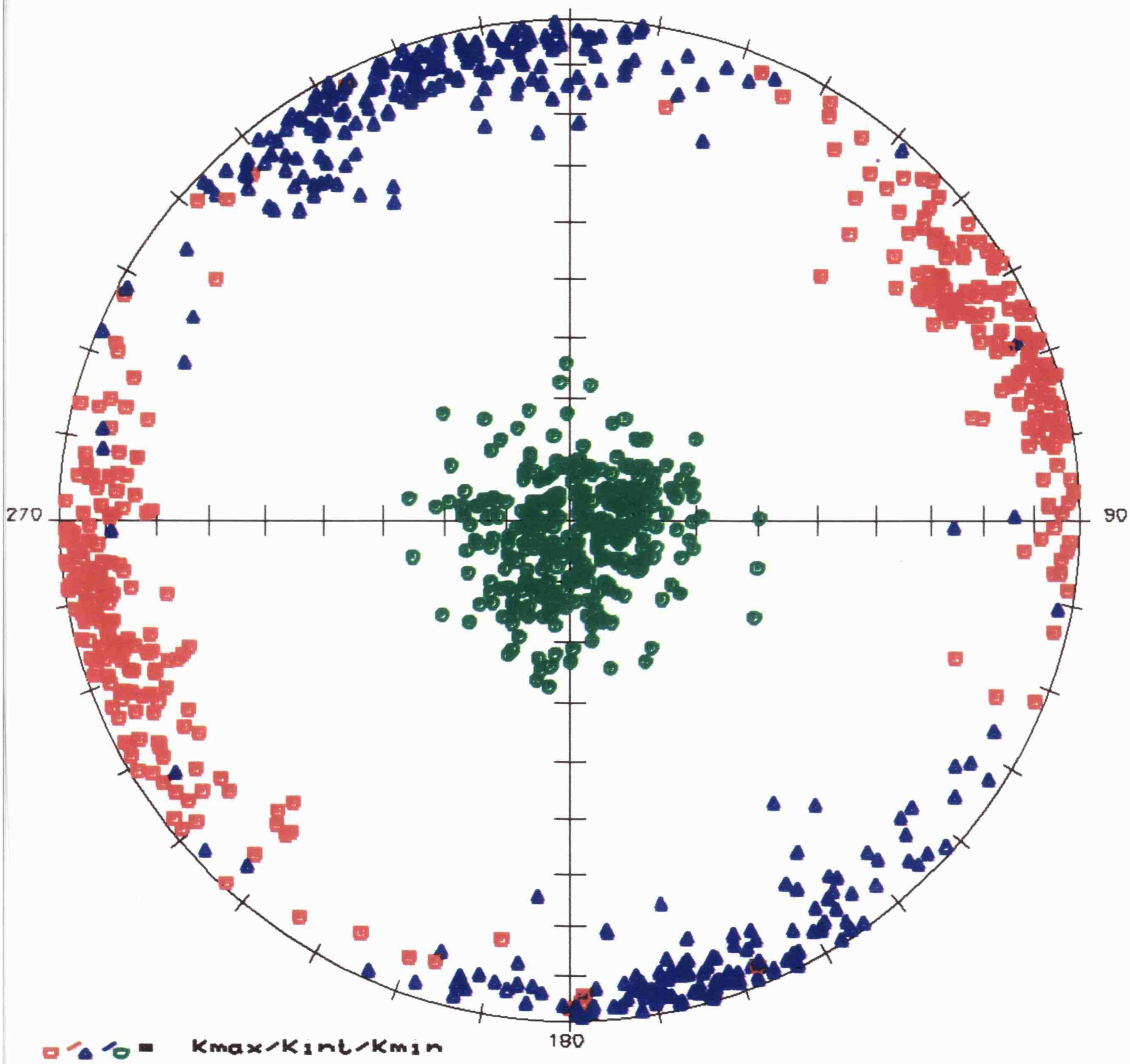

Figure 8.14 Lower hemisphere equal area plot of the principal axes of susceptibility for Dawan loess I.

DAWAN - PALAEOSOL I

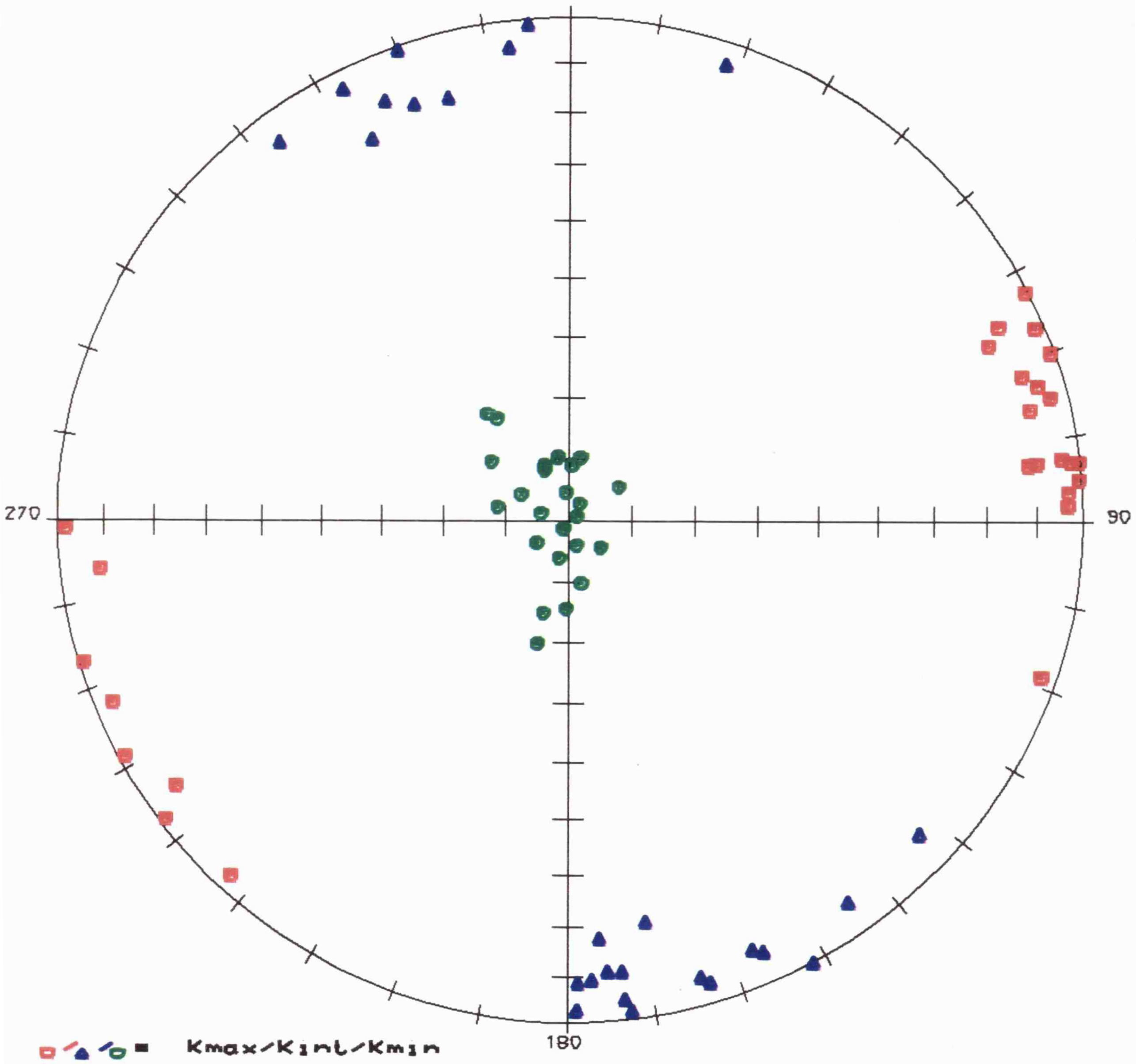

Figure 8.15 Lower hemisphere equal area plot of the principal axes of susceptibility for Dawan palaeosol I.

DAWAN - LOESS II

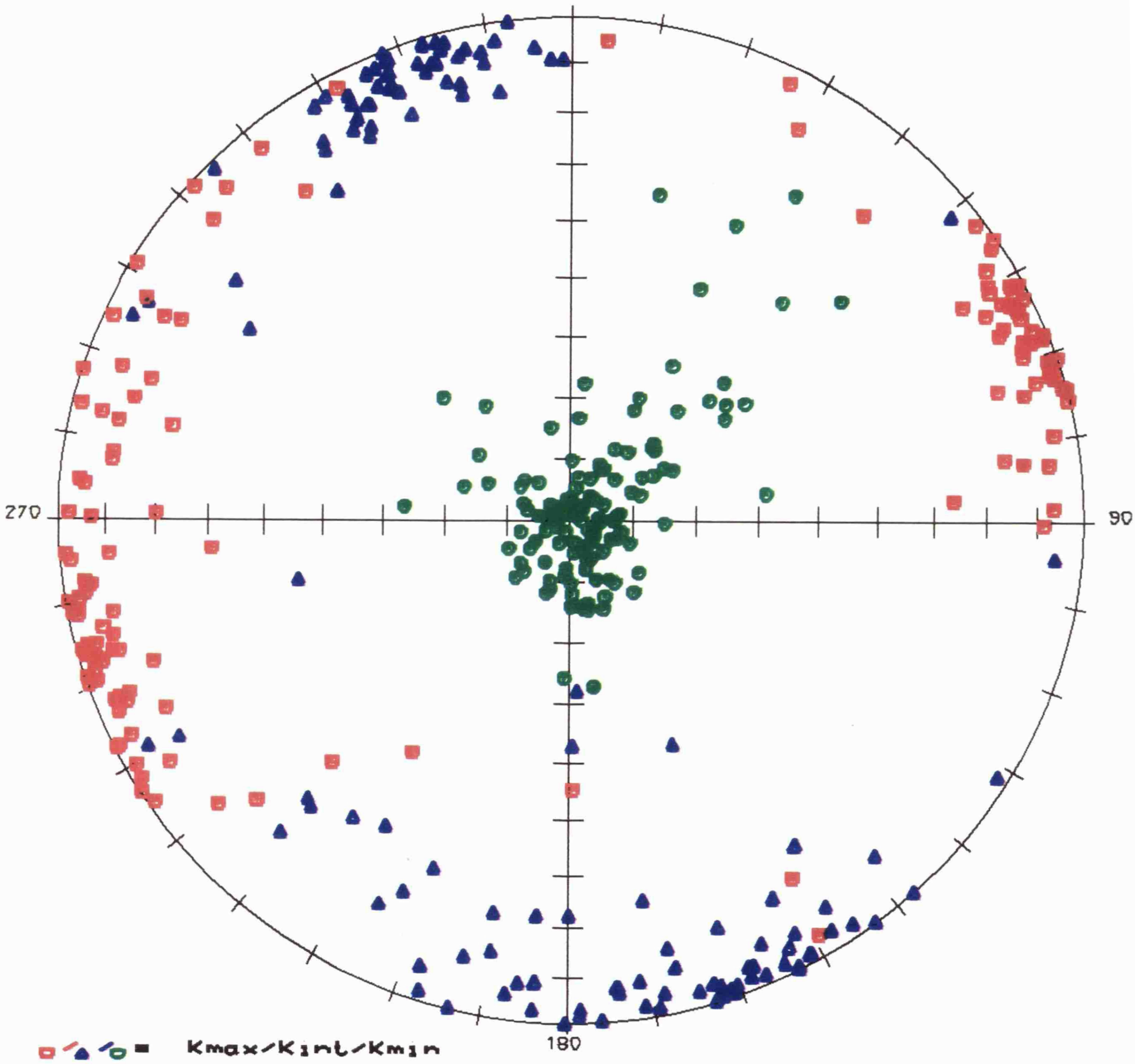

Figure 8.16 Lower hemisphere equal area plot of the principal axes of susceptibility for Dawan loess II.

DAWAN - PALAEOSOL II

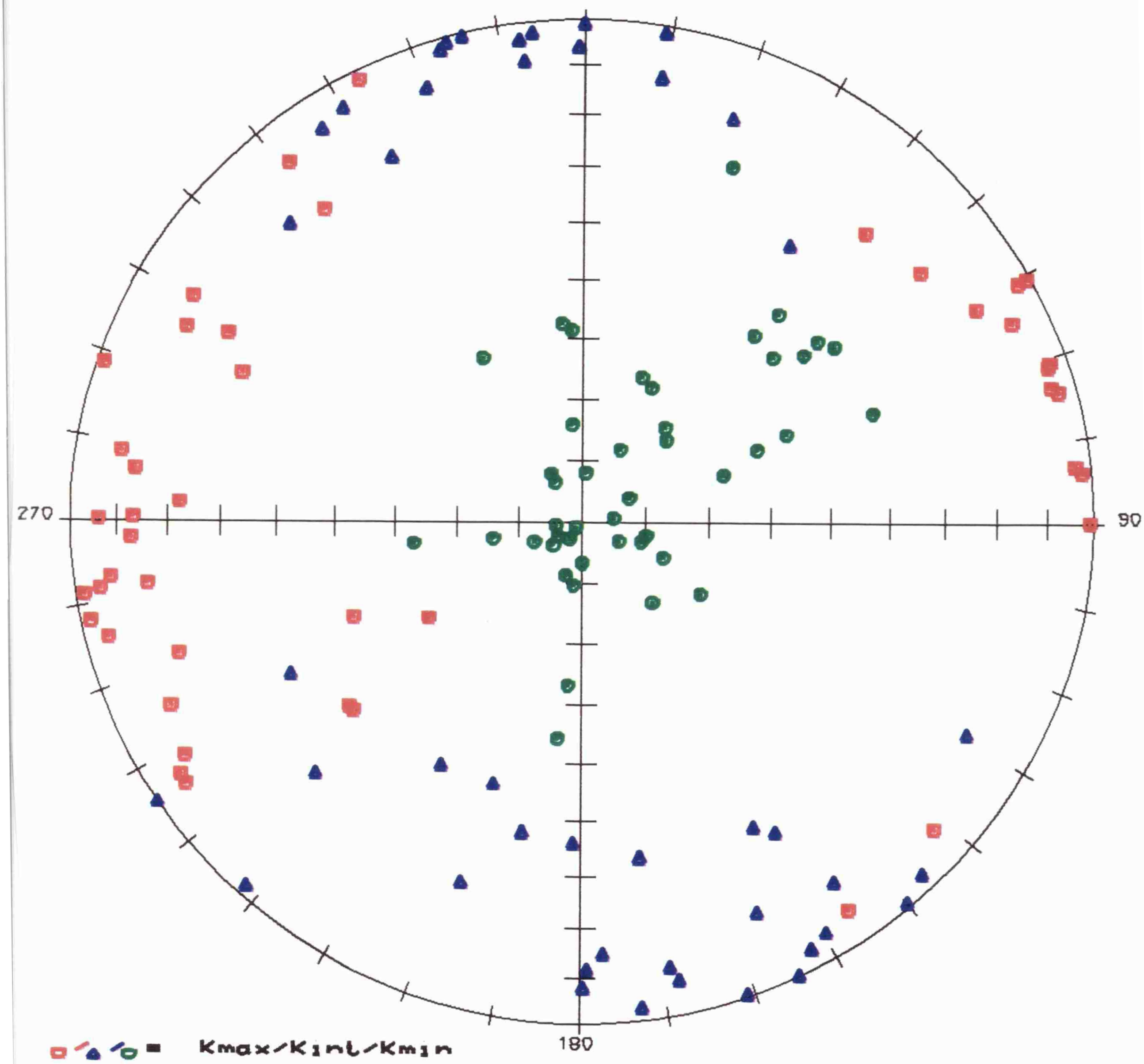

Figure 8.17 Lower hemisphere equal area plot of the principal axes of susceptibility for Dawan palaeosol II.

DAWAN - LOESS III

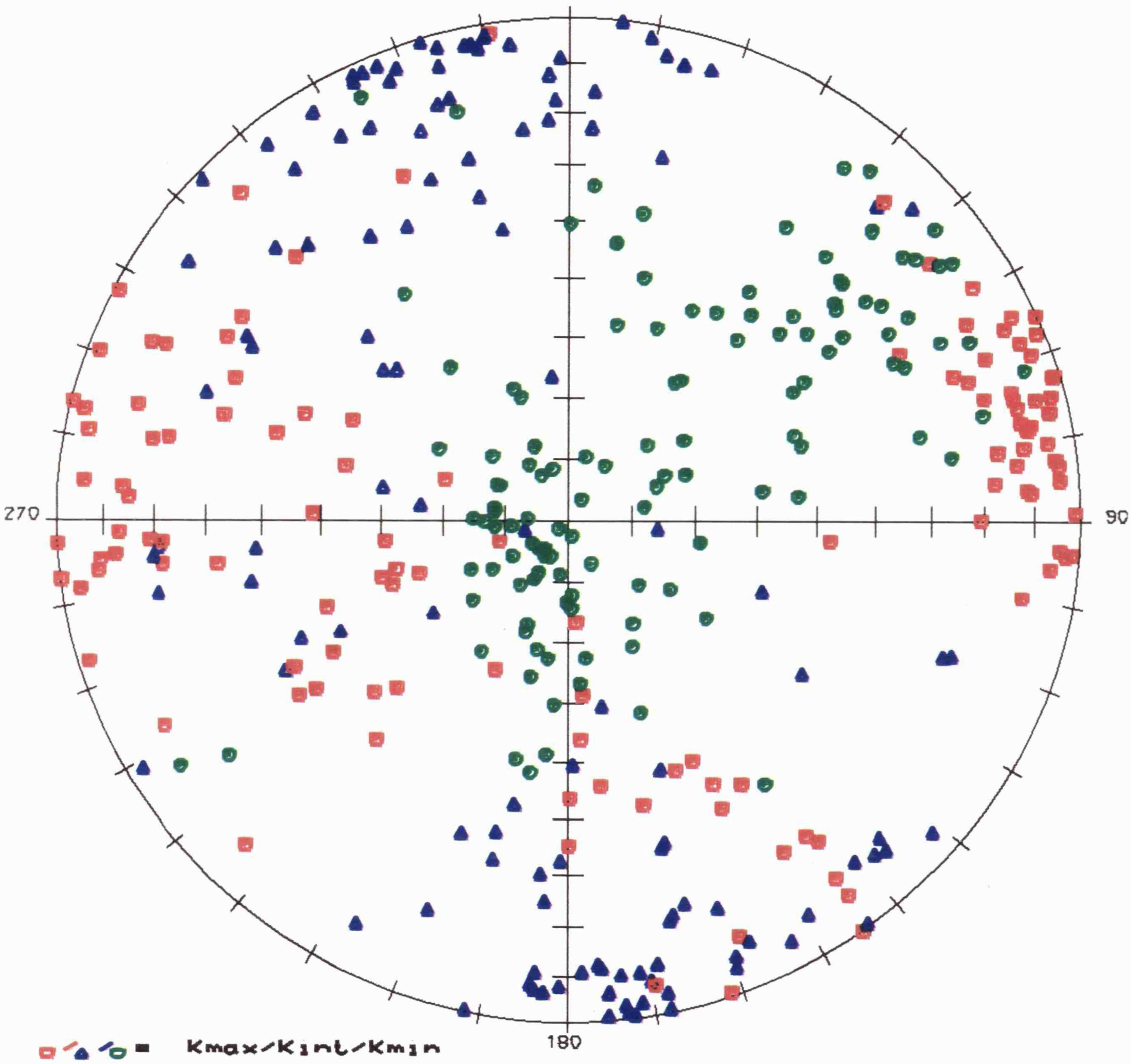

Figure 8.18 Lower hemisphere equal area plot of the principal axes of susceptibility for Dawan loess III.

DAWAN - PALAEOSOL III

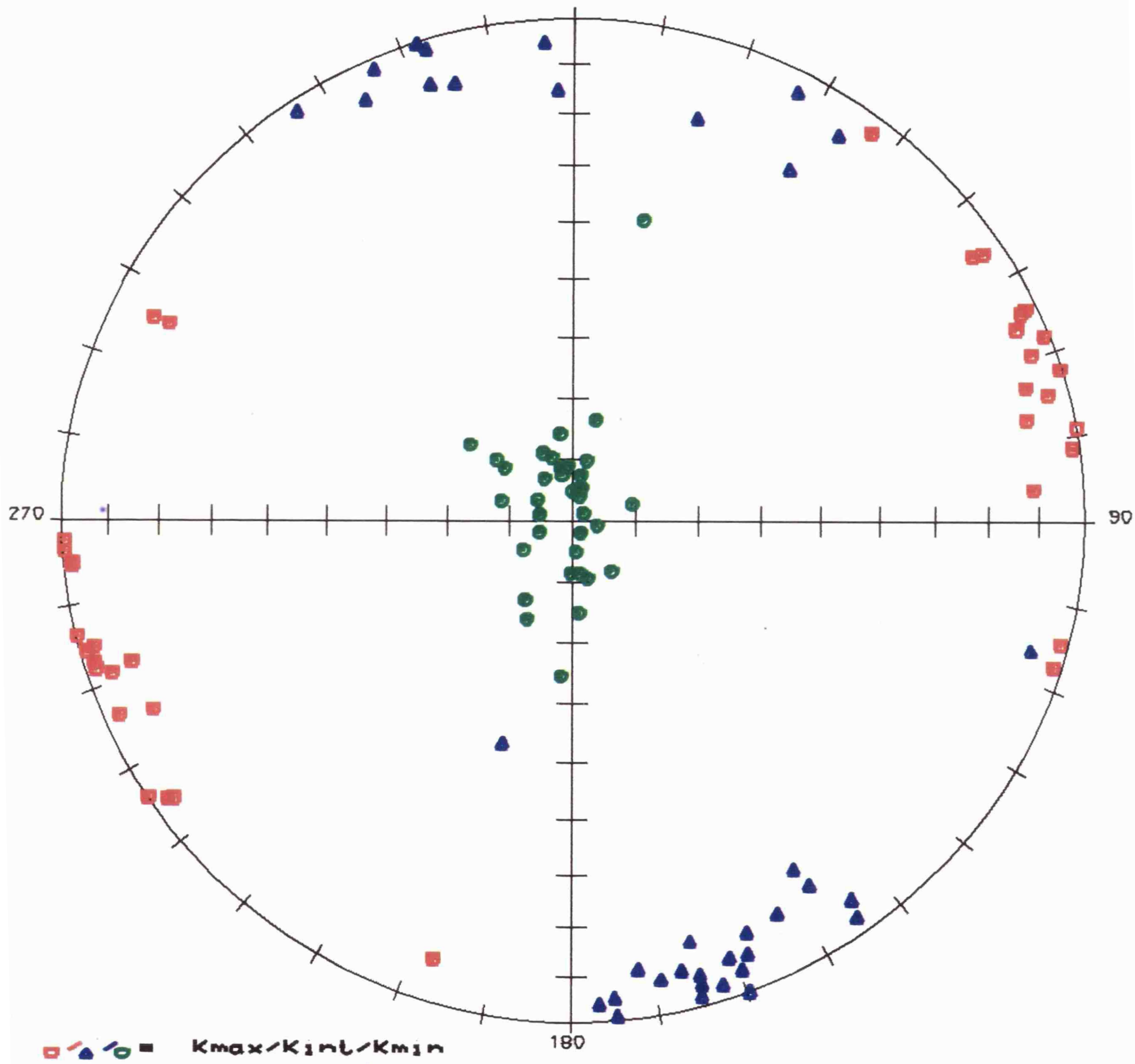

Figure 8.19 Lower hemisphere equal area plot of the principal axes of susceptibility for Dawan palaeosol III.

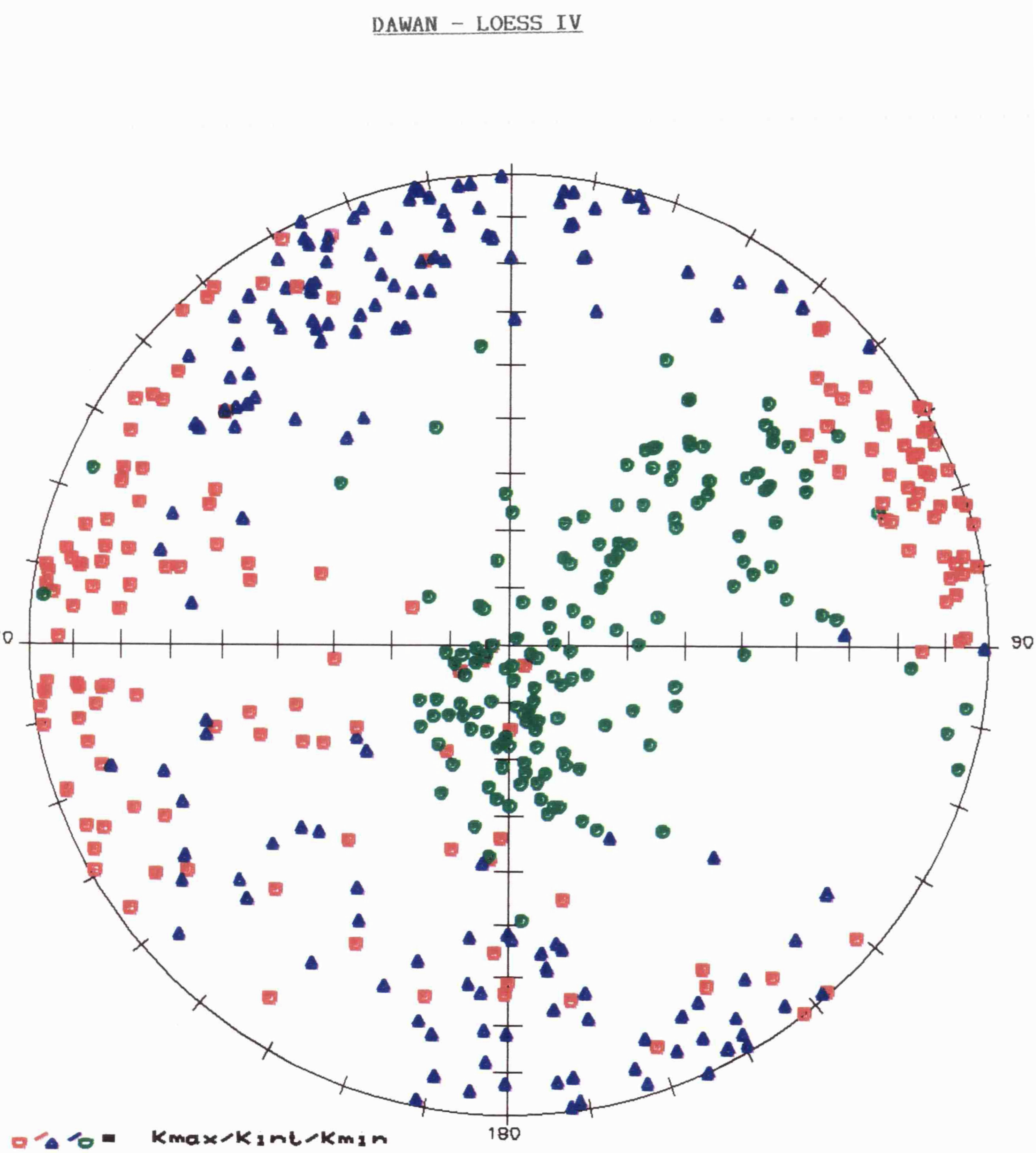

Figure 8.20 Lower hemisphere equal area plot of the principal axes of susceptibility for Dawan loess IV.

DAWAN - PALAEOSOL IV

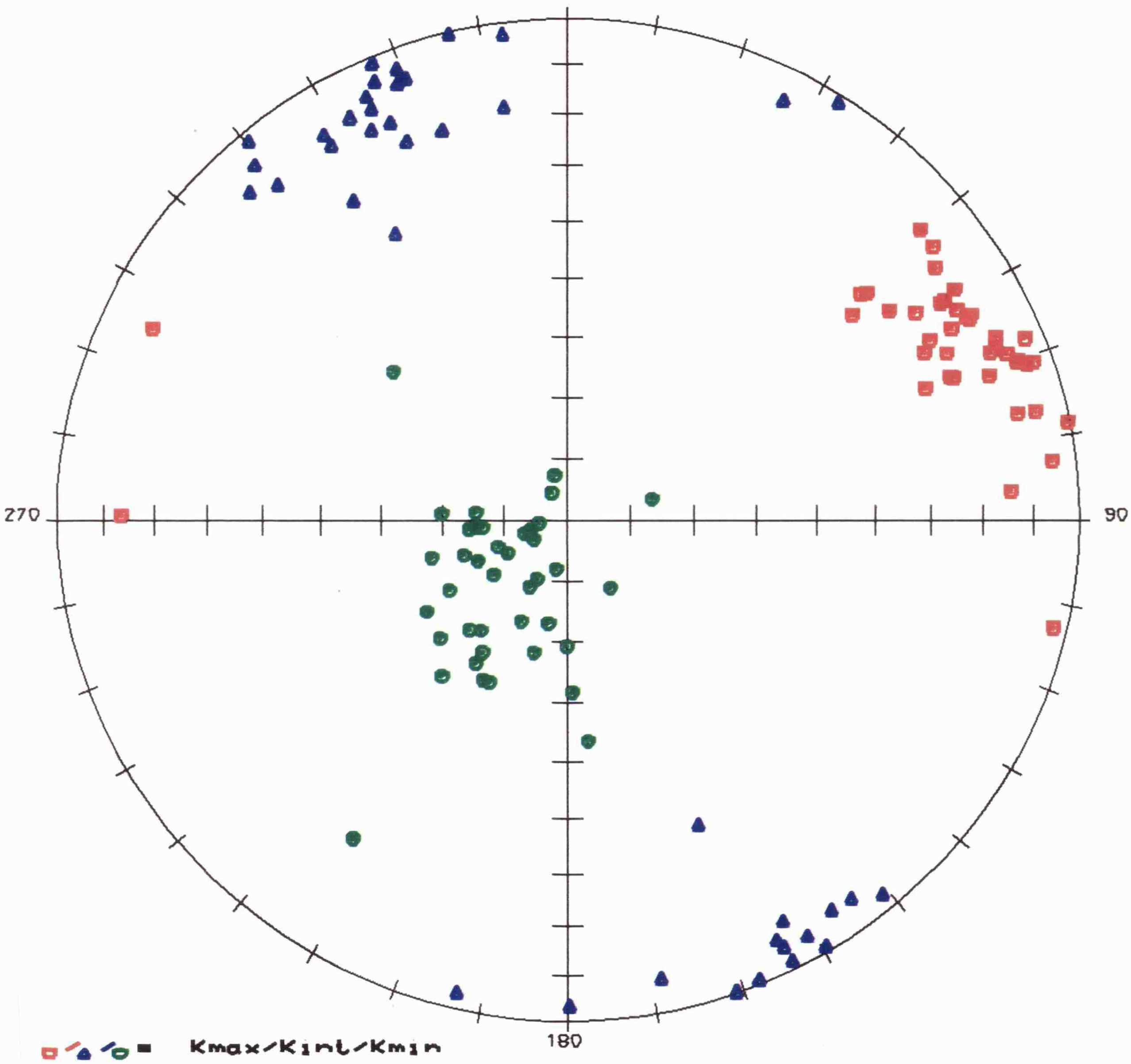

Figure 8.21 Lower hemisphere equal area plot of the principal axes of susceptibility for Dawan palaeosol IV.

DAWAN - LOESS V

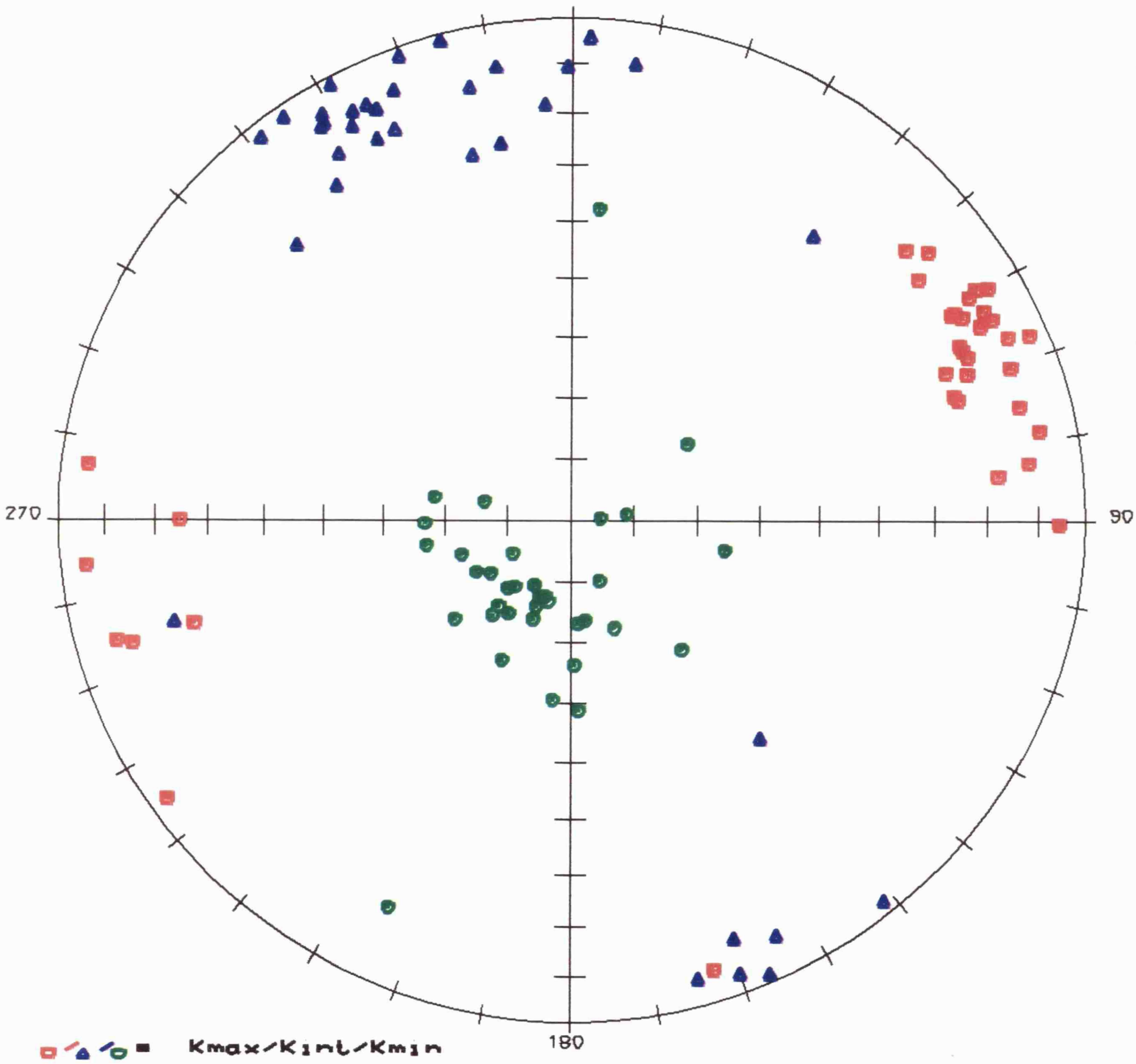

Figure 8.22 Lower hemisphere equal area plot of the principal axes of susceptibility for Dawan loess V.

DAWAN - PALAEOSOL V

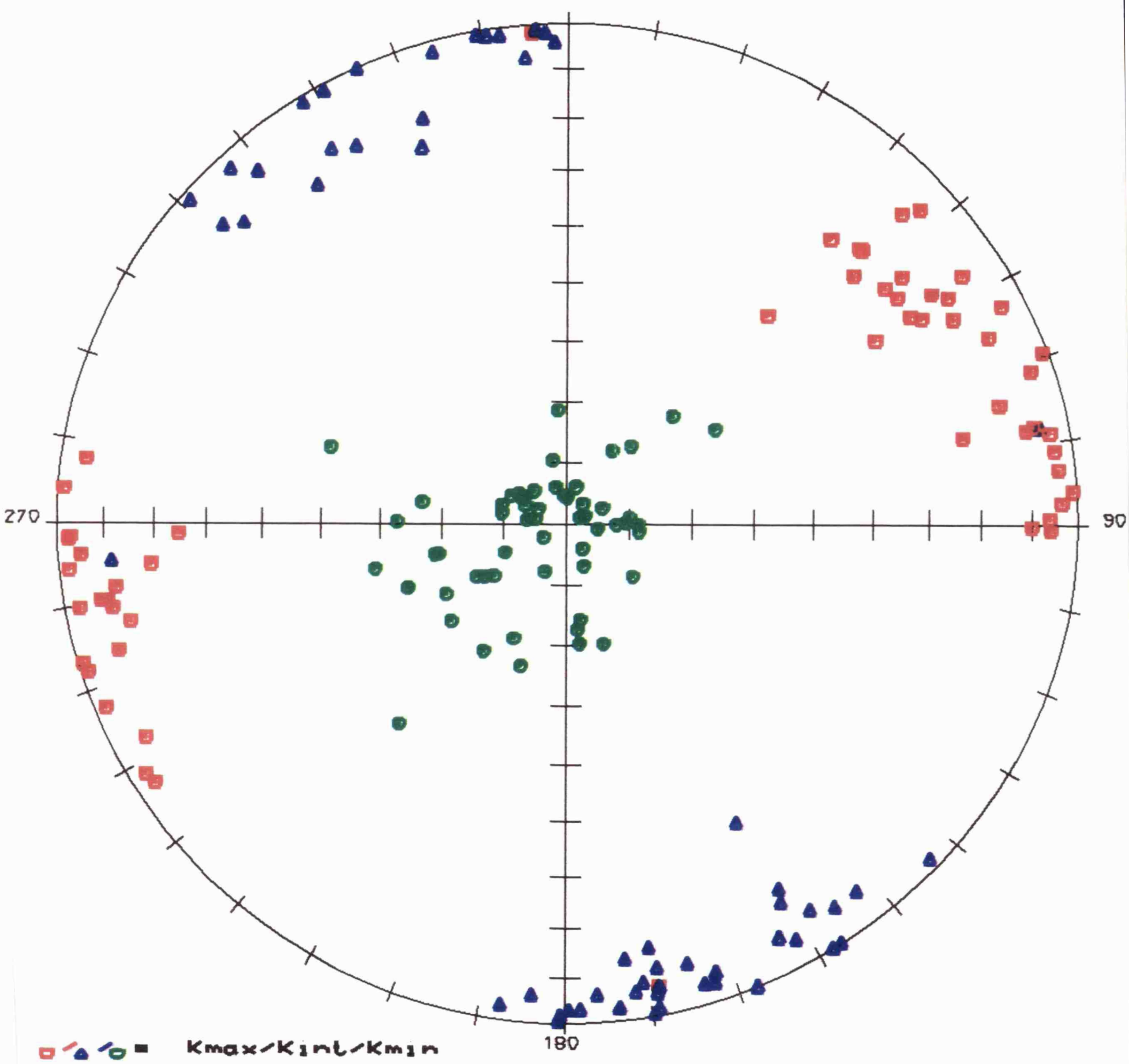

Figure 8.23 Lower hemisphere equal area plot of the principal axes of susceptibility for Dawan palaeosol V.

DAWAN - LOESS VI

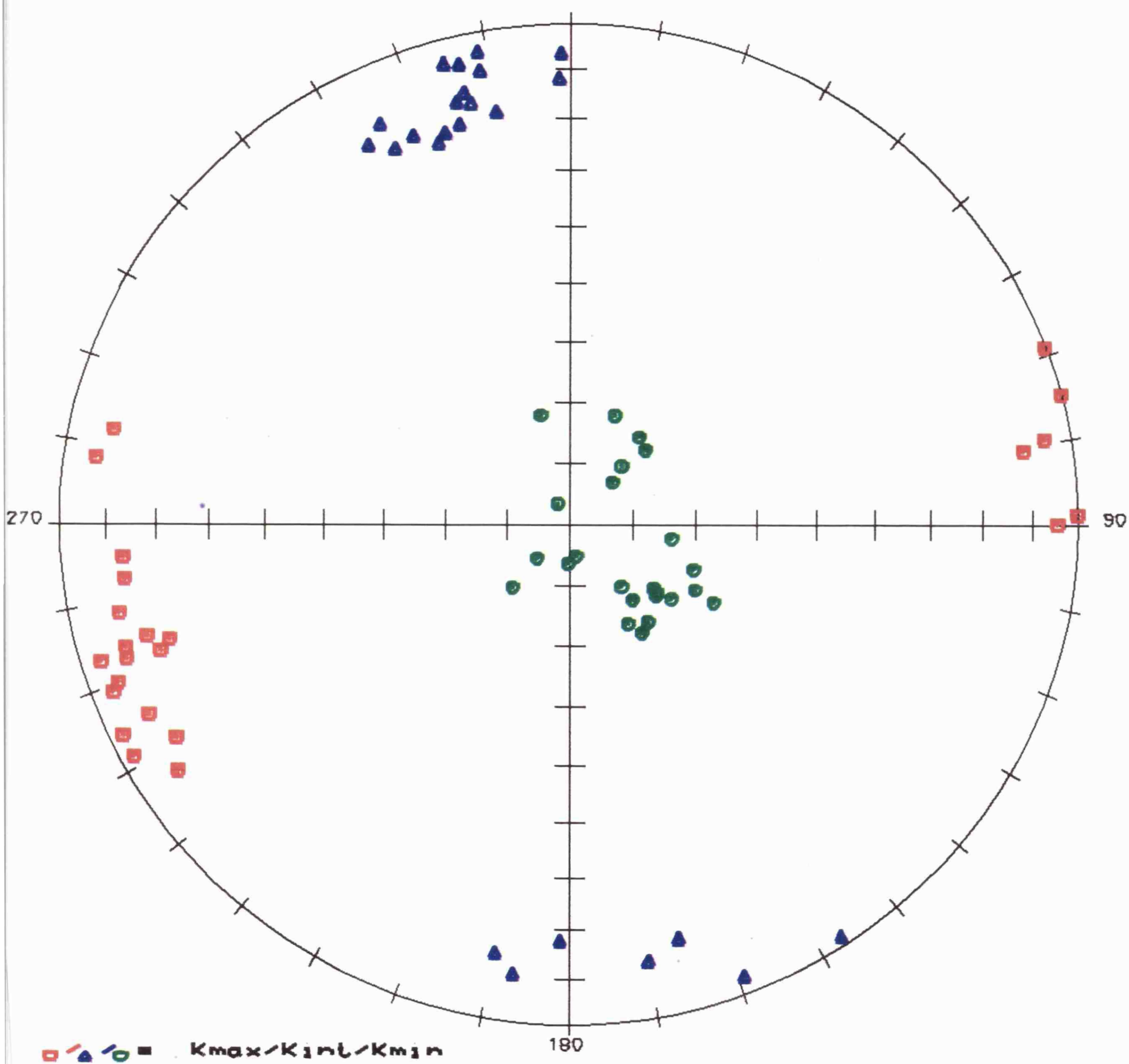

Figure 8.24 Lower hemisphere equal area plot of the principal axes of susceptibility for Dawan loess VI.

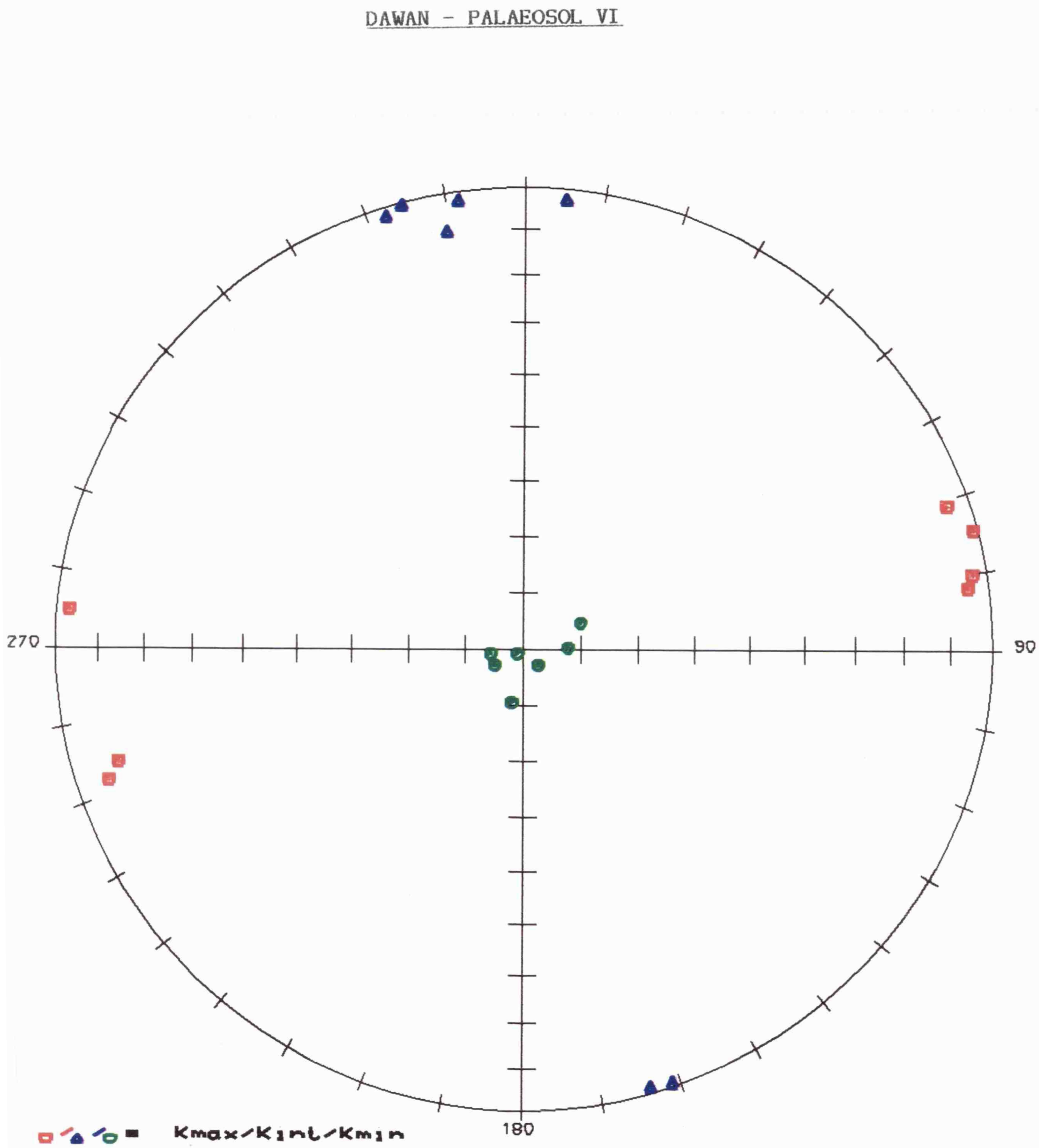

Figure 8.25 Lower hemisphere equal area plot of the principal axes of susceptibility for Dawan palaeosol VI.

8.2.3 Southern Gansu: Sala Shan and Labrang

29 samples of alluvial redeposited loess from Sala Shan and 54 samples of loess from Labrang were tested. The Sala Shan alluvial silt is visibly stratified, reworked loess (plates 2.6 and 2.7) and was sampled and measured as a control.

Table 8.4 Mean lineation, foliation, total anisotropy and q parameter, with standard deviations (SD), for Labrang loess and Sala Shan fluvially deposited alluvial loess. n is the number of samples measured.

site	lineation		foliation		total anisotropy		q		n
	mean	SD	mean	SD	mean	SD	mean	SD	
Labrang	0.0137	0.0080	0.0138	0.0102	0.0275	0.0142	0.695	0.405	54
Sala Shan	0.0060	0.0045	0.0670	0.0133	0.0610	0.0121	0.093	0.472	29

The mean fabric parameters calculated for the Labrang loess and Sala Shan silt are illustrated in table 8.4. The Labrang loess is as linear as it is foliar illustrated by a mean q of 0.695 with a weak anisotropy. The Sala Shan loessic alluvial silt on the other hand is strongly anisotropic dominated by a strong foliation in the order of six times greater than at the other sites (figure 8.26). Lineation is very weak with a mean value of 0.006 and a mean q of 0.093 illustrating the dominance of oblate grains. These results are similar to those found by Liu Xiuming et.al. (1988b) for waterlain loess from Xifeng.

The magnetic fabric from Labrang is plotted in stereographic form in figure 8.27 The fabric is isotropic with no particular ordering of axes. As the mass specific susectpibilities of the Labrang samples do not differ significantly from those of Jiuzhoutai and Dawan (see section 4.1), the isotropy is unlikely to be the result of scatter to increased signal to noise ratios. The Labrang loess is situated in the foothills of the A'nyêmaqen Mountains at the edge of the Tibetan Plateau and is terraced by the Daxia river. The loess is most probably formed within the mountain environment and deposited by wind within the narrow valleys. The fabric of the Labrang loess conforms to the expectations of an air fall deposit which has undergone no reworking or orientation within a current.

The lower hemisphere stereographic projection for the Sala Shan alluvial silt is illustrated in figure 8.28. The distribution of axes suggests a horizontal fabric with closely clustered vertical minimum axes and maximum and intermediate axes ranging from 110°-285° declination with dip angles less than 15°. The close association of minimum axes and variation in declination of maximum and intermediate axes are the result of deposition of strata in shallow braided channels which are affected by sinusoidal changes in channel and thus have varying current orientation. Each sample within the perspex cubes comprised at least 8 stratigraphic layers of silt which may each have been deposited under different flow régimes.

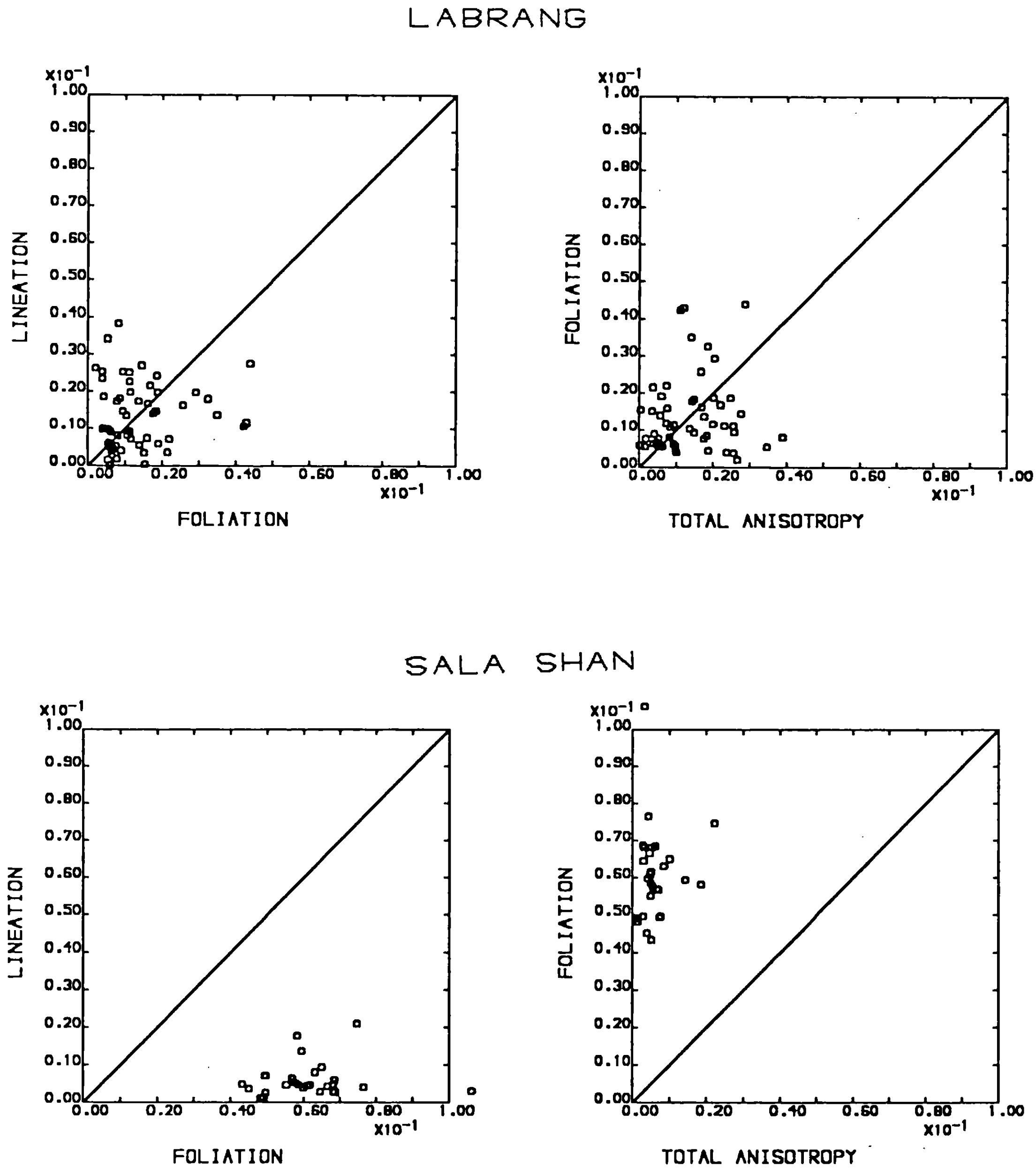

Figure 8.26 Lineation-foliation and foliation-total anisotropy plots for Labrang loess and Sala Shan loessic alluvium.

LABRANG LOESS

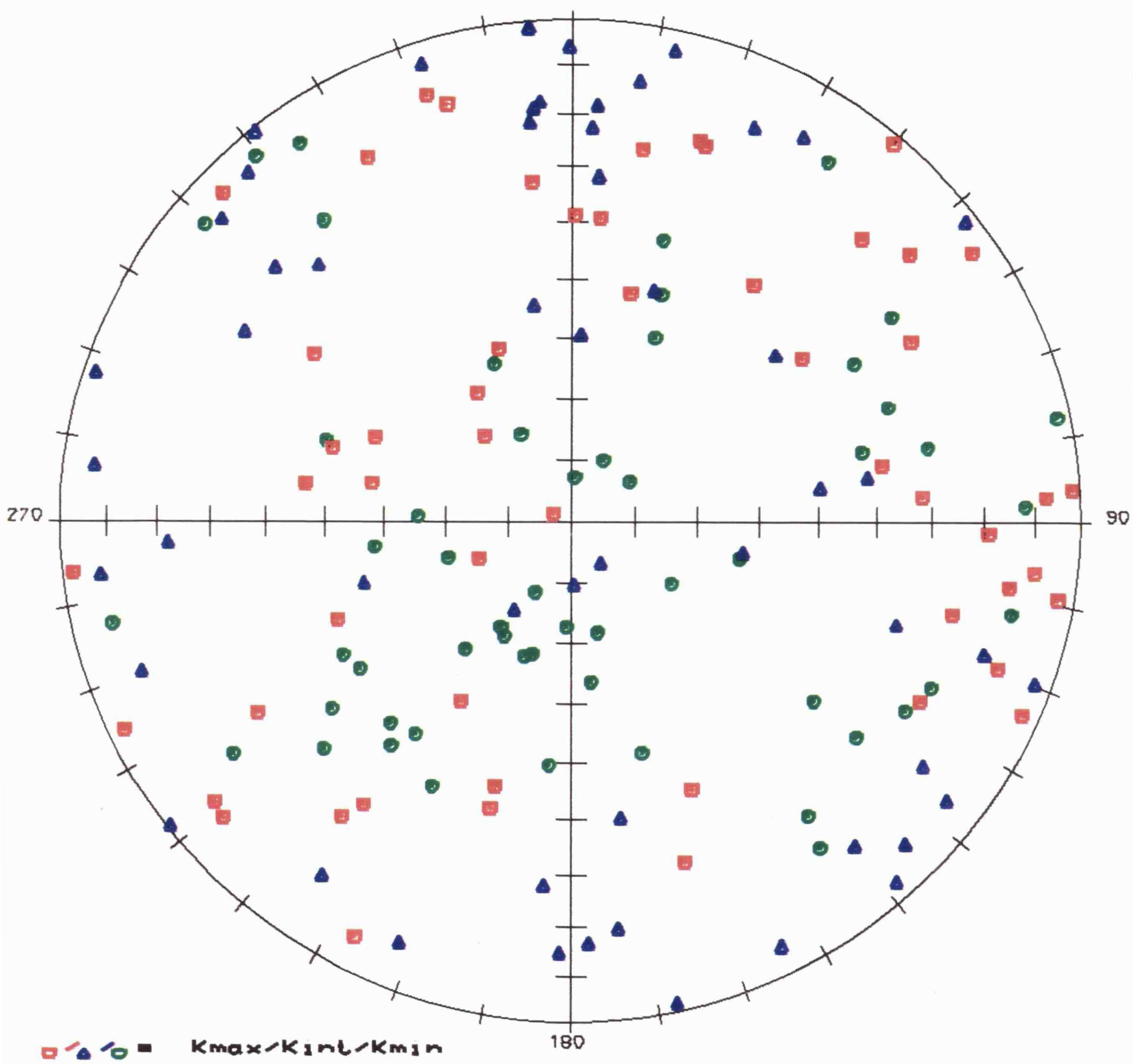

Figure 8.27 Lower hemisphere equal area plot of the principal axes of susceptibility for Labrang loess.

SALA SHAN LOESSIC ALLUVIUM

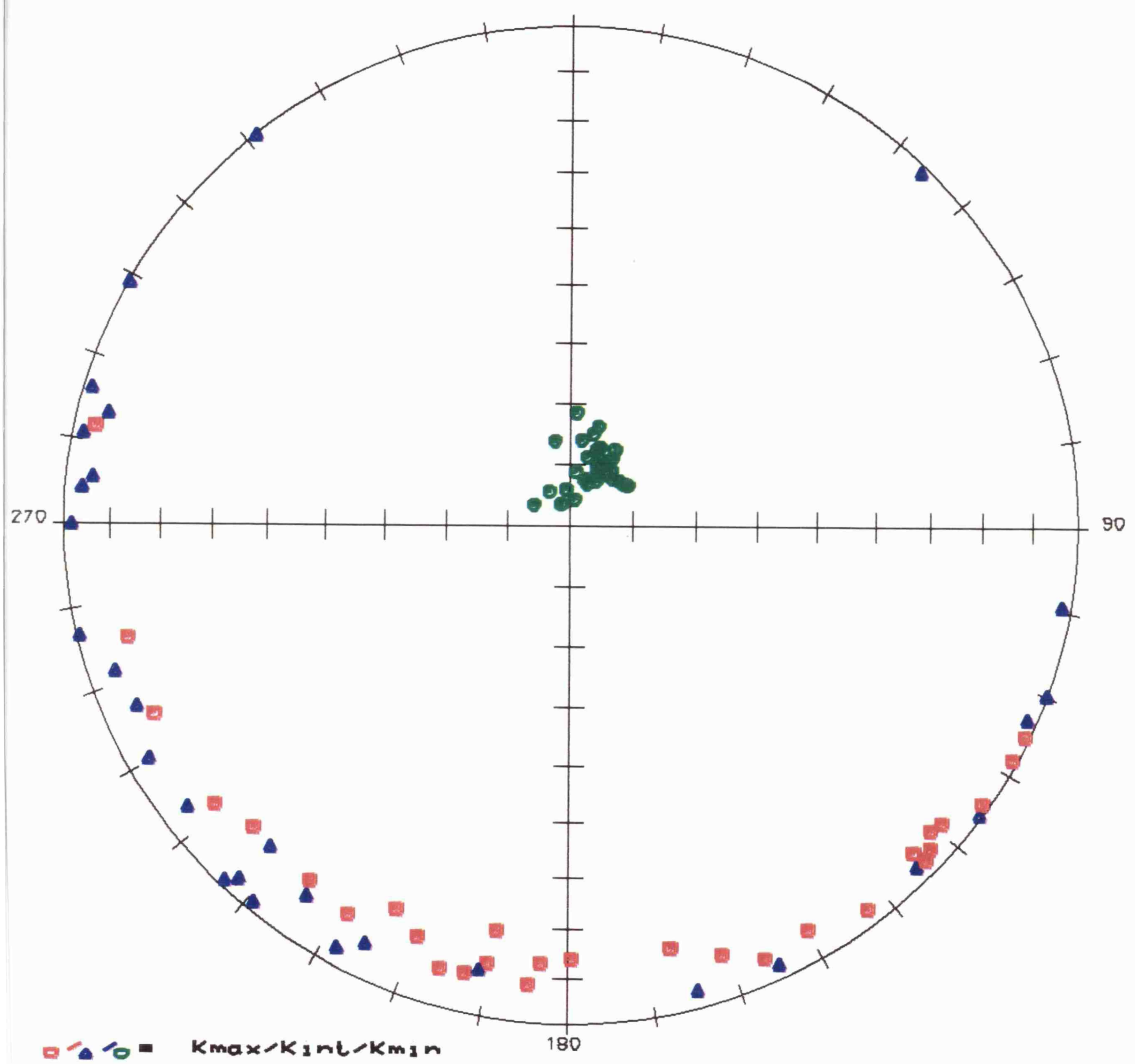

Figure 8.28 Lower hemisphere equal area plot of the principal axes of susceptibility for Sala Shan loessic alluvium.

8.3 Discussion of Minisep fabric

The primary fabric at Jiuzhoutai appears to be orientated NE/SW with a secondary component indicative of slope reworking which occurred during the last glacial stage. The sediment at Dawan shows a primary NE/SW fabric. The low foliation values in the Dawan sediment, when compared with waterlain silts from Sala Shan and published results from Xifeng (Liu Xiuming *et. al.*, 1988) shows the preferred grain orientation is most likely to be the result of wind action.

The textural differences between the Xian (central Loess Plateau) and Lanzhou sediment (see plate 2.2) coupled with the presence of gypsum in the Lanzhou loess are indicative of the different climatic régimes under which they have accumulated. The influence of the East Asian monsoon, which brings moist, warm air is strong within the central Loess Plateau but weaker at Lanzhou. The mean annual precipitation is a good illustration of this effect: 604mm falls at Xian compared to only half of this (330mm) at Lanzhou and a mere 38mm in the Qaidam Basin to the west (Zhao Songqiao, 1986). The occurrence of gypsum nodules throughout the Lanzhou sections testifies to the perennial aridity of the climate. The southerly monsoon winds impinge upon the A'nyêmaqen Mountains resulting in a high annual precipitation of 800mm at the snowline (Wang Jingtai, 1987; see section 2.1.5). The mountains to the south and southeast of Lanzhou (Mahan Shan, Min Shan and Qinling Shan) are all over 3000m in altitude and, together with the regional attenuation of the summer monsoon rainfall amounts from the southeast to the northwest, account for the strong rainfall gradients in this region and the rapid fall off in mean annual precipitation westwards through the Hexi Corridor and to the Qaidam Basin. The other climatic influence in this region is the Mongolian High Pressure system (MHPS). This causes convergence of warm air descending from the Tibetan Plateau and cold air of Siberian origin to be drawn northwestwards along the Hexi Corridor and into the Qaidam Basin, the Kunlun and Qilian mountains being an important influence in this movement. The Liupan Shan and Quwu Shan to the east of Lanzhou, which are well over 2000m in height, would attenuate any effect from northeasterly winds flowing into the Tengger Desert. Thus it is essential to stress the importance of regional topography in understanding the factors influencing the Lanzhou deposits. The loess sections of the central Loess Plateau are not effected by the same extreme topography.

The fabric of the Lanzhou sections suggests that the primary flow direction is NE/SW. However, taking the above discussion into account, it is more likely that the predominant winds effecting the Lanzhou area are those associated with the MHPS. Hrouda (1982) proposes that in conditions of strong current the long axes rotate to lie orthogonal to the current direction. Thus it is possible to interpret this Dawan and primary Jiuzhoutai fabric as resulting from deposition in a strong NW wind associated with the MHPS. It is also possible that it is a primary NE orientated fabric associated with weaker NE winds from the MHPS. The fabric is not likelv to result from SW winds due to the presence of the mountain front. A SE wind associated with the monsoon is likely to have been severlev attenuated by the presence of the 3000m mountains lying southeast of Lanzhou. Whilst a NE/SW current cannot be discounted, the strength of the MHPS implies that the fabric is more likelv to result from this than from NE/SW or local components.

The fabric results show some depositional variations between Dawan, Jiuzhoutai and Labrang. The Labrang loess appears to be random and isotropic conforming to the criteria of Derbyshire *et.al.* (1988) for unreworked loess. Labrang is situated at an altitude of about 3000m in the mountain range which forms the northeastern frontier of the Tibetan Plateau. This mountain range forms an extension of the A'nyêmaqen Mountains. The loess at Labrang takes the form of a 60 metre river terrace but is not visibly stratified. Its rare earth element geochemistry shows it to be of a different genesis from the deposits of the Loess Plateau and probablv formed within the local mountain environment. The narrow high altitude valleys would preclude substantial post-depositional sorting by wind and the absence of stratification and high foliation values also points to an absence of fluvial redeposition. The evidence therefore favours a primary aeolian origin for the Labrang loess, which has not undergone subsequent reworking.

The deposits from the Loess Plateau at Dawan and Jiuzhoutai both show evidence of post-depositional grain re-orientation. At Dawan, the fifteen metres of loess and palaeosol both show a weakly foliar horizontal fabric with a NE-SW orientation of grain long axes. This grain orientation lies orthogonal to the direction of predominant winds which are northwesterlies associated with the Mongolian High Pressure system (MHPS). One possible explanation could be that post-depositional grain alignment by wind has occurred, but due to the strength of the wind current, the grain long axes have rolled transverse to the current direction. Both Jiuzhoutai and Dawan show a NE-SW grain orientation, although much of the Jiuzhoutai loess appears to have undergone post-depositional realignment by slope processes. Only the Sala Shan loessic alluvium, which has visible stratification, showed high foliation values consistent with reworking by water.

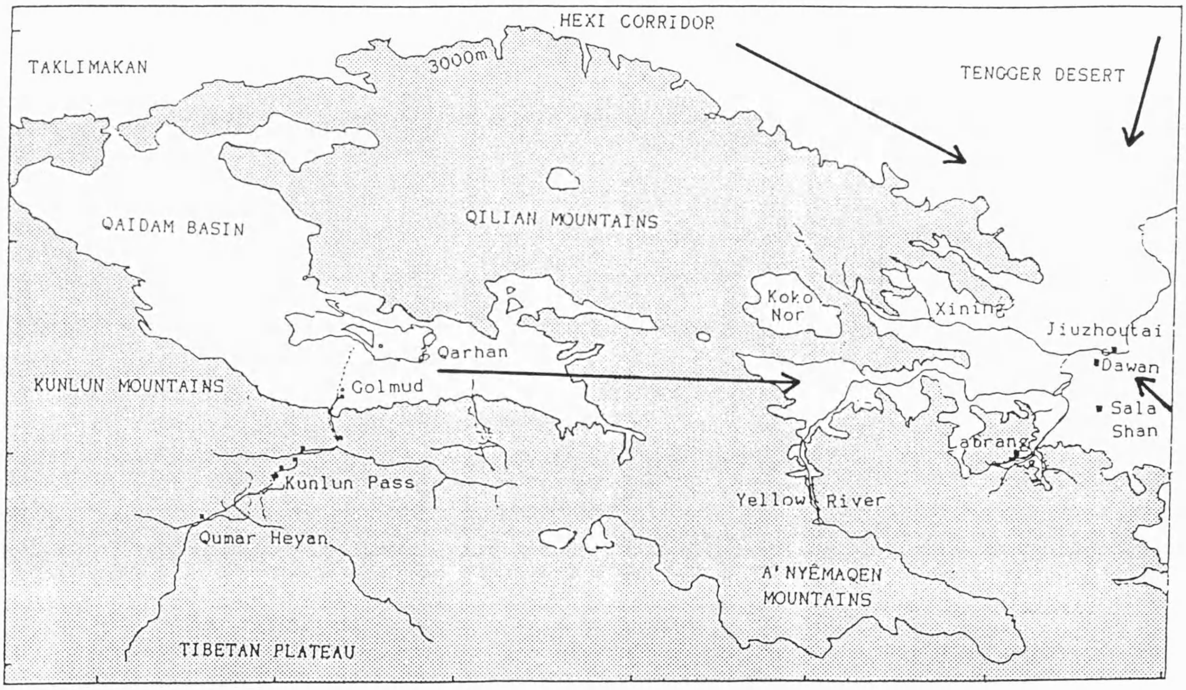

Figure 8.29 Wind directions associated with Lanzhou sediment fabrics.

8.4 Measurement of AMS using a low field torque magnetometer.

In addition to the Minisep samples, ten cubes of loess from Dawan and Jiuzhoutai were sent to the Department of Oceanography at the University of Southampton, where the AMS was measured by Dr. E.A. Hailwood on a low-field torque magnetometer. Although, in retrospect sample for sample comparisons between the Minisep and torque equipment would have been profitable, the difficulty involved in obtaining these results prevented further more comprehensive comparison.

8.4.1 The low-field torque magnetometer

The torque magnetometer at Southampton is of the suspended sample type (King and Rees, 1962), in which a sample is placed in a perspex chamber situated on a glass rod which is suspended from a phosphor-bronze torsion fibre. Around the sample chamber and glass rod are situated a pair of coaxial Helmholtz coils. A current of 5mT is passed through the coils, with a frequency of 50Hz, causing the sample to rotate according to its degree of anisotropy, with the maximum anisotropy axes aligning with the field direction. Movement of the glass rod is damped by an oil bath. Deflection of the sample is measured about three axes, with the change in torque on the specimen in the field giving a measure of the susceptibility difference in the plane of measurement.

8.4.2 Results

Ten 2.2cm cubes of loess from Jiuzhoutai and ten cubes of loess from Dawan were run on the low field torque magnetometer at Southampton University. Lower hemisphere equal area projections of the maximum (Kmax) and minimum (Kmin) axes of susceptibility are presented.

8.4.2.1 Jiuzhoutai

Both loess I and loess III samples show a foliar fabric with weak lineation and mean q values of 0.09 and 0.04, well below the 0.67 transition from foliar to linear. Total anisotropy is weak for both loesses.

The mean total anisotropy results are similar to those derived from the spinner magnetometer although the mean foliation is somewhat larger and the mean lineation smaller, with subsequent lower mean q values. However this may be due to the fact that only five samples from each loess were tested with the torque magnetometer whereas 103 samples were tested with the spinner magnetometer.

Table 8.5 Mean magnetic fabric parameters for loess samples from Jiuzhoutai obtained from the low field torque magnetometer.

unit	lineation		foliation		total anisotropy		q	
	mean	SD	mean	SD	mean	SD	mean	SD
Loess I	0.0030	0.0008	0.0324	0.0017	0.0354	0.0017	0.0902	0.0232
Loess III	0.0015	0.0017	0.0385	0.0026	0.0445	0.0075	0.0392	0.0441

The lower hemisphere equal area projection for the maximum and minimum susceptibility axes is illustrated in figure 8.30. The slightly dipping NW orientation of maximum axes shown by eight of the samples, lies orthogonally to the ENE-WSW orientation of the other two samples, reflecting the foliar nature of the susceptibility ellispoid and the subsequent similarity in Kmax and Kint axes. The dominance of foliation in this torque fabric is reflected in both foliation and q values, implying that Kmax ≅ Kmin and thus that the orthogonal axes are interchangeable. This explains the difference between the Minisep and torque fabrics.

8.4.2.2 Dawan

The two loess units from Dawan were both dominated by a foliar fabric with a small lineation component and mean q values in the range 0.31 to 0.35 (table 8.6).

Table 8.6 Mean magnetic fabric parameters for loess samples from Dawan obtained from the the low field torque magnetometer.

unit	lineation		foliation		total anisotropy		q	
	mean	SD	mean	SD	mean	SD	mean	SD
Loess I	0.0134	0.0030	0.0362	0.0058	0.0494	0.0079	0.3132	0.0582
Loess IV	0.0166	0.0026	0.0403	0.0059	0.0566	0.0068	0.3448	0.0538

Total anisotropy results are slightly higher than those obtained using the Minisep but again only five samples were run from each unit compared with 326 for loess I and 154 for loess IV on the spinner magnetometer. The orientation of principle axes of susceptibility (figure 8.31) is similar to those obtained from the Minisep. The q values are higher than for the Jiuzhoutai samples indicating that the foliation is not as dominant.

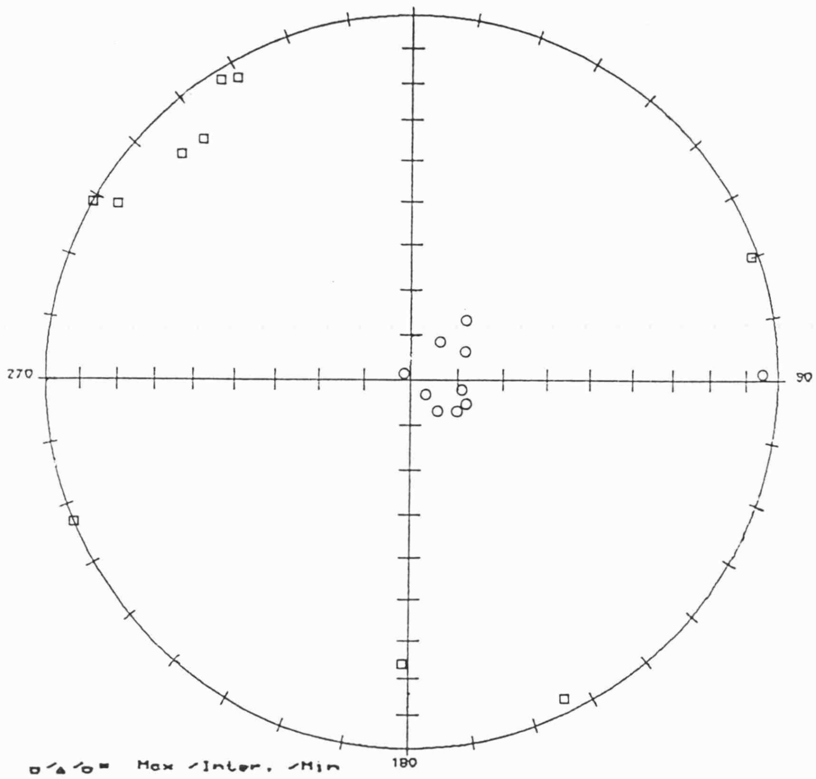

Figure 8.30 Lower hemisphere equal area plots of principal susceptibility axes measured in the torque magnetometer for samples from Jiuzhoutai.

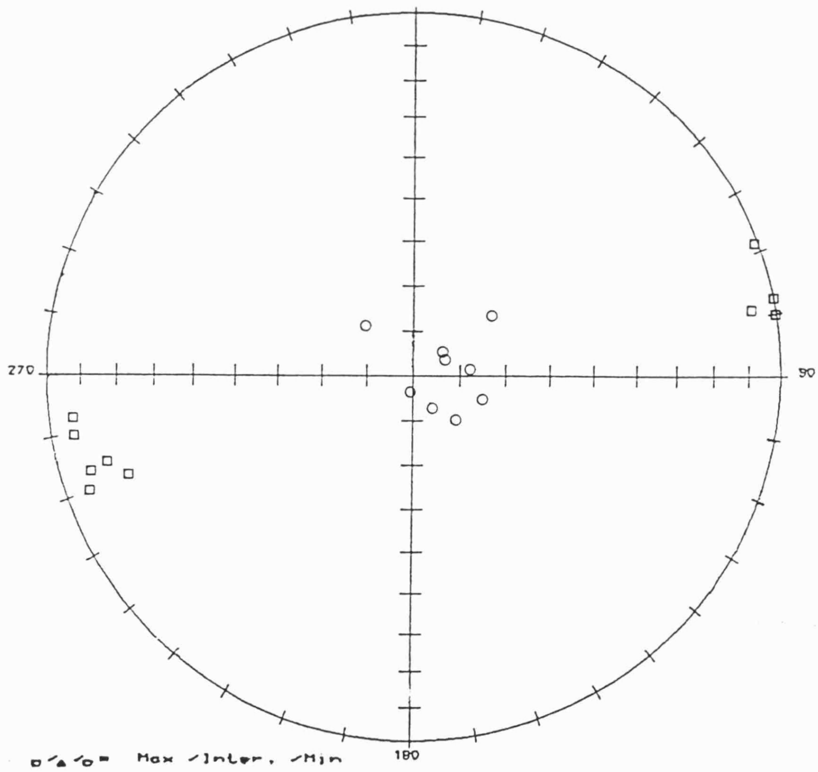

Figure 8.31 Lower hemisphere equal area plots of principal susceptibility axes measured in the torque magnetometer for samples from Dawan.

9. SUMMARY AND CONCLUSIONS

The particle size envelopes of the sediments from the Tibetan Front show that the samples from the high altitude mountain environments (Tibet, the Qaidam Basin and Labrang) have a coarser particle size than the Loess Plateau sediments. However, the mountain silts did not show a unimodal particle distribution and fines of the size prevalent in the Loess Plateau (less than 30µm) are abundant, contributing from 49% (Kunlun Pass) to 77% (Labrang A) of the overall particle size distribution in these mountain silts. The deposition model proposed by Bowler *et.al.* (1987) states that northwesterly winds associated with the Mongolian high pressure system deflate fines resident within the Qaidam Basin and carry them to the western Loess Plateau. The Mongolian High Pressure system (MHPS) causes winds to be funnelled past the Kunlun Mountains, northwest down the Hexi Corridor and across the Qaidam Basin. Bowler *et.al.* (1987) infer that these fine silts were formed in the Kunlun mountain environment from where they were transported into the Basin. The particle size of the surface silts studied here (chapter 3.1) indicates that particles of this size are present within the Kunlun Mountains and Tibetan Plateau. The Kunlun River represents one mechanism of transporting these silts down into the Qaidam Basin and the presence of the barchan dune field shows that an aeolian transport system is presently operating in the mountains carrying particles down from the vicinity of the Kunlun Pass. Although this only shows that sediments of the relevent size are being produced today in the mountains and transported into the Qaidam Basin, there is no reason to suggest that this process did not occur in the past.

The rare earth element abundances of the Kunlun Mountain silts are similar to those of Lanzhou loess. Wen Qizhong (1983; 1985) proposed that the similarity of distribution of REE between Luochuan loess and Tengger desert sand showed that the loess derived from the desert, although the concentrations of REE were different. If this proposition was applied to the silts studied here (chapter 3.3) then there constitute a convincing argument that the Lanzhou loess derived from the Kunlun Mountains. However, although the REE patterns are similar the data are not sufficient to support this hypothesis. It is therefore only possible to suggest that these sediments may be related, with both showing higher $(La/Yb)_N$ than the crustal average.

The Labrang loess shows a distinct REE abundance, with 5.5 to 6 times lower REE concentrations than the Lanzhou loess or Kunlun silt. Its location within the A'nyêmaqen Mountains southwest of the Loess Plateau suggests that it is the product of local mountain processes (cold weathering and glacial grinding) and the thickness of the deposit (60 metre loess terraces located on either side of the Daxia Valley) suggests that the formation and transport processes are efficient. Magnetic fabric indicates that the loess is a primary aeolian deposit that has not undergone any reworking. Thus the Labrang loess holds good potential for further study. The close proximity to its source suggests that if formation is related to palaeoclimate then the lag between climate change and deposition is minimised.

The magnetic mineralogy of the Tibetan Front sediments appears to be dominated by ferrimagnetic cation-deficient (CD) magnetite, although IRM acquisition suggests that there is also a high coercivity antiferromagnetic mineral present which may be hæmatite or defect goethite and is more prevalent in loess than palaeosols. The CD magnetite may exist as a coating around a cation-rich magnetite core. Such coatings are formed in oxidising environments such as that which exists in the arid northwest of China. Comparison of loess and palaeosols from Lanzhou shows that the palaeosols are characterised by a finer assemblage of superparamagnetic (SP) and stable single domain grains (SSD) whilst the loess contains coarser multidomain (MD) and single domain grains.

Magnetostratigraphies were compiled for sections of the Jiuzhoutai and Dawan profiles in an attempt to locate the Blake Event. However, no reversals or excursions were observed (see figures 7.3 and 7.5). The Blake Event has been principally documented in the Caribbean (Denham, 1976, Denham *et.al.*, 1977), Japan and Indonesia (Yaskawa *et.al.*, 1973; Yaskawa, 1974; Manabe, 1977; Sasajima *et.al.*, 1984) and in the Mediterranean (Creer *et.al.*, 1980; Tucholka *et.al.*, 1987; Tric *et.al.*, 1991) and is therefore thought to be a global event occurring during the last interglacial period at about 115-120ka (Tric *et.al.*, 1991). Thus if it were present in China it would occur within the last interglacial palaeosol. Thermoluminescence dates from the Scorpion Pit indicate that the dual palaeosol sampled here represents the last interglacial (Chen Fahu *et.al.*, 1991; Musson, *pers. comm.*). Fabric measurements indicate that there has been reworking of the sediment in the Scorpion Pit: however, the TL dates (Chen Fahu *et. al*, 1991; Musson *unpub. data*) suggest that the reworking occurred between 50ka and 80ka and the slope of the fabric (110°E) indicates that the topographic surface was different from that of today. As the reworking occurred after the Blake Event, it is likely that remagnetisation will have taken place. This is borne out by the NRM results (section 7.4) which show declination and inclinations which approximate the normal field direction and do not suggest rotation or tilting of the particles since the magnetisation was locked in. Therefore remagnetisation by powder flows or slumping between 50-80ka is likely.

The dual palaeosol representing the last interglacial occurs within the Scorpion Pit, Jiuzhoutai, at a depth of 48 to 52 metres. Two triple pedocomplexes of decreasing weathering intensity were found between depths of 25 and 35 metres at Dawan. The apparent difference in sedimentation rate between Dawan and Jiuzhoutai may be explained by their different topographic settings. Jiuzhoutai is located on the banks of the Yellow River in the Lanzhou Basin, whereas Dawan is situated on the Shua Jia valley (the Shua Jia is a minor tributary of the Yellow River) approximately 8km south of the Lanzhou Basin. Silts transported by the Yellow River may be deposited on point bars or braids during periods of low flow, from which they may be deflated and deposited on bluffs, in a manner similar to that described by Péwé (1975) for Alaskan loess, Alaska being one of the few places on earth where conditions have remained similar to those that prevailed during the last glacial period. As Jiuzhoutai is situated on the Yellow River it is possible to envisage a higher deposition rate compared to Dawan. The Dawan section has no geochronological control so it is not possible to define accurately the position of the last interglacial palaeosol. Two triple soils occur within 10 metres. The uppermost soils (I - III) are each separated by about 2 metres of loess. There is 2.5 metres of loess separating the two soil complexes, with the lower complex soils (IV - VI) each separated by between 0.5 and 1.0 metres of loess. Soils III and VI are well developed brown horizons, with II and V less well developed and I and IV poorly developed and difficult to distinguish from the surrounding loess.

Fabric studies indicate that the loess at Dawan is predominantly foliar and sub-horizontal showing a primary wind orientated fabric. The low foliation values, when compared with Sala Shan redeposited loessic alluvium (section 8.1.4.4; plate 2.10) and the published data of Liu Xiuming *et.al.* (1988) for fluvially redeposited Wucheng loess, suggest that deposition did not occur within a water medium. Therefore the preferred grain orientation must be due to wind, as proposed by Matalucci *et.al.* (1969) for the Vicksberg loess.

The preferred grain orientation at both sites is either broadly NW/SE or NE/SW depending upon the foliation. The dominant climate conditions are the winter MHPS and the southerly summer East Asian monsoon. The aridity of the Tibetan Front area (see section 2.1) testifies to the decreased penetration of the summer monsoon which impinges upon the mountains of Tibet. The presence of gypsum throughout the loess sections (section 2.2) shows that this aridity affected the loess and palaeosols sampled here. Therefore it is unlikely that the southerly monsoon winds would have a dominant effect upon the Lanzhou loess. However, the direction of monsoon winds reaching Lanzhou are influenced by the mountains to the west and their general southeasterly flow reinforced. Such southeasterly summer winds may augment the effect of MHPS northwesterlies funnelled through the Hexi Corridor and the Qaidam Basin but are unlikely to have a dominant effect due to attenuation by the Mahan, Min and Qinling Shan. Northeasterly winds also associated with the MHPS may also have affected the grain orientation of the Lanzhou loess after attenuation by the Quwu and Liupan Shan. Thus it is possible that the fabric orientation results from a combination of these factors.

9.1 Conclusions.

1. Dawan loess II shows a similar rare earth element distribution to surface silt derived from the Kunlun Mountains. Both of these samples have $(La/Yb)_N$ ratios higher than the crustal average.

2. The Labrang loess is a primary aeolian deposit produced within the local mountain environment and has a different source from that of the other deposits studied. Due to its topographic location it is likely that it represents silt particles formed by the processes of cold weathering and glacial grinding associated with mountain environments.

3. The magnetic mineralogy of the Tibetan Front sediments shows that they are dominated by ferrimagnetic magnetite with a cation-deficient coating. A harder magnetic component, which may be hæmatite or defect goethite is also present in the Gansu loessic silts. Palaeosols contain a higher concentration of ultrafine-grained minerals formed during pedogenesis.

4. Fabric results from Dawan indicate a weakly foliar horizontal fabric with no substantial reworking. The preferred grain orientation is probably a result of orientation by wind, with the grain long axes lying orthogonal to the predominant northwesterly wind direction.

6. No excursions of the magnetic field were found at Dawan. However the lack of chronological control precludes discussion of the absence of certain magnetic features *e.g.* the Blake Event.

7. The Jiuzhoutai sediment appears to have been partially reworked by slope processes bringing into doubt the authenticity of the magnetostratigraphy results. The evidence of slumping at Jiuzhoutai implies that, if the Blake Event were present in the sediment tested, post-depositional reworking will have overprinted the reversed NRM direction. Luminescence dates imply that the reworking was a Pleistocene event.

10. APPENDICES I - II

APPENDIX I: MAGNETIC MINERALOGY

Table I.1 Hysteresis Parameters for Jiuzhoutai samples

Sample depth (m)	Ms (Am^2kg^{-1})	Mrs ($x10^{-3}Am^2kg^{-1}$)	Mrs/Ms	Hc (kAm^{-1})
Loess I				
47.000	0.026	3.63	0.139	12.00
47.500	0.027	3.20	0.125	7.63
Palaeosol I				
48.275	0.029	4.32	0.148	7.21
48.600	0.028	4.21	0.151	8.60
48.975	0.024	3.97	0.159	8.55
49.175	0.025	3.99	0.154	9.61
Loess II				
49.675	0.018	2.43	0.135	10.80
50.000	0.025	3.55	0.139	10.90
50.425	0.013	1.90	0.142	10.30
Palaeosol II				
51.100	0.027	4.37	0.160	8.37
Loess III				
52.100	0.018	2.83	0.152	9.27
52.500	0.024	2.86	0.117	9.77
53.000	0.029	3.92	0.133	10.00

Table I.2 Hysteresis parameters for Dawan samples

Sample depth (m)	Ms (Am^2kg^{-1})	Mrs ($x10^{-3}Am^2kg^{-1}$)	Mrs/Ms	Hc (kAm^{-1})
Loess I				
20.000	0.029	3.49	0.117	9.70
20.025	0.023	2.69	0.113	9.48
21.500	0.022	2.42	0.109	9.74
21.550	0.031	3.80	0.120	10.10
21.800	0.028	3.18	0.115	9.56
22.500	0.022	2.78	0.126	10.10
22.800	0.022	2.67	0.120	9.78
23.500	0.029	3.71	0.127	9.47
24.000	0.030	3.00	0.100	6.57
24.200	0.015	1.98	0.128	9.67
24.500	0.027	2.73	0.120	9.50
24.875	0.019	2.67	0.137	11.20
Palaeosol I				
25.000	0.024	3.85	0.157	11.40
Loess II				
25.500	0.030	4.25	0.141	9.86
26.000	0.018	2.45	0.134	10.60
26.225	0.028	3.81	0.136	9.84
26.500	0.026	3.64	0.139	11.20
26.975	0.022	3.01	0.136	10.50
27.000	0.021	2.90	0.135	10.40
Palaeosol II				
27.200	0.030	4.53	0.150	8.75
Loess III				
28.500	0.026	3.36	0.127	9.89
29.000	0.022	3.52	0.155	10.70
Palaeosol III				
29.950	0.020	3.09	0.152	8.14
29.975	0.021	2.72	0.130	11.40
30.200	0.027	4.30	0.158	8.39
30.325	0.042	6.58	0.155	8.07
Loess IV				
30.500	0.019	2.89	0.151	10.40
31.000	0.040	6.44	0.161	6.58
31.175	0.035	5.53	0.158	7.83
31.500	0.023	2.83	0.121	10.60
31.775	0.026	3.43	0.131	9.54
32.000	0.023	3.01	0.129	9.48
32.500	0.023	2.75	0.123	9.44

Table I.2 continued.

Sample depth (m)	**Ms (Am^2kg^{-1})**	**Mrs ($x10^{-3}Am^2kg^{-1}$)**	**Mrs/Ms**	**Hc (kAm^{-1})**
Palaeosol IV				
33.000	0.023	3.61	0.155	8.73
Loess V				
33.550	0.024	2.86	0.117	7.55
33.700	0.028	3.82	0.134	10.80
Palaeosol V				
33.850	0.025	3.78	0.149	9.28
34.500	0.031	4.85	0.153	9.31
Loess VI				
34.800	0.026	3.42	0.130	10.20
35.000	0.024	3.75	0.152	10.60
Palaeosol VI				
35.250	0.038	6.39	0.167	7.51
35.275	0.032	4.96	0.153	6.58

Table I.3 Hysteresis parameters for Labrang and Sala Shan samples

Sample depth (m)	**Ms (Am^2kg^{-1})**	**Mrs ($x10^{-3}Am^2kg^{-1}$)**	**Mrs/Ms**	**Hc (kAm^{-1})**
LA000	0.029	3.74	0.127	8.20
LA025	0.022	2.29	0.100	8.22
LA050	0.029	2.82	0.097	7.72
LA075	0.021	2.07	0.099	8.54
LB000	0.019	2.56	0.132	7.71
LB025	0.028	2.89	0.104	8.53
LB050	0.027	2.68	0.098	7.71
LB075	0.021	2.08	0.096	7.98

Table I.4 Hysteresis parameters for Tibetan sediment

Sample depth (m)	**Ms (Am^2kg^{-1})**	**Mrs ($x10^{-3}Am^2kg^{-1}$)**	**Mrs/Ms**	**Hc (kAm^{-1})**
Golmud	0.025	1.13	0.044	2.35
KunlA	0.022	1.38	0.061	3.09
Glacier	0.018	1.77	0.094	7.43
Barchan	0.040	0.075	0.019	0.72
Pingo	0.017	4.51	0.260	20.50
Kun Pass	0.017	1.88	0.108	8.09
Qum Heyan	0.039	0.47	0.120	5.88

APPENDIX II: MAGNETOSTRATIGRAPHY

Table II.1 Palaeomagnetic directions and NRM intensities derived from thermal demagnetisation of loess and palaeosol samples from Jiuzhoutai. The maximum angle of deviation (MAD) is quoted along with the number of vector points used to derived it (n).

Depth (metres)	MAD	n	dec°	inc°	NRM ($x10^{-6} Am^2kg^{-1}$)
46.825	6.6	4	11.5	47.6	0.43
46.900	18.4	7	1.9	51.0	0.44
47.000	10.6	7	1.3	44.9	0.46
47.100	6.9	6	355.5	38.2	0.78
47.250	12.2	7	354.1	54.6	0.48
47.350	11.6	7	340.9	57.1	0.54
47.500	7.1	7	351.6	49.9	0.74
47.600	10.1	7	14.4	60.5	0.53
47.750	4.9	6	353.0	61.0	0.56
47.825	8.1	7	30.5	48.1	0.57
47.900	7.8	6	9.3	42.9	0.61
48.000	5.6	7	15.4	44.4	0.58
48.200	12.6	7	14.5	47.1	1.18
48.300	10.9	7	3.1	54.4	1.77
48.400	5.7	5	26.8	53.4	1.37
48.600	5.3	7	359.9	54.7	1.29
48.700	8.8	7	13.6	64.1	0.77
48.800	7.6	7	356.2	54.5	1.54
49.000	5.5	7	6.2	33.0	1.49
49.100	11.5	7	18.3	44.8	1.17
49.200	17.1	7	355.4	40.7	0.82
49.300	9.8	7	32.7	21.9	1.04
49.500	30.1	5	10.2	45.1	0.29
49.600	13.4	7	17.9	68.1	0.61
49.700	6.3	7	359.9	44.6	0.47
49.775	5.5	5	357.4	50.9	0.32
49.950	5.4	6	3.3	48.3	0.39
50.000	4.9	6	12.0	33.4	0.33
50.100	2.7	6	13.0	49.9	0.77
50.250	5.4	6	49.9	48.5	0.62
50.350	4.5	6	356.1	44.4	0.46
50.425	5.0	6	22.5	55.8	0.42
50.550	4.3	6	41.1	79.1	0.47
50.600	5.4	6	7.7	59.3	0.30
50.700	12.5	6	354.7	53.9	0.31
50.800	5.6	6	356.9	56.9	0.32
50.900	4.7	6	9.0	54.6	0.28
51.100	4.4	7	5.4	40.0	0.73
51.200	4.8	7	357.5	42.8	0.73
51.300	1.4	7	9.8	44.7	1.47
51.400	1.9	7	5.5	50.9	1.15
51.500	2.4	7	3.1	53.3	0.79
51.600	3.8	7	357.5	50.0	0.57
51.700	2.9	7	1.4	40.9	0.65

Table II.1 continued..

Depth (metres)	MAD	n	dec°	inc°	NRM ($x10^{-6} Am^2kg^{-1}$)
51.800	3.5	7	352.8	52.0	0.39
51.900	5.8	7	354.5	48.3	0.34
52.000	2.8	6	12.5	60.0	1.08
52.100	2.0	6	351.5	49.5	1.21
52.200	5.7	6	335.7	50.9	0.89
52.400	4.9	6	359.8	34.7	0.26
50.500	3.2	6	0.2	34.7	0.44
50.600	1.5	5	20.0	37.8	1.17
50.750	1.4	6	0.0	42.3	1.04
50.850	1.7	6	356.5	34.7	0.96
50.925	1.9	6	352.2	46.5	1.12
51.000	2.4	6	350.6	44.6	0.71

Table II.2 Demagnetisation characteristics of Jiuzhoutai loess and palaeosols

Depth (metres)	%NRM loss @ 100°C	temp of 50% NRM loss (°C)	temp of 90% NRM loss (°C)
Loess I			
46.800	25.6	170	415
46.900	32.1	160	510
47.000	24.6	150	500
47.100	13.2	230	500
47.250	27.7	160	480
47.350	27.2	180	500
47.500	33.0	150	470
47.600	34.3	150	380
47.750	29.3	180	495
47.825	22.2	190	530
47.900	23.4	200	490
Palaeosol I			
48.100	57.0	80	>550
48.200	64.2	80	410
48.300	73.2	75	370
48.400	72.9	60	400
48.600	82.2	50	280
48.700	67.1	85	350
48.800	61.3	80	430
49.000	61.1	80	440
49.100	69.8	70	310
49.200	72.4	70	360
49.300	70.0	75	330
Loess II			
49.500	60.7	80	550
49.600	54.8	80	435
49.700	46.6	220	440
49.775	30.1	170	420
49.950	25.7	180	>450
50.000	23.7	200	>450
50.100	22.8	180	440
50.250	28.8	180	410
50.350	28.4	175	340
50.425	28.6	170	460
50.550	34.0	150	430
50.600	10.9	210	460
50.700	14.7	210	450
50.800	21.5	190	440
50.900	26.4	180	460
Palaeosol II			
51.100	38.2	130	430
51.200	32.7	160	500
51.300	10.7	250	>550
51.400	19.5	215	510
51.500	31.8	150	515

(table II.2 continued)

depth (metres)	%NRM loss @ 100°C	temp of 50% NRM loss	temp of 90% NRM loss
Loess III			
51.600	17.8	210	520
51.700	24.5	190	>550
51.800	19.8	210	>550
51.900	17.0	185	450
52.000	25.6	180	375
52.100	27.6	180	>450
52.200	19.6	195	>450
52.300	14.0	210	>450
52.400	0.0	250	>450
52.500	11.4	370	380
52.600	0.3	260	>450
52.750	3.4	230	>450
52.850	3.7	240	>450
52.925	6.1	240	>450
51.000	0.0	250	>450

Table II.3 Palaeomagnetic directions and NRM intensities derived from thermal demagnetisation of loess and palaeosol samples from Dawan. The maximum angle of deviation (MAD) is quoted along with the number of vector points used to derived it (n).

Depth (metres)	MAD	n	dec°	inc°	NRM ($x10^{-6} Am^2kg^{-1}$)
20.000	14.5	5	20.8	42.0	0.389
20.300	14.1	4	59.2	78.3	0.209
20.400	3.6	5	23.7	51.0	0.634
20.500	5.1	7	28.6	58.5	0.824
20.600	14.8	7	3.3	36.6	0.332
20.700	14.2	5	0.7	33.0	0.378
20.800	8.8	5	327.3	45.5	0.304
20.900	6.3	7	11.3	31.6	0.564
21.000	8.6	7	351.7	17.6	0.583
21.200	22.3	7	7.5	11.7	0.403
21.300	15.7	5	23.2	18.9	0.300
21.400	14.5	7	46.1	14.9	0.389
21.500	4.6	8	20.8	40.3	0.601
21.600	4.8	8	27.3	11.3	0.480
21.700	9.5	8	16.6	34.9	0.395
21.800	4.6	8	32.9	36.4	0.552
21.900	4.2	8	31.7	29.1	0.684
22.000	3.1	8	344.8	53.3	0.996
22.100	2.2	8	341.9	40.0	1.381
22.300	3.4	8	26.3	57.0	0.836
22.400	4.6	6	2.6	60.1	0.668
22.600	3.4	8	18.9	44.7	0.752
22.700	7.4	3	350.2	56.3	0.480
22.800	12.8	5	335.1	58.0	0.707
22.900	9.0	5	4.4	36.6	0.514
23.000	2.9	6	3.0	49.2	1.610
23.100	3.5	6	16.3	56.0	1.025
23.200	10.2	6	4.3	39.7	0.433
23.300	12.8	5	39.1	43.2	0.487
23.400	18.1	6	16.2	48.9	0.337
23.500	6.9	5	5.5	42.9	0.635
23.600	5.6	4	13.6	34.0	0.484
23.700	12.2	5	23.1	4.8	0.381
23.800	5.8	5	16.6	43.3	1.078
24.000	27.3	5	8.3	63.7	0.497
24.100	9.6	4	1.0	67.1	0.598
24.200	11.8	5	8.8	39.4	0.792
24.300	8.7	5	14.3	47.7	1.225
24.400	2.8	5	355.7	52.1	0.901
24.500	3.6	5	7.7	53.5	0.781
24.600	2.1	5	15.8	55.2	0.773
24.700	4.4	5	27.3	65.2	1.067
25.000	3.1	5	3.5	59.0	0.979
25.100	2.2	5	8.9	52.1	1.147
25.300	4.6	5	352.9	50.0	1.506
25.400	3.6	5	354.5	50.1	0.919

Table II.3 continued...

Depth (metres)	MAD	n	dec°	inc°	NRM ($x10^{-6} Am^2kg^{-1}$)
25.500	4.9	5	12.2	46.9	0.892
25.600	4.4	5	15.2	62.3	0.965
25.700	6.0	5	0.1	58.4	0.865
25.800	7.1	5	357.0	53.1	0.447
25.900	4.2	5	15.3	56.9	0.450
26.000	4.4	6	0.1	65.4	0.504
26.100	5.3	6	16.5	51.2	0.435
26.200	4.7	6	29.0	55.2	0.380
26.300	6.2	6	2.9	47.2	0.563
26.400	2.2	6	349.1	65.9	0.479
26.500	6.3	6	357.7	54.5	0.421
26.600	4.6	6	22.7	49.4	0.401
26.700	6.7	6	0.4	40.5	0.408
26.800	3.1	6	351.5	46.7	0.552
26.900	4.7	4	349.2	55.1	0.483
27.000	6.1	6	351.5	46.7	0.471
27.100	4.1	6	2.9	52.6	1.371
27.200	5.7	6	5.6	47.4	1.441
27.300	1.8	6	14.3	52.1	1.828
27.500	7.9	4	29.2	52.0	1.780
27.600	3.0	4	337.9	59.3	1.863
27.700	3.6	4	2.0	46.8	1.436
27.800	2.8	4	355.5	51.6	1.441
27.900	3.0	4	4.2	46.8	1.623
28.000	2.5	4	3.5	43.7	1.607
28.200	4.2	4	359.8	43.6	0.910
28.300	3.7	4	344.2	49.0	0.639
28.400	3.2	4	0.1	60.0	0.498
28.500	6.7	4	6.8	67.3	0.472
28.600	6.6	4	357.5	69.2	0.576
28.700	6.8	4	359.7	52.9	0.524
28.800	7.4	4	13.1	55.1	0.582
28.900	1.8	5	12.1	60.2	0.735
29.000	10.2	4	8.6	52.4	0.689
29.100	6.7	4	13.6	43.9	0.722
29.300	6.2	5	8.7	63.1	0.550
29.500	12.3	5	20.2	47.8	0.709
29.600	23.4	5	46.2	55.8	0.757
29.700	14.6	5	17.3	54.0	0.757
29.800	9.9	5	17.9	54.0	0.805
29.900	12.5	5	341.5	60.6	2.011
30.100	16.0	5	355.5	67.4	3.089
30.200	3.8	5	353.2	55.1	1.466
30.300	11.4	5	10.8	65.6	2.394
30.400	1.8	5	10.6	63.6	2.186
30.600	9.5	5	13.5	48.9	0.377
30.800	5.5	5	8.3	56.2	0.438
30.900	8.9	6	16.3	83.5	0.544
31.000	3.3	6	16.0	63.4	0.718

Table II.3 continued...

Depth (metres)	MAD	n	dec°	inc°	NRM ($x10^{-6}Am^2kg^{-1}$)
31.100	5.2	6	321.5	69.8	0.771
31.200	7.5	4	28.9	51.1	0.322
31.300	7.1	7	343.8	53.3	0.561
31.400	3.9	7	12.7	45.8	0.627
31.500	5.0	7	11.4	44.6	0.979
31.600	5.3	7	2.2	60.3	0.839
31.700	3.5	6	31.8	65.0	0.990
31.800	2.3	7	11.9	63.5	0.874
31.900	3.4	7	357.6	55.4	1.087
32.000	5.3	4	26.6	43.8	0.436
32.100	6.0	5	17.2	42.7	0.487
32.200	10.6	6	26.9	27.6	0.325
32.400	6.5	7	20.5	33.2	0.428
32.500	3.7	7	27.9	43.8	0.652
32.600	4.2	6	43.1	21.6	0.595
32.800	3.2	7	13.6	39.5	0.903
32.900	6.1	5	32.5	32.2	0.781
33.000	4.4	7	22.5	51.6	1.201
33.100	6.8	5	350.0	53.3	0.853
33.200	8.8	7	18.4	10.6	0.597
33.300	5.9	5	0.6	36.2	0.853
33.500	25.7	6	354.4	21.8	0.267
33.600	11.3	5	6.7	45.6	0.352
33.700	8.9	5	17.4	44.3	0.470
33.800	9.4	5	6.4	21.9	0.320
33.900	4.4	7	358.1	12.9	2.164
34.000	9.1	7	3.1	26.3	1.295
34.100	12.0	7	42.2	4.2	1.001
34.200	13.2	7	0.6	8.8	1.359
34.300	11.1	7	0.1	32.9	1.452
34.400	8.9	7	11.9	39.7	1.530
34.500	5.5	7	32.9	42.6	1.369
34.700	11.9	7	325.5	25.2	0.662
34.800	7.7	6	8.1	41.0	0.904
34.900	9.5	7	12.3	30.9	0.851
35.000	8.2	7	44.9	49.9	0.746
35.100	8.6	7	1.8	42.4	1.454
35.200	7.3	7	4.4	24.3	3.058
35.275	10.2	6	46.1	43.2	3.008

Table II.4 Demagnetisation characteristics of Dawan loess and palaeosols

Depth (metres)	%NRM loss @ 100°C	temp of 50% NRM loss (°C)	temp. of 90% NRM loss (°C)
Loess I			
20.000	36.2	210	>450
20.300	45.9	150	375
20.400	26.6	210	350
20.500	21.6	230	425
20.600	50.3	200	500
20.700	45.5	210	330
20.800	47.7	120	280
20.900	28.0	270	500
21.000	20.4	360	>550
21.100	25.3	250	>550
21.200	34.5	225	>550
21.300	50.0	100	540
21.400	33.4	250	>550
21.500	54.6	80	525
21.600	49.3	260	525
21.700	71.6	70	500
21.800	57.2	80	525
21.900	57.3	80	425
22.000	55.9	70	550
22.100	53.0	90	490
22.300	50.7	100	450
22.400	64.1	70	325
22.600	60.2	80	340
22.700	77.9	75	325
22.800	64.5	75	325
22.900	45.3	110	355
23.000	19.7	220	>450
23.100	25.4	190	>450
23.200	48.0	105	310
23.300	44.6	115	>450
23.400	34.2	120	>450
23.500	34.1	170	410
23.600	48.2	105	380
23.700	50.8	100	325
23.800	33.3	200	410
24.000	64.7	80	>400
24.100	57.9	80	360
24.200	61.3	85	330
24.300	50.7	100	360
24.400	29.8	190	370
24.500	20.5	190	405
24.600	27.2	170	375
24.700	31.6	150	420
24.800	18.4	220	>450
24.900	31.4	180	>400

Table II.4 continued.

Depth (metres)	%NRM loss @ 100°C	temp of 50% NRM loss (°C)	temp. of 90% NRM loss (°C)
Palaeosol I			
25.000	41.4	240	310
25.100	44.0	120	290
25.300	48.9	110	280
25.400	40.5	150	420
Loess II			
25.500	29.6	190	>400
25.600	31.7	160	420
25.700	43.7	115	460
25.800	54.2	80	405
25.900	44.0	170	410
26.000	35.2	150	455
26.100	22.8	200	>450
26.200	28.7	190	>450
26.300	23.3	210	>450
26.400	28.4	190	365
26.500	34.3	150	370
26.600	31.2	185	350
26.700	28.0	180	375
26.800	28.7	195	395
26.900	43.7	130	330
27.000	44.0	170	480
Palaeosol II			
27.100	43.7	180	440
27.200	41.7	120	390
27.300	48.0	110	340
27.500	44.9	115	210
27.600	68.1	60	250
27.700	70.4	40	250
27.800	76.0	35	190
27.900	64.3	60	270
28.000	70.0	55	220
Loess III			
28.200	63.3	80	280
28.300	45.3	115	410
28.400	50.3	100	290
28.500	47.5	110	350
28.600	46.9	120	370
28.700	52.0	95	350
28.800	61.4	90	280
28.900	57.2	90	295
29.000	70.7	60	325
29.100	78.1	50	300
29.200	74.2	55	350
29.300	69.9	60	330
29.500	76.2	55	305
29.600	80.4	40	280
29.700	78.9	40	280
29.800	88.9	30	110

Table II.4 continued.

Depth (metres)	%NRM loss @ 100°C	temp of 50% NRM loss (°C)	temp. of 90% NRM loss (°C)
Palaeosol III			
29.900	82.2	35	220
30.100	82.0	35	140
30.200	76.0	40	200
30.300	57.0	80	280
30.400	62.1	70	440
Loess IV			
30.500	39.9	130	450
30.600	27.6	210	>450
30.800	53.9	95	320
30.900	41.6	120	>450
31.000	35.5	160	>450
31.100	44.0	180	>450
31.200	26.1	250	>450
31.300	31.1	170	530
31.400	16.3	230	470
31.500	11.9	220	570
31.600	11.8	220	490
31.700	17.2	230	570
31.800	19.5	230	540
31.900	20.1	230	540
32.000	6.5	250	430
32.100	43.6	130	300
32.200	25.0	150	430
32.400	5.5	250	550
32.500	3.1	250	515
32.600	13.5	240	490
Palaeosol IV			
32.800	4.9	240	510
32.900	38.3	130	320
33.000	35.0	140	490
33.100	46.7	120	345
33.200	29.7	180	520
33.300	34.2	170	400
Loess V			
33.500	27.0	180	>550
33.600	25.3	170	>500
33.700	32.8	170	400
Palaeosol V			
33.800	23.5	170	375
33.900	33.5	140	330
34.000	62.1	80	345
34.100	62.4	75	450
34.200	67.6	70	340
34.300	64.1	75	330
34.400	61.0	80	340
34.500	42.9	140	425
34.700	50.2	100	380
34.800	45.3	120	410

Table II.4 continued.

Depth (metres)	%NRM loss @ 100°C	temp of 50% NRM loss (°C)	temp. of 90% NRM loss (°C)
Loess VI			
34.900	50.5	100	475
35.000	53.0	95	360
35.100	47.4	110	470
Palaeosol VI			
35.200	65.4	75	310
35.275	61.5	80	345

Table II.5 Demagnetisation characteristics of Labrang loess

Depth (metres)	%NRM loss @ 100°C	temp of 50% NRM loss (°C)	temp. of 90% NRM loss (°C)
Labrang B			
LB0.000	22.5	200	>350
LB0.025	27.3	200	340
LB0.050	27.2	205	>350
LB0.075	32.2	160	>350
Labrang A			
LA0.000	16.9	220	>350
LA0.025	23.0	190	340
LA0.050	16.5	225	>350
LA0.075	17.2	225	>350
LA0.100	13.5	230	>350

11. REFERENCES

An Zhisheng, Wu Xihao, Wang Pinxian, Wang Shuming, Dong Guangrong, Sun Xiangjun, Zhang De'er, Lu Yanchou, Zheng Shaohua and Zhao Shonglin (1991) 'Changes in the monsoon and associated environmental changes in China since the last interglacial'. In: Liu Tungsheng (ed) Loess, Environmental and Global Change, Science Press, Beijing. p. 1-29.

Argyle, K.S. and Dunlop, D.J. (1984) 'Theoretical domain structure in multidomain magnetite particles'. Geophys. Res. Lett., 11 (3), p. 185-188.

Argyle, K.S. and Dunlop, D.J. (1990) 'Low-temperature and high-temperature hysteresis of small multidomain magnetites (215-540nm)'. J. Geophys. Res., 95, p. 7069-7083.

Barton, C.E., McElhinny, M.W. and Edwards, D.J. (1980) 'Laboratory studies of depositional DRM'. Geophys. J.R. astr. Soc., 61, p. 355-377.

Boulton, G.S. (1978) 'Boulder shapes and grain size distribution of debris as indicators of transport paths througha glacier and till genesis'. Sedimentology, 25, p. 773-799.

Bowler, J.M., Chen Kezao and Yuan Baoyin (1987) 'Systematic variation in loess source areas: evidence from Qaidam and Qinghai Basins, western China'. In: Liu Tungsheng (ed) Aspects of loess research. China Ocean Press, Beijing. P. 39-51.

Bowler, J.M., Huang Qi, Chen Kezao, Head, J.M. and Yuan Baoyin (1986) 'Radiocarbon dating of playa-lake hydrological changes: examples from Northwestern China and Central Australia'. Palaeogeog., Palaeoclim., Palaeoeco., 54, p. 241-260.

Bradley, R.S. (1985) Quaternary paleoclimatology: methods of paleoclimatic reconstruction. Allen and Unwin, Boston, pp. 472.

Bradley, W.C., Hutton, J.T. and Twidale, C.R. (1978) 'Rôle of salts in the development of granitic taffoni, South Australia'. J.Geol., 86, p. 647-654.

Bull, P.A., Whalley, W.B. and Magee, A.W. (1986) 'An annotated bibliography of environmental reconstruction by SEM 1962-1985'. British Geomorphological Research Group, Technical Bulletin No. 35, 94pp.

Burbank, D.W. and Cheng Jiangcheng (1991) Relative dating of Quaternary moraines, Rongbuk Valley, Mt. Everest, Tibet: Implications for an ice sheet on the Tibetan Plateau'. Quaternary Research, 36, p. 1-18.

Burbank, D.W. and Li Jijun (1985) 'Age and palaeoclimatic significance of the loess of Lanzhou, North China'. Nature, 316, p. 429-431.

Chao Sungchiao (1984) 'The sandy deserts and the Gobi of China'. In: Farouk el-Baz (ed) Deserts and Arid Lands. Martinus Nijhoff, p. 95-113.

Chao Sungchiao and Xing, Jiaming (1982) 'Origin and development of the Shamo (sandy deserts) and the Gobi (stony deserts) of China'. Striae, 17, p.79-91.

Chen Fahu (1990) The studies of loess records and glacial cycles in the contiguous region between the Qinghai-Xizang Plateau and the Loess Plateau. PhD thesis, Lanzhou University, 173pp. [in Chinese]

Chen Fahu, Li Jijun and Zhang Weixin (1991) 'Loess stratigraphy of the Lanzhou profile and its comparison with deep-sea sediment and ice core record'. Geojournal, 24, p.201-209.

Chen Hongchen, Jahn Borming, Lee, T. Chen Chaohsia and Cornichet, J. (1990) 'Sm-Nd isotopic geochemistry of sediments from Taiwan and implications for the tectonic evolution of southeast China'. Chemical Geology, 88, p.317-332.

Chen Kezao and J.M. Bowler (1986) 'Late Pleistocene evolution of salt lakes in the Qaidam Basin, Qinghai Province, China'. Palaeogeog. Palaeoclim. Palaeoeco., 54, p. 87-104.

Chen Kezao, Zheng Xiyu and Yang Shaoxiu (1981) 'Salt lakes on the Qinghai-Xizang plateau'. Acta Geographica Sinica, 36, p.13-21. [English abstract]

Clark, D.A. (1984) 'Hysteresis properties of sized dispersed monoclinic pyrrhotite grains'. Geophys. Res. Lett., 11, 3, p.173-176.

Collinson, D.W. (1983) Methods in rock magnetism and palaeomagnetism. Chapman and Hall, London. 500pp

Cooke, R.U. (1979) 'Laboratory simulation of salt weathering processes in arid environments'. ESPL, 4, p.347-359.

Creer, K.M., Readman, P.W. and Jacobs, A.M. (1980) 'Palaeomagnetic and palaeoentological dating of a section at Gioia Tauro, Italy: Identification of the Blake Event'. Earth Plan. Sci. Lett., 50, p.289-300.

Dankers, P. (1981) 'Relationship between median destructive field and remanent coercive forces for dispersed natural magnetite, titanomagnetite and hematite'. Geophys. J. R. astr. Soc., 64, p.447-461.

De Menocal, P.B., Laine, E.P. and Ciesielski, P.F. (1988) 'A magnetic signature of bottom current erosion'. Phys. Earth Plan. Int., 51, p.326-348.

Dearing, J.A., Maher, B.A. and Oldfield, F. (1985) 'Geomorphological linkages between soils and sediments: the role of magnetic measurements'. In: Richards, K.S. (ed) Geomorphology and Soils. Allen and Unwin. London. p.245-266.

Debenham, N.C. (1985) 'Use of U.V. emissions in TL dating of sediments'. Nuclear Tracks, 10, p.717-724.

Dekkers, M.J. (1989) 'Magnetic properties of natural goethite - I. Grain-size dependence of some low- and high-field related rockmagnetic parameters measured at room temperature'. Geophys. J., 97, p.323-340.

Dekkers, M.J. (1990) 'Magnetic monitoring of pyrrhotite alteration during thermal demagnetisation'. Geophys. Res. Lett., 17 (6), p.779-782.

Dekkers, M.J. and Linssen, J.H. (1989) Rockmagnetic properties of fine-grained natural low-temperature haematite with reference to remanence acquisition mechanisms in red beds'. Geophys. J. Int., 99, p.1-18.

Dekkers, M.J., Mattéi, J.-L., Fillion, G. and Rochette, P. (1989) 'Grain-size dependence of the magnetic behaviour of pyrrhotite during its low-temperature transition at 34K'. Geophys. Res. Lett., 16, p.855-858. pyrrhotite

Denham, C.R. (1976) 'Blake polarity episode in two cores from the Greater Antilles Outer Ridge', Earth Plan. Sci. Lett., 29, p.422-434.

Denham, C.R., Anderson, R.F. and Bacon, M.P. (1977) 'Palaeomagnetic and radiochemical age estimates for the Brunhes Polarity episodes'. Earth Plan. Sci. Lett., 35, p.384 - 397.

Derbyshire, E. (1983) 'On the morphology, sediments and origin of the loess in central China'. In: Gardener, R. and Scoging, H. (eds) Megageomorphology. C.U.P., London. p.172-194.

Derbyshire, E. (1984) 'Granulometry and fabric of the loess at Jiuzhoutai, Lanzhou, Peoples Republic of China'. In: Pecsi, M. (ed) Lithology and stratigraphy of loess and palaeosols, Hungarian Acad. Sci., Budapest. p.95-104.

Derbyshire, E. (1987) 'A history of glacial stratigraphy in China'. Quat. Sci. Rev., 6. p.301-314.

Derbyshire, E. (1988) 'Granulometry and fabric of Quaternary silts from Eastern Asia'. In: The Palaeoenvironment of East Asia from the Mid-Tertiary, Proc. 2nd Conf., Vol.1., p. 36-48.

Derbyshire, E., Billard, A., Van Vliet-Lanoë, B., Lautridou, J.-P. and Cremaschi, M. (1988) 'Loess and palaeoenvironment: some results of a European joint programme of research'. J. Quat. Sci., 3, p.147-169.

Derbyshire, E., Shi Yafeng, Li Jijun, Zheng Benxing, Li Shijie and Wang Jingtai (1991b) 'Quaternary glaciation of Tibet: the geological evidence'. Quaternary Science Reviews, p.485-510.

Derbyshire, E., Wang Jingtai, Jin Zexian, Billard, A., Egels, Y., Kasser, M., Jones, D.K.C., Muxart, T. and Owen, L. (1991a) 'Landslides in the Gansu loess of China'. Catena Suppl., 20, p. 119-145.

Derbyshire, E., Wang Jingtai, Shaw, J. and Rolph, T. (1987) 'Interim results of studies of the sedimentology and remanent magnetization of the loess succession at Jiuzhoutai, Lanzhou, China'. In: Liu Tungsheng (ed) Aspects of Loess Research, China Ocean Press, Beijing. p 175-191

Dunlop, D.J. (1970) 'Hematite: instrinsic and defect ferromagnetism'. Science, 169, p.858-860.

Dunlop, D.J. (1973) 'Superparamagnetic and single domain threshold sizes in magnetite'. J. Geophys. Res., 78, p.7602-7613.

Dunlop, D.J. (1987) 'Temperature dependence of hysteresis in 0.04-0.22μm magnetites and implications for domain structure'. Phys. Earth Plan. Int., 46, p. 100-119.

Ellwood, B.B., Hrouda, F. and Wagner, J.-J. (1988) 'Symposia on magnetic fabrics: introductory comments'. Phys. Earth Plan. Int., 51, p. 249-252.

Fisher, R.A. (1953) 'Dispersion on a sphere'. Proc. R. Soc. Lond., 217A, p. 295-305.

Fort, M. (1989) 'The Gongba conglomerates: glacial or tectonic ?'. Z. Geomorph. N.F. Suppl. 76, p. 181-194.

Fullard, H. and Darby, H.C. (1978) The University Atlas. George Philip and Son Ltd, London.

Goudie, A.S. (1974) 'Further experimental investigation of rock weathering by salt and other mechanical weathering processes'. Z. Geomorph. N.F. Suppl. 21, p. 1-12.

Goudie, A.S. (1983) 'Dust storms in space and time'. Prog. Phys. Geog., 7, p. 502-530.

Goudie, A.S., Cooke, R.U. and Doornkamp, J.C. (1979) 'The formation of silt from salt dune sand by salt weathering processes in deserts'. J. Arid Env., 2, p. 105-112.

Griffiths, D.H., King, R.F., Rees, A.I. and Wright, A.E. (1960) 'The remanent magnetisation of some recent varved sediments'. Proc. R. Soc. London, A256, p.359-383.

Gromet, L.P., Dymek, R.F., Haskin, L.A. and Korotev, P.L. (1984) 'The "North American Shale Composite": its compilation, major and trace element characteristics'. Geochim. Cosmochim. Acta, 48, p.2469-2482.

Grommé, C.S., Wright, T.L. and Peck, D.L. (1969) 'Magnetic properties of iron-titanium oxide minerals in Alae and Makaopuhi Lava Lakes, Hawaii'. J.Geophys. Res., 74 (22), p.5277-5293.

Halgedahl, S.L. (1987) 'Domain pattern observations in rock magnetism: progress and problems'. Phys. Earth. Plan. Int., 46, p.127-163.

Hamilton, N. and Rees, A.I. (1970) 'The use of magnetic fabric in palaeocurrent estimation'. In: Runcorn, S.K. (ed) Palaeogeophysics. Academic Press, London. p.445-464.

Hartstra, R.L. (1982) 'Grain-size dependence of initial susceptibility and saturation magnetisation-related parameters of four natural magnetites in the PSD-MD range'. Geophys. J.R. astr. Soc., 71, p. 477-495.

Haskin, M.A. and Haskin, L.A. (1966) 'Rare earths in European shales: a redetermination'. Science, 154, p.507-509.

Heider, F., Dunlop, D. and Sugiura, N. (1987) 'Magnetic properties of hydrothermally recrystallised magnetite crystals'. Science, 236, p.1287-1290.

Heller, F. and Liu Tungsheng (1982) 'Magnetostratigraphical dating of loess deposits in China'. Nature, 300, p.431-435.

Heller, F. and Liu Tungsheng (1984) 'Magnetism of Chinese loess deposits'. Geophys. J. R. astr. Soc., 77, p.125-141.

Heller, F. and Liu Tungsheng (1986) 'Palaeoclimatic and sedimentary history from magnetic susceptibility of loess in China'. Geophys. Res. Lett., 13, no.11, p.1169-1172.

Hodych, J.P. (1986) 'Evidence for the magnetostrictive control of intrinsic susceptibility and coercive force of multidomain magnetite in rocks'. PEPI, 42, p.184-194.

Hovan, S.A., Rea. D.K. and Shackleton, N.J. (1989) 'A direct link between the China loess and marine $\delta^{18}O$ records: aeolian flux to the north Pacific'. Nature, 340, p.296-298.

Hövermann, J. (1987) 'Morphogenetic regions of the northeast Xizang (Tibet)'. In: Hövermann, J. and Wang Wenying (eds) Reports on the northeastern part of the Qinghai-Xizang (Tibet) Plateau, Science Press, Beijing. p. 112-139.

Howell, D.G. (1989) Tectonics of suspect terranes - mountain building and continental growth. Chapman & Hall, London. p. 167-173.

Hrouda, F. (1982) 'Magnetic anisotropy of rocks and its application in geology and geophysics'. Geophysical Surveys, 5, p. 37-82.

Ising, G. (1943) 'On the magnetic properties of varved clay'., Arvik. f. Matematik, Ast. Fysik, 29A, p.1-37.

Jackson, M., Sprowl, D. and Ellwood, B. (1989) 'Anisotropies of partial anhysteretic remanence and susceptibility in compacted black shales: grainsize- and composition-dependent magnetic fabric'. Geophys. Res. Lett., 16 (9), p.1063-1066.

Jacobs, J.A. (1984) Reversals of the Earth's magnetic field. Adam Hilger Ltd., Bristol, pp. 218.

Jolly, W.L. (1984) Modern inorganic chemistry. McGraw Hill. Singapore. pp.610.

Jouzel, J., Petit, J.R. and Raynaud, D. (1990) 'Palaeoclimatic information from ice cores: the Vostok records'. Trans. Roy. Soc. Edin., Earth Sci., 81, p.349-356.

Kashiwaya, K., Yaskawa, K., Yuan Baoyin, Liu Jiaqi, Gu Zhaoyan, Cong Shaoquang and Toshiyuki, M. (1991) 'Paleohydrological processes in Siling-Co (lake) in the Qing-Zang (Tibetan) Plateau based on the physical properties of its bottom sediments'. Geophys. Res. Lett., 18, p.1779-1781.

King, J.A. (1990) Magnetic remanence and petrology of some loessic and lacustrine sediments from central China, unpub. PhD thesis. Liverpool University. pp.181.

King, J., Banerjee, S.K., Marvin, J. and Özdemir, Ö. (1982) 'A comparison of different magnetic methods for determining the relative grain size of magnetite in natural minerals: some results from lake sediments'. EPSL, 59, p.404-419.

King, R.F. (1955) 'The remanent magnetisation of artificially deposited sediments'. Mon. Not. R. Astr. Soc. Soc. Geophys. Suppl., 7, p.115-134.

King, R.F. and Rees, A.I. (1962) 'The measurement of anisotropy of magnetic susceptibility of rocks by the torque method'. J. Geophys. Res., 67, p.1565-1572.

King, R.F. and Rees, A.I. (1966) 'Detrital magnetism in sediments: an examination of some theoretical models'. J. Geophys. Res., 71 (2), p.561-571.

Kirschvink, J.L. (1980) 'The least squares line and plane and the analysis of palaeomagnetic data'. Geophys. J. R. astr. Soc., 62, p.699-718.

Konischev, V.N. (1987) 'Origin of loess-like silt in Northern Jakutia, USSR'. Geojournal, 15, p. 135-139.

Krinsley, D.H. and Doornkamp, J.C. (1973) Atlas of quartz sand surface textures. Cambridge University Press, 91pp.

Kuhle, M. (1986) 'The upper limit of glaciation in the Himalayas'. GeoJournal 13 (4), p.331-346.

Kuhle, M. (1987a) 'The problem of Pleistocene inland glaciation of the northeastern Qinghai-Xizang Plateau'. in: Hövermann and Wang Wenying, *op. cit.*, p.250-315.

Kuhle, M. (1987b) 'Subtropical mountain- and highland- glaciation as ice age triggers and the waning of the glacial periods in the Pleistocene'. GeoJournal, 13 (6), p. 1-29.

Kuhle, M. (1988) 'Geomorphological findings on the build-up of Pleistocene glaciation in southern Tibet and on the problem of inland ice - results of the Shisha Pangma and Mt. Everest Expedition 1984'. GeoJournal, 17 (4), p.457-511.

Kuhle, M. (1989) 'On the ice age glaciation of the Tibetan Highlands and its transformation into a 3-D model'. GeoJournal, 19 (2), p. 201-206.

Kuhle, M. (1990a) 'The probability of proof in geomorphology - an example of the application of information theory to a new kind of glaciagenic morphological type, the ice marginal ramp (Bortensander)'. Geojournal, 21 (3), p. 195-222.

Kuhle, M. (1990b) Ice marginal ramps and alluvial fans in semi-arid mountains: convergence and difference'. In: Rachocki, A. & Church, M. A. (eds) Alluvial fans - a field approach. Wiley & Sons, Chichester.

Kukla, G. (1988) 'The mystery of the Chinese Magnetic dust'. Lamont Doherty Geological Observations, Columbia University, p. 32-37.

Kukla, G. and An Zhisheng (1989) 'Loess stratigraphy in central China'. Palaeogeog, Palaeoclimatol, Palaeoecol., 72, p. 203-225.

Kukla, G., An Zhisheng, Melice, J.L., Gavin, J. and Xiao Jule (1990) 'Magnetic susceptibilty record of Chinese Loess'. Trans. R. Soc. Edin., 81, p. 263-288.

Kukla, G. and Briskin, M. (1983) 'The age of the 4/5 isotopic stage boundary on land and in the oceans'. Palaeogeog., Palaeoclim., Palaeoeco., 42, p. 35-45.

Kukla, G., Heller, F., Liu Xiuming, Xu Tonchun, Liu Tungsheng and An Zhisheng (1988) 'Pleistocene climates in China dated by magnetic susceptibility'. Geology, 16, p. 811-814.

Levi, S. and Banerjee, S.K. (1990) 'On the origin of inclination shallowing in redeposited sediments'. J. Geophys. Res., 95, B4, p. 3690-3698.

Li Baosheng, Dong Guangrong, Shao Yajun, Sheng Jianyou, Gao Shangyu and Din Tonghu (1988) 'Preliminary observation and research on the loess in the northern piedmont of the Kunlun Mounatins south of Pulu, Xinjiang'. Geological Review, 35, no. 5, p. 84-92. [in Chinese]

Li Jijun, Zhou Shangzhe and Pan Baotian (1991) 'Studies on Quaternary glaciation in the eastern part of the Qinghai-Xizang Plateau'. Abstracts, XIII INQUA Congress, Beijing. p. 195.

Liu Tungsheng and Ding Menglin (1985) 'Pleistocene stratigraphy and Plio/Pleistocene boundary in China'. In: Liu Tungsheng (ed) Quaternary geology and environment of China. Quaternary Research Association of China, China Ocean Press, Beijing, p. 1-9.

Liu Tungsheng, Gu Xiongfei, An Zhisheng and Fan Yongxiang (1981) 'The dust fall in Beijing, China on April 18, 1980. Geol. Soc. Am. Sp. Paper, 186, p. 159-167.

Liu Tungsheng et. al. (1985) Loess and the Environment. China Ocean Press. Beijing. 301pp.

Liu Xiuming, Liu Tungsheng, Heller, F. and Xu Tongchun (1990) 'Frequency dependent susceptibility of loess and Quaternary palaeoclimate'. Quaternary Sciences, 3, (1), p. 42-50 [English abstract]

Liu Xiuming, Liu Tungsheng, Xu Tongchun, Li Chun and Chen Mingyang (1987) 'A preliminary study on magnetostratigraphy of a loess profile in Xifeng area, Gansu Province'. In: Liu Tungsheng (ed) Aspects of loess research. China Ocean Press, Beijing. p. 164-174.

Liu Xiuming, Liu Tungsheng, Xu Tongchun, Liu Chun and Chen Mingyang (1988a) 'The Chinese loess in Xifeng, I. The primary study of magnetostratigraphy of a loess profile in Xifeng area, Gansu province'. Geophys. J., 92, p. 345-348.

Liu Xiuming, Xu Tongchun and Liu Tungsheng (1988b) 'The Chinese loess in Xifeng II. A study of anisotropy of magnetic susceptibility of loess from Xifeng'. Geophys. J., 92, p. 349-353.

Liu Xiuming, Shaw, J., Liu Tungsheng, Heller, F. and Yuan Baoyin (1992) 'Magnetic mineralogy of Chinese loess and its significance'. Geophys. J. Int., 108, p. 301-308.

Liu Zechun, Sun Siying, Li Xuesong, Wang Yongjin, Li Qingchen and Chen Yanan (1991) 'Stratigraphic and geochronological analyses of the Quaternary deposits in the middle part of Qaidam Basin, western China'. In: Liu Tungsheng (ed) Loess, Environmental and Global Change, Science Press, Beijing. p. 358-370.

Løvlie, R., Lowrie, W. and Jacobs, M. (1971) 'Magnetic properties and mineralogy of four deep-sea cores'. EPSL, 15, p. 157-168.

Maher, B. (1988) 'Magnetic properties of some synthetic sub-micron magnetites'. Geophys. J., 94, p. 83-96.

Maher, B. A. and Taylor, R. M. (1988) 'Formation of ultrafine-grained magnetite in soils'. Nature, 336, p. 368-370.

Maher, B. A. and Thompson, R. (1991) 'Mineral magnetic record of the Chinese loess and palaeosols'. Geology, 19, p. 3-6.

Manabe, K. I. (1977) 'Reversed magneto-zone in the Late Pleistocene sediments from the Pacific coast of Odaka, northeast Japan'. Quaternary Research, 7, p. 372 - 379.

Matalucci, R. V., Shelton, J. W. and Abdel-Hardy, M. (1969) 'Grain orientation in Vicksberg loess'. J. Sed. Petr., 39 (3), p. 969-979.

McGown, A. and Derbyshire, E. (1974) 'Technical developments in the study of particulate matter in glacial tills'. J. Geol., 83, p. 225-235.

McGreevy, J. P. (1982) 'Frost and salt weathering: further experimental results'. ESPL, 7, p. 475-488.

McGreevy, J.P. and Smith, B.J. (1982) 'Salt weathering in hot deserts: observations on the design of simulation experiments'. Geog. Ann., 64A, p. 161-170.

McKenna, L.W. and Walker, J.D. (1990) 'Geochemistry of crustally derived leucocratic igneous rocks from the Ulugh Muztagh area, northern Tibet and their implications for the formation of the Tibetan Plateau'. J. Geophys. Res., 95, B13, p.21483-21502.

Middleton, J., Goudie, A.S. and Wells, S.G. (1986) 'The frequency and source area of dust storms'. Aeolian Geomorphology. Allen and Unwin, New York, p.237-289.

Minervin, A.V. (1974) 'Cryogenic processes in loess formation in Central Asia'. In: Velichko, A.A. (ed) Late Quaternary Environments of the Soviet Union, Longman, London, p.133-140.

Molnar, P. (1986) 'The geologic history and structure of the Himalaya'. American Scientist, 74, p.144-154.

Moskowitz, B.M., Frankel, R.B., Bazylinski, D.A., Jannasch, H.W. and Lovley, D.R. (1989) 'A comparison of magnetite particles produced anaerobically by magnetotactic and dissimmilatory iron-reducing bacteria'. Geophys. Res. Lett., 16 (7), p. 665-668.

Moss, A.J. and Green, P. (1975) 'Sand and silt grains: predetermination of their formation and properties by microfractures in quartz'. J. Geol. Soc. Austr., 22 (4), p.485-495.

Mullins, C.E. (1977) 'Magnetic susceptibility of the soil and its significance in soil science - a review'. J. Soil. Sci., 28, p.223-246.

Nahon, D. and Trompette, R. (1982) 'Origin of siltstones: glacial grinding vs. weathering'. Sedimentology, 29, p.25-35.

Nakamura, N. (1974) 'Determination of REE, Ba, Fe, Mg, Na and K in carbonaceous and ordinary chondrites'. Geochim. Cosmochim. Acta, 38, p.757-775.

Nance, W.B. and Taylor, S.R. (1976) 'Rare earth element patterns and crustal evolution - I. Australian post-Archean sedimentary rocks'. Geochim. Cosmochim. Acta., 40, p.1539-1551.

Nöel, M. (1983) 'The magnetic remanence and anisotropy of susceptibility of cave sediments from Agen Allwedd, South Wales'. Geophys. J. R. astr. Soc., 72, p. 557-570.

Nöel, M. (1986) 'The palaeomagnetism and magnetic fabric analysis of sediments from Peak Cavern, Derbyshire'. Geophys. J.R. astr. Soc, 84, p.445-454.

O'Reilly, W. (1984) Rock and Mineral Magnetism. Blackie, Glasgow. pp220.

Osmaston, H.A. (1989) 'Problems of Quaternary geomorphology of the Xixabangma region in South Tibet and Nepal'. Z. Geomorph. N.F. Suppl. 76., p.147-180.

Özdemir, Ö and Banerjee, S.K. (1982) 'A preliminary magnetic study of soils samples from west-central Minnesota'. EPSL, 59, p.393-403.

Özdemir, Ö and Banerjee, S.K. (1984) 'High temperature stability of maghemite (γ-Fe_2O_3)'. Geophys. Res. Lett., 11, no.3, p.161-164.

Péwé, T.L., Liu Tungsheng and Slatt, R.M. (1987) 'Retransported loess in the southern part of the Qinghai-Xizang (Tibet) Plateau, China'. In: Liu Tungsheng (ed) Aspects of loess research, China Ocean Press, Beijing. p.70-75.

Péwé, T.L., Liu Tungsheng, Slatt, R.M. and Li Bingyuan (in press) 'Origin and character of loesslike silt in the southern Qinghai-Xizang (Tibet) Plateau, China'. U.S.G.S. Prof Paper.

Piper, D.Z. (1974) 'Rare earth elements in the sedimentary cycle: a summary'. Chemical Geology, 14, p.285-304.

Potter, D.K. and Stephenson, A. (1988) 'Single-domain particles in rocks and magnetic fabric analysis'. Geophys. Res. Lett., 15 (10), p.1097-1100.

Prebble, M.M. (1967) Cavernous weathering in the Taylor Dry Valley, Victoria Land, Antarctica'. Nature, 216, p.1194-1195.

Pullaiah, G.E., Irving, E., Buchan, K.L. and Dunlop, D.J. (1975) 'Magnetisation changes caused by burial and uplift'. Earth Plan. Sci. Lett., 28, p. 133-143.

Pye, K. (1983) 'Formation of quartz silt during humid tropical weathering of dune sands'. Sedim. Geol., 34, p.267-282.

Pye, K. (1987) Aeolian dust and dust deposits. Academic Press, London. pp.334.

Pye, K. and Sperling, C.H.B (1983) 'Experimental investigation of silt formation by dry static breakage processes: the effect of temperature, moisture and salt on quartz dune sand and granitic regolith'. Sedimentology, 30, p.49-62.

Pye, K. and Tsoar, H. (1987) The mechanics and geological implications of dust transport and deposition in deserts with particular reference to loess formation and sand dune diagenesis in the northern Negev, Israel'. In: Frostick, L. and Reid, I. (eds) Desert sediments: ancient and modern. Geol. Soc. Spec. Pub., 35, p.139-156.

Pye, K. and Zhou Liping (1989) 'Late Pleistocene and Holocene aeolian dust deposition in North China and the Northwest Pacific Ocean', Palaeogeog. Palaeoclim. Palaeoeco., 73, p.11-23.

Radhakrishnamurty, C., Likhite, S.D., and Sahasrabudhe, W. (1977) 'Nature of magnetic grains and their effect on the remanent magnetisation of basalts'. Phys. Earth Plan. Int., 13, p. 289-300.

Rankama, K. and Sahama, Th. G. (1950) Geochemistry. University of Chicago Press. Chicago. pp803.

Riezebos, P.A. and Van de Waals, L. (1974) 'Silt-sized quartz particles: a proposed source'. Sed. Geol., 12, p.279-285.

Rochette, P. and Fillion, G. (1989) 'Field and temperature behaviour of remanence in synthetic goethite: paleomagnetic implications'. Geophys. Res. Lett., 16, (8), p. 851-854.

Rolph, T.C., Shaw, J., Derbyshire, E. and Wang Jingtai (1989). 'A detailed geomagnetic record from Chinese loess'. Phys. Earth. Plan. Int. 56, p.151-164.

Rutter, N., Ding Zhingli, Evans, M.E. and Liu Tungsheng (1991) 'Baoji-type pedostratigraphic section, Loess Plateau, north-central China'. Quat. Sci. Rev., 10, p.1-22.

Sasajima, S., Nishimura, S. and Hirooka, K. (1984) 'The Blake geomagnetic Event as inferred from Late Brunhes ignimbrites in southwest Japan and west Indonesia'. J. Geomag. Geoelectr., 36, p.203-214.

Schreiber, J. and Ellwood, B.B. (1988) 'The coincidence between microscopic paleocurrent indicators and magnetic lineation in shales from the Precambrian Belt Basin'. J.Sed. Petr., 58, p.830-835.

Senanayake, W.E. and McElhinny, M.W. (1981) 'Hysteresis and susceptibilty characteristics of magnetite and titanomagnetites: interpretation of results from basaltic rocks'. Phys. Earth Plan. Int., 26, p.47-55.

Senanayake, W.E. and McElhinny, M.W. (1982) 'The effects of heating on low temperature susceptibility and hysteresis properties of basalts'. Phys. Earth Plan. Int., 30, p.317-321.

Shackleton, N.J., Berger, A. and Peltier, W.A. (1990) 'An alternative astronomical calibration of the lower Pleistocene timescale based on ODP site 677'. Trans. Roy. Soc. Edin., Earth Sci., 81, p.250-261.

Shackleton, N.J. and Opdyke, N.D. (1973) 'Oxygen isotope and palaeomagnetic stratigraphy of equatorial Pacific core V28-238: oxygen isotope temperatures and ice volumes on a 10^5 and 10^6 year scale'. Quaternary Research, 3, p.39-55.

Sherwood, G.J. (1988) 'Rock magnetic studies of Miocene volcanics in eastern Otago and Banks Peninsula, New Zealand: comparison between Curie temperature and low temperature susceptibility behaviour'. N.Z. Jour. Geol. Geophys., 31, p.225-235.

Shi Yafeng, Li Binyuan and Li Jijun (1991) Quaternary glacial distribution map of Qinghai-Xizang (Tibet) Plateau. Science Press, Beijing. 10pp and map at 1:3M scale.

Smalley, I.J. (1966) 'The properties of glacial loess and the formation of loess deposits'. J. Sed. Petr., 36, p.669-676.

Smalley, I.J. (1980) 'The formation of loess materials and loess deposits: some observations on the Tashkent loess'. Geophys. u. Geol., 2 (2), p.247-257.

Smalley, I.J. (1991) 'Possible formation mechanisms for the modal coarse-silt quartz particles in loess deposits'. Quaternary International, 7, p.52-56.

Smalley, I.J. and Cabrera, J.G. (1970) 'The shape and surface texture of loess particles'. Geol. Soc. Am. Bull., 81, p. 1591-1595.

Smalley. I.J. and Derbyshire, E. (1990) 'The definition of 'ice-sheet' and 'mountain' loess'. Area, p.300-301.

Smalley, I.J. and Krinsley, D.H. (1978) 'Loess deposits associated with deserts'. Catena, 5, p.53-66.

Smalley, I.J. and Smalley, V. (1983) 'Loess material and loess deposits; formation, distribution and consequences'. In: Brookfield, M.E. and Ahlbrandt, T.S. (eds) Eolian sediments and processes, Elsevier, Amsterdam, p.51-68.

Smalley, I.J. and Vita-Finzi, C. (1968) 'The formation of fine particles in sandy deserts and the nature of 'desert' loess'. J. Sed. Pet., 38, p.766-774.

Smart, P. and Tovey, N.K. (1982) Electron microscopy of soils and sediments: techniques. Clarendon Press. Oxford. pp.264

Smith, J.D. and Foster, J.H. (1969) 'Geomagnetic reversal in Brunhes normal polarity epoch'. Science, 163, p.565-567.

Sparks, N.H.C., Mann, S., Bazylinski, D.A., Lovely, D.R., Jannasch, H.W. and Frankel, R.B. (1990) 'Structure and morphology of magnetite anaerobically-produced by a marine magnetotactic bacterium and a dissimilatory iron-reducing bacterium'. EPSL, 98, p.14-22.

Spender, M.R., Coey, J.M.D. and Morrish, A.H. (1972) 'The magnetic properties and Mössbauer spectra of synthetic samples of Fe_3S_4'. Can. J Phys., 50, p.2313-2326.

Stolz, J.F., Lovley, D.R. and Haggerty, S.E. (1990) 'Biogenic magnetite and the magnetisation of sediments'. J. Geophys. Res., 95, B4, p.4355-4361.

Sun Jiangzhong and Li Xingguo (1986) 'Palaeo-environment of the last glacial (Dali) stage in North China'. In: Gardiner, V. (ed) International Geomorphology, Vol. 2., p.763-773.

Sun, T.C. and Yang, H.J. (1961) 'The Great Ice Age glaciation in China'. Acta Geological Sinica, 41, p.234-244. [in chinese]

Tarling, D.H. (1983) Palaeomagnetism - principles and applications in geology, geophysics and archaeology. Chapman and Hall. London. pp. 379.

Taylor, S.R. and McLennan, S. (1985) The continental crust: its composition and evolution. Blackwell Scientific Publications. Oxford. p.36-45.

Taylor, S.R., McLennan, S.M. and McCulloch, M.T. (1983) 'Geochemistry of loess, continental crust composition and crustal modal ages'. Geochem. Cosmochem. Acta., 47, p.1897-1905.

Thistlewood, L. and Sun Jianzhong (1991) 'A palaeomagnetic and mineral magnetic study of the loess sequence at Liujiapo, Xian, China'. J. Quat. Sci., 6, (1), p.13-26.

Thompson, R. and Oldfield, F. (1986) Environmental magnetism. Allen and Unwin, London. pp. 217.

Thompson, L.G., Mosley-Thompson, E., Davis, M.E., Bolzan, J.F., Dai, J., Yao, T., Gundestrup, N., Wu, X., Klein, L. and Xie, Z. (1989) 'Holocene-Late Pleistocene climatic ice core records from the Qinghai-Tibetan Plateau'. Science, 246, p.474-479.

Thompson, M. and Walsh, J.N. (1983) A handbook of inductively coupled plasma spectrometry. Blackie, Glasgow. pp. 273.

Tian Junliang, Chou Chenlin and Ehmann, D. (in press) 'Determination of major and trace elements in loess, palaeosol and precipitation layers in a Pleistocene loess section, China, by INAA'. J. Radioanalyt. Nucl. Chem., Articles, 110, no.1, p.261-274.

Tong Boliang (1981) 'Some features of permafrost on the Qinghai-Xizang Plateau and the factors influencing them'. In: In: Geological and ecological studies of the Qinghai-Xizang Plateau Vol.II: Environment and Ecology of the Qinghai-Xizang Plateau, Science Press, Beijing. p.1795-1802.

Tric, E., Laj., Valet, J-P., Tucholka, P., Paterne, M. and Guichard, F. (1991) 'The Blake geomagnetic event: transition geometry, dynamical characteristics and geomagnetic significance'. EPSL, 102, p.1-13.

Tsoar, H. and Pye, K. (1987) 'Dust transport and the question of desert loess formation'. Sedimentology, 34, p. 139-153.

Tucholka, P. (1977) 'Magnetic polarity events in Polish loess profiles'. Biul. Inst. Geol. Warsaw, 305, p. 117-123.

Tucholka, P., Fontugne, M., Guichard, F. and Paterne, M. (1987) 'The Blake magnetic polarity episode in cores from the Mediterranean Sea. EPSL, 86, p.320-326.

Urrutia-Fucuguachi, J., Radhakrishnamurty, C. and Negendank, J.F.W. (1984) 'Magnetic properties of a columnar basalt from central Mexico'. Geophys. Res. Lett., 1, (9), p. 832-835.

Vinogradov, A.P. (1959) The geochemistry of rare and dispersed chemical elements in soils. Chapman and Hall, London. pp. 209.

Wang Fubao and Fan C.Y. (1987) 'Climatic changes in the Qinghai-Xizang (Tibetan) region of China during the Holocene'. Quat. Res., 28, p.50-60.

Wang Fubao and Li Bingyuan (1985) 'The lower boundary of the Quaternary in the Himalayan region in China'. In: Liu Tungsheng (ed) Quaternary geology and environment of China, p. 18-22.

Wang Jingtai (1987) 'Climatic geomorphology of the northeastern part of the Qinghai-Xizang Plateau'. In: Hövermann, J. and Wang Wenying (eds) Reports on the northeastern part of the Qinghai-Xizang (Tibet) Plateau, Science Press, Beijing. p. 140-175.

Wang Jingtai (1988) 'Climatic geomorphology of the A'nyêmaqen Mountains' In: The Palaeoenvironment of East Asia from the Mid-Tertiary, Proc. 2nd Conf., Vol. 1, p. 121-127.

Wang Jingtai, Derbyshire, E. and Shaw, J. (1986) 'Preliminary magnetostratigraphy of Dabusan Lake, Qaidam Basin, central Asia'. Phy. Earth. Plan. Int., 44, p.41-46.

Wang Jingtai and Derbyshire, E. (1987) 'Climatic geomorphology of the north-eastern part of the Qinghai-Xizang Plateau, Peoples Republic of China'. Geog. J., 153, p.59-71.

Wang Yongyan (1983) Rock desert, gravel desert, sand desert, loess. Science Press, Beijing. 234pp.

Wang, Y., Evans, M.E., Rutter, N. and Ding, Z. (1990) 'Magnetic susceptibility of Chinese loess and its bearing on paleoclimate'. Geophys. Res. Lett., 17, (12), p.2449-2451.

Wen Qizhong, Diao Guiyi and Yu Suhua (1987) 'Geochemical environment of loess in China'. In: Pecsi, M. (ed) Loess and Environment, Catena suppl., 9, p.35-46.

Wen Qizhong, Diao Guiyi, Yu Shuhua, Sun Fuqing, Gu Xiongfei, Chen Qingmu and Liu Yuluan (1982) 'Some problems of loess geochemistry in China'. In: Wasson, R.J. (ed) Quaternary dust mantles of China, New Zealand and Australia. ANU Press, Canberra. p.69-83.

Wen Qizhong, Yang Weihua, Diao Guiyi, Sun Fuqing, Yu Suhua and Liu Youmei (1984) 'The evolution of geochemical elements in loess of China and palaeoclimatic conditions during loess deposition'. In Pécsi, M. (ed) Lithology and stratigraphy of loess and palaeosols. Geographical Research Institute, Hungarian Academy of Sciences, Budapest. p. 161-169.

Wen Qizhong, Yu Suhua, Gu Xiongfu and Lei Jianquan (1983) 'Preliminary investigation of REE in loess'. Geochemistry, 2 (1), p.81-88.

Wen Qizhong, Yu Suhua, Sun Fuqing, Wang Yuqi, Chen Bingru, Tu Shuda and Sun Jingxin (1985) 'Rare-earth elements in Luochuan loess, Shaanxi Province'. Geochemistry, 4 (2), p.172-180.

Westgate, J.A., Walter, R.C., Pearce, G.W. and Gorton, M.P. (1985) 'Distribution, stratigraphy, petrochemistry and palaeomagnetism of the Late Pleistocene Old Crow tephra in Alaska and the Yukon'. Can. J. Earth Sci., 22, p.893-906.

Whalley, W.B., Douglas, G.R. and McGreevy, J.P. (1982b) 'Crack propagation and associated weathering in igneous rocks'. Zeit. f. Geomorph., 26 (1), p.33-54.

Whalley, W.B., Marshall, J.R. and Smith, B.J. (1982a) 'Origin of desert loess from some experimental observations'. Nature, 300, p.433-435.

Whalley, W.B., Smith, B.J., McAlister, J.J. and Edwards, A. (1987) 'Aeolian abrasian of quartz particles and the production of silt-size fragments, preliminary results and some possible implications for loess and silcrete formation'. In: Reid, I. & Frostick. L.(eds) Desert sediments ancient and modern. Blackwell, Oxford. p. 129-138.

Williams, R.G.B. and Robinson, D.A. (1981) 'Weathering of sandstone by the combined action of frost and salt'. Earth Surf. Proc. Land, 6, p.1-9

Wintle, A.G. (1990) 'A review of current research on TL dating'. Quat. Sci. Rev., 9, p.385-398.

Wintle, A.G. and Westgate, J.A. (1986) 'Thermoluminescence of Old Crow tephra in Alaska'. Geology, 14, p.594-597.

Wu Zirong and Gao Fuqing (1985) 'The formation of loess in China'. In: Liu Tungsheng et.al. (ed) Quaternary Geology and Environment of China, China Ocean Press, Beijing. p. 137-138. (abstract)

Xu Shuying (1981) 'The evolution of the palaeogeographic environments in the Tanggula Mountains in the Pliocene Quaternary'. In: In: Geological and ecological studies of the Qinghai-Xizang Plateau Vol.I: Geology, geological history and origin of the Qinghai-Xizang Plateau, Science Press, Beijing. p.247-256.

Yaskawa, K. (1973) 'Reversals in Brunhes normal polarity epoch'. Rock Mag. and Paleogeophys., 1, p.44-46.

Yaskawa, K. (1974) 'Reversals, excursions and secular variations of the geomagnetic field in the Brunhes normal polarity epoch'. Palaeolimnology of Lake Biwa and the Japanese Pleistocene, 2, p.77-88.

Zhang Hongyi and Han Shudi (1987) 'The palaeosols in the loess of Xinjiang and their paleoclimatic significance'. In: Liu Tungsheng (ed) Aspects of Loess Research, China Ocean Press, Beijing. p.52-57.

Zhang Jing, Huang Weiwen, Liu Minguang, Gu Yuqiao and Gu Zhaoyan (1990) 'Element concentration and partitioning of loess in the Huanghe (Yellow River) drainage basin, north China'. Chemical Geology, 89, p. 189-199.

Zhang Linyuan, Dai Xuerong and Shi Zhengtao (1991) 'The sources of loess material and the formation of the Loess Plateau in China'. Catena Suppl., 20, p. 1-14.

Zhao Songqiao (1986) Physical Geography of China. Science Press and J. Wiley and Sons.

Zhao Sonqiao and Xing Jiaming (1988) 'Origin and development of the Shamo (sandy deserts) and the Gobi (stony deserts) of China'. In: The Palaeoenvironment of East Asia from the Mid-Tertiary, Proc. 2nd Conf., Vol. 1, p. 230-251.

Zheng Benxing (1989a) 'The influence of Himalayan uplift on the development of Quaternary glaciers'. Zeit. f. Geomorph. Suppl., 76, p. 89-115.

Zheng Benxing (1989b) 'Controversy regarding the existence of a large ice sheet on the Qinghai-Xizang (Tibetan) Plateau during the Quaternary period'. Quaternary Research, 32, p. 121-123.

Zheng Benxing (1991) 'Quaternary geology in Kunlun Mountains'. In: Liu Tungsheng (ed) Loess, Environmental and Global Change, Science Press, Beijing. p. 396-402.

Zheng Benxing and Li Jijun (1981) 'Quaternary glaciation of the Qinghai-Xizang Plateau' In: Geological and ecological studies of the Qinghai-Xizang Plateau Vol. II: Environment and Ecology of the Qinghai-Xizang Plateau, Science Press, Beijing. p. 1631-1640.

Zheng Zuoxin, Feng Zuojian, Zhang Yongzu and Hu Shuqin (1981) 'On the land-vertebrate fauna of Qinghai-Xizang Plateau with considerations concerning its history of transformation'. In: Geological and ecological studies of the Qinghai-Xizang Plateau Vol. II: Environment and Ecology of the Qinghai-Xizang Plateau, Science Press, Beijing. p. 975-989.

Zhou Liping, Oldfield, F., Wintle, A. G., Robinson, S. G. and Wang Jingtai (1990) 'Partly pedogenetic origin of magnetic variations in Chinese loess'. Nature, 346, p. 737-739.

Zhu Zhenda, Liu Shu, Wu Zhen and Di Xinmin (1986) 'Deserts in China'. Inst. Desert Res. Academia Sinica, Lanzhou.